Sphingolipid Biosynthesis as an Antileishmanial Target and the Confounding Effects of Genome Plasticity

YASMINE PRECIOUS KUMORDZI

Sphingolipid Biosynthesis as an Antileishmanial Target and the Confounding Effects of Genome Plasticity

Yasmine Precious Kumordzi

A thesis submitted in partial fulfilment of the requirements for the degree of Doctor of Philosophy in Science

Department of Chemistry
Durham University

2023

Abstract

Leishmania parasites cause devastating diseases in tropical areas around the world. With a lack of vaccine, treatment relies entirely on the current drugs in the market which have several limitations, including severe side effects and emerging resistance. These are major concerns worldwide which has led to the use of genomic and proteomic approaches for the detection and characterization of new targets to help formulate newer, better drugs.

Sphingolipids are major components of the plasma and intracellular membranes, playing an essential role in maintaining structural integrity as well as being involved in cell signalling functions. Due to this, sphingolipid metabolism is very tightly regulated to maintain balance of the sphingolipidome, allowing the generation of sphingolipids when needed and to degrade toxic sphingoid bases and ceramides to avoid accumulation. Many enzymes within the sphingolipid biosynthetic pathway are employed in this homeostasis, with dysregulation of within this pathway linked to diseases such as hereditary sensory neuropathy, type 1 caused by a mutation in serine palmitoyl transferase (SPT). In *Leishmania* spp, mutations and genetic manipulation of the enzymes within this pathway results in loss of parasite viability and infectivity. Targeting sphingosine kinase, a key enzyme within the sphingolipid pathway with a divergent structure compared with the human orthologue, as well as other enzymes within the pathway shows the genome to be highly plastic as previously reported. However, when studying genes which caused detrimental effects such as LCB2, probing the pathway genetically has been showed to result in many off-target genetic changes which has impact on the final clone generated and studied. A greater understanding of *Leishmania* genome plasticity has been gained and evidence of *Leishmania* parasites genetically adapting to conform to wanted genotype is shown in the ΔLmLCB2-/- population. Overall, these results suggest a need for the monitoring of genome stability in the clones generated and the essentiality of the sphingolipid biosynthetic pathway for *Leishmania* drug target.

List of Tables

List of Figures

Abbreviations

ABC	ATP binding cassette
ALT-EJ	alternative end joining
ATP	adenosine triphosphate
Cas9	CRISPR-associated gene 9
CE-MS	Capillary electrophoresis–mass spectrometry
CER	Ceramide
CHO	Chinese hamster ovary
CL	Cardiolipin
CN	Copy Number
CNV	Copy Number Variation
CRISPR	Clustered regularly interspaced short palindromic repeats
DAG	Diacylglycerol
DAGK	diacylglycerol kinase catalytic domain
DALY	disability-adjusted life year
DHS	dihydrosphingosine
DHS1P	dihydrosphingosine 1-phosphate
DKO	double knock out
DMSO	dimethyl sulfoxide
DNA	Deoxyribonucleic acid
DR	downstream reverse
EC50	Half maximal effective concentration
EDTA	Ethylenediaminetetraacetic acid
ER	endoplasmic reticulum

ESI-MS	electrospray ionization mass spectrometry
FBS	Fetal Bovine Serum
FP	Forward Primer
FPLC	Fast protein liquid chromatography
G418	Neomycin
GBD	Global Burden of Disease
GOI	Gene of Interest
GPI	glycosylphosphatidylinositol
GSL	Glycosphingolipid
HCl	Hydrochloric Acid
HEPES	4-(2-hydroxyethyl)-1-piperazineethanesulfonic acid
HR	homologous recombination
HSAN1	Hereditary Sensory and Autonomic Neuropathy
IC50	Half maximal inhibitory concentration
IP_3	inositol trisphosphate
IPC	Inositol phosphorylceramide
IPTG	isopropyl-β-D-thiogalactopyranoside
KDS	keto-dihydrosphingosine
KO	knock out
LB	Lysogeny Broth
LCB	long chain base
LPC	Lysophosphatidylcholine
LPE	Lysophosphatidylethanolamine
LPG	lipophosphoglycan
LPI	Lysophosphatidylinositol

MAG	Monoacylglycerol
MCL	mucocutaneous leishmaniasis
MMEJ	microhomology-mediated end joining
MS	mass spectrometry
MT	miltefosine transporter
MTT	3-(4,5-dimethylthiazol-2-yl)-2,5-diphenyltetrazolium bromide
NHEJ	non-homologous end joining
NI	non induced
NTD	neglected tropical disease
OD	optical density
ORF	open reading frame
PBS	Phosphate Buffered Saline
PC	Phosphatidylcholine
PCR	polymerase chain reaction
PE	Phosphatidylethanolamine
PFA	paraformaldehyde
PG	Phosphatidylglyvcerol
PI	Phosphatidylinositol
PIP_2	phosphatidylinositol 4,5-bisphosphate
PM	plasma membrane
PNPP	PNPP
PS	Phosphatidylserine
QPCR	quantitative polymerase chain reaction
RNA	Ribonucleic acid
RP	reverse primer

S1P	sphingosine-1-phosphate
SB	spingoid base
SDS PAGE	Sodium dodecyl-sulfate polyacrylamide gel electrophoresis
SE	Sterol ester
SK	sphingosine kinase
SL	sphingolipid
SNP	single nucleotide polymorphism
SSA	single-strand annealing
SSG	sodium stibogluconate
TAE	Tris-acetate-EDTA
TAG	Triacylglycerol
TLC	thin layer chromatography
UF	upstream forward
UK	United Kingdom
UR	Upstream reverse
USA	United States of America
UTR	untranslated region
UV	Ultraviolet
VL	visceral leishmaniasis
WGS	Whole Genome Sequencing
WHO	World Health Organisation
WT	wild type

Declarations

The work presented in this thesis was carried out in the Department of Chemistry at Durham University, UK. All work is the author's own. Some results showed and discussed in chapter six has been published in journal Frontiers in Cellular and Infection Microbiology, titled 'Genome deletions to overcome the directed loss of gene function in *Leishmania*'. No other part of this thesis has been submitted for any other degree at this or any other University.

Statement of Copyright

.

Chapter 1: Introduction

The leishmaniases are a group of vector-borne zoonotic neglected tropical diseases (NTDs) caused by species of the protozoan parasite *Leishmania*. Manifestations of the disease in humans can take differing pathologies, from self-resolving cutaneous ulcers to a systemic illness and death. The parasites manifest in two main forms: the mammalian intracellular amastigote parasite and the flagellated promastigote vector form. With no prophylactic drug or vaccine on the market, a suitable treatment for the disease is necessary. However, with all current treatment having disadvantages such as long treatment regimes, painful injections and unpleasant side-effects, the need for better drugs is clear. Due to the intracellular location of these parasites in its mammalian host, specific targeting of the *Leishmania* parasite, along with the need to cross into the phagolysosome without inactivation in the acidic environment, are essential features of any new therapy (Zulfiqar et al., 2017, Russell et al., 1992). The first step in this discovery process is the identification of essential proteins that can be specifically targeted by a compound. This involves both genetic (Jones et al., 2018) and chemical approaches and has led to the identification of essential enzymes within the sphingolipid biosynthetic pathway, including sphingosine kinase (Harrison et al., 2018, Zhang et al., 2003, Zhang et al., 2007, Zhang and Beverley, 2010, Ali et al., 2012, Zhang et al., 2013a).

1.1 Leishmaniasis

The leishmaniases are a group of vector-borne, mostly zoonotic, Neglected Tropical Diseases (NTD) caused by protozoan parasites of the genus *Leishmania*. Leishmaniasis is endemic in over 90 countries (Alvar et al., 2012) and is prevalent in areas in tropical and subtropical regions, including the Mediterranean Basin. The Global Burden of Disease (GBD) study in 2019 showed between 498,000 and 862,000 new cases of leishmaniasis were estimated each

year leading to 18,700 deaths and 1.6 million disability-adjusted life years (DALYs) lost annually. These factors in addition to the limited diagnostic, treatment, and control measures, have led leishmaniasis to be considered one of the most neglected of the NTDs (Bern et al., 2008) and categorized as a class I disease (emerging and uncontrolled) by the World Health Organisation (WHO).

Leishmaniasis is known to have strong associations with poverty (Alvar et al., 2012) and environmental changes leading to the burden of this NTD falling disproportionally on the poorest global populations. Poverty is associated with poor nutrition, housing conditions and sanitation, as well as migration; all of which brings nonimmune hosts into proximity to domestic animals (potential reservoir), other infected persons and the insect vector, sandflies. This, in addition to the lack of access to healthcare and delays in diagnosis and treatment, increases the risk of disease progression, leading to a proliferation of the clinically manifested disease (Alvar et al., 2012). The costly diagnosis and treatment of leishmaniasis leads to further hardship for the families involved, reinforcing the cycle of the disease and poverty. In many poverty-stricken prevalent areas, periodic epidemics are known to occur (Ethiopia (2005, 2006), Kenya (2008) and Sudan (2009-2011) (Gillespie et al., 2016). Epidemics have also emerged due to conflicts and war, where public health systems have broken down and housing conditions have deteriorated, leading to untreated patients and the migration of immunologically naive people from non-endemic to endemic areas (Alvar et al., 2012). An example of this was seen in 2013 when an outbreak of leishmaniasis in Lebanon occurred following the migration of refugees from endemic Syria (Alawieh et al., 2014). The high burden of leishmaniasis is linked to the great impact that it has on the magnitude of morbidity and mortality (Alvar et al., 2012). Furthermore, with symptomatic cases taking months to show clinical manifestation after exposure (Alawieh et al., 2014) representing 5-16% of all

cases, and the lack of proper reporting, the actual burden of leishmaniasis could exceed the estimates.

The causative *Leishmania* spp are kinetoplastids transmitted by the bite of an infected hematophagous female phlebotomine sandfly. With a heteroxenous life cycle, *Leishmania* exists in two morphological forms: the flagellated insect form (promastigote) and the rounded mammalian intracellular form (amastigote). The *Leishmania* parasites are categorized into two distinct groups with differential global distributions, the Old World, and the New World species, which determines the pathology of leishmaniasis that occurs within a region. There are over 20 species of *Leishmania* parasites that cause disease in humans and other mammals. With a wide distribution of vector and *Leishmania* species worldwide, there are various interplays between vector, parasite and host leading to various clinical manifestations of the disease. These differential pathologies have been classified into three main forms which can be further divided: cutaneous leishmaniasis (CL), visceral leishmaniasis (VL) and mucocutaneous leishmaniasis (MCL). VL occurs when parasite is disseminated throughout the body and manifests in hepatosplenomegaly, pancytopenia and hypergammaglobulinemia. CL and MCL are localised to the skin and mucosal membranes respectively, resulting in lesions or ulcers.

1.1.1 Treatments for Leishmaniasis

Treatment for leishmaniasis can be systemic, local, or topical. Systemic drug treatments include the use of pentavalent antimonials such as sodium stibogluconate (SSG) and meglumine antimoniate, amphotericin B, pentamidine and paromomycin. These can be administered both intravenously or intramuscularly, and in some cases are used in

combination. Miltefosine is the only oral administered drug that has recently been repurposed for the treatment of all three forms of leishmaniasis.

Miltefosine

Miltefosine is a phospholipid drug and the only oral treatment available. It was originally developed for the treatment of cancer, however, was shown to be effective against *Leishmania* parasites. In March 2002, it was the first oral antileishmanial agent to be registered for use in India. Miltefosine was seen to have a high efficiency (94% cure rate) at a dose of 50-100 mg/kg for 28 days (Sundar et al., 2002), however this has dropped since its introduction (Rijal et al., 2013). However, this effectiveness comes with a plethora of side effects including gastrointestinal side effects leading to anorexia, nausea, vomiting and diarrhoea, occasional hepatotoxicity, nephrotoxicity and teratogenicity (Chakravarty and Sundar, 2010). When taken orally, miltefosine has a wide distribution throughout the body, however extensive uptake occurs in the skin (Marschner et al., 1992), liver, lungs, kidney, and spleen. With a long elimination half-life (Rijal et al., 2013), metabolism slowly eliminates miltefosine until it is excreted in the urine at <0.2% of the dose administered at day 23 of a 28-day treatment regime. The mode of action of miltefosine unknown, however is possibly linked to apoptosis and lipid-dependent cell signalling pathways being disrupted (Rijal et al., 2013).

Within the intracellular amastigote parasite, miltefosine is proposed to lead to dysfunctional fatty acid and sterol metabolism (Rakotomanga et al., 2005), apoptosis (Paris et al., 2004) and dysfunctional mitochondrial effects (Luque-Ortega and Rivas, 2007). The notion of fatty acid and sterol metabolism as a possible target for miltefosine is supported by changes seen in resistant *L. donovani* promastigotes: decreased unsaturated phospholipids, a higher content of short alkyl chain fatty acid due to a possible inactivation of the fatty acid elongation system

pathway and 24-alkylated sterol content decreased 2-fold (Rakotomanga et al., 2005). Apoptosis is another mode by which miltefosine is proposed to exhibit its antileishmanial properties. This is supported by the changes seen in treated *L. donovani* promastigotes related to indirect apoptosis-like death: cell shrinkage, DNA fragmentation and phosphatidylserine exposure (Paris et al., 2004). Mitochondrial dysfunction is seen in miltefosine-treated *L. donovani* promastigotes, including the possible disruption of cytochrome c oxidase function which causes a decline in intracellular ATP and oxygen consumption and mitochondrial depolarization (Luque-Ortega and Rivas, 2007).

The reduction in cure rate seen since introduction (Rijal et al., 2013), from 94% to 90.3% (Sundar et al., 2012) gives cause for concern and suggests that miltefosine may become obsolete. Resistance can be through many avenues: *L. donovani* miltefosine transporter (*Ld*MT) and LdRos3 inactivation in *L. donovani* (Perez-Victoria et al., 2003a), and efflux of miltefosine through ATP-binding cassette (ABC) transporter overexpression (Castanys-Munoz et al., 2007). Resistance by defective translocation of the drug via *LdMt* has already been reported in field isolates from India (Srivastava et al., 2017).

Amphotericin B

The large-scale resistance to pentavalent antimonials in Bihar state pushed the development of amphotericin B as the first line drug for VL in this region with a 90%-95% cure rate in VL cases in India (Olliaro et al., 2005). Limitations with amphotericin B, however, include the side effects associated with the treatment such as infusion related fever, nausea, chills, nephrotoxicity, and hypokalaemia which may require hospitalization (Sundar et al., 2007), as well as the cost of treatment. These side effects are more severe when using amphotericin B in its free deoxycholate (Ponte-Sucre et al., 2017). Liposomal amphotericin B (L-Amp), a

formulation packaged with cholesterol and phospholipids forming a small unilamellar liposome improves the side effects (Stone et al., 2016). Liposomal formulations may be administered with a reduced toxicity due to the reduced exposure of the free drug to the organs, however this is at a higher cost restricting its use. The VL elimination programme in the Indian subcontinent has led to the use of AmBisome (L-Amp) and in 2006 it was declared as the first-line treatment in areas of drug resistance, replacing miltefosine (Bern et al., 2006). The amphotericin B site of action is the cell surface membrane of the parasite, interacting with ergosterol (the primary membrane sterol of *Leishmania*) leading to the formation of transmembrane channels, the loss of osmotic integrity of cell, ion leakage and cell death (Saha et al., 1986).

These facts give priority to the development of a more effective, affordable, and safer drugs, either through repurposing as seen with miltefosine, improvement of current drugs through reformulation or the development of new drugs.

1.2 Drug Discovery for Leishmaniasis

Developing a drug is a long process that can take 12-15 years (Hughes et al., 2011). Before the selection of a candidate compound, there are many key stages that precede this process such as the initial target identification and validation, through assay development, high throughput screening, hit identification, lead optimization and finally molecule selection for clinical development (Hughes et al., 2011). This process usually begins with the hypothesis of the inhibition or activation of a particular protein or pathway leading to a therapeutic effect on the disease.

Drug discovery within leishmaniasis begins with drug target validation; having evidence that a target molecule (e.g., an enzyme) can be selectively inhibited leading to the death of the parasite. This evidence usually comes from genetic and/or chemical manipulations such as over-expression and analyses of the molecular signalling pathways, however this has yet to yield the target protein leading to a compound which gives the therapeutic qualities of many of the antileishmanial drugs (miltefosine, paromomycin, antimonials and pentamidine).

For leishmaniasis, the search for therapeutically significant compounds has typically employed a process of phenotypic screening, target-based screening, or drug repurposing. In phenotypic screening, the specific molecular target or compounds' mechanism of action is unknown. The whole parasite is used to screen compounds to assess the impact on parasite fitness and suggest therapeutic potential based on the toxicity towards the parasite. Target-based screening assays compounds against a specific target, usually in a biochemical or biophysical assay (Zulfiqar et al., 2017). This process requires a good understanding of the target selected, with evidence defining it as essential and 'druggable' through inhibition and gene knockout studies. Drug repurposing is a cheaper alternative to identifying a new

compound. Many of the current antileishmanials have been discovered this way: miltefosine, amphotericin B, paromomycin and pentamidine (Jones et al., 2018).

With the need for better drugs for leishmaniasis, many assays for the screening of *Leishmania* parasites have been developed (Zulfiqar et al., 2017) including the use of techniques such as absorbance and fluorescence assays (Bodley et al., 1995), flow cytometry (Delgado et al., 2001), fluorescence and bioluminescent transgenic parasites (Chan et al., 2003), imaging (Siqueira-Neto et al., 2010) and *ex vivo* assays (Aulner et al., 2013). Absorbance and fluorescence screening assays have many different types of methodologies utilising measurements to compare compound activity in both promastigotes and axenic rather than intracellular amastigotes. Acid phosphatase (Bodley et al., 1995), resazurin (Nakayama et al., 1997), and 3-(4,5-dimethylthiazol-2-yl)-2,5-diphenyltetrazolium bromide (MTT) (Maarouf et al., 1997) assays are the fluorescent assays most used for compound screening against *Leishmania* parasites. They all use similar methodology; the incubation of log stage parasites with compounds followed by the addition of screening agent (P-nitrophenyl phosphate (PNPP), resazurin or MTT). After a short incubation period the metabolically active cells either hydrolyse (PNPP) or reduce (resazurin and MTT) the reagent to a chromogenic product that can be read to give the metabolic activity of cells (Zulfiqar et al., 2017).
(Frearson et al., 2007)

1.2.1 Genetic Target Validation in *Leishmania*

Genetic methods can be used to establish which genes are essential to the parasite, thus identifying potential drug targets (Jones et al., 2018). The genome of *Leishmania* is generally considered to be diploid, however a few chromosomes have been described as aneuploid (aberrant number of chromosomes) with the transmission of genetic material during mitosis

highly unstable (Sterkers et al., 2011). This means that the modification of essential genes can also be unstable (Jones et al., 2018). Genetic manipulations are commonly performed using the promastigote stage; these are not relevant to human disease so the confirmation of essentiality of target needs to ultimately be done using the amastigote stage, preferably intracellularly using macrophages (Jones et al., 2018).

RNA-mediated interference (RNAi) is the silencing of a gene through the degradation of RNA into short fragments that activate ribonucleases to target homologous mRNA (Agrawal et al., 2003). This method of genetic manipulation for knockdown is, however, not available in almost all *Leishmania* species through the loss of RNAi machinery during evolution, possibly through viral pressure or 'freeing' the genome from constraints to increase genome plasticity (Lye et al., 2010).

Genetic manipulation techniques often lead to double strand breaks which require fixing by the cell. There are four pathways for double strand breaks; non-homologous end joining (NHEJ), single-strand annealing (SSA), alternative end joining (ALT-EJ), and homologous recombination (HR) (Kelso et al., 2017). These are essential for the maintenance of genome stability and diversity. *Leishmania* has a very efficient DNA HR that has been used to study essential and non-essential genes. Utilising *Leishmania* HR mechanism, gene replacement is done by the transfection of promastigotes with a linear vector containing a drug resistance cassette flanked by sequence homologous for the target gene locus, resulting in loss of heterozygosity (Cruz et al., 1991). Single genes on disomic chromosomes only require two rounds of transfection with different drug selection markets to generate a null mutant. These promastigote mutants can be used for the evaluation of metacyclogenesis, amastigogenesis or infection. The identification of essential genes can be manifested by giving a lethal

phenotype, cell survival depending on growth conditions, or showing essentiality in one stage and not the other (e.g. arginase is only essential in promastigotes) (Boitz et al., 2017). The inability to create a fully null mutant implies essentiality and therefore a putatively validated drug target (Duncan et al., 2017). The genetic drug target validation molecular toolbox in *Leishmania* has expanded in the recent years to include more refined methods for assessing gene essentiality (plasmid shuffle, DiCre recombinase, CRISPR/Cas9), regulating gene expression (RNAi, tetracyclic gene expression, DiCre recombinase) and endogenous protein tagging (fusion PCR tagging, destabilising domain and CRISPR/Cas9 tagging) (Duncan et al., 2017).

1.2.2 Clustered Regularly Interspaced Short Palindromic Repeats (CRISPR)/ CRISPR-associated gene 9 (Cas9) system in *Leishmania*

Clustered regularly interspaced short palindromic repeats (CRISPR)/ CRISPR-associated gene 9 (Cas9) system offers precise cleavage of double-stranded DNA using the Cas9 nuclease. *L. mexicana* promastigote have been engineered to express the humanized *Streptococcus pyogenes* Cas9 nuclease and T7 RNA polymerase (T7 RNAP). Transfection of two single-guide RNA (sgRNA) for transcribed sgRNA allows sequence specificity of the site where two double stranded breaks will occur, targeting a specific locus where precise modifications of a target site can be achieved (Beneke et al., 2017a). Due to *Leishmania* parasites lacking a functional NHEJ pathway due to absence of Artemis and XRCC4 (Uzcanga et al., 2017), this induced double-strand break must be repaired by microhomology-mediated end joining (MMEJ) using repair templates. During transfection a repair cassette generated by PCR amplification using pT plasmid containing a drug resistance marker is also introduced for repair and importantly the integration of a drug resistance marker within the two double strand breaks (Beneke et al., 2017a). Flanking the drug-resistance genes are *L. mexicana* 5′ and 3′untranslated region (UTR) sequences, selected

based on length and transcript abundance to promote robust expression of the resistance gene independent of target locus and life cycle stage. The targeted gene can be reinserted into the genome and integrated into the β-tubulin locus of *L. mexicana* using an addback strategy (Beneke et al., 2017a). This *L. mexicana* T7/Cas9 system uses PCR amplification for both sgRNA and repair templates with no cloning steps, allowing both alleles to be targeted in a single transfection, an easy and fast knockout strategy. CRISPR/Cas9 has been shown to result in an increased throughput and efficiency in assessing the essentiality of specific *Leishmania* genes (Jones et al., 2018). However, due to this system being non-inducible, only non-essential genes can be fully knocked out to give a null mutant (Duncan et al., 2017).

1.2.3 The Impact of Genome Plasticity in *Leishmania*

With a wide global distribution and clinical manifestation, adaptations to gain parasite fitness in response to environmental fluctuations such as transfer into the host or drug treatment, have led to large genetic variations within and between species (Peacock et al., 2007, Zackay et al., 2018), even in cultured *Leishmania* parasites (Sinha et al., 2018, Imamura et al., 2020). Although previously thought to be a diploid genome, *Leishmania* species have a degree of aneuploidy, dependent on the species, termed 'mosaic aneuploidy' (Sterkers et al., 2011, Lachaud et al., 2014). Other genome differences include gene copy number variation (CNV), telomeric amplification (Bussotti et al., 2018) and single nucleotide polymorphism (SNP) (Zackay et al., 2018). Therefore, genome plasticity involves different molecular modifications such as the amplification or up-regulation of genes, the loss or down-regulation of genes and aneuploidy.

These genetic variations are not random but an essential mechanism in the adjustment of levels of critical proteins through gene dosage changes. During adaptation to different *in*

vivo environments, changes in the chromosome CNV correlate with transcript levels in a manner described as 'aneuploidy-independent regulation of gene expression' (Dumetz et al., 2017). This shows parasite adaptation to the environment through dosing the expression of specific genes required for each stage of the *Leishmania* life cycle (Dumetz et al., 2017). Evidence of CNV conferring essential responses to stressful environment was shown by Bussotti et al. The genes shown to undergo CNV changes in different *Leishmania* spp are heat shock proteins, transporters and known virulence factors (Bussotti et al., 2018). Thus, changes in gene CNV may be driven by adaptation for differences in stress resistance, nutrition, and infectivity (Bussotti et al., 2018). Gene copy numbers can be changed by the addition (Ouellette and Borst, 1991) or deletion of genes or extrachromosomal elements (Grondin et al., 1993, Leprohon et al., 2009). Furthermore, due to the lack of transcription regulators in *Leishmania* parasites, aneuploidy may the main strategy for the dosage of genes in specific environments (Clayton, 2016).

Importantly, in the laboratory creation of *Leishmania* gene knockouts, high plasticity, and adaptation to changes in the environment such as addition of antibiotics can lead to the selection of parasites that display genetic changes that do not match that specifically targeted.

1.3 The significance of phospholipids and sphingolipids in *Leishmania*

Phospholipids (PLs) and sphingolipids (SLs) are abundant in all eukaryotic membranes, playing an essential role in signalling and the structure of the plasma membrane (PM). Cellular responses triggered by extracellular signalling molecules result in the hydrolysis of PLs located on the PM such as phosphatidylinositol 4,5-bisphosphate (PIP_2) generating intracellular messengers such as diacylglycerol (DAG) and inositol trisphosphate (IP_3) which play a role in signal activation within the cell and are further converted to a variety of inositol phosphates (Rhee, 2001). As well as this production of signalling molecules, PLs are also involved in highly regulated cellular processes such as actin remodelling (Coppolino et al., 2002) and the presentation of apoptosis for recognition by phagocytosis (Fadok et al., 1992, Vance and Steenbergen, 2005).

Phosphatidylserine (PS) is a PL found in the inner leaflet of eukaryotic cellular membrane, the loss of this asymmetric distribution is used as a signal of apoptosis (Verhoven et al., 1995) to macrophages (Fadok et al., 1992, Chaurio et al., 2009). This presentation to macrophages is through surface expression of PS, PS has been mimicked by parasitic protozoans such as *Leishmania* parasites to allow entry into host phagocytes (Wanderley et al., 2006). This mechanism facilitates parasite survival as complement-mediated lysis does not occur, allowing disease propagation in a process known as 'apoptotic mimicry' (de Freitas Balanco et al., 2001). As well as PLs, the plasma membrane of *Leishmania* parasites comprises complex glycolipids and glycoproteins such as lipophosphoglycans (LPGs), glycosylphosphatidylinositol (GPI)-anchored glycoproteins and proteophosphoglycans. These complex molecules differ in their amount and structure through the developmental stages of parasites and can determine the virulence of parasite (Wanderley et al., 2006, Fadok et al., 1992, de Freitas Balanco et al., 2001). Similar to PS, LPGs have been adapted to promote

parasite survival by phagocytosis. This is achieved after phagocytosis and occurs by delaying the formation of the phagolysosomes, allowing *Leishmania* promastigotes to differentiate into amastigote forms before being exposed to the low pH and hydrolytic conditions that characterize the mature phagosome (Winberg et al., 2009).

SLs, and their intermediates, are also major components of the plasma and intracellular membranes (van Meer et al., 2008), playing essential roles in maintaining structural integrity as well as being involved in cell signalling functions (Hannun and Obeid, 2008). As such, the sphingolipid pathway, and so SL levels, are tightly controlled in a process mediated by a variety of enzymes and second messengers. All SLs are derived from a backbone of sphingoid base (SB), also known as long chain base (LCB), composed of L-serine and a fatty acid acyl-CoA. Unlike in mammalian cells, *Leishmania* species preferentially use myristoyl-CoA (C14) over palmitoyl-CoA (C16) in the LCB and the resultant ceramide, the core unit of SLs (Hsu et al., 2007, Williams et al., 1984). The wide diversity of SLs is derived from the differences in the fatty acid chains (Ternes et al., 2011) and the C1 head group (Merrill et al., 2007, Merrill, 2011) in combination to form the complexity of SLs. Due to the essentiality of SLs, dysregulation of the metabolic pathway is linked to diseases such as hereditary sensory neuropathy, type 1 (Bejaoui et al., 2001) when a subunit of serine palmitoyltransferase, the first and rate limiting step in the pathway, is mutated. As well as mammals, SLs are also found in *Leishmania* species and other protozoa.

In *Leishmania* promastigotes, SLs account for ~10% of the total cellular lipids, with the most abundant cellular lipids being of PLs (~70%, made up of 33% of phosphatidylcholine (PC), 10% phosphatidylethanolamine (PE), 10% phosphatidylinositol (PI) and 7% other PLs such as phosphatidylglycerol (PG), cardiolipin (CL), and phosphatidic acid (PA)) (Zhang and Beverley, 2010). The vast majority of SLs in *Leishmania* are inositol phosphorylceramide

(IPC), which are not present in mammals (Zhang et al., 2003, Denny et al., 2004) Conversely, mammalian SLs such as sphingomyelin or glyco-SLs are clearly not synthesised by *Leishmania* parasites.

With *Leishmania* surface membrane components being important in infection and survival within the macrophages (Wanderley et al., 2006, Fadok et al., 1992, de Freitas Balanco et al., 2001, Winberg et al., 2009) the composition of SLs differing from the mammalian hosts (Zhang et al., 2003, Denny et al., 2004, Hsu et al., 2007, Williams et al., 1984), and clinical antileishmanial miltefosine shown to affect lipid biosynthesis (Rakotomanga et al., 2005, Armitage et al., 2018), targeting essential membrane components within the SL biosynthesis pathway may prove a sensible route to drug discovery for leishmaniasis.

There are many enzymes involved in SL biosynthesis and catabolism which maintain SL homeostasis, however focus here will be given to serine palmitoyltransferase (SPT) the first enzyme in *de novo* biosynthesis, and sphingosine kinase (SK) which is key to linking the SL pathway to the PL synthesis via ethanolamine phosphate (EtN-P) (Figure 1).

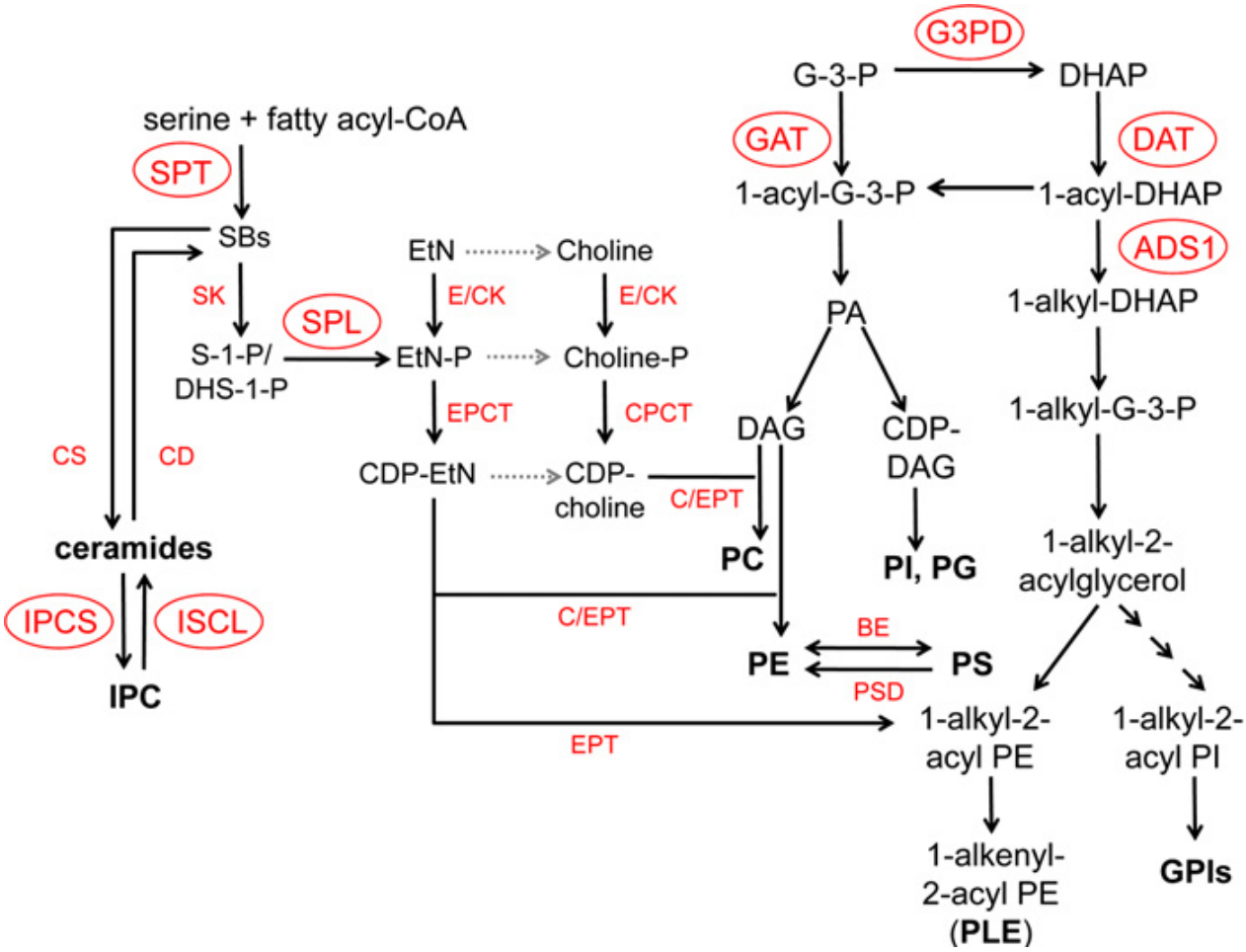

Figure 1: Predicted metabolism of SLs and PLs in Leishmania (Zhang and Beverley, 2010). Enzymes showed in red.

1.4.1 Enzymes Involved in Sphingolipid Metabolism: Serine Palmitoyltransferase

The first step in SL biosynthesis is the condensation of L-serine with palmitoyl-CoA, catalysed by serine palmitoyltransferase (SPT), to form the SB 3-keto-dihydrosphingosine (3-KDS) which is then reduced to dihydrosphingosine (DHS) (Zhang et al., 2003, Denny et al., 2004) (Figure 1). SPT is the first enzyme, and rate limiting step, in SL biosynthesis and is conserved across all eukaryotes. The SBs forms are subsequently used as intermediates to produce high order SLs through the *N*-acylation of sphingoid bases in the endoplasmic reticulum (ER) to form ceramide and later complex SLs. Through research in *Saccharomyces cerevisiae,* it was found that the activity of SPT requires two genes, lcb1 (long chain base 1)

and lcb2 which form a heterodimer in the ER membrane (Buede et al., 1991). The SPT complex in humans has been further complicated by the identification of a second orthologue of SPTLC2 (equivalent to Lcb2 in yeast), SPTLC3 with 68% homology (Hornemann et al., 2006). Mutations of SPT in humans have been linked to diseases such as HSAN1 (Bejaoui et al., 2001), a rare autosomal dominant disease which leads to progressive sensory neuropathy. Disfunction of either LCB1 (Dawkins et al., 2001) or LCB2 (Murphy et al., 2013) subunits results in increased deoxy-SB accumulation and disease (Duan and Merrill, 2015).

Due to SPT's importance in regulation, and the unfavourable pathologies that arise from mutations and/or lack of homeostasis of the sphingolipid biosynthetic pathway, SPT inhibitors have been seen as useful therapeutic tools. Myriocin, is an antibiotic and antifungal which potently inhibits SPT (Chen et al., 1999).

In *L. major*, SPT contains both LCB1 and LCB2, with *Lmj*LCB2 shown to reside in the ER. *Lmj*SPT2 mutants were disabled in metacyclogenesis, the generation of infective form promastigotes, suggesting that SL biosynthesis plays a role in infectivity (Zhang et al., 2003). These mutants also resulted in the complete loss of IPC and ceramide synthesis (Zhang et al., 2003, Denny et al., 2004) confirming that this pathway was essential for their *de novo* synthesis. Sphingosine-1-phosphate lyase (SPL) breaks down phosphorylated sphingoid bases, such as sphingosine-1-phosphate (S-1-P) or dihydrosphingosine-1-phosphate (DHS-1-P), to generate ethanolamine phosphate (EtN-P) and fatty aldehydes. *Lmj*SPL mutants (Zhang et al., 2007) showed similarity to the *Lmj*LCB2 mutants in growth, reaching stationary phase at a lower density and lower number of parasites undergoing metacyclogenesis. Unlike *Lmj*LCB2 mutants, *Lmj*SPL mutants retained the ability to synthesise ceramides and IPC as

normal wild type. However, a similar reduction in PC and PE synthesis to *Lmj*LCB2 mutants was seen in *Lmj*SPL mutants (Zhang et al., 2003, Zhang et al., 2007).

1.4.2 Enzymes Involved in Sphingolipid Metabolism: Sphingosine Kinase

Sphingosine kinase (SK) phosphorylates the terminal hydroxyl group of SBs such as sphingosine and dihydrosphingosine. This gives sphingosine-1-phosphate (S-1-P) and dihydrosphingosine-1-phosphate (DHS-1-P) respectively. These are important signalling molecules both inside and outside of the cell. In mammalian cells S-1-P binds to specific G-protein coupled receptors triggering a cascade of SL-dependent cellular events (Harrison et al., 2018). The mammalian SK is encoded by two genes, SK1 (also known as SPHK1) is predominantly cytosolic whilst SK2 (also known as SPHK2) is predominantly located in the nucleus. Unlike SPT, deletion of both SK1 and SK2 is required to create a mutant, with a single knockout not having an effect (Allende et al., 2004, Mizugishi et al., 2005). Overexpression of SK1 has been reported to contribute to cancer (Nava et al., 2002, Loveridge et al., 2010) which is supported by murine studies where blood levels of S1P were higher in mice with colon cancers and SK1 expression increased (Kawamori et al., 2009). In addition, as mutations in SK have not been recorded (Hatoum et al., 2017) this may signify its core importance. Due to the overexpression of SK1 seen in many cancers, the design of drugs to inhibit SK have led to many compounds such as PF-543 (Schnute et al., 2012) and ABC294640 (French et al., 2010).

In *Leishmania* S-1-P and DHS-1-P can also be converted to ethanolamine-phosphate (EtN-P), an essential metabolite for the synthesis of phospholipids such as phosphatidylethanolamine (PE), an abundant phospholipid (Zhang et al., 2013a). Only one isoform of SK has been found in *Leishmania* species and it is divergent from other eukaryotic orthologues and is

predicted to be expressed as a large cytoplasmic enzyme. *Leishmania* SK has not been isolated and analysed to date and has only ~20% homology to human SK1 which mostly comes from 3 highly conserved regions; the diacylglycerol kinase catalytic domain (DAGKc C1, C2 & C3), C4 and the NAD kinase/diacylglycerol kinase-like superfamily (containing C5) domain shown in graphical form in Figure 21. The catalytic active site of human SK1 is located in the cleft between the two domains and a hydrophobic lipid-binding pocket is buried in the C-terminal domain within which sphingosine binds (Wang et al., 2013).

SK null *L. major* promastigotes had defective growth, dying in 3-4 days. A phenotype that was reversed by blocking SPT with myriocin and supplementing the media with EtN (Zhang et al., 2003, Zhang et al., 2013a). This suggested that the defect was caused by the accumulation of toxic SBs and the lack of conversion of S-1-P and DHS-1-P to EtN-P. However, these rescued mutants are more sensitive to heat, acidic pH and oxidants suggesting a role for S-1-P and/or DHS-1-P in the control of stress tolerance (Zhang et al., 2013a).

Furthermore, whilst the SK null mutants could invade murine macrophages and survive for 3-4 days, they failed to proliferate even when supplemented with myriocin and EtN (Zhang et al., 2013a).

1.4.3 Salvage of Phospholipids and Sphingolipids

Another process in parasite survival is the use of endocytosis to scavenge host factors for immune evasion or energy, this is increased in the amastigote stage (Ali et al., 2012). The *de novo* biosynthesis of SBs and ceramide is non-essential for the proliferation of *L. major* amastigotes within phagolysosomes in the mammalian host, as complex SLs are synthesized using precursors from the host (Zhang and Beverley, 2010). *L. major* SMase (*Lmj*ISCL) is

used to convert scavenged host sphingolipids into ceramide (Zhang and Beverley, 2010). This ceramide can be used to generate IPC and these complex species are found at the same level as promastigote parasites in amastigotes lacking SPT and *de novo* ceramide synthesis. In *L. donovani* this scavenging is achieved through the stimulation of the host macrophage to upregulate ceramide production (Ghosh et al., 2001). With the host sphingolipid biosynthesis inhibited and/or the removal of serum from the media (exogenous source of lipids) *L. mexicana* amastigotes still successfully proliferated (Ali et al., 2012). This suggested that, unlike *L. major, L. mexicana* amastigotes do not use the host SL as the substrate for ceremide production and complex SL biosynthesis.

The *de novo* biosynthesis of SBs and ceramide is therefore likely to be essential for the proliferation of New World *Leishmania* species such as *L. mexicana*, contrasting with the Old World *Leishmania* species *L. major* and *L. donovani.* These differences may allow the SL biosynthetic pathway to be a target for New World *Leishmania* species that require *de novo* biosynthesis of SBs for invasion and proliferation (Ali et al., 2012).

1.5 Project Aims and Objectives

Considering the potential of SK as a potential drug target for leishmaniasis, this thesis sought to target SK along with other enzymes within the sphingolipid biosynthetic pathway. The aims of this project therefore include:

1. The expression and purification of *Leishmania* SK protein to facilitate an understanding of the full-length protein, including the expression of *Lmj*SK and *Lmex*SK conserved regions detailed in Chapter 4.
2. The use of known *Hs*SK inhibitors to determine differences between conserved regions detailed in Chapter 3.

3. The generation and selection of a SK knockout in *L. mexicana* using CRISPR Cas9 to assay parasite viability detailed in Chapter 5, with unwanted phenotypes investigated further.
4. Monitoring the multiple non-targeted gene ablations in *L. major* Δ*Lm*LCB2-/- using CRISPR Cas9 and monitoring of the sphingolipidome to investigate the lipidomic changes that occur when the sphingolipid biosynthesis pathway is genetically probed detailed in Chapter 6. These compensatory deletions' drug resistance are further investigated.

Chapter 2: Materials and Methods

2.1 Solutions, Buffers, and media compositions

Medium 199 (M199)

Medium 199 (M199) (Fisher Scientific, 10165142) was used for the culturing of *Leishmania mexicana* and prepared according to manufacturer advice, with the addition of 1% (v/v) Penicillin/Streptomycin (PenStrep 5,000 U/mL, ThermoFisher Scientific, 15070063), 0.1% Hemin and 20% (v/v) Fetal Bovine Serum (FBS, Sigma Aldrich, F9665). Filtered media was adjusted to the final pH of 7.0 for promastigotes and 5.5 for amastigotes prior to storage at 4 °C. Where required, M199 was supplemented with the addition of drugs for selection at the following concentrations: 50 $\mu g/ml^{-1}$ Nourseothricin sulphate (Sigma Aldrich, 74667); 32 $\mu g/ml^{-1}$ Hygromycin B (50 mg/mL, ThermoFisher Scientific, 10687010); and 20 $\mu g/ml^{-1}$ Puromycin Dihydrochloride and/or 5 $\mu g/ml^{-1}$ Blasticidin S Hydrochloride.

Schneider's media

Schneider's media (ThermoFisher Scientific, 21720001) was used for the culturing of *Leishmania major* and was prepared according to manufacturer advice with the addition of 1% v/v Penicillin/Streptomycin (PenStrep 5,000 U/mL, ThermoFisher Scientific, 15070063), and 15 or 20% v/v Fetal Bovine Serum respectively (FBS, Sigma Aldrich, F9665). Filtered media was adjusted to the final pH of 7.0 for promastigotes and 5.5 for amastigotes prior to storage at 4 °C. Where required, media was supplemented with Neomycin (G418, Sigma Aldrich, N1142) to a final concentration of 40 $\mu g/ml^{-1}$.

Lysogeny Broth (LB)

For liquid LB, 25 g of LB powder (Melford, GL1704) was added to 1 L sterile water, mixed and sterilized by autoclaving for 15 minutes at 121 °C. Ampicillin was added when required to gain a final concentration of 100 μg/ml.

For LB agar plates, 30.5 g of LB with agar powder (Sigma Aldrich, L3272) was added to sterile water, mixed and sterilized by autoclaving for 15 minutes at 121 °C. After the addition of ampicillin, plates were poured and stored in 4 °C for a maximum of 2 weeks.

Tris-acetate-EDTA (TAE) buffer (1X)

4.84 g of Tris base, 1.2 mL of 100% acetic acid and 292 mg EDTA (Ethylenediaminetetraacetic acid) was added to sterile water to make up 1 L of 1X TAE buffer.

Sodium dodecyl sulfate (SDS) buffer

30.3 g of tris base, 144.4 g of glycine and 10 g of SDS was dissolved in 1.0 L of sterile filtered H_20.

Ampicillin stock solution (100 mg/mL)

1 g of ampicillin sodium salt powder (Sigma Aldrich, 69-52-3) was dissolved completely in 10 mL of sterile water. Using a prewet 0.22 μm pore size syringe filter, 100 mg/mL ampicillin stock solution was sterilized and aliquoted in 1mL Eppendorf tubes for storage at -20 °C.

Resazurin solution (0.8 mg/mL)

40 mg resazurin sodium salt powder (Sigma Aldrich, 62758-13-8) was dissolved in 50 mL PBS. Stored in foil wrapped tube and stored at 4 °C.

SDS-PAGE gel

Resolving gel (Res) and stacking gel (Stack) was prepared as shown in

Table 1: Resolving gel was first poured into the gel cassette with isopropanol used to remove any bubbles. After polymerization of the resolving gel, the isopropanol was removed, and Stack poured above the resolving gel with the comb inserted. All prepared protein samples were run using 12.5% SDS PAGE gels and 1X SDS electrophoresis buffer for the separation of protein based on molecular weight.

Table 1:12.5% SDS-PAGE gel recipe dependent on the number of gels required and thickness of the gel required.

	1 gel x 1 mm thick		2 gel x 1 mm thick		4 gel x 1 mm thick	
	Res / µL	Stack / µL	Res / µL	Stack / µL	Res / µL	Stack / µL
SDS Buffer	2400	1200	4800	2400	9600	4800
40 % BisAcrylamide	1875	712.5	3750	1425	7500	2850
H_2O	1575	1487	3150	2974	6300	5948
APS	62.0	31.3	124.0	62.6	248.0	125.2
TEMED	6.3	3.1	12.5	6.3	25.0	12.5
Total Volume / mL	5.9	3.4	11.8	6.9	23.7	13.7
	1 gel x 1.5 mm thick		2 gel x 1.5 mm thick		4 gel x 1.5 mm thick	
	Res / µL	Stack / µL	Res / µL	Stack / µL	Res / µL	Stack / µL
SDS Buffer	3600	1800	7200	3600	14400	7200
40 % BisAcrylamide	2812.5	1068.75	5625	2137.5	11250	4275
H_2O	2362.5	2230.5	4725	4461	9450	8922
APS	93.0	47.0	186.0	93.9	372.0	187.8
TEMED	9.4	4.7	18.8	9.4	37.5	18.8
Total Volume	8.9	5.2	17.8	10.3	35.5	20.6

Leishmania parasites freezing media

1 mL dimethyl sulfoxide (DMSO) was added to 9 mL media resulting in a 10% (v/v) in the suitable medium.

2.2 General experimental methods

Polymerase chain reaction (PCR)

PCR reagents: Phusion® High-Fidelity DNA Polymerase, 5X Phusion HF Buffer, 5X Phusion GC Buffer, dimethyl sulfoxide (DMSO), 10 mM dNTPS and 50 mM $MgCl_2$ solution (Thermo Scientific, F530S).

Unless stated otherwise, DNA fragments were amplified using Phusion® High-Fidelity DNA Polymerase. PCR reactions mixes were set up as instructed by manufacturer Thermo Scientific, detailed in Table 2 and amplification was achieved using 3Prime Thermal Cycler (Techne) detailed in Table 3. All primers detailed in Table 4. Amplified products were resolved in 1% agarose gel electrophoresis.

Table 2: PCR mixture composition

PCR reaction mix	1x reaction (µL)	
10ng DNA template	5	
10mM Forward Primer	1	(0.5mM)
10mM Reverse Primer	1	(0.5mM)
5X Phusion GC/HF Buffer	4	
10mM dNTPS	0.4	(0.5mM)
Phusion® High-Fidelity DNA Polymerase	0.2	
DMSO	0.6	
water	Up to 20ul	

Table 3: PCR reaction programme- LmjSK protein expression

PCR reaction steps	Temperature °C	Time
Initial denaturation	98	30 seconds
Denaturation	98	10 seconds
Annealing	70	30 seconds
Elongation	72	90
Final elongation	72	10 minutes

Table 4: Primers used for PCR amplification- LmjSK protein expression

Primer name	DNA sequence
SK_F	5'-AAGTTCTGTTTCAGGGCCCGATGCACTCTCTCAGCTCCAACAACACGC-3'
SK_F	5'-ATGGTCTAGAAAGCTTTACTACCCACTGCGCACGAACTGC-3'

Agarose TAE gel electrophoresis

For a 1% agarose gel, 1 g of agarose was added to 100mL 1x TAE buffer and heated until fully dissolved. When cooled, 2 µl of SYBR Safe DNA gel stain (Invitrogen S33102) was added before pouring and adding a comb.

6x Gel Loading Dye (Thermo Scientific) was added to the amplification reaction for a 1x final solution and loaded into a well of the 1% agarose TAE gel containing SYBR Safe DNA gel stain. 5 µl of GeneRuler DNA Ladder (Thermo Scientific) was used for a standard ladder and the loaded gel was run immersed in 1x TAE buffer for 30-45minutes at 100 volts for the separation of DNA based on sizes. For separating larger size DNA, a 0.7% agarose TAE gel was used and for smaller DNA fragments 1.5% agarose TAE gel used. DNA bands were visualized by UV transilluminator using Gel Doc XR imager (Bio-Rad).

DNA purification from agarose TAE gel

DNA fragment required from the agarose TAE gel was excised from the gel, weighed, and transferred to a clean 1.5 mL Eppendorf tube. DNA product from the gel was extracted and purified using QIAquick Gel Extraction Kit (QIAGEN), according to manufacturer's instructions.

Restriction enzyme digestion

Unless stated otherwise, restriction enzymes (Thermo Fisher) were used for digestion according to manufacturer's protocol. Restriction enzymes were selected using Snapgene and protocol determined using NEBcloner (version 1.13.4). Digested DNA fragments were confirmed using agarose gel electrophoresis.

Gene sequencing

Miniprep purified plasmids, PCR and restriction digestion products purified from agarose TAE gel electrophoresis were submitted to gene sequencing. Purified plasmids were sequenced using the T7 promoter and terminator, and purified DNA products from agarose gel electrophoresis were sequenced using primers detailed in

Table 4 at Durham University DBS GENOMICS. DNA sequences generated were aligned with their respective genetic sequence from TryTrypDB using Clustal Omega alignment programme.

Ethanol precipitation

To the PCR products, 1x volume of 3M sodium acetate at pH 5.2, 3x volume of ice cold 100% ethanol and 2 µl of glycogen (20 mg/ml) solution was added. This is mixed gently and left on dry ice pellets for 5-10 minutes or stored at -80 °C for 30 minutes- 1 hour. Following centrifugation at 4 °C for 30 minutes at maximum speed, supernatant is removed and 75% ice cold ethanol is used to rinse the pellet. Pellet is centrifuged and supernatant removed ensuring as little ethanol remains. Using a heat block, pellet is dried for ~10 minutes and pellet is fully dissolved in water for storage at -80 °C or ready for use in transfections.

Quantitative Polymerase Chain Reaction (QPCR)

qPCRBIO SyGreen Mix Separate-ROX was used for the QPCR reaction mix without the use of RO and using the recommended reaction setup according to manufacturer's instructions. For each reaction 10 µl of 100 ng/µl of Leishmania genomic DNA was used.

2.3 Leishmania methods

Leishmania strains used are listed below.

Leishmania major: L. major (strain: Freidlin Virulent 1 [FV1]); *L. major* FV1 *ΔLmlcb2::HYG/ΔLmLCB2::PAC [pX NEO LmLCB2]* (pXΔ*Lm*LCB2); and *L. major* FV1 *ΔLmlcb2::HYG/ΔLmLCB2::PAC* (Δ*Lm*LCB2)

Leishmania mexicana: Leishmania mexicana (strain: MNYC/BZ/62/M379 [M379]) and *L. mexicana* Cas9 T7 RNA polymerase.

L. major were cultivated using Schneider's medium and *L. mexicana* using M199 medium. pXΔ*Lm*LCB2 had the addition of 40 µg/ml Neomycin. *L. mexicana* Cas9 T7 polymerase parasites had the addition of 50 µg/ml Nourseothricin sulphate and 32 µg/ml Hygromycin B.

Promastigotes were passaged 1:100 into a T25 closed cap flask using the correct media and antibiotic supplements in pH 7.0. The culture was incubated at 26 °C and maintained at log stage by passaging every 3-4 days.

Amastigotes were similarly passaged however in Schneider's media with a higher FBS content of 20% (v/v) and a lower pH of 5.5. The culture was incubated at 34 °C and maintained by passaging every 5-7 days.

Leishmania **parasite transformation**

For the transformation of *L. mexicana* promastigotes to amastigotes, a series of changes in pH, temperature and FBS (v/v) was made in a stepwise manner protocol from (Bates and Tetley, 1993).

Counting *Leishmania* parasites

Viable cells were counted from suspension using a Neubauer haemocytometer under x40 magnification using a light microscope.

A small amount of the cell culture was added to 4% paraformaldehyde (PFA) in an Eppendorf tube and mixed gently using a pipette making note of the dilution factor. Using capillary action, 10 µL of the cell suspension was used to fill the chamber under the coverslip. Cells were counted using microscopy (Olympus CKX31) within the set of 25 squares. This was multiplied by 10^4 and the dilution factor to give the parasite/mL in the culture.

Leishmania genomic DNA extraction

Leishmania genomic DNA (gDNA) was isolated using the QIAamp® DNA Blood Miniprep kit using the DNA Purification from Blood or Body Fluids (Spin Protocol), with eluted concentration of gDNA quantified using nanodrop (DeNovix DS-11 + Spectrophotometer).

Leishmania cryofreezing and revival

Leishmania promastigotes were cryofrozen in the log phase of growth. Cells were counted for a final concentration of $2x10^7$ cells/mL, freezing media (1.1.8) was prepared, and the counted cells mixed in a 1:1 ratio to give a final of 10% (v/v) DMSO in media with 10^7 promastigotes/mL. These were aliquoted into cryovials and frozen in a stepwise manner.: -20 °C, followed by -80 °C and finally -150 °C for long term storage.

For the revival of frozen stocks, *Leishmania* from the -150 °C was quickly thawed and placed into the prewarmed media. Due to the high levels of DMSO in the media, recovered parasites were passaged into 10mL of fresh media when a good level of recovered cells was visualised.

2.4 *Escherichia coli* methods

Bacterial inoculation and glycerol stock

From colonies grown on petri dishes, using a sterile pipette tip or loop, a single colony was picked. The pipette tip was dropped into a tube containing 5 ml LB broth with appropriate antibiotic selection, if using a loop, it was swirled in the broth. The culture tube was loosely closed and shaking incubated at 37 °C overnight.

500 µl of the overnight growth was added to 500 µl of 50% (v/v) glycerol in sterile water and the isolates were stored at -80 °C in cryovials.

Recovering bacteria from glycerol stocks required prior preparation of prewarmed LB plates. Using a sterile loop, some of the frozen bacterial stock was removed from the top without thawing and streaked directly on the agar petri dish with appropriate antibiotic. Bacteria were grown overnight at 37 °C.

X-Gal and IPTG selection

The identification of recombinant bacteria can be done using IPTG (isopropyl-β-D-thiogalactopyranoside) selection.

X-Gal is hydrolysed into 5-bromo-4-chloro-indoxyl which dimerizes to produce an insoluble blue pigment and is used to show incorrect insertion during cloning. With correct insertion within the lacZ operon on a plasmid during cloning, a functional β-galactosidase enzyme is not produced therefore X-Gal cannot be hydrolysed leading to recombinant *E.coli* appearing as white colonies. 20 mg/mL X-Gal (5-bromo-4-chloro-3-indolyl-β-D-galactopyranoside, Sigma Aldrich, 7240-90-6) in DMSO is stored at -20 °C in a glass container.

To a premade LB agar plate, 40 µl of 20 mg/mL X-Gal and 4 µl 1M IPTG was spread over the entire surface and incubated at 37 °C until fully absorbed into the plate.

2.5 CRISPR Cas9 knockout system

Protocol followed was adapted from (Beneke et al., 2017b). Primers were designed using the online resource LeishGEdit (*Leishmania* Genome Editing) to generate an Upstream Forward (UF) and Reverse (UR) primer, Downstream Forward (DF) and Reserve (DR) primer, 5'sgRNA primer and 3'sgRNA. These primers were designed to create a knockout of the specific genes in *L. mexicana* using pTBlast (pTBlast_v1), pTNeo (pTNeo_v1) and pTPuro (pTPuro_v1) plasmids.

sgRNA Template PCR

Primers were all diluted to 100µM. For the sgRNA PCR master mix, a 4µM primer stock of each 3'sgRNA and 5'sgRNA was made in sterile water. The sgRNA PCR master mix was made by adding the following: 0.4 µL of 100 µM G00 primer, 0.4 µL 100 µM dNTPs, 4 µL 5X GC reaction buffer, 5 µL ddH_20 and 0.2 µL High-Fidelity DNA Polymerase.
To run the PCR, 10 µL of the 4 µM sgRNA primer stock was added to 10 µL of the sgRNA PCR master mix. Amplification was achieved using the following PCR protocol: 98 °C initial denaturation for 30 seconds; 35 cycles of: 98 °C for 10 seconds, 60 °C for 30 seconds and 72 °C for 15 seconds. This was followed by 72 °C for 10 minutes. Using this, 3'sgRNA and 5'sgRNA were amplified.

Donor (plasmid) Template PCR

Primers were all diluted to 100 µM. For the donor plasmid PCR master mix, a 10 µM primer stock of UF and DR for KO or, for N-terminal tagging UF and UR or for C-terminal tagging DF and DR, was made in sterile water. The Donor (plasmid) PCR master mix was made by adding the following: 0.5 µL of plasmid, 0.8 µL 100 µM dNTPs, 1.2 µL DMSO, 1.5 µL 50

mM $MgCl_2$ solution, 8 µL 5X GC reaction buffer, 19.6 µL ddH_20 and 0.4 µL High-Fidelity DNA Polymerase.

To run the PCR, 10 µL of the 10 µM UF and DR primer stock were added to 32 µL of the Donor (plasmid) PCR master mix using the following PCR protocol: 94 °C initial denaturation for 30 seconds; 40 cycles of: 94 °C for 10 seconds, 65 °C for 30 seconds and 72 °C for 2 minutes. This was followed by 72 °C for 7 minutes.
Using this, Puromycin and Blasticidin drug resistance cassettes were amplified.
Gel electrophoresis, using a 1% (w/v) agarose gel, was used to confirm sizes of DNA amplified by PCR. 2 µL of the PCR product was used and added to 2 µL of DNA loading dye (Thermo Fisher, R0611) before loading into the wells. The gel was run at 120 volts for 30 minutes. Following this, the gel was analysed to visualize the DNA fragments separated using a GelDoc™ XR+ System (Bio-Rad).

Transfection and Selection

Prior to transfection, PCR products (3'sgRNA, 5'sgRNA and donor drug resistance cassettes), and *L. mexicana* promastigotes expressing Cas9 and T7 RNAP were prepared. Parasites were cultured in M199 media supplemented with 50 µg/ml Nourseothricin sulphate and 32 µg/ml Hygromycin B and used for transfection at log stage of growth. PCR products were pooled for ethanol precipitation using standard ethanol precipitation protocol.

Buffer preparation and PCR pooling

Transfection buffer at 1x and 4x was made using the following protocol. For 1 mL of 1x transfection buffer, 90 µl of sodium phosphate ($NaPO_4$), 3 µl of calcium chloride ($CaCl_2$), 50 µl of potassium chloride (KCl), 100µl of 4-(2-hydroxyethyl)-1-piperazineethanesulfonic acid

(HEPES) and 757 µl of sterile water was mixed. For 1mL of 4x transfection buffer, 360 µl of $NaPO_4$, 12 µl of $CaCl_2$, 200 µl of KCl, 400 µl of HEPES and 28 µl of sterile water was mixed. Both buffers were sterile filtered prior to transfection.

DNA concentration of PCR products following ethanol precipitation was measured using a nanodrop (DeNovix DS-11 + Spectrophotometer). For a single KO, 10,000 ng of each product (3'sgRNA, 5'sgRNA and pTBlast or donor pTPuro) was pooled with the addition of 10 µl 4x transfection buffer and sterile water to make volume up to 40 µl. A mock transfection was achieved by pooling 10 µl 4x transfection buffer and 30 µl sterile water.

Transfection and Clonal selection

$1x10^7$ cells/mL promastigotes at log stage growth were used for each transfection. Parasites were counted and spun down for 10 minutes, washed in cold PBS and respun for 5 minutes. The pellet containing $1x10^7$ cells was resuspended in 60 µL 1x transfection buffer and the promastigote suspension transferred into the Eppendorf tube containing the pooled PCR product. The 100 µl solution containing $1x10^7$ cells and pooled PCR products was gently mixed and transferred to the Lonza 100 µl Nucleocuvette cuvettes (Lonza, V4XP-3024). Using an Amaxa Nucleofector 2b, cuvettes were pulsed using programme X-001 and quickly transferred into 3mL of prewarmed M199 in each flask. Flasks were incubated at 26 °C for at least 24 hours before adding the drug selection of 20 µg ml^{-1} Puromycin Dihydrochloride and/or 5 µgml^{-1} Blasticidin S Hydrochloride.

Following selection using drug selective pressure, clonal selection was achieved by diluting early log stage promastigotes to a concentration of 2.5 promastigotes/mL. 20 ml of 2.5 promastigotes/mL was used to fill a 96 well plate at 200 µL per well achieving an average of

0.5 promastigote per well. Growth achieved in each well was assumed to be generated from a single clone creating a clonal population adapted from (Ommen et al., 2009)

Validation

To validate the knockout, gDNA was extracted from the KO transgenic lines. Primers synthesized for flanking the open reading frame (ORF) and within the ORF of the specific gene were used for PCR. Following PCR amplification products were analysed by gel electrophoresis.

Addback

Plasmid pGL2277 containing a kanamycin resistance gene was used for the gene addback preparation. Primers were prepared to clone the gene (SK) into the plasmid. The infusion cloning procedure was used. DNA of plasmid pGL2277 containing the gene of interest was isolated using the PureYield Plasmid Midiprep system (Promega, A2496). The pGL2277 plasmid containing the GOI was linearised by restriction enzymes NdeI and SacI, ethanol precipitated and transfected into the KO promastigotes and selected for using the addition of antibiotic in medium.

2.6 Anti-promastigote screening

Screening of Human SK inhibitors against *L. major* parasites and miltefosine against *L. mexicana* null mutants

For the compound inhibition assays, mammalian SK inhibitory compounds ABC294640, RB-005, PF-543 and 55-21 were provided by Prof Michael Barrett (Glasgow University). Each compound was dissolved in DMSO to produce a 10mM stock solution, with aliquots stored at -4 °C and the working aliquot stored at 15 °C.

For the miltefosine sensitivity assays, miltefosine was dissolved in water to produce a 50Mm stock stored at -4 °C and the working aliquot stored at 15 °C.

Promastigote activity

Leishmania promastigotes ($1x10^6$/mL) at log stage growth were incubated with SK inhibitors, DMSO (negative control), Miltefosine and Amphotericin B (positive control) in Schneiders medium in 96-well plates (Corning) using a 2-fold dilution for differing concentrations. Parasites were incubated for 44 hours at 26 °C before the addition of 10 µL resazurin solution (0.125 mg/mL). After a further 4 hours incubation, fluorescence was read using a Biotek FLx800 fluorescence microplate reader (excitation λ 540nm, bandwidth 35nm and emission λ 600nm, bandwidth 40nm).

To ensure robust data, miltefosine and each of the SK inhibitors were screened in triplicate in a set of three independent assays. This was then repeated a further three times.

Statistical analysis

The average positive control value (*RCtrlp*) was subtracted from all experimental values (*Rx*). The resultant values were then divided by the difference between the averages of the positive and negative controls (*RCtrln*) and multiplied by 100 to yield the normalised values.

$$\%\ Response = ((RCtrlp - Rx)/(RCtrlp - RCtrln)) \times 100$$

IC50 values and 95% confidence intervals for each compound were calculated using GraphPad Prism 7 software. These values were obtained from non-linear regression analysis of dose-response curves. R squared values above 0.9 indicated that the data was well fitted to the non-linear regression model. Furthermore, all IC_{50} values were calculated as an average of at least three independent assays, in which compounds were tested in triplicate.

2.7 Protein expression and purification

The full-length *LmjSK* open reading frame (ORF) was cloned into the expression vector pOPINF (N-His) using the In-Fusion system (Takara Bio). Constructs containing the truncated *L. major* and *LmxSK* flanked by a sequence encoding the N-terminal His6-tag was incorporated into the rhamnose-inducible vector pJOE5751.1 plasmid (Wegerer et al., 2008) were ordered from GenScript.

Infusion cloning

PCR primers. OPTIC/OPINE (https://www.oppf.rc-harwell.ac.uk/Opiner/AddTemplate) was used to design primers flanking the full-length *LmjSK* ORF with homology for the pOPINF plasmid vector at the 3' InFusion site and the 5' InFusion site to ensure correct cloning.

***Lmj*SK region of interest amplification.** The full-length *LmjSK* was amplified from *L. major* gDNA using PCR set up: 12.5 µL CloneAmp HiFi Premix, 2.5 µL 10mM FWD_IF_LmjSK primer, 2.5 µL 10mM REV_IF_LmjSK primer, 60 ng *L. major* wt gDNA, distilled water to 24.5 µL and 0.5 µL Phusion Polymerase. PCR protocol: 98°C initial denaturation for 1 minute; 35 cycles of 98 °C for 10 seconds, 55 °C for 15 seconds and 72°C for 1 minute 25 seconds; followed by 72 °C for 5 minutes. PCR products were fractionated on a 0.7% (w/v) agarose gel for confirmation and fragments of the correct size (2.8 kb) isolated by gel extraction using spin-column purification (QIAquick Gel Extraction Kit 28704) and quantified.

pOPINF cloning vector linearization. *E. coli* containing the pOPINF vector was grown overnight in LB culture at 37 °C and the plasmid isolated using a Miniprep kit (QIAprep Spin

Miniprep Kit 27104). Isolated plasmid was linearized: 5 µL10x Buffer Tango with BSA (Thermo Fisher), 1 µg pOPINF, 2 µL Fastdigest KpnI (Thermo Fisher), 4 µL Fastdigest HindIII (Thermo Fisher) and 26 µL distilled water. This solution was heated to 37°C for 15 minutes and inactivated at 80 °C for 10 minutes. Following linearization, products were run on a 0.7% (w/v) agarose gel and fragments of the correct size (5.2 kbp) isolated by gel extraction using spin-column purification and DNA quantified.

Insert *Lmj*SK into pOPINF cloning vector. To set up the In-Fusion cloning reaction, 50 ng of linearized pOPINF vector, 200 ng of *Lmj*SK isolated PCR product, 2 µL 5x In-Fusion enzyme premix and distilled water to 10 µL were incubated at 50°C for 15 minutes in an Eppendorf tube before placing on ice. 50 µL Stellar^{TM} competent *E.coli* HST08 strain cells were thawed on ice for 30 minutes. Subsequently, 2.5 µL of the In-Fusion cloning reaction containing pOPINF_SK recombinant plasmid was added to 50 µL of competent bacteria, mixed gently and maintained on ice for 30 minutes, before being heat shocked for 45 seconds at 42 °C and maintained on ice for a further 2 minutes. 450 µL of warm SOC media was then added and the bacteria incubated by shaking at 160 rpm for 1 hour at 37°C.

Recombinant DNA selection. LB agar plates with ampicillin and X-Gal IPTG selection were warmed to room temperature. Following the 1 hour shaking incubation, 50 µL transformed cells were spread on each plate and these incubated overnight at 37 °C.
The growth of white colonies indicated the presence of SK inserted into the lacZ region of the pOPINF vector. Clones were picked and individually grown in overnight cultures. These were then stored in 50% (v/v) glycerol solution a 1:1 dilution and frozen at -80°C. Recombinant plasmid DNA was isolated using QIAprep Spin Miniprep Kit (QIAGEN) according to manufacturer's instructions.

pOPINF_SK recombinant plasmid validation. To validate the presence of the SK ORF, isolated plasmid DNA was used in PCR (primers SK_F and SK_R), restriction enzyme digestion using ScaI and HindIII (Thermo Fisher) according to manufacturer's instructions and DNA sequencing (primers SK_F and SK_R).

Transformation into competent *E.coli* cells

pOPINF plasmids containing the *Lmj*SK were transformed into expression *E.coli* cells according to manufacturer's instructions detailed in Table 5. Transformed *E.coli* were then spread on LB-agar plates containing ampicillin and validated by PCR and DNA sequencing. Confirmed clones were stored in 50% v/v glycerol stocks at -80 °C.

Table 5: Competent cells used for protein expression.

Competent cell type	Manufacturer and catalogue numbers
ArcticExpress	Agilent #230191
BL21 (DE3)	Thermo Scientific #EC0114
Lemo21 (DE3)	NEB #C2528J
Shuffle T7	NEB #C3026J
T7 Express Competent (High Efficiency)	NEB #C2566

Expression of Sphingosine Kinase full-length protein in *E.coli*

For the expression of *L. major* sphingosine kinase, pOPINF_SK, transformed into cells listed in Table 5 was confirmed by PCR before expression. Troubleshooting of expression is discussed in Chapter Leishmania SK protein is highly disordered with final expression

procedure mentioned below. Before protein expression, PCR confirmation of competent *E.coli* containing the correct insert in the recombinant vector (pOPINF) was achieved.

Expression of Sphingosine Kinase full-length protein in BL21 (DE3) & Shuffle T7

For each competent cell line, glycerol cell stock was thawed and grown overnight shaking at 37 °C in LB broth supplemented with ampicillin. This was used as a starter culture to inoculate 1 litre LB media containing ampicillin in a baffled flask shaking at 180 rpm at 37 °C. When an absorbance value of 0.7 at 600 nm was reached, Isopropyl β-D-1-thiogalactopyranoside (IPTG) was added to a final concentration of 0.4 mM for induction. Protein expression proceeded for 14 hours shaking at 180 rpm at 20°C. Before harvesting, an absorbance reading of cells at 600nm was read and cells harvested by centrifugation.

Expression of Sphingosine Kinase full-length protein in Lemo21 (DE3)

Starter culture of 10 ml of LB broth containing chloramphenicol and ampicillin was inoculated using a glycerol cell stock and grown overnight at 37 °C shaking at 1800 rpm overnight. 10 ml of the starter culture was used to inoculate 500 ml LB broth chloramphenicol and ampicillin shaking at 180 rpm at 37 °C. When an absorbance value of 1.0 at 600 nm was reached, culture was induced by adding IPTG to a final concentration of 400µm L-rhamnose. A concentration of 500 µm Rhammnose for truncated SK protein and 500 µm for full-length SK protein was used for induction. Protein expression proceeded overnight shaking at 180 rpm at 18 °C for truncated protein and 15 °C for full length protein. Cells were harvested by centrifugation.

Expression of Sphingosine Kinase full-length protein in ArcticExpress

Starter culture LB broth containing gentamycin and ampicillin was inoculated using a glycerol cell stock and grown overnight at 37 °C shaking at 250 rpm. 10 ml of the starter culture was used to inoculate 500 ml LB broth containing no antibiotics shaking at 250rpm at 30 °C for 3 hours. For induction IPTG was added to a final concentration of 1 mM IPTG. Protein expression proceeded for 24 hours shaking at 250 rpm at 10 °C. Cells were harvested by centrifugation.

Expression of truncated proteins in *E.coli*

Constructs of truncated *L. major* and *LmxSK* within the pJOE5751 plasmid were ordered from GenScript. These domains contain the conserved regions of SK, removing the proposed disordered regions. Constructs containing the truncated *L. major* and *LmxSK* within the pJOE plasmid were transformed directly into the BL21 cell line according to manufacturer's instructions detailed in table 6. Constructs were also inserted into pOPINf vector using infusion cloning (Section 2.6) and confirmed vectors transformed into expression cells Lemo21 (DE3), ArcticExpress, Shuffle T7 and BL21 (DE3) *E.coli* cells.

Whole cell lysate

After protein expression absorbance reading of cells at 600 nm allowed for 0.7OD volume of cells to be harvested, spun down (4000 rpm, 5 minutes, 4 °C) and cells resuspended in 100 µL of protein loading buffer before boiling at 96°C for 10 minutes to lyse the cells. Then, the lysates were centrifuged for 5 minutes at maximum speed. 10 µL from the top layer was loaded onto an SDS page gel which was then run at 400 mA (200 volts) for 50 minutes and stained using Coomassie Blue (Thermo Fisher) overnight before visualising using a light box

to detect bands. This allowed for comparison of exact number of cells before and after expression.

Soluble and insoluble fractions

Lysis buffer consisting of 50 mM Tris HCl, 500 mM NaCl, 30 mM Imidazole and 2 mM B-mercaptoethanol, elution buffer consisting of 50 mM Tris HCl, 500 mM NaCl, 500 mM Imidazole and 2 mM B-mercaptoethanol was used.

For the confirmation of expression of protein expression levels: After protein expression absorbance reading of cells at 600 nm allowed for 0.7 OD volume of cells to be harvested, spun down (4000 rpm, 5 minutes, 4 °C) and cells resuspended in 100 µL lysis buffer. The resuspended cells were mixed and placed on ice briefly before sonication for 15 seconds at power 35-40. The solution was spun down at 14,000 rpm for 10 minutes at 4°c. 10 µL of the supernatant was added to 10 µL 2x loading buffer and run as the soluble fraction. A small amount of the pellet was added to 10 µL 2x loading buffer and run as the insoluble fraction on a SDS page gel.

For the accumulation of all expressed protein present in the soluble fraction: After protein expression, the culture was centrifuged at 4000 rpm, 30 minutes, 4 °C and cells resuspended in 25 ml of lysis buffer containing one tablet of Sigma-Fast protease inhibitors. Cells were agitated by sonication (4 cycles of 50% intensity for 30 seconds on ice). This lysate was centrifuged at 4000 rpm, 30 minutes, 4 °C and supernatant filtered using a 0.45 µm syringe filter.

His-tagged protein purification

HisTrap HP-5 ml (Cytiva) was used for each recombinant protein purification. Columns were equilibrated with distilled water (5x column volume), elution buffer (5x column volume) and lysis buffer (10x column volume). Using a peristaltic pump (Econo Pump, Bio-Rad) at 1 ml/min, the filtered lysate was loaded on the column.

For the full-length protein, the loaded column remained on the peristaltic pump where binding buffer (15x column volume) was used followed by elution buffer (10x column volume) to elute bound protein. The desired protein was purified by affinity chromatography on Ni+2-NTA columns by FPLC elution with increasing imidazole concentration. For truncated SK protein, the loaded column was eluted from His-Trap column with increasing amounts of elution buffer using a AKTA Pure system (GE healthcare). For both purification methods, samples were taken and fractions analysed by SDS-PAGE gels. Samples were collected during all purification steps and analysed by SDS- PAGE.

Purified proteins were concentrated using a Protein Concentrator PES 10K MWCO (Thermo Scientific) spin concentrator and quantified using a NanoDrop spectrophotometer (ThermoFisher). For mass spectrometry analysis, proteins were dialyzed into against 1 L ultra-pure water overnight at 4 °c using a Mini Slide-A-Lyser 10K MWCO. To 50 µL protein suspension, 50 µL acetonitrile and 1 µL formic acid is added and this was submitted to the Durham University Mass Spectroscopy service.

Denaturation

For the denaturation of protein, denaturation buffer consisting of 8 M urea, 100 mM Tris pH 8.5 and 10 mM EDTA was used. Following separation of the soluble and insoluble fraction 3

mL of denaturation buffer was added to the insoluble pellet, solution was vortexed and placed on ice for 30 minutes. Solution was sonicated for 15 seconds at power 35-40, followed by the addition of 500 μL of denaturation buffer and sonication repeated. The solution was spun down at 14,000 rpm for 50 minutes at 4 °c. Numerous series of sonication and centrifugation may be required for denatured protein to be present in the soluble fraction.

Mass spectrometry analysis

Proteins in the supplied gel bands were analysed by Dr Adrian Brown. Provided gel bands were digested, Liquid Chromatography-Electrospray Ionization-Mass Spectrometry (LC-ESI-MS) of resulting peptides was performed on a Sciex TripleTOF 6600 mass spectrometer linked to an Eksigent nanoLC 425 chromatography system operating in micro-flow mode and acquisition was data-dependent, top 10. Precursor and fragment-ion peak lists were generated by MSConvert and used to search a database containing ~30,000 Arabidopsis sequences, known proteomic contaminants and the provided sphingosine kinase sequences. The database search engine was PEAKS X.

2.8 Lipid analysis of *L. mexicana* parasites

Lipidomic analysis followed the protocol previously used by (Denny et al., 2004). Pellet containing $2.5x10^9$ cells was wash in ice cold PBS 3 times. Within a glass tube, cells were stored at -80 °c overnight. 250µL chloroform-methanol-water mix (4:8:3 v/v/v) was added and contents treated in a sonicating water bath twice for an hour. Supernatant from both sonication treatment was pooled and adjusted to a biphasic mixture of chloroform-methanol-water mix (4:8:5.6 v/v/v). The mixture was mixed using a vortex and sample collected following centrifugation. Bottom phase sample was collected in a glass tube and dried. Contents were frozen for analysis.

Global lipidomic analysis was performed by Phillip Whitfield at Glasgow Polyomics as stated in (Alpizar-Sosa et al., 2022). High resolution liquid chromatography-mass spectrometry (LC-MS) using an Exactive Orbitrap mass spectrometer (Thermo Scientific, Hemel Hempsted, UK) interfaced to a Thermo UltiMate 3000 RSLC system. Samples (10 µl) were injected onto a Thermo Hypersil Gold C18 column (1.9 µm; 2.1 mm x 100 mm) maintained at 50 °C. Mobile phase A consisted of water containing 10 mM ammonium formate and 0.1% (v/v) formic acid. Mobile phase B consisted of a 90:10 mixture of isopropanol-acetonitrile containing 10 mM ammonium formate and 0.1% (v/v) formic acid. The initial conditions for analysis were 65%A-35%B, increasing to 65%B over 4 min and then to 100%B over 15 min, held for 2 min prior to re-equilibration to the starting conditions over 6 min. The flow rate was 400 µl/min. Samples were analyzed in positive and negative-ion modes at a resolution of 100,000 over the mass-to-charge ratio (m/z) range of 250 to 2,000. Analyses were performed in negative ion mode at a resolution of 100,000 over the mass-to-charge ratio (m/z) range of 250 to 2,000. Progenesis QI v3.0 (Nonlinear Dynamics, Newcastle upon Tyne, UK) was used to process the data sets and determine the relative

intensities of signals associated with ceramide and inositol phosphorylceramide (IPC) molecular species. Graphs were plotted with Prism v9.4 (GraphPad, San Diego, USA).

For metabolomic analysis, pellet cells and transfer to a 50 mL falcon tubes. Quench cells by rapidly cooling to 4 °c. Centrifuge for 10 minutes at 4 °c. Move pellet into a glass tube and wash cells in 1 mL ice cold PBS twice. Resuspend pellet in 4 °c 300 µL chloroform-methanol-water mix (1:3:1 v/v/v). Leave on a shaker at 4°c for 1 hour. Centrifuge at max speed for 10 minutes at 4 °c, collecting supernatant into a glass tube. Store contents for a maximum of 24 hours at 4 °c for analysis.

Chapter 3: Conserved regions is retained between Human Sphingosine Kinase and *Leishmania* Sphingosine Kinase

With no known structure of the *Leishmania* sphingosine kinase (SK) protein and a variety of known Human SK inhibitors available on the market as anticancer drugs, an inhibition study using Human SK inhibitors against *Leishmania* parasites may facilitate an understanding of the similarity between *Leishmania* and Human SK. As a potential drug target for an intracellular parasite, inhibition to the *Leishmania* SK would suggest SK to not be a suitable drug target for Leishmaniasis due to cross-species interaction. Using populations of WT *Leishmania* parasites and *Leishmania* parasites without a functional sphingolipid biosynthetic pathway (Δ*Lm*LCB2-/-); result from this experiment may answer the following questions:

1. How similar is the *Leishmania* SK protein to the Human SK protein?
2. Are there cross-species interaction due to conserved regions?

SK inhibitors known from literature to target human Sphingosine Kinase (SK) PF-543 (HsSK1, IC_{50} 2 nM) (Schnute et al., 2012) , ABC29640 (HsSK2, IC_{50} 60 µM) (French et al., 2010), 55-21 (HsSK1, IC_{50} 7.1) (Byun et al., 2013) and RB-005 (HsSK1, IC_{50} 3.6 µM) (Baek et al., 2013) were used to determine their inhibition against *LmjSK* (Figure 2).

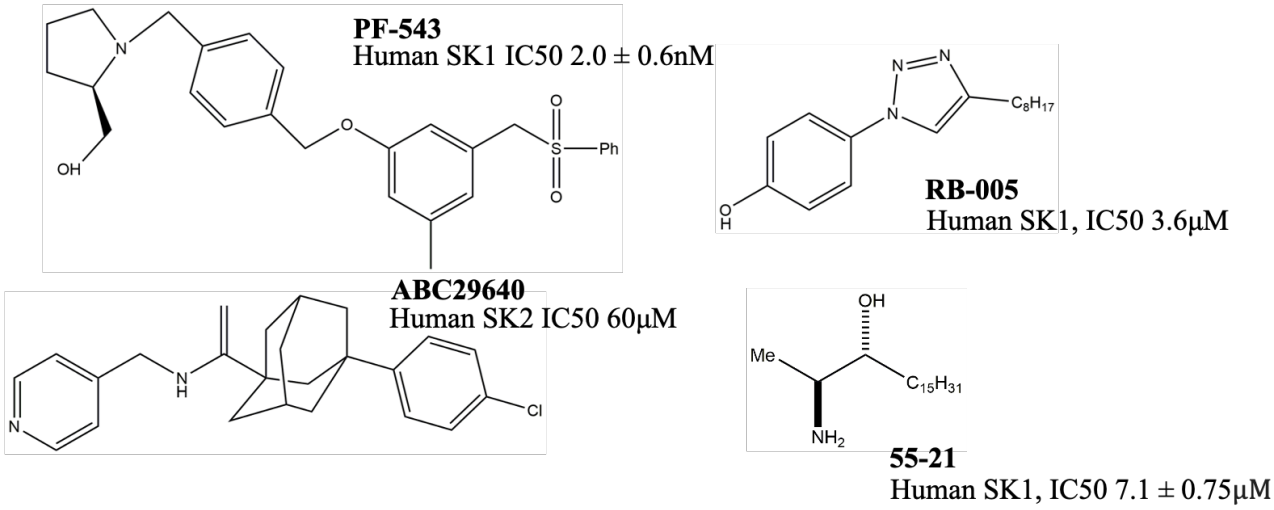

Figure 2: Chemical Structures of SK inhibitors. Structures of 55-21, ABC29640, PF-543 and RB-005 and their IC50s from enzymatic assays using Human SK and Leishmania cell-based assay. PF-543 (1-[[4-[[3-methyl5[(phenylsulfonyl)methyl]phenoxy]methyl]phenyl]methyl]-2R- pyrrolidinemethanol) RB-005 (1-(4-octylphenethyl)piperidin-4-ol) 55-21 (2S,3R)-1-Deoxy-2-amino-3-octadecanol) ABC294640, (3-(4-Chlorophenyl)-N-(4-pyridinylmethyl)-1- adamantanecarboxamide)

3.1 Conserved regions of human Sphingosine Kinases

Sphingosine kinases (SKs) catalyses the ATP-dependent phosphorylation of sphingosine to sphingosine-1-phosphate (S1P). This process plays an important role for diverse cellular functions. There are two main mammalian isozymes of SK, SK1 and SK2 (Figure 3). The main differences between SK1 and SK2 are, SK2 is 236 amino acids longer in the N terminus, contains a BH3 binding domain and contains protein rich insertions in the C terminus (Liu et al., 2000). Both SK isozymes catalyses the same the conversion of sphingosine to S1P however have origins from two separate genes and have different substrate specificities, intracellular distribution, and tissue distributions (Kohama et al., 1998, Liu et al., 2000). Within the *Hs*SK proteins there are regions conserved within both isozymes, the C1-C3 domains are found in the N terminus, and C4 and C5 domains found in the C terminus of the protein (Wang et al., 2013). C1 and C3 domains contain a ATP binding site (for sphingolipid phosphorylation) (Pitson et al., 2002), residue 81 within the C2 domain contains the active site (Wang et al., 2013), C4 contains sphingosine binding sites and is

unique domain to SKs enabling their unique ability of catalysing sphingosine to S1P (Wang et al., 2013) and C5 contains magnesium ion binding site (Wang et al., 2020). The arrangement is similar in *Lmj*SK (Figure 6) where the C1-C5 domains are conserved.

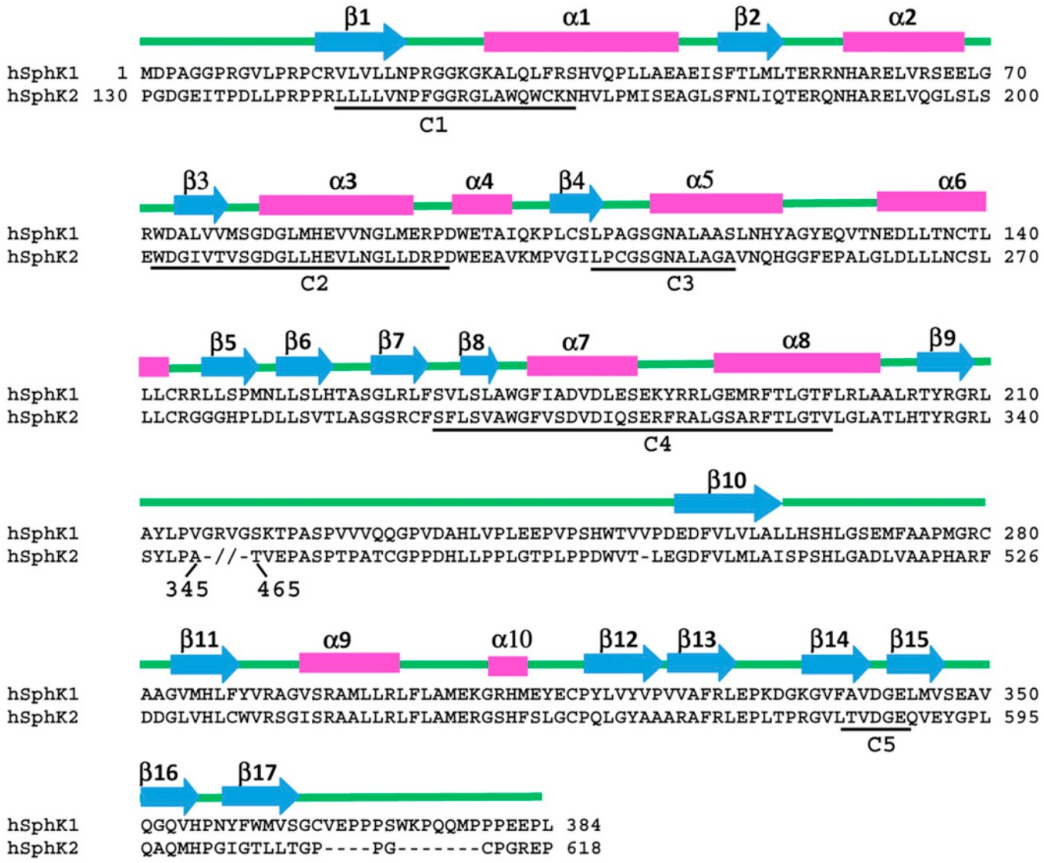

Figure 3: Sequence alignment with of Human Sphingosine Kinase isozymes 2 and 3. Double slashes indicate a large insertion in the sequence of SphK2 (Wang et al., 2014).

Due to alternative splicing, *Hs*SK1 exists in three different protein isoforms SK1a (the original SK1 described prior), SK1b and SK1c, *Hs*SK2 exists in three different isoforms SK2a (the original SK2 described prior), SK2-L, SK2b, SK2c and SK2d (Table 6). These isoforms differ only in their N terminus and isoform specificity and function knowledge in humans is limited (Haddadi et al., 2017).

Table 6: Nomenclature of SK1 and SK2 isozymes and protein isoforms

Isozymes	Isoform Name	Isoform No.	Variant No.	GenBank Accession	Uniprot ID
Sphingosine kinase 1 (SK1)	SK1a	3	3 4 X1	NM_001142601 NM_001142602 XM-005257766	Q9NYA1-1
	SK1b	2	2	NM_182965	Q9NYA1-2
	SK1c	1	1	NM_021972	Q9NYA1-3
Sphingosine kinase 2 (SK2)	SK2a SK2-L	1 3	1 3	NM_020126 NM_001204159	Q9NRA0-1 Q9NRA0-3
	SK2b	2	2	NM_001204158	Q9NRA0-2
	SK2c	4	4	NM_001204160	Q9NRA0-4
	SK2d	5	5 X1 X2 X3 X4 X5 X6	NM_001243876 XM_017027008 XM_011527133 XM_006723292 XM_011527134 XM_017027009 XM_017027010	Q9NRA0-5 Q9NRA0-5 Q9NRA0-1 Q9NRA0-2 Q9NRA0-2

3.2 Human Sphingosine Kinase inhibitors

PF-543, the most potent HsSK1 inhibitor binds into the lipid binding pocket within HsSK1 (Figure 4). For anchoring within the lipid-binding pocket of HsSK1, PF-543 adopted a bent conformation with the terminal phenol ring occupying the hydrophobic pocket and the (R)-2-(hydroxymethyl)-pyrrolidine head group bound in the expected position for a lipid head group. Residues important for the binding of the phenol ring in the binding pocket include F374, L347, L354 and L405 whilst the sphingosine recognition residue D264 is important for the binding of the head group. With the binding site of PF-543 situated between F259 and L405, other important residues for binding included F259, F389 and L385, L286 (Figure 4) (Wang et al., 2014).

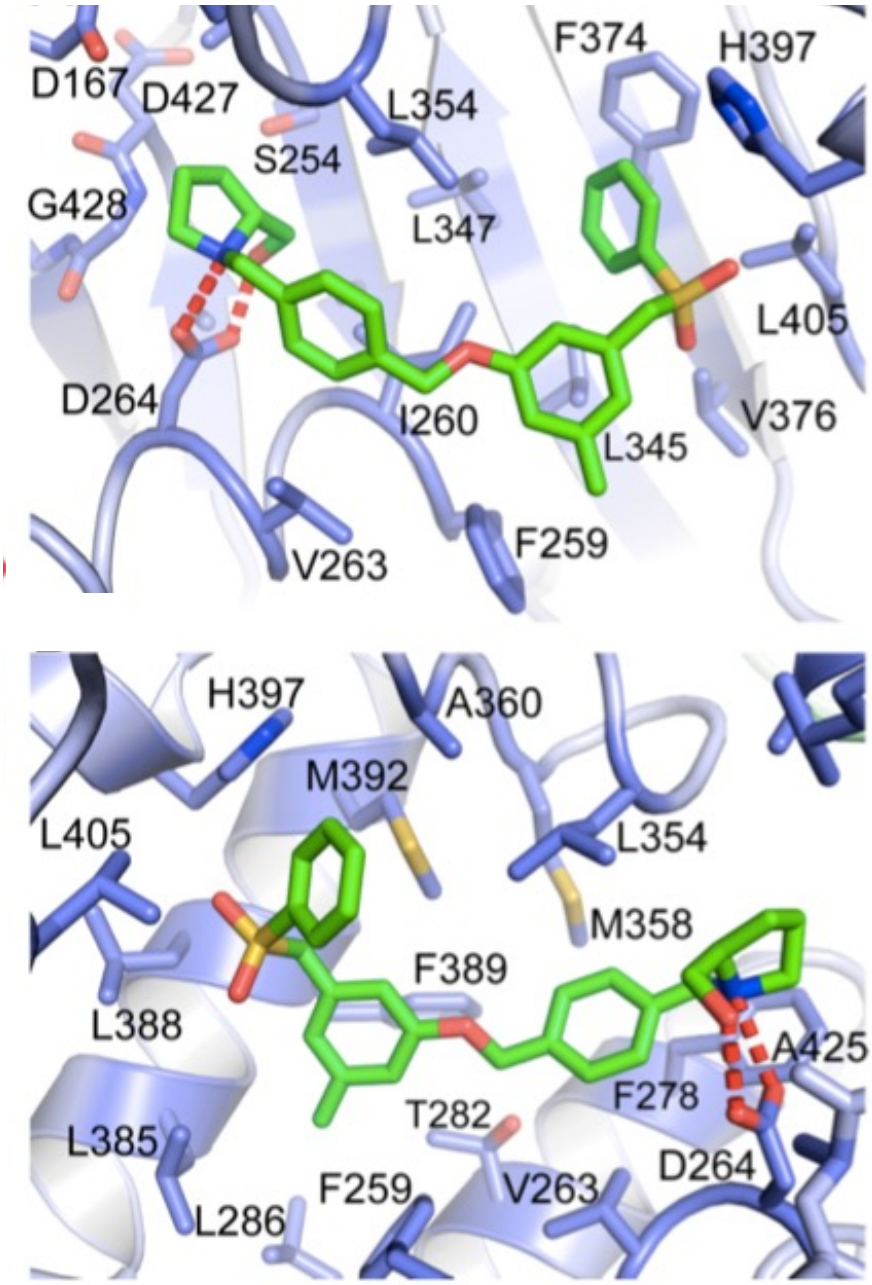

Figure 4:Binding of PF-543 from two opposite directions. Residues numbered for sphingosine kinase 1 isoform 2. (Wang et al., 2014)

RB-005 is another selective *Hs*SK1 inhibitor, however unlike PF-543 is not competitive with the sphingosine substrate. Although there have been no co-crystals reported, there have been various published modelling analyses to identify important residues for the interaction between RB-005 and *Hs*SK1 (Figure 5) (Baek et al., 2013). These analyses identified key residues, including D81, L116, A115, L268, D178 and S168 which equates to D167, L202,

A201, L354, D264 and S254 when *Hs*SK1 is aligned with *Hs*SK2. Interestingly, residues L354 and D264 are important for the interaction between *Hs*SK1 and both inhibitors RB-005 and PF-543.

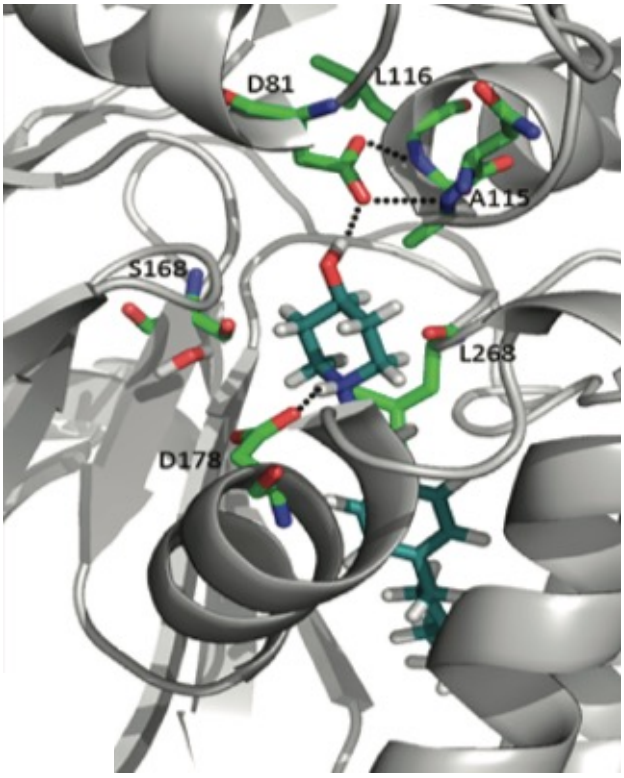

Figure 5:Modelled poses of RB-005 in the catalytic site of SK1, key residues which numbered according to HsSK1 (isoform 1) D81, L116, A115, L268, D178 and S168 (Baek et al., 2013)

There is no *Leishmania* SK crystal structure, however using bioinformatic analysis the protein sequence of *L.major* SK (LmjF.26.0710), COBALT MSA (Figure 6) alignment and BLAST global alignment (using program Needleman-Wunsch alignment of two sequences) showed that despite a low percentage identity of 14% in human SK1 and 19% in human SK2 (Altschul et al., 1997), there are areas of high homology such as the main hydrophobic pocket that makes up the C5 active site found within HsSK1 which can also be found in both *L. major* and *LmxSK (*Figure 6*)*.

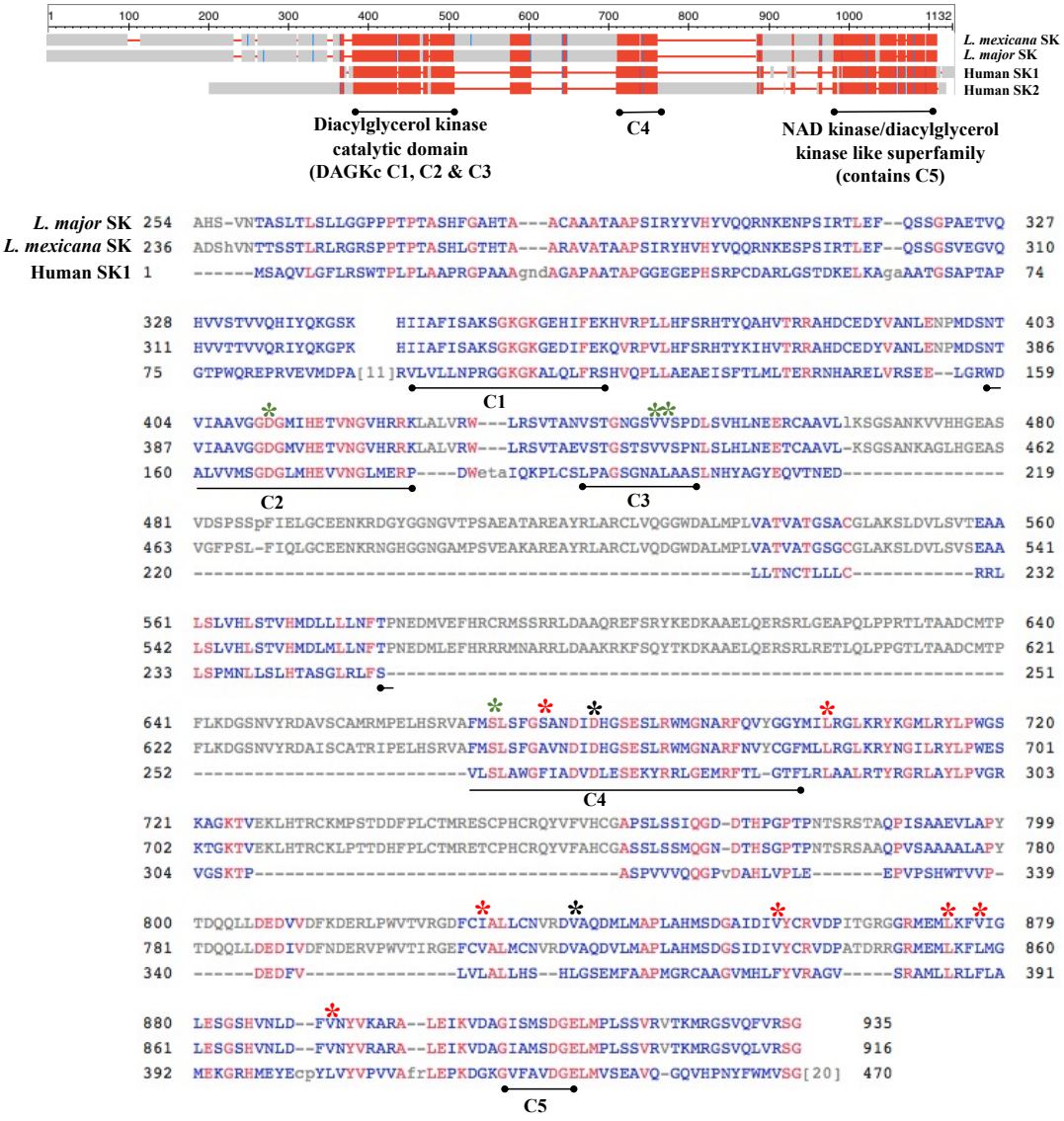

Figure 6: COBALT MSA overview of LmjSK, LmjSK, HsSK1 and HsSK2 (A) and COBALT MSA alignment of LmxSK, LmjSK, and HsSK1 with HsSK1 (isoform 2) C1-C5 regions noted (B). Residues important for PF-543 binding to HsSK1 (F259, D264, L286, L347, L354, F374, L385, F389 and L405) indicated by red star (*). Residues important for RB-005 binding to HsSK1 (D167, A201, L202, S254, D264 and L354) indicated by green star (*). Star (*) indicates residues important for both RB-005 and PF-543. Multiple sequence alignment columns with no gaps are colored in blue or red. The red color indicates highly conserved columns and blue indicates less conserved ones.

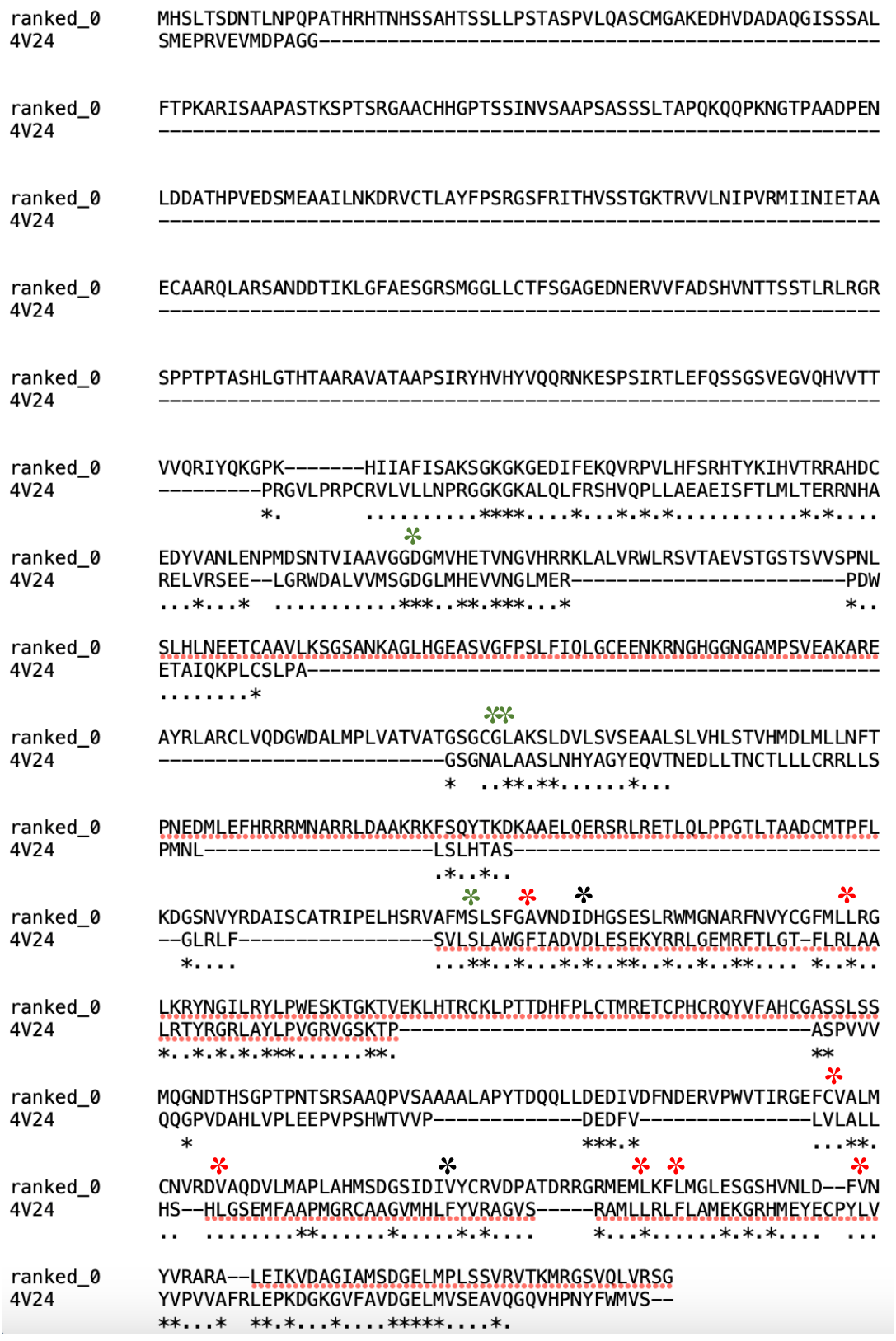

Figure 7: CLUSTAL sequence alignment between LmxSK and HsSK1 (Isoform 2) used for AlphaFold model. Residues important for PF-543 binding to HsSK1 (F259, D264, L286, L347, L354, F374, L385, F389 and L405) indicated by red star (*). Residues important for RB-005 binding to HsSK1 (D167, A201, L202, S254, D264 and L354) indicated by green star (*). Star (*) indicates residues important for both RB-005 and PF-543.

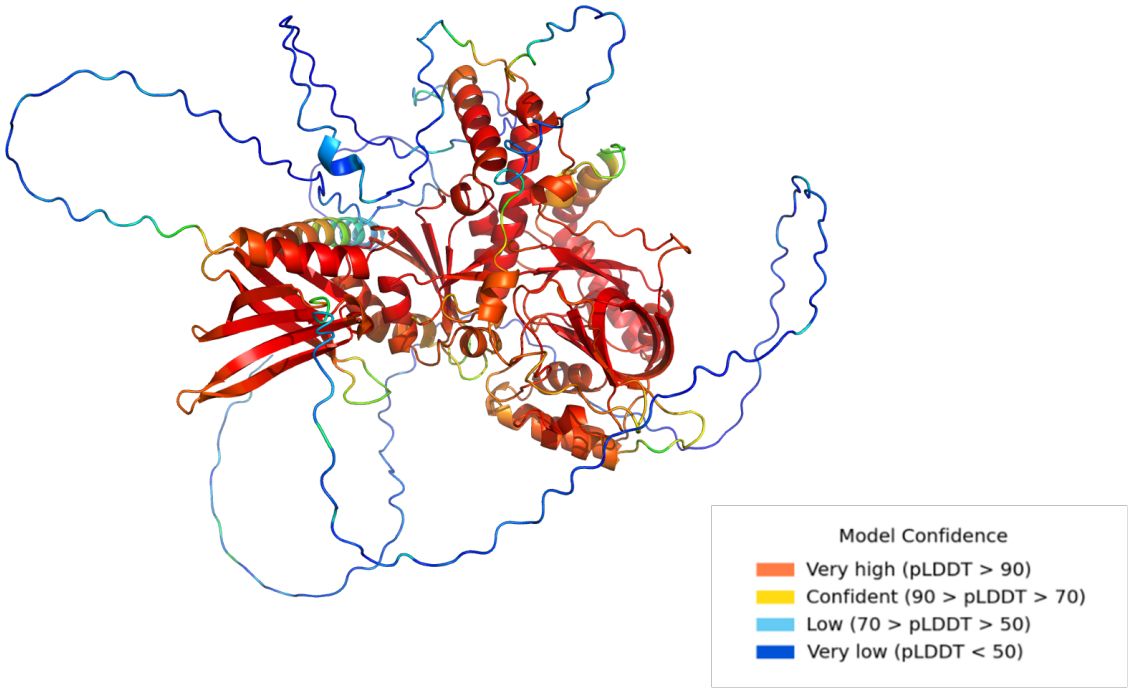

Figure 8:Alphafold prediction of Lmx SK protein.

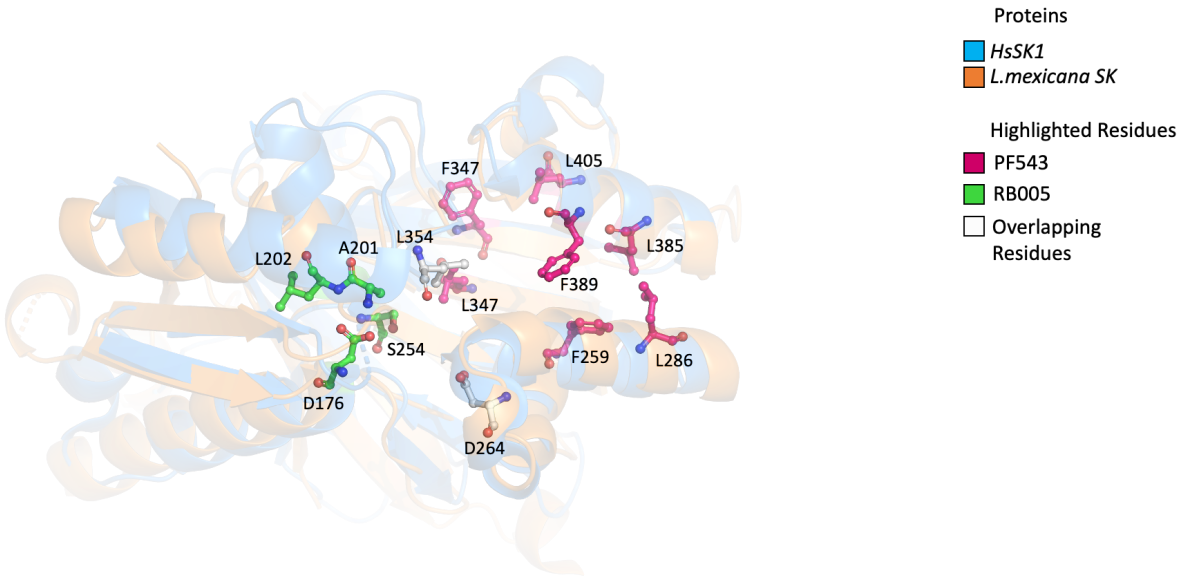

Figure 9:Overlay of alphafold of HsSK1 and LmxSK showing the regions containing important residues for PF-543 and RB-005 binding to HsSK1.

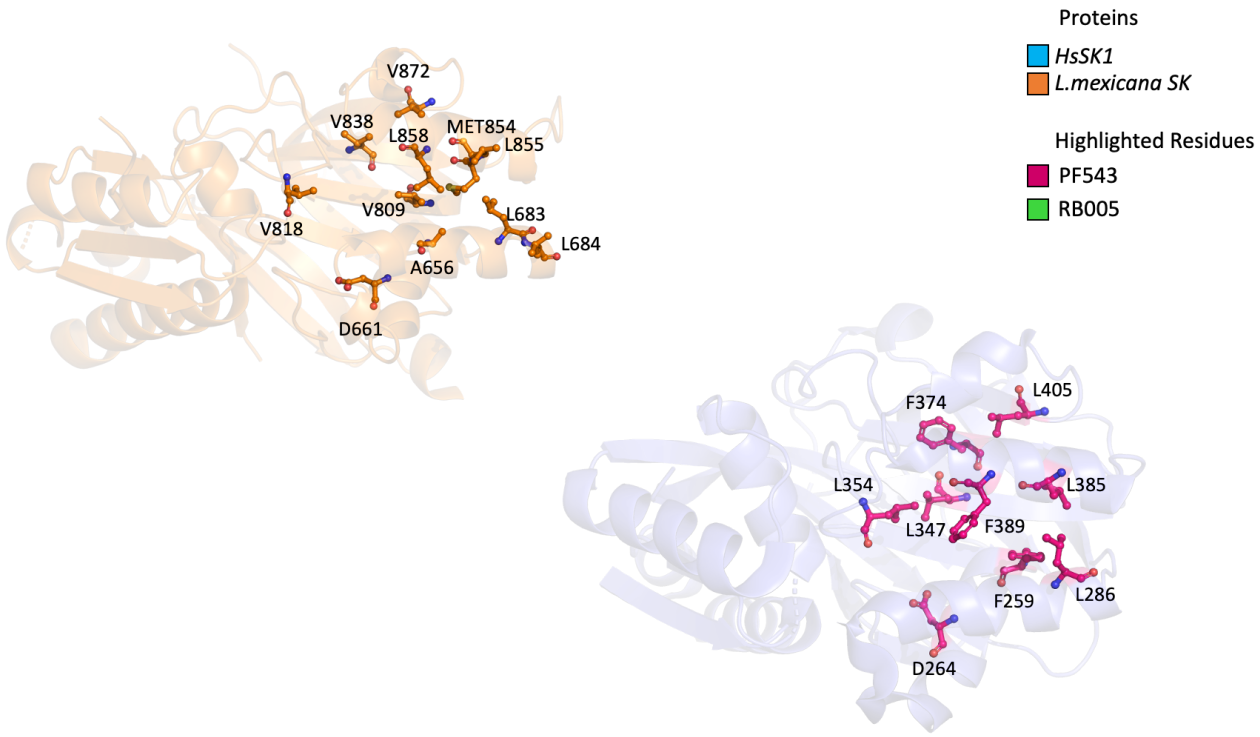

Figure 10: Overlay alphafold of HsSK (blue ribbon) and Lmx SK (orange ribbon). Residues important for PF-543 and binding to HsSK1 (F259, D264, L286, L347, L354, F374, L385, F389 and L405) indicated by red sticks.

The binding region of PF-543 to *Hs*SK1 contains important residues F259 to L405 (starred in red in Figure 6 and Figure 7) is within the C4-C5 region containing a high level of homology between *Lmj*SK and *LmxSK* (Figure 5). *Hs*SK1 F259, an aromatic amino acid is aligned with S in *Lmj*SK which is not hydrophobic and A in *Lmx*SK which is a much smaller amino acids and hydrophobic similar to F, however a F is located two amino acids away. *Hs*SK1 D264 important for the binding of the head group (Wang et al., 2014), L385 and L286, are all aligned with the same amino acid in *Lmj*SK and *Lmx*SK. *Hs*SK1 L347, L354 and L405 are aligned with V in *Lmx*SK and I in *Lmj*SK, however these are interchangeable as they are similar aliphatic amino acids. *Hs*SK1 F374 aligned with V in *Lmx*SK which is also hydrophobic however slightly smaller. F389 is aligned to L in *Lmx*SK however, can be aligned with a 1 amino acid shift (Figure **6**). The alignment of this conserved region (C4-C5)

aligns in the same manner with cobalt MSA (**Figure 6**) and clustal alignment (Figure 7) used for the AlphaFold diagram in Figure 10.

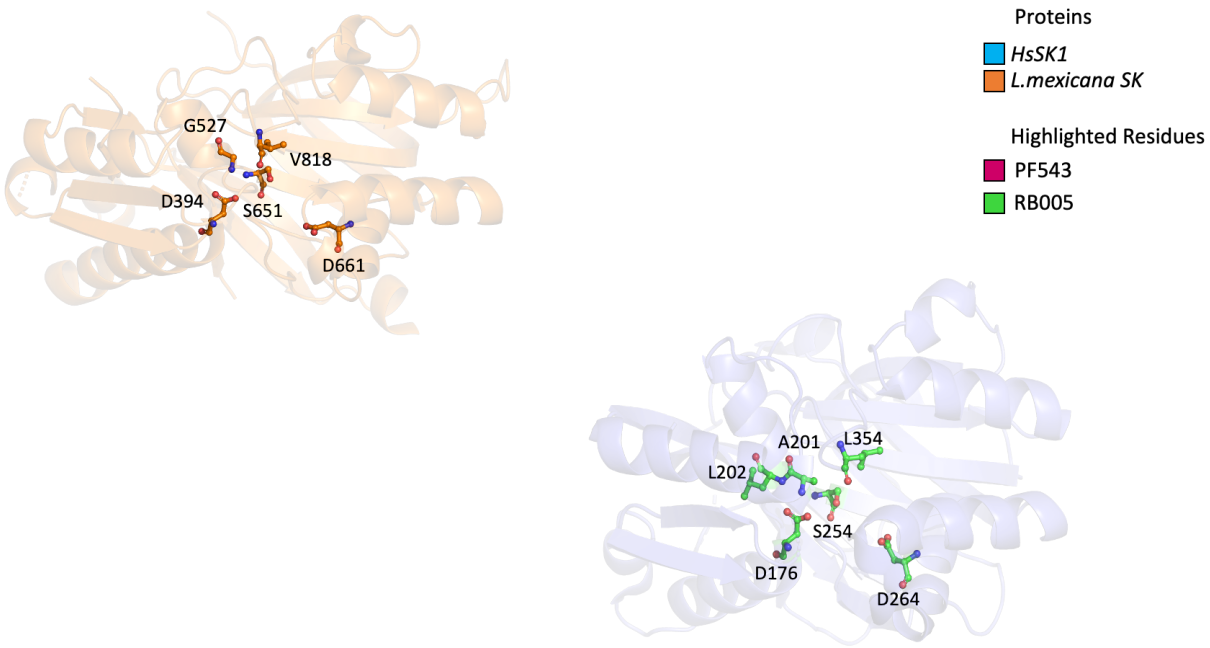

Figure 11: Alphafold of HsSK (blue ribbon) and LmxSK (orange ribbon). Residues important for RB-005 binding to HsSK1 (D167, A201, L202, S254, D264 and L354) indicated by green sticks.

The alignment of *Lmx*SK conserved regions C1 to C3 differs between cobalt MSA and clustal alignment used for AlphaFold. The important binding residues of RB-005 (starred in green in Figure 7 and Figure 8) covers a wider range of *Lmx*SK and *LmjSK* in the alignment to *Hs*SK1 (D167 to L354), however the key residues are similar or homologous to those aligned in *Lmx*SK and *Lmj*SK. *Hs*SK1 D167 and S254 both align with *Lmx*SK and *Lmx*SK. L201 and A202 are aligned with V a similar size amino acid when using cobalt MSA, with Clustal alignment A and L is changed to G and L respectively in *Lmx*SK. With this level of conservation within residues important for the binding of PF-543 and RB-005, it was considered that these *Hs*SK inhibitors may inhibit the divergent *Leishmania* SK (Figure 11).

Residues important for RB-005 and PF-543 binding are found in *Hs*SK within the C1-C5 regions (Wang et al., 2014, Baek et al., 2013). These conserved regions have a high level of

conservation between *Hs*SK and *Leishmania* SK shown by the sequence alignment (**Figure 6** and Figure 7), with amino acid changes between species retaining similar chemical properties (Figure 10 and Figure 11). Although the *Leishmania* SK protein shows high disorder (Figure 8), the regions in which *Hs*SK inhibitors bind to *Hs*SK is conserved in *Leishmania* SK; it is therefore hypothesised that *Hs*SK inhibitors may have some inhibition to *Leishmania* SK.

3.3 Human Sphingosine Kinase inhibitors against sphingolipid-free *L. major*

To identify which *Hs*SK inhibitors may elicit an effect towards *Leishmania*, *Hs*SK1 inhibitors PF-543, ABC-29640, 55-21 and RB-005 were screened against *L. major* wild type parental line (Friedlin Virulent [FV] 1), Δ*Lm*LCB2-/-, and the mutant complemented by LCB2 expressed from a plasmid ΔLCB2-/-pXLCB2 in a cell based assay (Denny et al., 2004) (Figure 12). The half maximal inhibitory concentration (IC_{50}) is a measure of the effectiveness of a compound in inhibiting a biochemical function, in this case the activity of SK enzyme. Directly targeting SK causes the accumulation of spingoid bases (SBs) which are toxic to the cell. However, in the *L. major* Δ*Lm*LCB2-/- promastigotes, the ablation of serine palmitoyl transferase (SPT) activity means that SBs are not synthesized, and therefore no ceramide and IPC are produced resulting in a sphingolipid-free membrane and SK redundancy (Denny et al., 2004). Therefore, these transgenic parasites should be insensitive to any specific SK inhibitors.

These four compounds were selected due to previous studies (Schnute et al., 2012, French et al., 2010, Byun et al., 2013, Baek et al., 2013) in which they showed good inhibitory activity against *Hs*SK enzymatic activity.

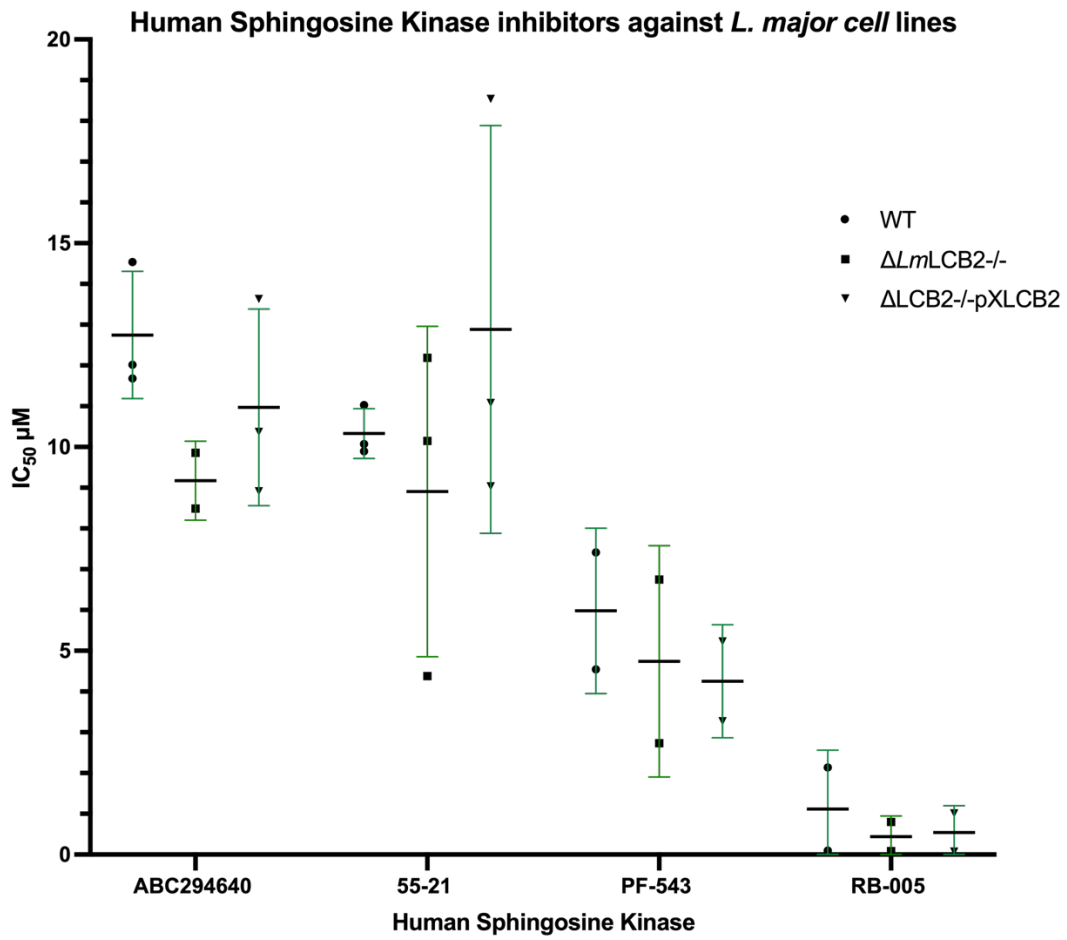

Figure 12: Sphingosine kinase inhibitors 55-21 (A), ABC294640 (B), PF-543 (C) and RB-005 (D activity against L. major wild-type (WT) in black, ΔLmlcb2::HYG/ΔLmLCB2::PAC [pX NEO LmLCB2] (ΔLCB2-/- pxLCB2) in yellow and (ΔLmlcb2::HYG/ΔLmLCB2::PAC) ΔLmLCB2-/- in red. Each point represents an average of 3 technical repeats of 3 biological repeats, n=3. GraphPad Prism 7 software was used for analysis as described in Materials and Methods.

Each of the four compounds inhibited *L. major* growth with micromolar efficiency, IC_{50} between 2nM (PF-543, (Schnute et al., 2012) and 60µM (ABC29640, (French et al., 2010) (Figure 2). PF-543 is the second most potent of the 4 inhibitors (Figure 12), perhaps reflecting its status as the most active human SK inhibitor used in this study (Schnute et al., 2012).

Table 7:IC50 of L.major populations and HumanSK

Inhibitor IC50 (μM)	PF-543	RB-005	55-21	ABC29640
Human SK	0.002 ± 0.0006	3.6	7.1 ± 0.75	60
***L. major* wild-type (WT)**	5.98	1.12	10.33	12.75
Δ*Lm*LCB2-/-	4.74	0.44	8.91	9.17
ΔLmLCB2-/-pXLCB2	4.25	0.54	12.88	10.97

Δ*Lm*LCB2-/- showed slight increase in sensitivity to the four tested human SK inhibitors (Figure 12 & Table 7). RB-005 showed to be the most potent of the inhibitors tested with an IC_{50} of 1.12μM in the *L. major* wild type cell line, reducing to 0.44μM in Δ*Lm*LCB2-/- and increasing to 0.54μM in Δ*Lm*LCB2-/-pXLCB2. This slight revival of resistance does not reach the 1.12μM of the *L. major* wild type cell line. Δ*Lm*LCB2-/- also showed increased sensitivity to PF-543 (4.74μM) compared to parental (5.98μM). The addback Δ*Lm*LCB2-/-pxLCB2 is recorded to be more sensitive to PF-543 (4.25μM) than Δ*Lm*LCB2-/-, suggesting that the sensitivity to PF-543 that Δ*Lm*LCB2-/- exhibits is not due to the changes within the sphingolipid biosynthetic pathway as the recovery of the SPT enzyme does not increase resistance back to normal WT levels. ABC294640 and 55-21 both show an increase in sensitivity when SPT is ablated (9.17μM and 8.91μM respectively in Δ*Lm*LCB2-/-), with the recovery of SPT in the addback cell line (10.97μM and 12.88μM respectively in Δ*Lm*LCB2-/-pxLCB2) increasing resistance to near *L. major* WT levels (Figure 12).

The trend of increase of sensitivity of Δ*Lm*LCB2-/- compared to *L. major* WT levels which is recovered by Δ*Lm*LCB2-/-pxLCB2 seen in RB-005, ABC294640 and 55-21 is the opposite of what is expected. This trend of increased sensitivity of the sphingolipid-free Δ*Lm*LCB2-/- indicates that the activity of these SK inhibitors does not inhibit within the sphingolipid

biosynthetic pathway as the SK enzyme is redundant in these cells and therefore should be resistant to SK inhibitors rather than sensitive.

3.4 Conclusion

Generally, each of the four compounds showed inhibition against the *L. major* lines (Figure 12). With the most activity *Hs*SK1 inhibitor PF-543 (Schnute et al., 2012), showing the second highest potency in the *Leishmania* cell-based assay. RB-005 was the most potent compound. However, in all cases Δ*Lm*LCB2-/- was more sensitive to the inhibitors indicating that SK and/or the sphingolipid biosynthetic pathway is not the target. This lack of specific *Leishmania* SK inhibition using inhibitors known to target *Hs*SK could be due to the overall divergence of sequence identity when looking outside of the conserved regions. The result from this chapter gives insight into the research questions and aims stated previously. It has confirmed the tested *Hs*SK inhibitors has suggested differences between the areas outside and potentially within the conserved regions. Bioinformatic analysis of the protein sequence of using COBALT MSA (Figure 6) alignment and BLAST global alignment (using program Needleman-Wunsch alignment of two sequences), CLUSTAL sequence alignment (Figure 7) and Alphafold predictions (Figure 8-11) supported this divergence outside of the conserved regions. *LmjSK* has a sequence identity 14% to *Hs*SK1 and 19% to *Hs*SK2 (amino acid sequence alignment shown in Figure 6 and Figure 7). Looking at the predicted tertiary structure of *LmjSK* shows large amount of disorder in the Alphafold prediction (Figure 8). The data collectively shows that the stark difference between *LmjSK* and *Hs*SK does not allow for the tested *Hs*SK inhibitors to inhibit *LmjSK.* Overall, the tested Human SK inhibitors suggests that the folded *LmjSK* protein is possibly divergent enough for cross-species interaction due to conserved regions to not occur. This however requires a study into the structure of the *Leishmania* SK protein which is discussed in Chapter 4.

Chapter 4: Expression of the *Leishmania* SK protein using microbial expression systems

Bioinformatic analysis of the protein sequence of using COBALT MSA alignment, BLAST global alignment, CLUSTAL sequence alignment and Alphafold predictions in Chapter 3 suggests divergence outside of the conserved regions. This alludes that the *Leishmania* SK protein is divergent despite the conserved regions across species due to the regions outside the conserved regions inferring fold changes in the final *Leishmania* SK protein not allowing the inhibitors to bind strongly. The identification of very low level of activity from human SK inhibitor activity against *Leishmania major* parasites directed the need to produce the *Leishmania* sphingosine kinase enzyme.

Using microbial expression systems, the expression and purification of *Leishmania* SK protein will be attempted. This will facilitate an understanding of the full-length protein and would allow further characterisation on whether current SK inhibitors such as PF-543 inhibits the *Leishmania* enzyme directly and the divergence of structure between Human SK isoforms and *Leishmania* SK to be studied. Objectives from Chapter 4 are:

1. Probing different *E.coli* expression systems for the *Leishmania* SK protein
2. Improve the expression of toxic and insoluble protein using specialist *E.coli* expression cells

Using ClustalW, sequence alignment was performed of SK from *Leishmania* species, *Trypanosoma* species and Human: *L. major*, *L. mexicana*, *L. braziliensis, L. infantum,, Trypanosoma brucei, T. cruzi,* Human SPHK1 and Human SPHK2 (Figure 13).

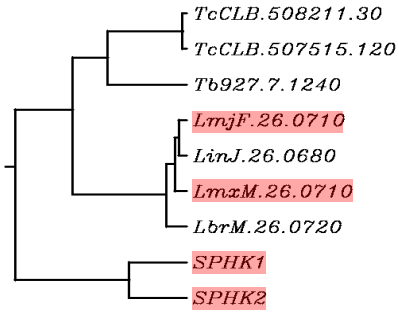

Figure 13: ClustalW sequence alignment of SK from Leishmania species, Trypanosoma species and Human: LmjF.26.0710 (L. major), LmxM.26.0710 (L. mexicana), LbrM.26.0720 (L. braziliensis), LinJ.26.0680 (L. infantum), Tb927.7.1240 (Trypanosoma brucei), TcCLB.508211.30 (T. cruzi), TcCLB.507515.120 (T. cruzi), Homo sapiens (SPHK1, 8877) and H. sapiens (SPHK2, 56848)

Unsurprisingly, the protein sequence alignment scores were highest between the *L. major* and *L. infantum* sequences (87.4%), followed by *L. major* and *L. mexicana* (81.0%). However, none of the *Leishmania* sequences showed any significant alignment with SPHK1 (12.2%-16.6%) and SPHK2 (13.6%). With such low identity, the tertiary structure of *Lmj*SK seen in the AlphaFold prediction in Figure 8 is likely to be very divergent and inhibitors of Human SK therefore unable to bind and inhibit *Lmj*SK specifically. This is likely to explain the inhibitor results above, however such divergence, coupled with a probable essential function, suggests the *Leishmania* SK as a possible novel drug target.

To investigate the structure and function of the *Leishmania* SK enzyme, the *LmjSK* coding sequence (~2800 bp, amplified from a cDNA clone acquired from GenScripT) was cloned into the pOPINF expression system (Takara Bio) as described in Materials and Methods. Following validation by PCR and DNA sequencing, pOPINF_SK plasmid was transformed into T7 Express cells, Rosetta2, ERZ566 cells, and BL21 DE3 pRARE cells for the expression of SK protein as instructed by manufacturer. Expression of the 101 kDa *LmjSK* protein was not achieved in the initial test expressions using T7 Express cells, Rosetta2, ERZ566 cells and BL21 DE3 pRARE cells (refer to

below for the different expression conditions used). This lack of SK protein expression was deduced by a lack of protein band in the induced sample when compared to non-induced sample run on SDS page gel. Solving this was approached firstly by codon optimization of the sequence for *E.coli,* to overcome the difference in codon usage between the bacteria and *Leishmania*. This codon optimisation however did not improve expression in the cell lines previously used cells (refer to Table 7 for the different expression conditions used).

Table 8: Table 9: Expression level of L.major SK using E.coli cells T7 Express cells, Rosetta2, ERZ566 cells, and BL21 DE3 pRARE cells with a combination of different expression conditions (- no expression deduced by no protein band in induced samples analysed on SDS page gel, + low expression, ++ mid expression, +++ high expression).

		Non codon optimised								Codon optimised							
	Induction concentration	1mM IPTG				2mM IPTG				1mM IPTG				2mM IPTG			
	Temperature °c	15	18	30	37	15	18	30	37	15	18	30	37	15	18	30	37
E.coli cell type	T7 Express	-	-	-	-	-	-	-	-	-	-	-	-	-	-	-	-
	Rosetta2	-	-	-	-	-	-	-	-	-	-	-	-	-	-	-	-
	ERZ566	-	-	-	-	-	-	-	-	-	-	-	-	-	-	-	-
	BL21 DE3 pRARE	-	-	-	-	-	-	-	-	-	-	-	-	-	-	-	-

4.1 Solving problematic Shingosine Kinase (SK) protein expression

Due to the previous expression cells not resulting in SK expression, Lemo21 (DE3) E.*coli* cells known for the expression of difficult targets was tested. Using Lemo21 (DE3) E.*coli* cells, expression can be tuned down by the addition of rhamnose during induction. These were tested using a range of temperatures, IPTG concentrations and Rhamnose concentrations shown in the Table 10.

Table 10: Expression level of LmjSK using E.coli cells Lemo21 (DE3) with a combination of different expression conditions (- no expression, + low expression, ++ mid expression, +++ high expression).

	0µM rhamose					100µM rhamnose					500µM rhamnose					2000µM rhamnose				
Temperature °c	15	20	25	30	37	15	20	25	30	37	15	20	25	30	37	15	20	25	30	37
Non codon optimised	+	-	-	-	-	+	-	-	-	-	+	-	-	-	-	+	-	-	-	-
Codon optimised	+	-	-	-	-	+	-	-	-	-	+	-	-	-	-	+	-	-	-	-

Lemo (DE3) cells grown at 15°c showed a >100 kDa protein expressed (**Figure** 14) in the whole cell fraction. This expression occurred in cells containing both the codon optimised sequence and the non-codon optimised sequence showing a slight bias to the non-codon optimised sequence. Testing expression of *Lmj*SK in Lemo cells at higher temperatures (20°c, 25°c, 30°c, and 37°c) showed no protein expression, making 15°c induction with 500µM Rhamnose and 400µM IPTG the optimum condition for *Lmj*SK protein expression in these cells.

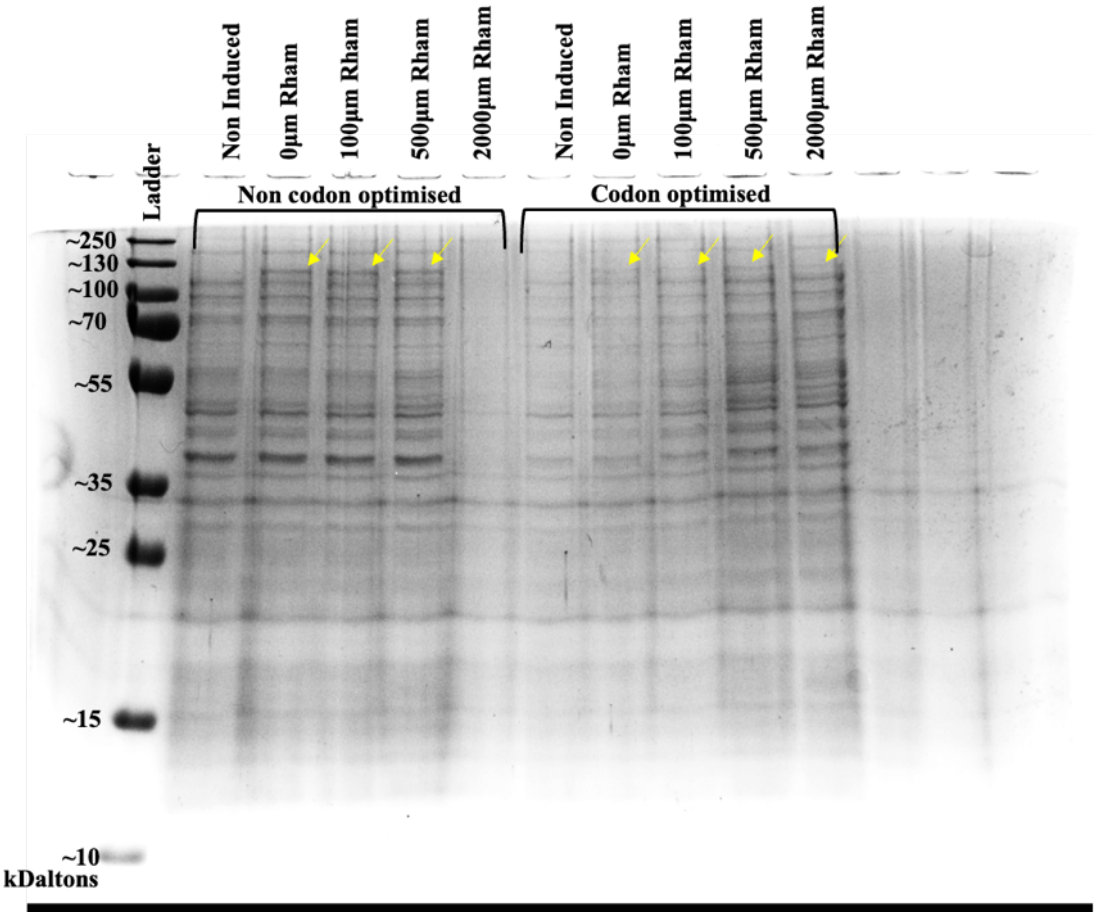

Figure 14. Test expression of full-length LmjSK protein in pOPINf vector expression using Lemo(DE3)competent E.coli cells showing whole cell lysate. Lemo cells containing pOPINF plasmids containing non codon optimised and codon optimised SK sequences were analysed separately. Yellow arrows show the presence of a ~ 115kDalton expressed protein deduced by the band not present in the non-induced fraction.

Investigations of the location of the protein in the soluble and insoluble fractions by separating the whole cell lysate into the soluble and insoluble fraction described in Materials and Methods showed that the protein was only found in the insoluble fraction (Figure 15). This indicated potential problems in aggregation and protein folding.

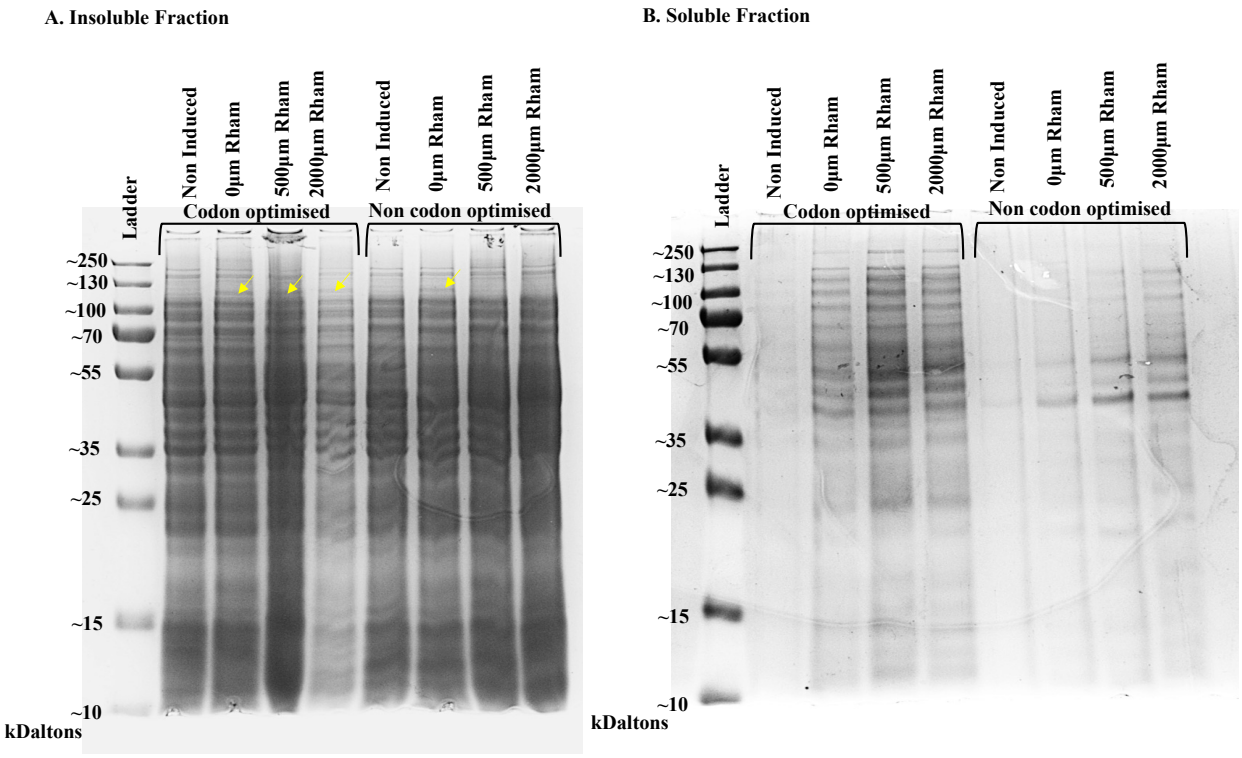

Figure 15.Test expression of full-length LmjSK protein in pOPINf vector expression using Lemo(DE3)competent E.coli cells showing (A) insoluble and (B) soluble fraction. Lemo cells containing pOPINF plasmids containing non codon optimised and codon optimised SK sequences were used. The insoluble fraction (A) and soluble (B) expression samples were analysed. Both non-codon and codon optimised samples had a control sample that was not induced. Yellow arrows show the presence of a ~115kDalton expressed protein deduced by the band not present in the non-induced fraction.

Due to the insolubility and low protein expression, the extraction of the protein from the insoluble fraction was attempted by denaturation followed by refolding (Figure 16). Prior to the denaturation process, the sample was separated using binding buffer sonication as usual (Materials and Methods) for separation of the soluble and insoluble fractions followed by the insoluble fraction denaturation using a denaturation buffer. During this denaturation process, pellets each containing 5 litres worth of induced culture were used. *L. major* expressed protein

was found within the soluble fraction prior to the denaturation process however in low expression levels.

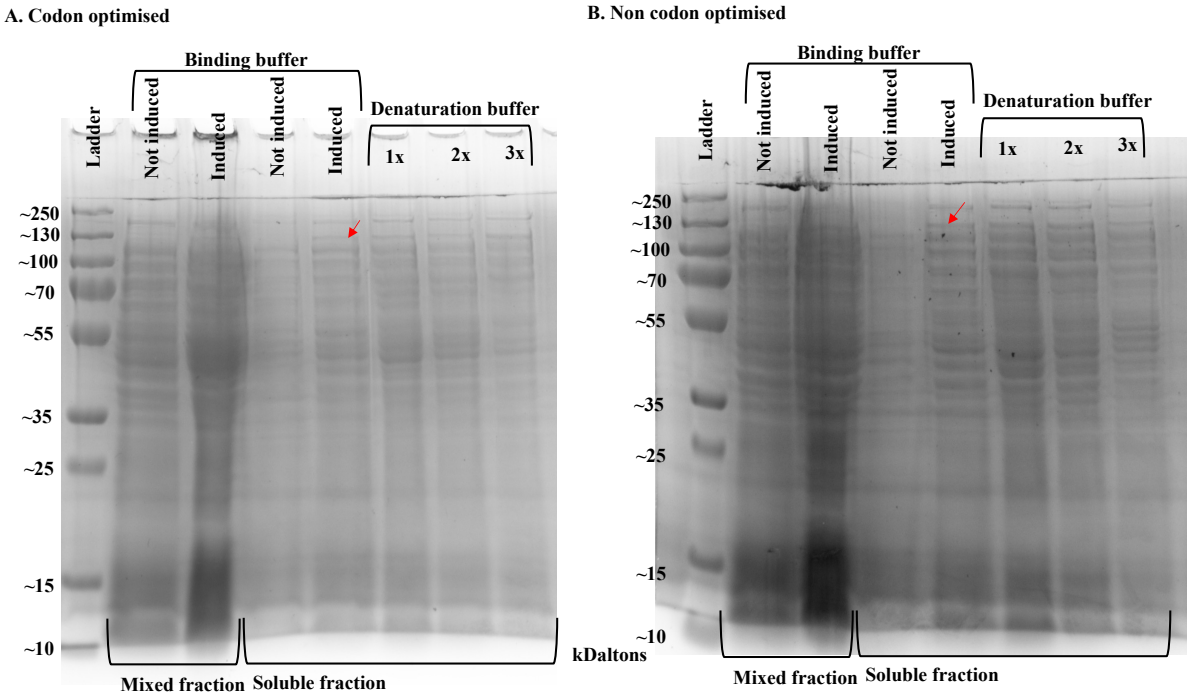

Figure 16.Test expression of full-length LmjSK protein expression using Lemo(DE3)competent E.coli cells using denaturation of codon optimised (A) and non-codon optimised (B) SK sequence in pOPINf vector. The mixed fraction (soluble and insoluble fraction) and soluble fraction samples from overnight expression at 15°c induced with 400um 1PTG and 500um Rhamnose were run on 12.5% SDS PAGE gel. Soluble and insoluble fractions were initially separated using binding buffer, with the insoluble fraction denatured 3 times using denaturation buffer and the soluble fraction of the sample run. Red arrow show the presence of an expressed protein analysed by MS.

Although the expressed protein found in the induced samples was consistent in terms of predicted molecular weight visually on the SDS Page gel, mass spectrometry (MS) was used to confirm the expressed band was *LmjSK*. Protein bands from Figure 16 (shown by red arrows) were analyzed. 47 proteins were detected, 46 of which were contaminants such as keratin and *E. coli* beta galactosidase/HSPs, including the expected *LmjSK*. Using the average theoretical mass of 101,018 Daltons and the sequence of *LmjSK*, MS found a 12% coverage of the sequence. Although this confirmed the successful expression of *LmjSK* protein using Lemo cells, the low expression arrested further expression trials of the full-length *Lmj*SK.

4.2 Expressing the conserved domain of *Leishmania* Sphingosine Kinase

Expression of large proteins such as this, particularly within a heterologous host, can be challenging due to a vast number of factors including significant differences in codon usage.

4.2.1 Design of truncated constructs

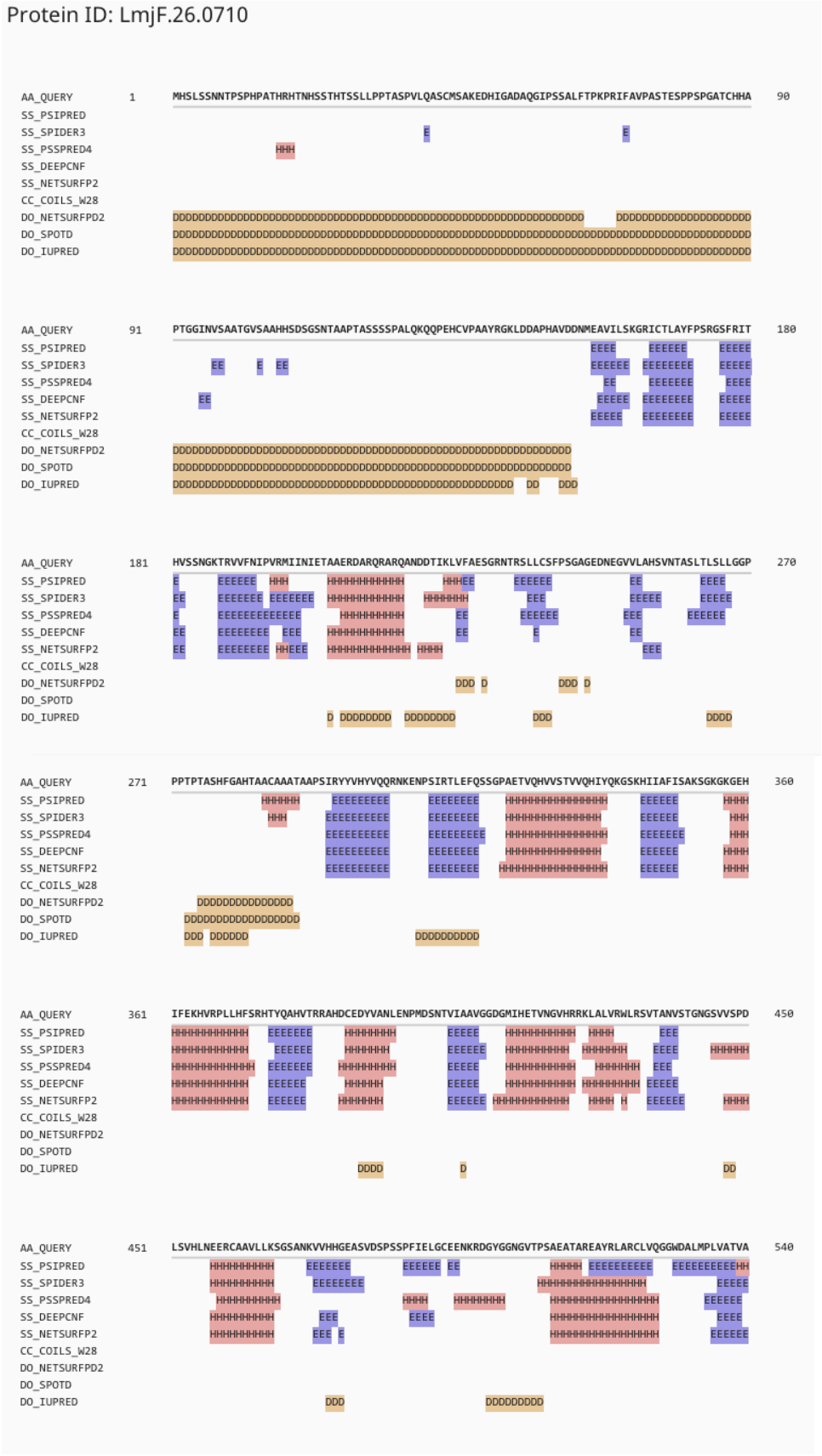

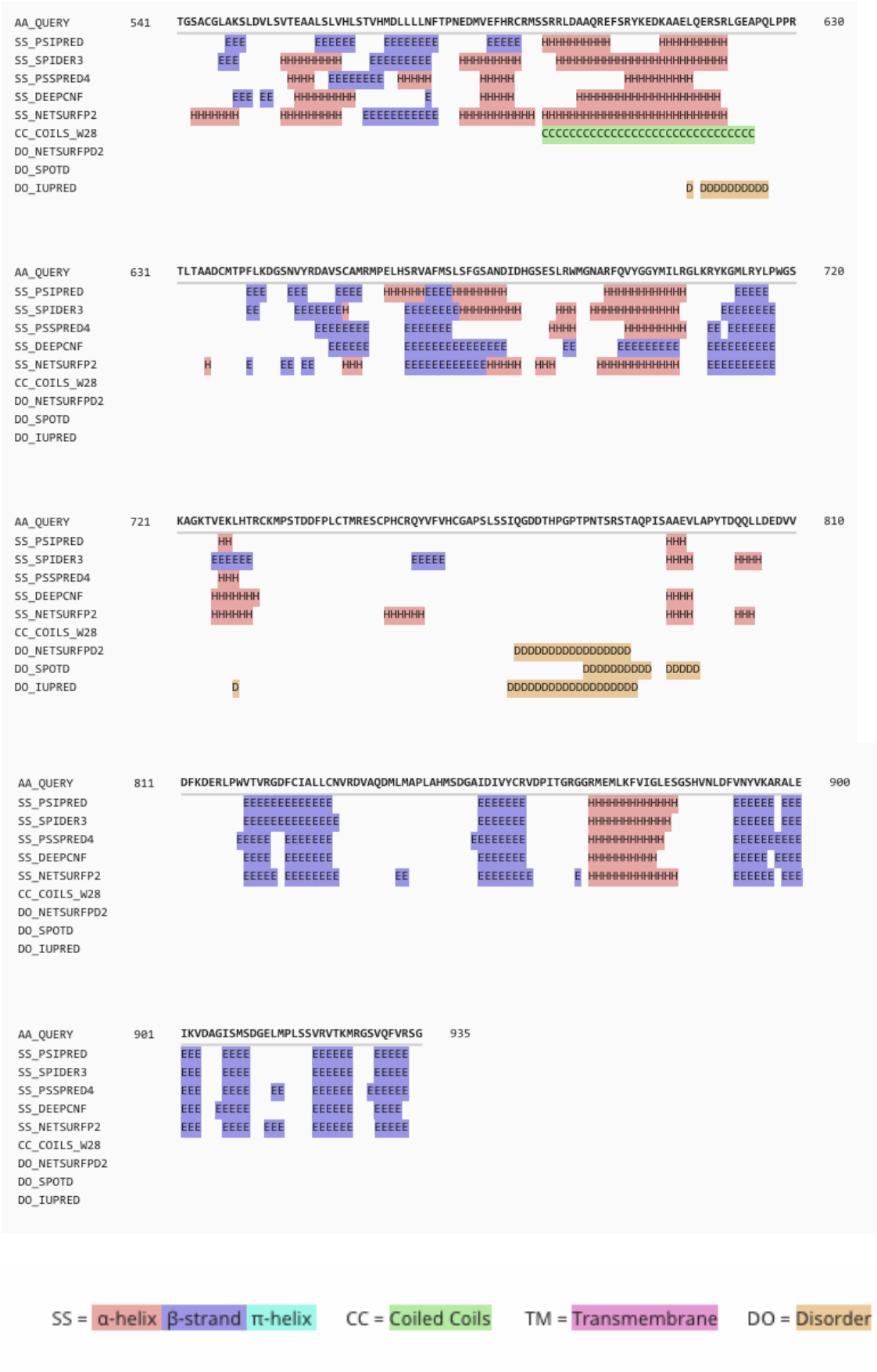

Figure 17:HHPred report of LmjSK

Protein ID: LmxM.26.0710

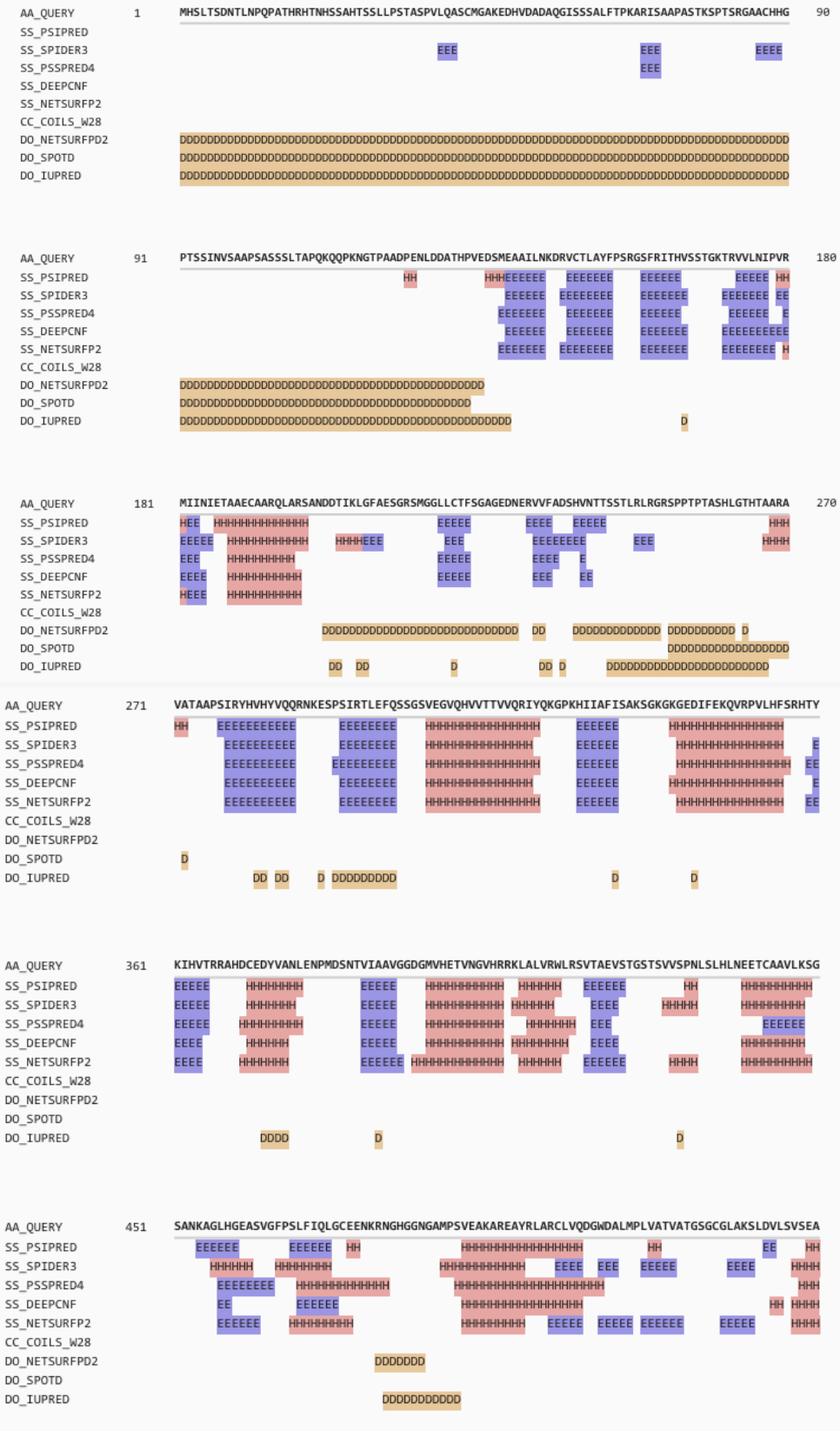

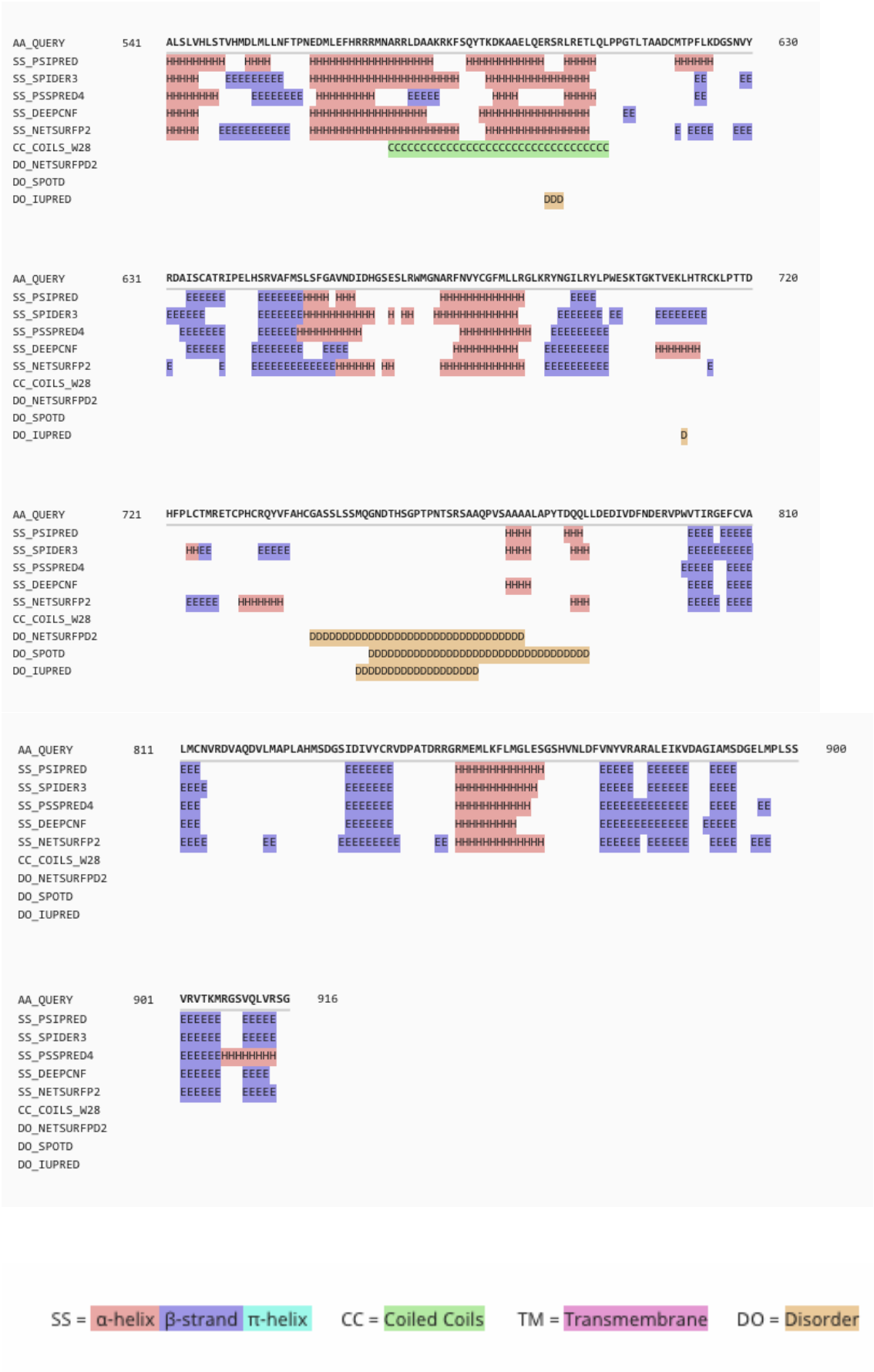

Figure 18: HHPred report of LmxSK

In this case, looking at the predicted tertiary structure of *LmjSK* (Figure 17 and 18), there are various regions of disorder within the N-terminal 180 amino acids which could affect the expression of the protein due to their 3D structure not being well-defined and unstable within the cell. This may lead to the aggregation of expressed proteins which is sensitive to proteolytic cleavage by *E. coli* leading to no production of target protein (Graether, 2019). This led to the design of domains from the full-length SK *L. major* and *L. mexicana* proteins to exclude the disordered segments as predicted by the HHpred report (Figure 17 and Figure 18) (Zimmermann et al., 2018) but contain the conserved C1-C4 regions expected to contain the catalytic domain (Figure 6) and residues important for SK inhibitors PF-543 (Wang et al., 2014) and RB-005 (Baek et al., 2013) (Figure 6). This should increase folding and stability of the expressed protein.

4.2.2 Expression trials

These constructs were ordered from GeneScript in the pJOE expression vector. Due to full length *LmjSK* protein showing to not express in high enough levels due to solubility issues, as well as T7 Express Competent *E.Coli* High Efficiency cells, BL21(DE3) Competent *E.coli* cells and Lemo21 (DE3) *E.coli* cells, Shuffle T7 and ArcticExpress *E.coli* cells were employed for their enhanced protein folding and stability capabilities.

T7 Express Competent *E.Coli* High Efficiency cells (C2566) and BL21(DE3) Competent *E.coli* cells (C2527) were used for initial expression of the 4 constructs. These followed the expression described in Materials and Methods. Expression confirmed by MS was achieved from all 4 constructs on both T7 Express and BL21 *E.coli* cells as shown in Figure 19 below however the protein of interest is also expressed in the 'not induced' sample. This suggests that

the expression of these constructs in high levels is causing the known toxic SK proteins to be leaked out due to toxicity to the *E.coli* cell and potentially be inclusion bodies. Due to this, a tunable Lemo21 (DE3) was employed for the expression of the constructs as these cells allows a reduction of the expression. By using both rhamnose and IPTG for expression, lysozyme (lysY) is induced by rhamnose to inhibit T7 RNA polymerase decreasing expression and therefore maintaining the concentration of a toxic target protein expressed just below a host strain's tolerance.

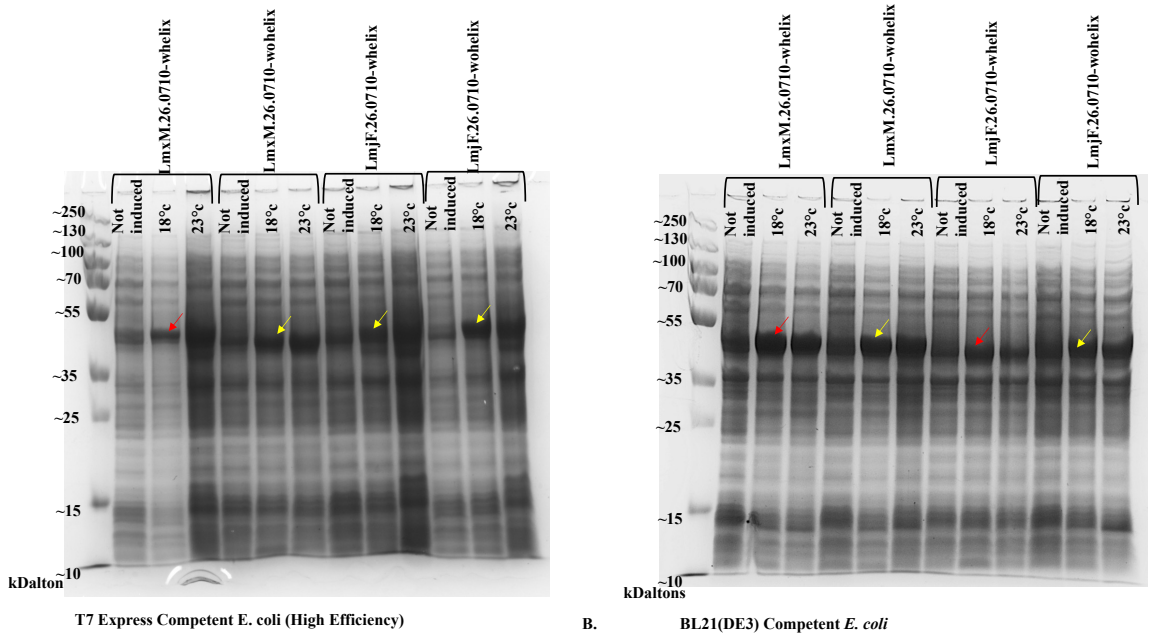

Figure 19. L. major and LmxSK constructs within the pJOE vector test expression in (A) T7 Express and (B) BL21(DE3) Competent E.Coli cell showing whole cell lysate. Red arrows show the presence of an expressed protein confirmed by MS. Yellow arrows show the presence of a ~42-44kDalton expressed protein which may be the expressed SK construct.

The use of Lemo21 (DE3) for the construct's expression required the construct to be transformed into the pOPINf vector from the pJOE vector. This is due to the pJOE vector using rhamnose for induction which would interact with Lemo system in the Lemo21 (DE3) cells. This was achieved using the protocol described in Materials and Methods and results showed

in Figure 20. Clones 1 of all constructs are shown to contain the constructs within the pOPINf vector.

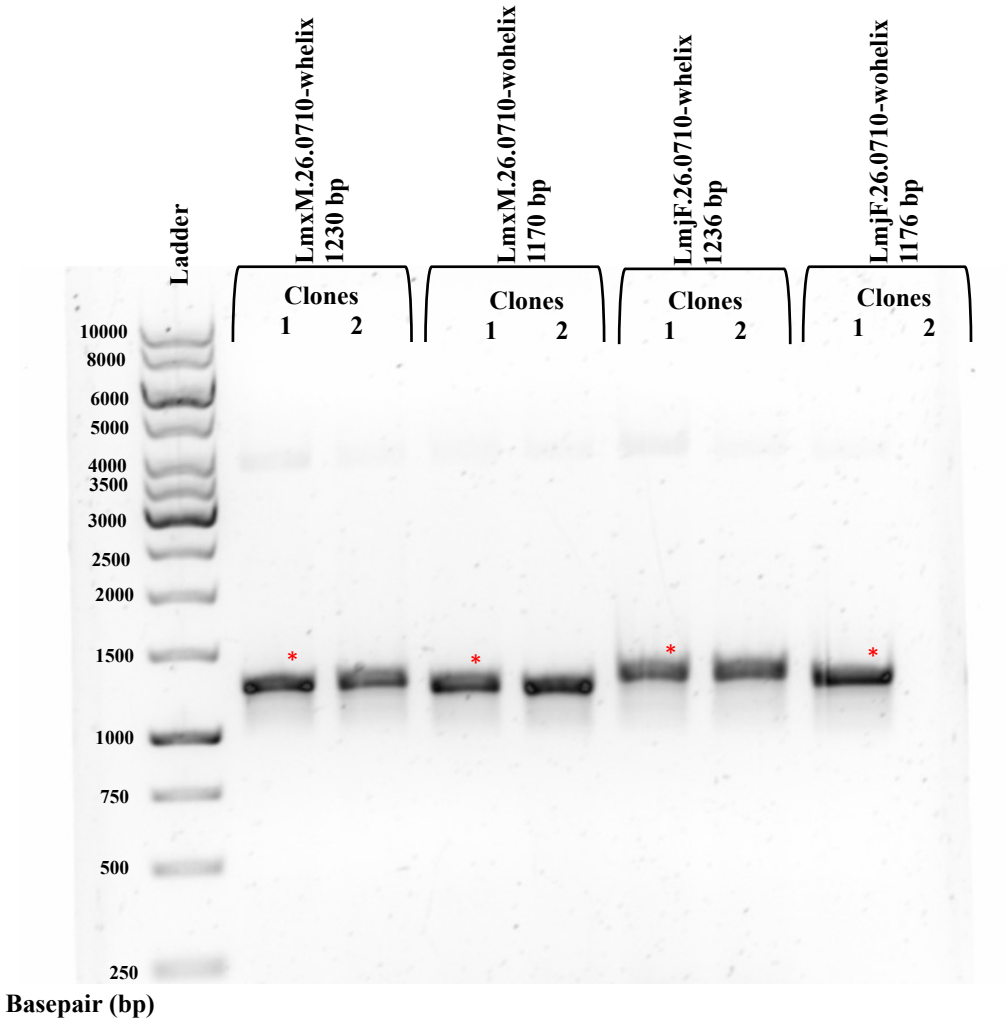

Figure 20. PCR Confirmation of L. major and LmxSK constructs clones within the pOPINf expression vector. Red starred results show the clones that were taken forward for use in expression tests in Lemo21 (DE3), Shuffle and ArcticExpress E.coli cells.

POPINf vectors containing the constructs were extracted after confirmation (Figure 20) and transformed into Lemo21 (DE3) cells. These were used for expression shown in Figure 21. Unlike in the BL21 and T7 Express competent cells shown in Figure 19, visually on a SDS page gel there is no 'leaky' expression suggesting that the use of a tunable system reducing expression using 500µM rhamnose, expression is not toxic to the cells. However, when equal

amounts of cells for each construct was prepared and run on the gel it shows that the amount of expressed protein in the soluble fraction is extremely low and this cell line cannot be used for enough production of protein used downstream.

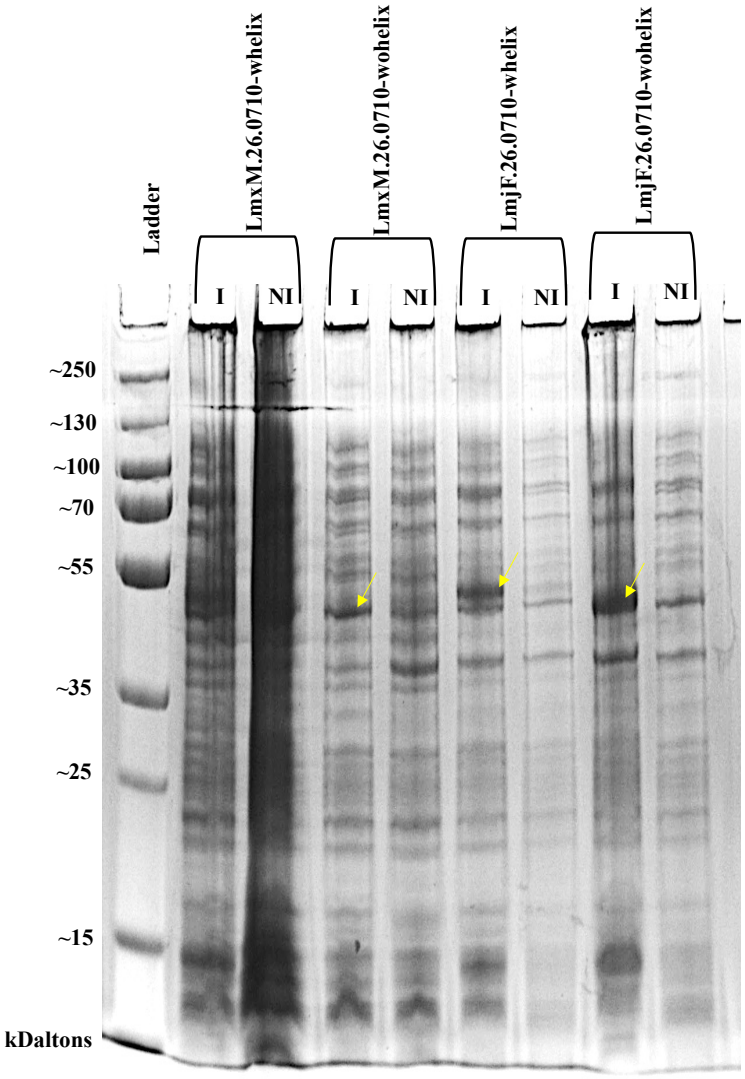

A. **Insoluble Fraction**

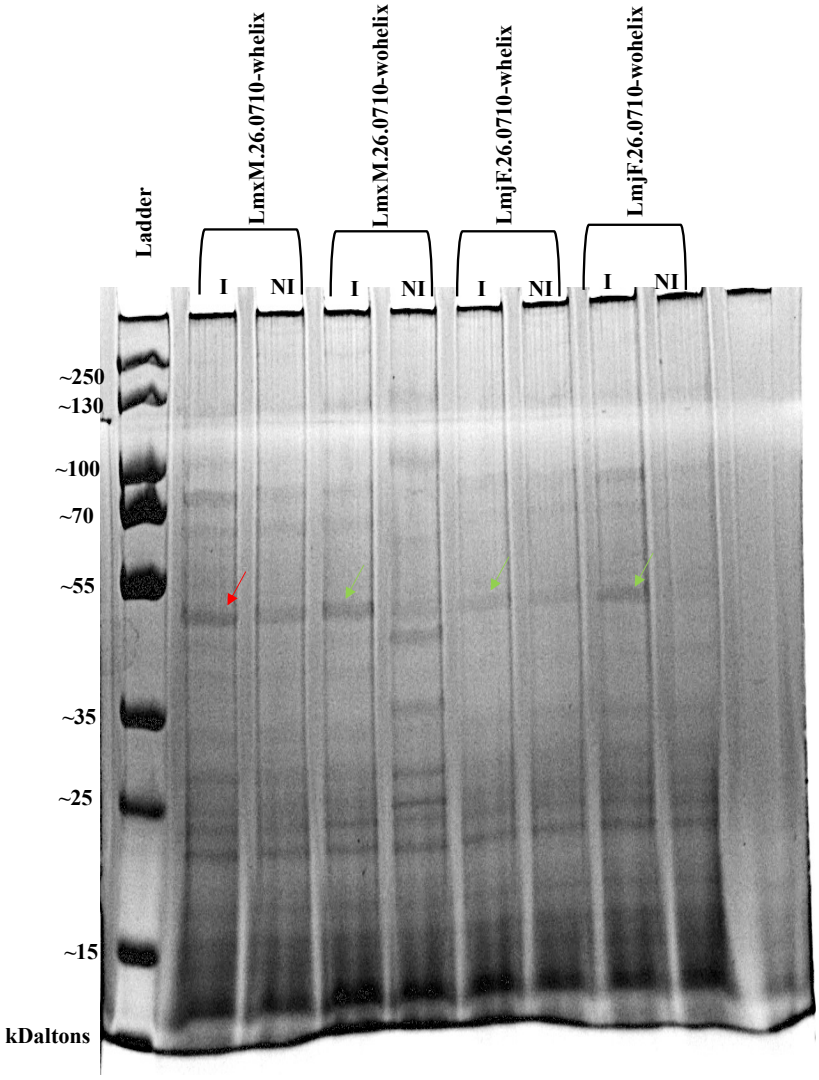

B. **Soluble Fraction**

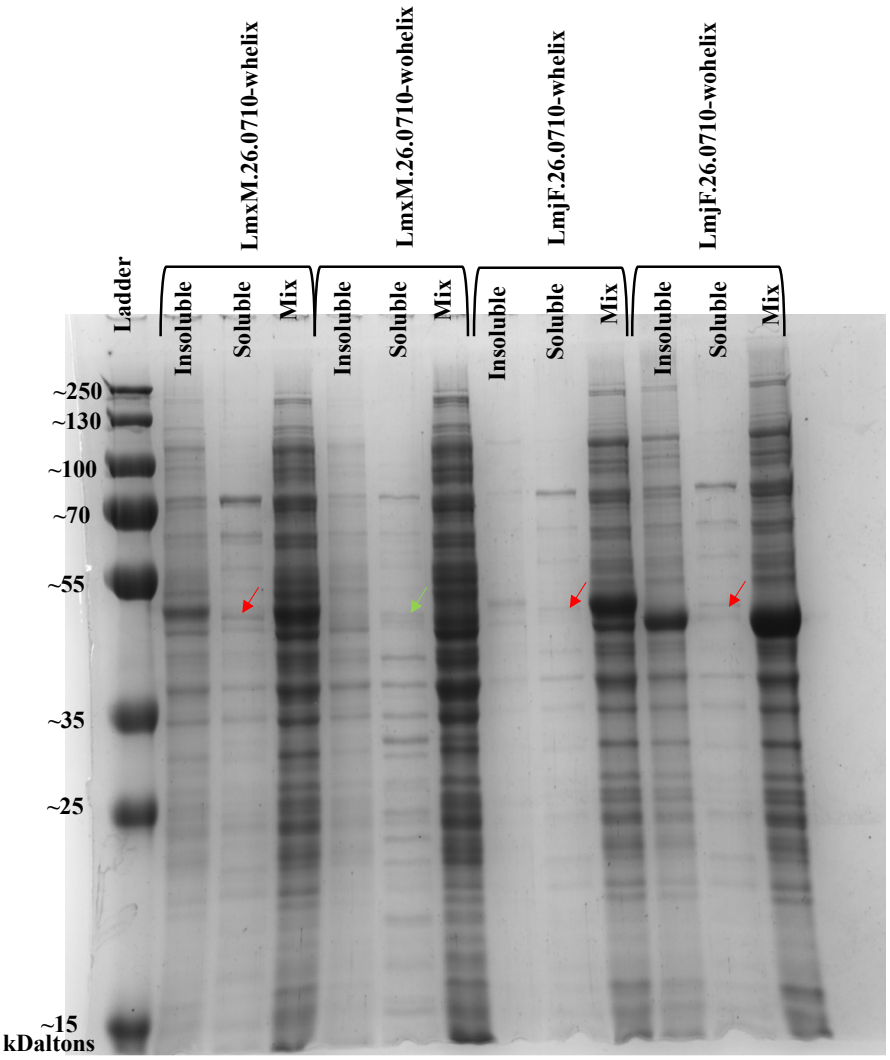

C. Equal number of cells used for both soluble and insoluble fraction

Figure 21.Test expression of L. major and LmxSK constructs within the pOPINf vector in Lemo21(DE3) competent E.coli cells showing the (A) insoluble, (B) soluble fractions and (C) both fractions using OD600 of 1.0 . Red arrows show bands which are within the region of constructs confirmed by MS, green arrows show bands which were checked however returned to not have construct present. Yellow arrows show the presence of a ~42-44kDalton expressed protein which may be the expressed SK construct. I (Induced samples), NI (Non induced control samples)

With insolubility continuously being the problem that arose in both full length protein and constructs when using Lemo21 (DE3) cells even at low temperature, an expression cell type that increased the yield of soluble protein was required. ArcticExpress competent *E.coli* cells which express at lower temperatures and contains chaperones Cpn60 and Cpn10 with refolding

properties, and Shuffle competent *E.coli* cells which express disulfide bond isomerase (DsbC) for enhancing protein folding were employed.

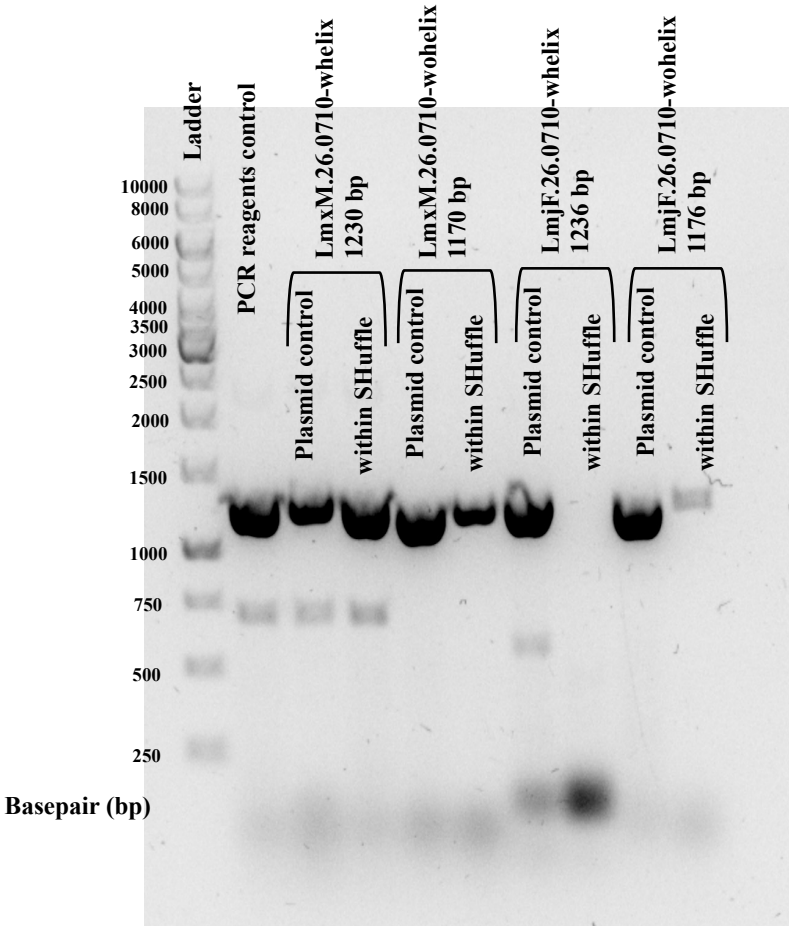

Figure 22.Confirmation of pOPINf containing construct transformed into SHuffle competent E.coli cells by PCR. PCR products analysed on 1% agarose gel and imaged using Gel Doc XR imager (Bio-Rad). Red starred results show the clone that were taken forward for use in expression tests in SHuffle E.coli cells.

POPINf vectors containing the constructs were transformed into SHuffle cells and confirmed by PCR. Figure 22 shows the successful transformation of constructs *Lmx*M.26.0710-_whelix and *Lmx*M.26.0710-wohelix, however the transformation of constructs *Lmj*F.26.0710-_whelix and *Lmj*F.26.0710-_wohelix was not successful into SHuffle

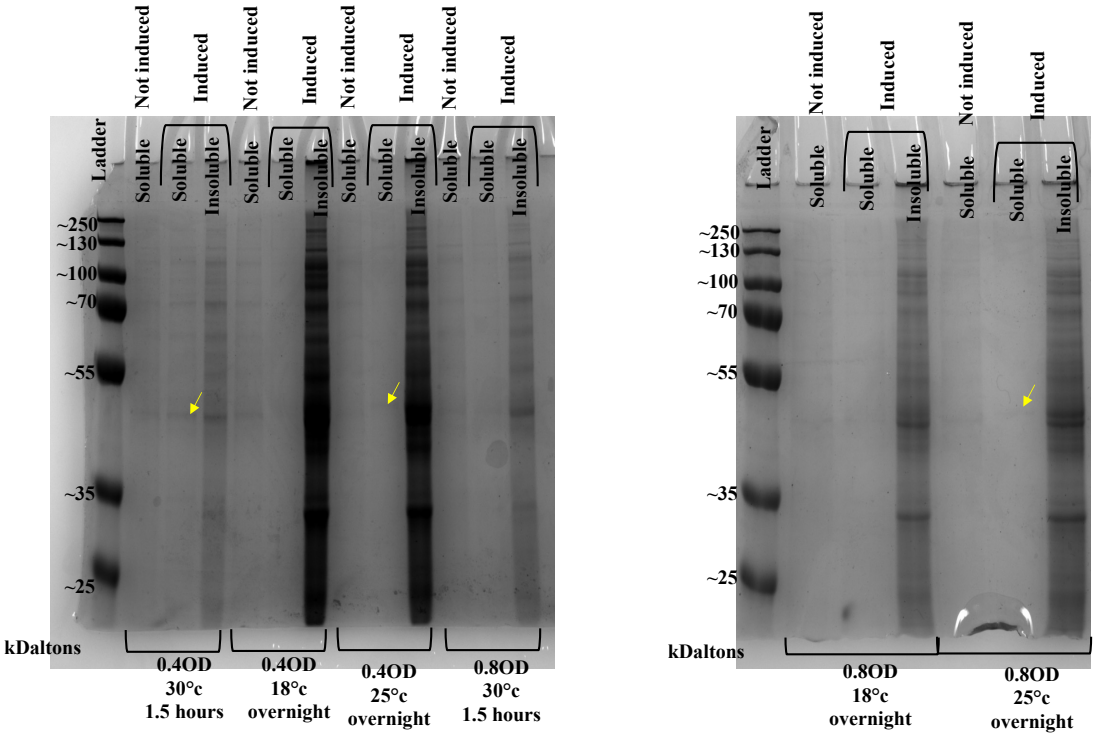

Figure 23.LmxM.26.0710-whelix construct expression in SHuffle cells using different conditions. Dependant on conditions, SHuffle cells were grown to an OD600 of 0.4 or 0.8 and induced using 0.4mM IPTG shaking at 180rpm for 1.5 hours (30°c sample) or overnight (18 and 25°c sample). Yellow arrows show bands which are within the region of constructs' size.

LmxM.26.0710-whelix and LmxM.26.0710-wohelix constructs within SHuffle cells was used for expression using various conditions including temperatures of 18°c, 25°c and 30°c and ODs of 0.4 and 0.8. Although these cells improve protein folding for protein to be expressed in the soluble fraction, there were very faint bands produced in the region of constructs' size within the soluble fraction (yellow arrow in Figure 23) and therefore the use of SHuffle cells for larger scale expression was ceased.

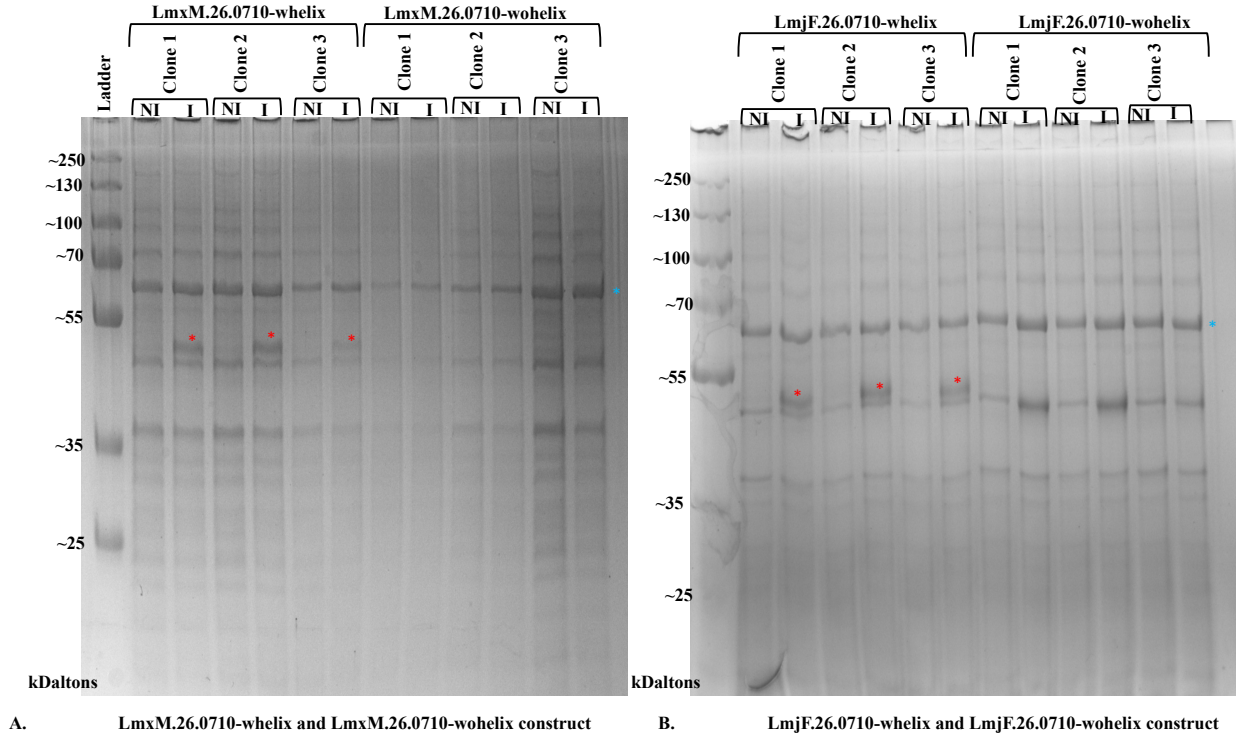

Figure 24. Whole cell lysate from test expression of L. mexicana (A) and L. major (B) SK constructs within the pOPINf vector in ArcticExpress competent E.coli cells showing both induced (I) and not induced (NI) samples. Fractions were analysed SDS page gel showing bands potentially containing the SK constructs. Red starred show bands which are within the region of constructs. Blue starred shows the region of chaperon protein Cpn60. I (Induced samples), NI (Non induced control samples)

All 4 constructs were transformed into ArcticExpress competent *E.coli* cells with expression of 3 clones containing construct in pOPINf vector induced at 10°c overnight using 1mM IPTG and shaking of 250rpm for 24 hours. Whole cell lysate of this test expression was run on 12.5% SDS page gel seen in Figure 24. LmxM.26.0710-whelix and LmjF.26.0710-_whelix resulted

in distinct bands which were within the correct size of protein (starred in red) and these bands were not present in the non-induced control samples (NI). There was also a distinct band in ~60kDa region of the gel present in both induced and non-induced samples (starred in blue) which was assumed to be the chaperone protein Cpn60.

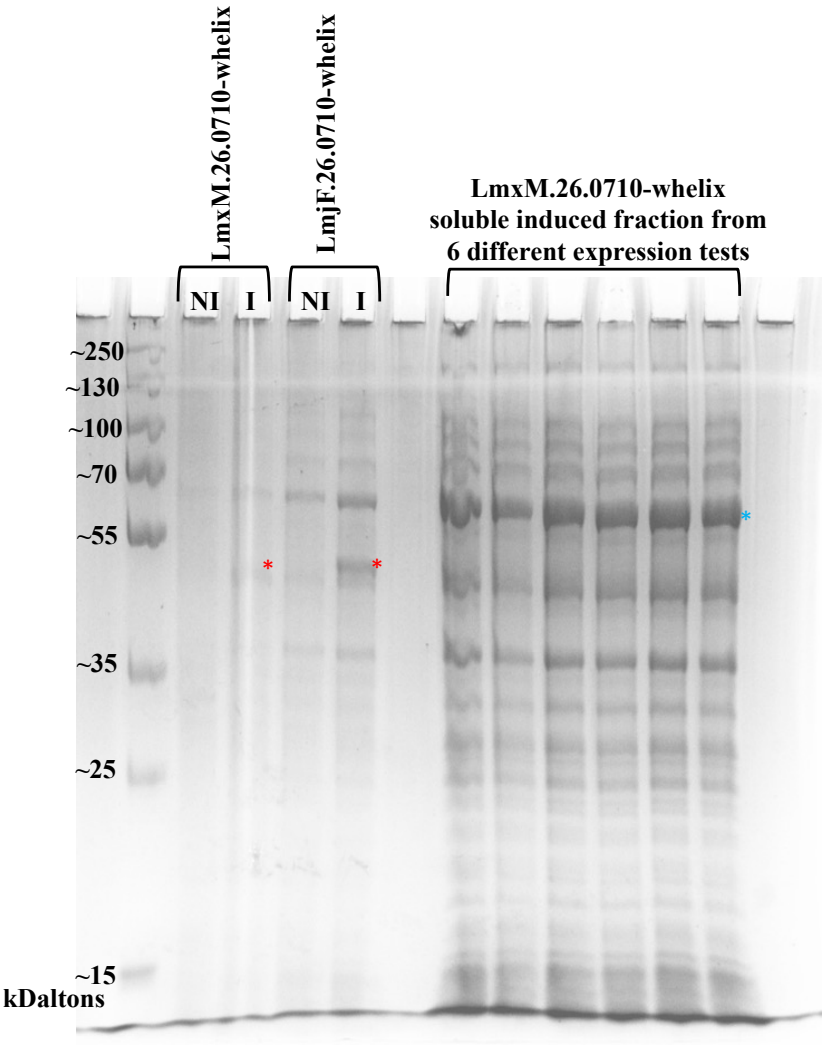

Figure 25. Expression in ArcticExpress competent E.coli cells of LmxM.26.0710-whelix and LmjF.26.0710-whelix. Red starred shows the MS confirmed LmxM.26.0710-whelix and LmjF.26.0710-whelix proteinBlue starred shows the region of chaperon protein Cpn60. I (Induced samples), NI (Non induced control samples)

4.2.3 Isolation/Purification of SK protein

With the success of ArcticExpress cells expressing showed in Figure 24 by the protein bands of ~45Daltons in the induced fraction, LmxM.26.0710-whelix was expressed in larger scale of 500mL six separate times for use in the protein purification procedure to acquire protein. Figure

25 shows the soluble fraction of LmxM.26.0710-whelix and LmjF.26.0710-whelix expression, with bands containing the protein of interest starred in red and the suspected chaperone protein Cpn60 starred in blue. A small amount of each of the 6x 500mL pellets of ArcticExpress cells containing the LmxM.26.0710-whelix was prepared as described in the Material and Method to show that protein was present in the soluble fraction and that storage did not affect protein viability before use.

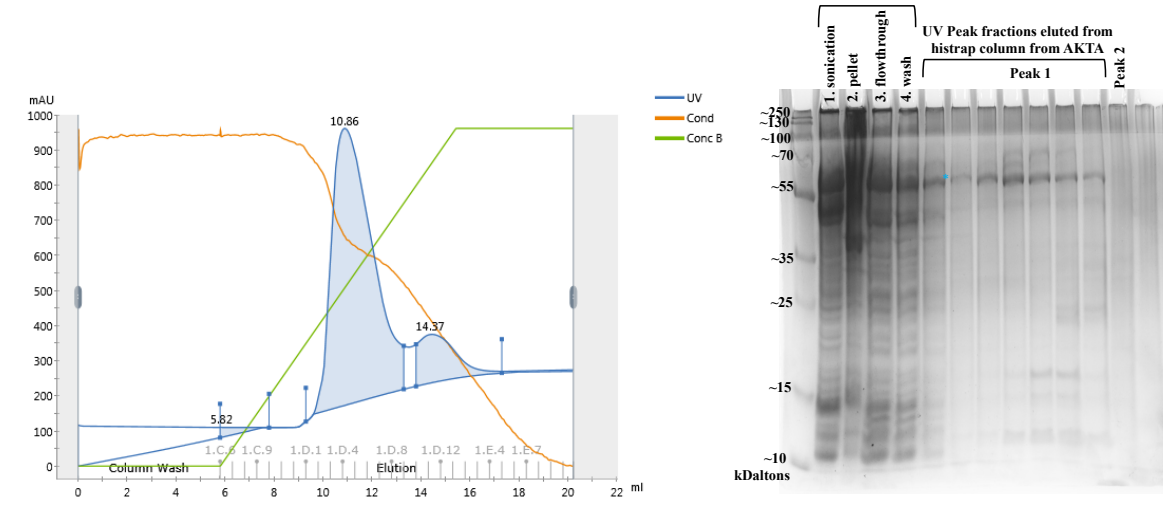

A. Output of LmxM.26.0710-whelix from HisTrap on AKTA Pure

B. Fractions from HisTrap preparation and AKTA Pure fractions

Figure 26. Output of Histagged protein expression from ArcticExpress cell containing LmxM.26.0710-whelix eluted (A), and fractions from HisTrap preparation and AKTA Pure fractions (B). ImL HisTrap elution giving 2 unique peaks detected. Fractions from both peaks labelled on B. Red starred shows the region in which the LmxM.26.0710-whelix construct would be found and blue starred shows a ~ 70kDalton expressed protein (chaperon protein Cpn60).

During the steps of protein purification, fractions of the pellet, sonicated pellet in lysis buffer, flowthrough during loading of the 1mL HisTrap and washing of the HisTrap was collected and run to check for protein lost in the many stages. Using the pOPINf vector, LmxM.26.0710-whelix contained a Histidine tag and therefore should tag to the HisTrap column. The elution detected two distinct peaks in the chromatogram (Figure 26A) resulting in the first larger peak having an elution volume of 10.86mL (Peak 1) and the smaller second peak 14.37mL (Peak 2). The fractions eluted from peak 1 and one fraction of peak 2 was collected and run on a 12.5% SDS page gel seen in Figure 26B. Peak 2 shows no protein that can be visualised on the SDS

gel, and peak 1 showed a ~60kDa protein (starred in blue) but not the expected 44.6kD (LmxM.26.0710-whelix) protein. Due to the size on the SDS gel (Figure 26B), this eluted protein from peak 1 was suggested to be the chaperone protein Cpn60. These fractions were collected and used for ESI-MS for confirmation (Figure 27). As none of the fractions from either peak produced a visible band on the SDS gel of 44.6kD, other fractions prior to elution within the protein purification procedure was analysed. The fractions of the insoluble fraction of pellet (2) produced a smear of which specific banding would not be distinguished however the 'sonicated' (1) fraction of whole cell in lysis buffer showed the 44.6kD protein banding (starred in). This band was also found in the 'flowthrough' fraction (3) and 'wash' fraction (4) prior to elution.

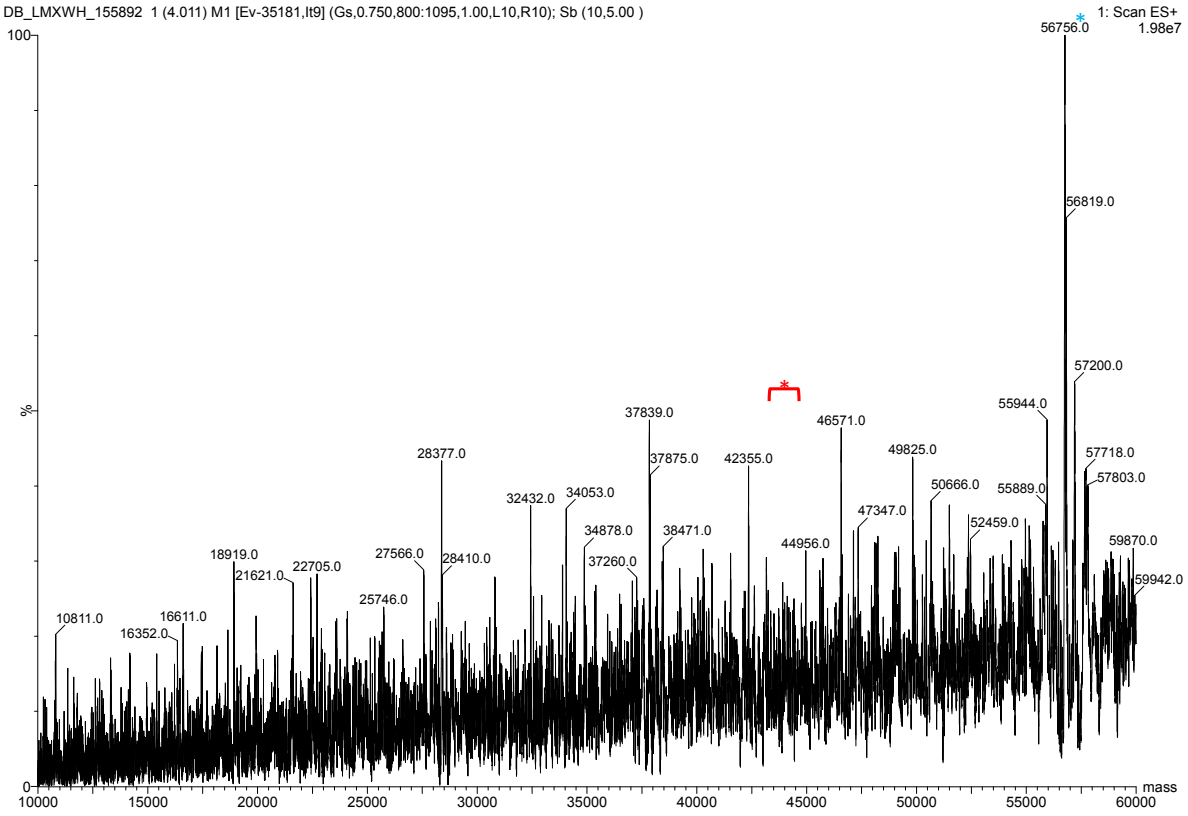

Figure 27.Mass spectrometry output of His-tagged protein expression from ArcticExpress cell containing LmxM.26.0710-whelix eluted a AKTA Pure system. UV peak of 10.86 from figure 21 was collected and concentrated to 1mg/ml for mass spectrometry analysis. Red starred show area of ~ 44517.96 where a peak of

LmxM.26.0710-whelix should be located. Blue starred shows the peak of ~ 57kDa of chaperon protein Cpn60 (exact mass 61281).

Mass spectrometry shows peak 1 to have eluted many proteins of varying sizes, however the largest portion to be the size of 56756.0Daltons (starred in blue in Figure 27) which is over 4.5kDaltons larger than the 61,281Daltons chaperone protein Cpn60. The red starred area in Figure 27 shows the region in which a peak of LmxM.26.0710-whelix should be located.

This data collectively suggests that the LmxM.26.0710-whelix protein was lost prior to the elution step possibly due to the histidine tag being hidden and therefore binding to the column. The eluted protein was of a mixed variety (Figure 27) which possibly includes the chaperone protein Cpn60 along with a larger population of a 56756.0Dalton sized protein.

4.3 Expression cells and commercial production

Although generally not successful protein expression, more protein expression success was achieved with the constructs containing the active site confirmed by MS in multiple expression (Figure 25) than the full-length SK protein (Figure 16). This was not sufficient for progressing to purification as showed in Figure 26 and Figure 27.

Commercial protein expression of *LmxM.26.0710-whelix* (Labelled as LmxM.26.0710.1A in GenScript report) and *LmxM.26.0710-wohelix* (Labelled as LmxM.26.0710.1B in GenScript report) from GenScript was used in hope for large scale expression. Initial expression using the pET-30a(+) vector in BL21 Star (DE3) *E.coli* cells showed expression of both constructs within the cell lysate with induction at 15°c for 16 hours giving a best expression level of 30 and 25 mg/L respectively however solubility of <1%. For better expression, the vector was changed to pSUMO-M. This gave a similar expression within the induced cell lysate fraction to pET-

30a(+) vector. However, at the best expressed condition of 4 hours at 37°c, the expression level reduces to 20 mg/L and solubility remains <1%. Brief conclusions of result found in Table 11.

Table 11:Best expression level and solubility of LmxM.26.0710-whelix (Labelled as LmxM.26.0710.1A in GenScript report) and LmxM.26.0710-wohelix (Labelled as LmxM.26.0710.1B in GenScript report) by GenScript with pET-30(+) and pSUMO-M vector.

	pET-30a(+)	pSUMO-M
Best condition	16h 15°c	4h 37°c
LmxM.26.0710-whelix	30 mg/L <1% solubility	20mg/L <1% solubility
LmxM.26.0710-wohelix	25mg/L <1% solubility	20mg/L <1% solubility

4.4 Conclusion and proposed future experiments

The various attempts of troubleshooting the *Leishmania* SK protein for expression, began with the attempt to express the full length 101 kDa *Lmj*SK protein. This was unsuccessful in four different expression cell types. However, some expression was achieved when using Lemo21 (DE3) expression cells containing properties for aiding in solubility. This was confirmed by MS and showed in Figure 16 however not sufficient expression was achieved for purification to be attempted. Attempt to solve this led to designing constructs that do not containing predicted disordered regions according to the HHpred report and only the active site and conserved regions. This however did not yield any soluble protein when using Shuffle, T7 Express and (B) BL21(DE3) Competent *E.coli* cell types. Lemo21 (DE3) did achieve a small amount of soluble protein seen in Figure 21. The change of expression cell type to ArcticExpress competent cell did show some success in the expression of soluble protein (Figure 24). However in the process of protein purification from Figure 24 to Figure 27 it is showed that LmxM.26.0710-whelix can be expressed within the soluble fraction in certain cells such as ArcticExpress cells in the correct conditions. The loss of

LmxM.26.0710-whelix from the flowthrough and wash suggests sequestered within a fold of the protein thus making it unable to interact with the immobilized Nickel ion responsible for the affinity. This may be fixed by denaturation of proteins prior to purification, moving the His-tag to the opposite terminus of the protein to make it more accessible or using a different tag.

The commercial production of LmxM.26.0710-whelix and LmjF.26.0710-whelix proteins not being successful also suggests that alternative expression systems may be required. Insect, yeast, or mammalian cell-based systems employ the benefits of protein folding and eukaryotic post-translational modifications. With the SK protein having effects within the highly homeostatic sphingolipid biosynthetic, intracellular expression of this protein may be unfavourable. This lends to a secreted expression system combined with perfusion. Without complex growth requirements, non-pathogenic *Leishmania* parasites such as *L.tarentolae* may be an attractive host to express the homologous LmxM.26.0710-whelix protein in its native state (Taheri et al., 2016).

The aim set in Chapter 1 of expression and purification of *Leishmania* SK protein was not possible despite the troubleshooting. The result from this chapter gives insight into the level of disorder found outside of the conserved regions as proposed in Chapter 3 which is further supported by the low expression of *Leishmania* SK in *E.coli* protein expression system where post translational modifications is not possible. Without a purified protein, further understanding of *Leishmania* SK requires genetic evidence of its essentiality which is discussed in Chapter 5. Knowledge of its essentiality by generating a SK free *Leishmania* cell line will aid in the understanding of the effect targeting the *Leishmania* SK directly using an inhibitor will result in unlike the non-specific targeting showed in Chapter 3.

Chapter 5: Genetic assessment of sphingosine kinase essentiality in *Leishmania mexicana*

Validation of sphingosine kinase (SK) as a suitable drug target includes genetic manipulation for evidence to suggest that the SK gene is essential for parasite survival and/or proliferation (Jones et al., 2018). Chapter 3 and 4 suggests divergence outside of the conserved regions and the *Leishmania* protein being difficult to express in *E.coli*. Due to the inability to adopt the expressed protein in further studies to gain further knowledge on whether *Leishmania* SK would be a good drug target, a genetic assessment on essentiality of the protein is required. Using CRISPR Cas9, the generation and selection of a SK knockout in *L. mexicana* will be used to assay parasite, with unwanted phenotypes investigated further. This will facilitate an understanding of lack of an active SK within the parasite and support further characterisation on whether targeting SK is as detrimental to the cell as assumed in Chapter 1. Objectives from Chapter 5 are:

1. Assessing published data where SK has been ablated from *Leishmania* parasite genome.
2. Generating clones of *L. mexicana* parasites with varying levels of SK knockout (KO)- full diploid KO (labelled DKO) and partial single allele KO (labelled SKO).
3. Addback of the SK gene to the ablated population to assess if WT phenotype returns.

The genetic drug target validation molecular toolbox in *Leishmania* has expanded over recent years, refining manipulations to assessing specific *Leishmania* genes including the use of CRISPR Cas9 system for *L. mexicana* (Beneke et al., 2017a). Deletion of genes within the tightly regulated sphingolipid biosynthetic pathway encoding enzymes such as serine palmitoyltransferase (SPT) (Denny et al., 2004) and SK (Zhang et al., 2013b)., have shown detrimental outcomes in *Leishmania* spp.

5.1 Analyses of published *Leishmania major* sphingosine kinase knockout

Zhang et al., 2013 reported the generation of a *L. major* SK null mutant using the methodology described by (Kapler et al., 1990) to replace the two SK encoding genes in this diploid organism through two rounds of drug selection (Zhang et al., 2013). These SK null parasites underwent lipid profiling (Zhang et al., 2013) and an *in vitro* activity assay to determine SK activity (Zhang et al., 2013) to detect changes in the production of sphingosine-1-phosphate (S1P). The composition of major phospholipids showed little altered difference between SK null (knockout, KO) and wild type (WT) parasites. The results of the *in vitro* activity showed the production of both dihydrosphingosine 1-phosphate (DHS1P), and S1P in WT parasites as expected, however the KO parasites also produced these products, although at 50% of WT. This suggested a 50% reduction of SK activity in the KO *L. major* parasites. From these results Zhang et al. deduced that LmjF26.0710 may not be the only functional SK present in *L. major.*

The KO promastigotes showed similar growth rates and doubling times to WT *L. major* parasites, however their viability rapidly reduced after reaching 6-8x10^6 cells/ml suggesting the accumulation of toxic metabolites. Ethanolamine (EtN) and myriocin was used to block SL synthesis, this restored the morphology of KO parasites from rounded to normal elongated promastigotes and improved growth and viability (Zhang et al, 2013). This indicated that SK plays a role in preventing the build-up of toxic sphingoid bases (SB) detrimental to the parasite. However, the activity of SK was maintained in the SK null cells, and it was suggested by Zhang et al,. that, despite a lack of genomic evidence, another SK is encoded in the *L. major* genome.

Due to the proposed essentiality of SK, we investigated the effect of the loss of the gene encoding this enzyme using the recently adopted CRISPR-Cas9 system.

5.2 Gene targeting using the CRISPR Cas9 system in *Leishmania mexicana*

CRISPR-Cas9 Knockout (KO) of the SK gene was attempted using the CRISPR-Cas9 system designed for use in *Leishmania mexicana.* Using the online resource LeishGEdit (Beneke et al., 2017a), primers were designed as described in Materials and Methods.

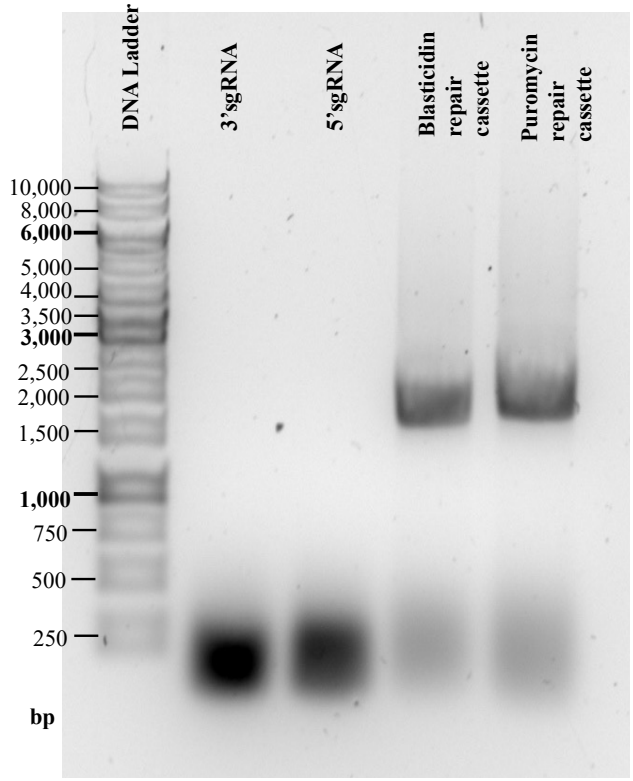

Figure 28: PCR products run on 1% agarose gel with SYBR Safe. Left to right: GeneRuler™ 1 kb ladder DNA indicated, 3'sgRNA, 5'sgRNA, pTBlasticidin repair cassette and pTPuromycin repair cassette.

3'sgRNA, 5'sgRNA, and blasticidin repair and puromycin repair cassettes were generated through PCR and analysed by agarose gel electrophoresis as shown in Figure 28. This confirmed that the DNA products generated matched the expected sizes of 124bp for the 3'sgRNA, 119bp for the 5'sgRNA, 1700bp for the blasticidin repair cassette and 1800bp for the puromycin repair cassette. These sgRNAs and repair cassettes were then transfected into

L. mexicana Cas9 T7 (Beneke et al., 2017a), selected using puromycin and/or blasticidin and cloned as described in Materials and Methods.

Initially both repair cassettes were used simultaneously for transfection, in the hope of creating of a double KO. However, transfected parasites were visually not healthy and the addition of blasticidin and puromycin lead to parasite death. This outcome suggested that a double KO could not be achieved, and SK is essential. The subsequent focus was therefore on using a single repair cassette for transfection.

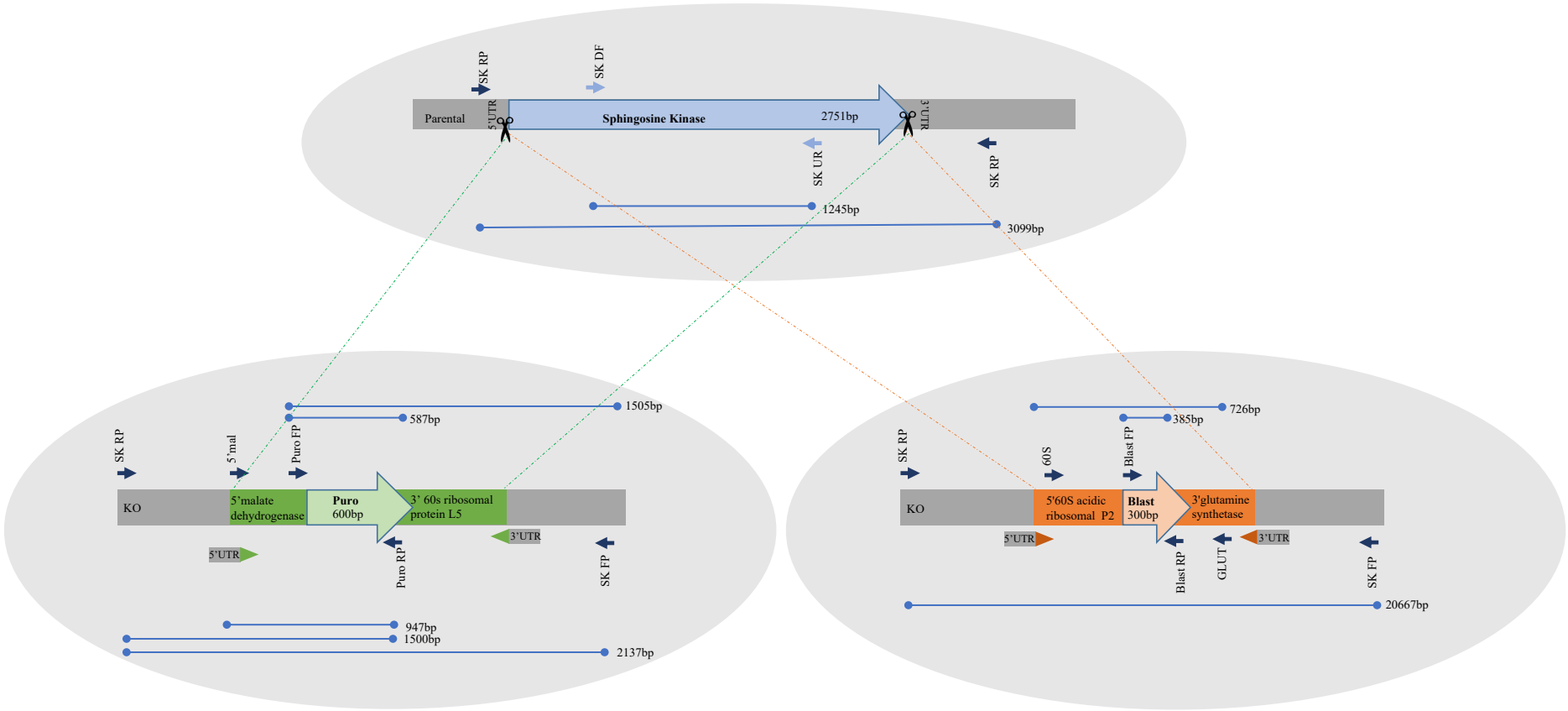

Figure 29: Primer sizes and location for SK diagnostics.

CRISPR-Cas9 Knockout (KO) using the blasticidin resistance marker. Genomic DNA from single clones generated from transfected *L. mexicana* promastigotes selected for blasticidin resistance were analysed using diagnostic primers (Figure 30).

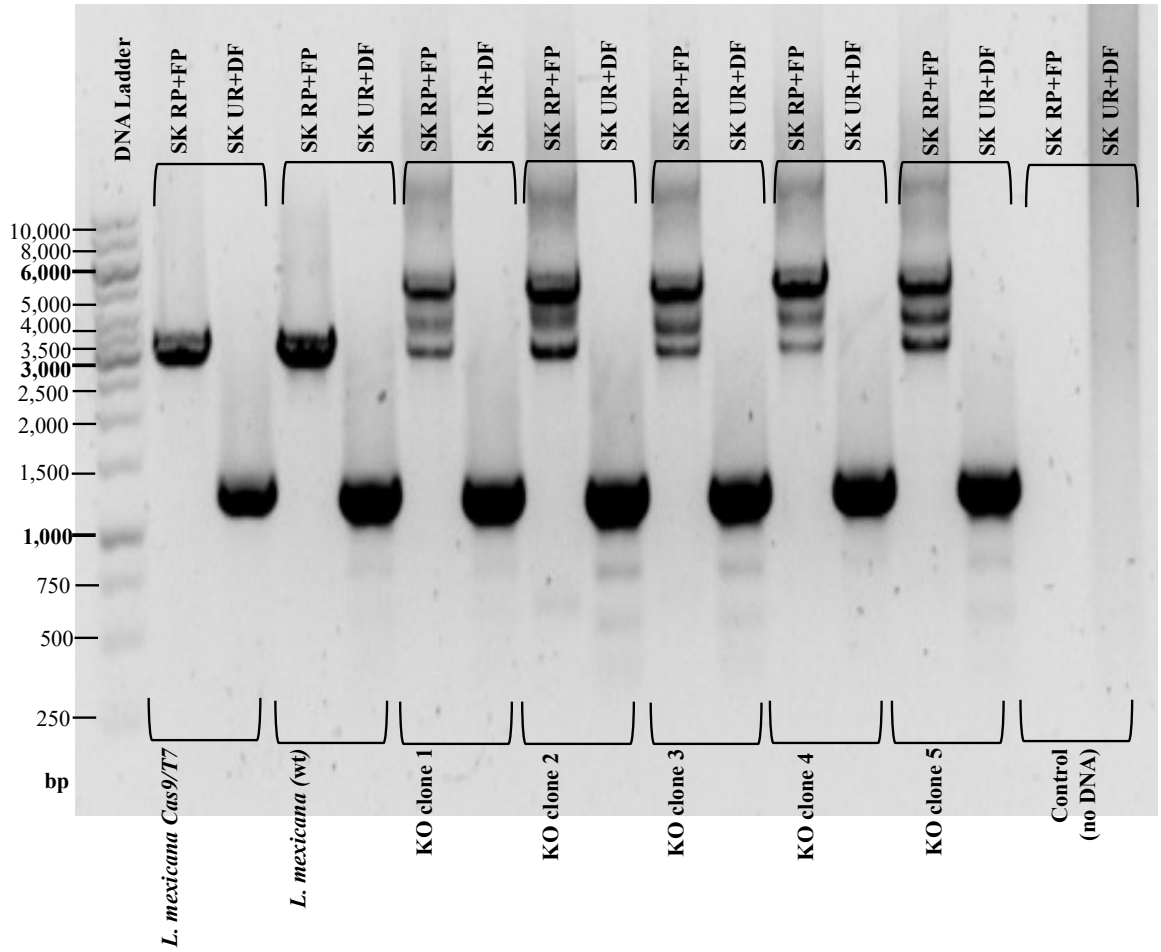

Figure 30: PCR diagnostic of the status of the potential sphingosine kinase knockout L. mexicana clones isolated by blasticin resistance. L. Mexicana M379 (wt) and L. mexicana Cas9/T7 were used as controls. Primer sets flanking the sphingosine kinase locus (RP and FP) and within the ORF (UR and DF) were used.

Diagnostic primers flanking the SK gene (FP and RP) resulted in a PCR product matching the predicted 3098bp from both the WT *L.* mexicana (M379) and the *L. mexicana* Cas9/T7 parental line. The second diagnostic primer pair from within the SK open reading frame (UR and DF) resulted in a PCR product matching the predicted 1245 bp (Figure 30). With the

correct insertion of the blasticidin donor DNA, the diagnostic primer pair FP and RP should give a PCR product size of 2066bp due to the excision of the SK gene and the insertion of the resistance cassette along with the 60S acidic ribosomal protein P2, the 5' untranslated region (UTR) and glutamine synthetase 3' UTR. In each of the five blasticidin resistant clones selected (Figure 30), the diagnostic primer pair UR and DF showed the product expected if the SK reading frame is maintained (1245 bp). Similarly, like the controls, the primer pair flanking the SK locus (FP and RP) gave a product matching the predicted 3098bp in each of the 5 clones demonstrating that the full-length SK gene was maintained. This demonstrated that a full knockout of the SK ORF was not achieved in any of the 5 clones tested. However, all 5 clones also gave 2 further unknown products of ~4000 bp and ~5000 bp which were not found in the controls. A single CRISPR Cas9 mediated cut at either 5' or 3' of the SK gene, followed by with the insertion of the blasticidin repair construct could explain the diagnostic primer pair of FP and RP amplifying the dominant upper band (~5000 bp). The origin of the ~4000 bp product remained unclear.

What is clear is that SK knockout has been unsuccessful, perhaps due to the quantity of one sgRNA being insufficient in the transfection for the full excision of the SK gene. Following these unsuccessful attempts, improvements to the protocol were made - PCR, transfection and selection (see Materials and Methods). Subsequently, the double KO using both puromycin and blasticidin repair cassettes was repeated and again resulted in no viable parasites following selection. This supported the conclusion that SK was likely to be essential, however single selectable marker experiments continued – beginning with repeating the KO using the blasticidin cassette.

The cells selected during this process were analysed using diagnostic primers shown schematically in Figure 29- flanking the SK gene (SK FP and RP); within the blasticidin resistance gene (Blast FP and RP); and flanking glutamine synthetase (GLUT) and 60S acidic

ribosomal protein P2 (60S) for the amplification of pTBlast and genomic DNA from the un-cloned mixed knockout population (Figure 31). As expected, using pTBlast, the SK FP and RP primers did not amplify any products. However, unexpectedly, no amplification was seen in the un-cloned knockout population. The SK diagnostic primers were designed upstream and downstream from the open reading frame and within the UTRs, with amplification of a fragment size of 2066bp was expected. The blasticidin diagnostic primer set and the 60S and GLUT primer set both showed positive results, giving the correct fragment sizes matching 385bp and 726bp respectively. Therefore, despite the uncertainty the diagnostic SK primer pair result, these data strongly suggested the presence of SK knockouts within this mixed parasite population. Notably, the mixed population of transfected parasites in culture viably were unhealthy and showed poor motility, this did not improve and resulted in very few parasites being viable for selection.

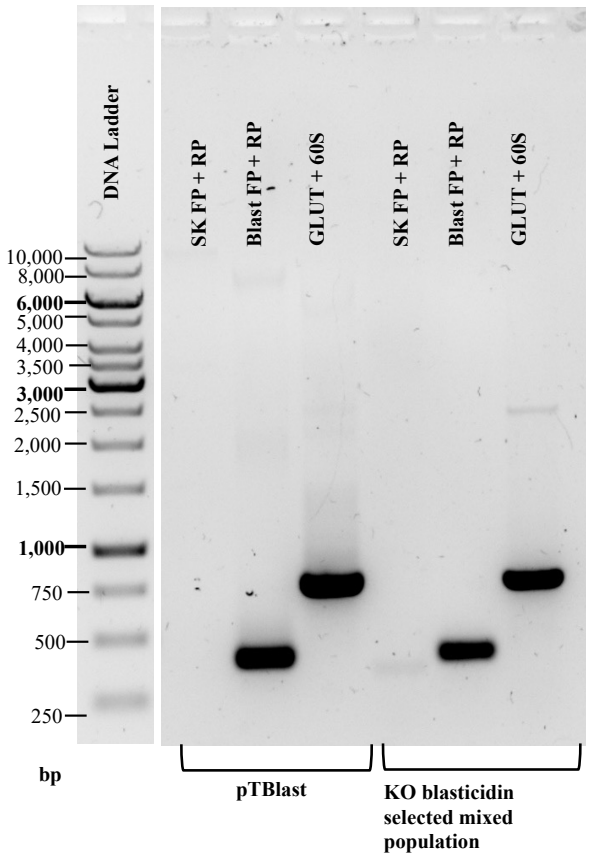

Figure 31:PCR diagnostic of the status of the potential sphingosine kinase knockout L. mexicana clones isolated containing blasticidin resistance. pTBlast was used as control. Primer sets flanking the sphingosine kinase locus (RP and FP), blasticidin (BlastFP and BlastRF) and GLUT primer and 60S primer were used.

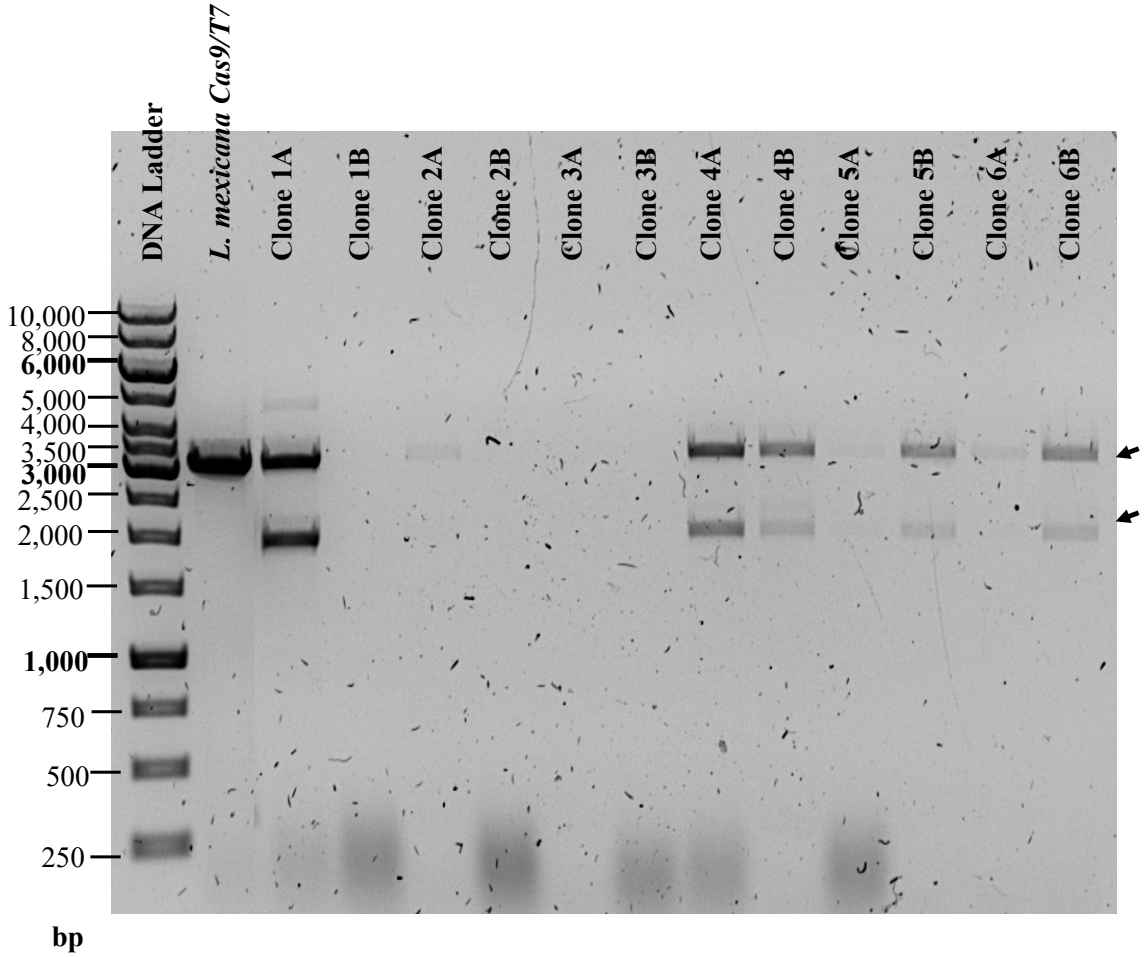

Figure 32:PCR diagnostic of the status of the potential SK knockout L. mexicana clones containing blasticidin resistance. L. mexicana Cas9/T7 genomic DNA was used as a control. Primer set flanking the sphingosine kinase locus (RP and FP) used.

Clones generated from the mixed population were PCR analysed using the diagnostic SK primer pair as previously (Figure 32). The 3099bp fragment was amplified from the *L. mexicana* Cas9/T7 parental line. Of the 12 clones analysed, two bands were amplified (shown by arrows). The larger fragment indicated the maintenance of SK, whilst the smaller band of 2137bp indicated the replacement of SK by the blasticidin repair cassette. Results from Clones 1A, 4A, 4B, 5B and 6B suggested that there was knockout in only a single allele, with a copy of SK maintained within the second allele. Clone 2A and 6A showed faint fragments

of ~3000bp suggesting that both alleles may have retained the SK gene. Again, these data supported that SK is an essential leishmanial activity.

CRISPR-Cas9 Knockout (KO) using the puromycin resistance marker. In parallel to the work above using the blasticidin castte, SK KO employing the puromycin cassette was attempted. Notably, this mixed population was visibly more viable and motile than the second blasticidin-based selection above. Genomic DNA from a transfected and puromycin selected population was analysed using diagnostic primers for SK and puromycin insertion (Figure 33).

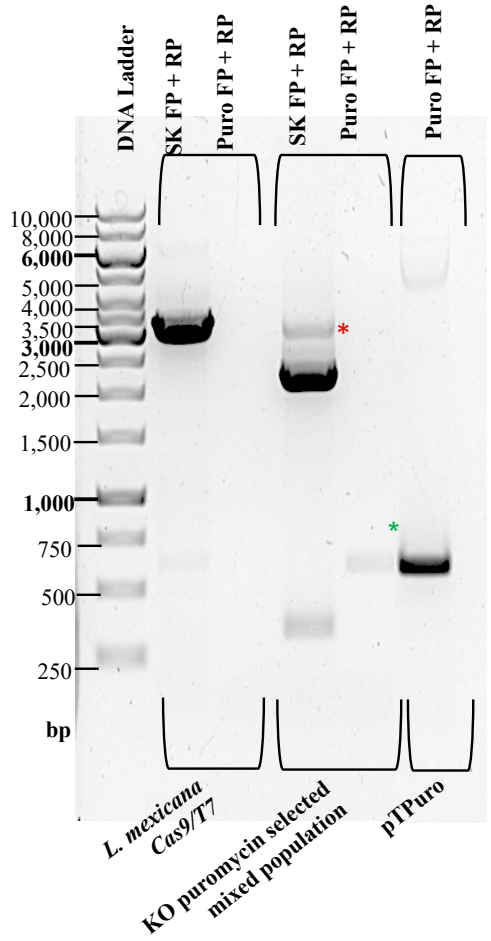

Figure 33:PCR diagnostic of the potential sphingosine kinase knockout L. mexicana population containing puromycin resistance. L. mexicana Cas9/T7 and pTPuro were used as controls. Primer sets flanking the sphingosine kinase locus (RP and FP) and puromycin (PuroFP and PuroRF) were employed. Starred (*) bands indicating 3099bp and 589bp**

The mixed (uncloned) population generated was analysed using two primer pairs (Figure 33). Diagnostic primers flanking the SK gene (FP and RP) resulted in a PCR product matching the predicted 3099bp from the *L. mexicana* Cas9/T7 parental line. The diagnostic primers flanking the puromycin resistance gene present in puromycin repair cassette (PuroFP and PuroRF) resulted in a PCR product matching the predicted 587bp (*) in the transfected line, which was not present in the parental, but was seen in the control pTPuromycin plasmid as expected (Figure 33). FP and RP amplification showed additional bands: a faint one matching the predicted 3099bp (*) of full-length SK, indicating maintenance in a subpopulation in this mixed population; and a dominant 2066bp band suggested that the SK gene had been replaced with the puromycin repair cassette containing the 587bp puromycin resistance gene, malate dehydrogenase 5' UTR and 60S ribosomal protein L5 3' UTR. These results strongly suggested the presence of SK KO within the mixed population, requiring clonal selection to establish whether the gene was successfully ablated from both alleles in the diploid *Leishmania.*

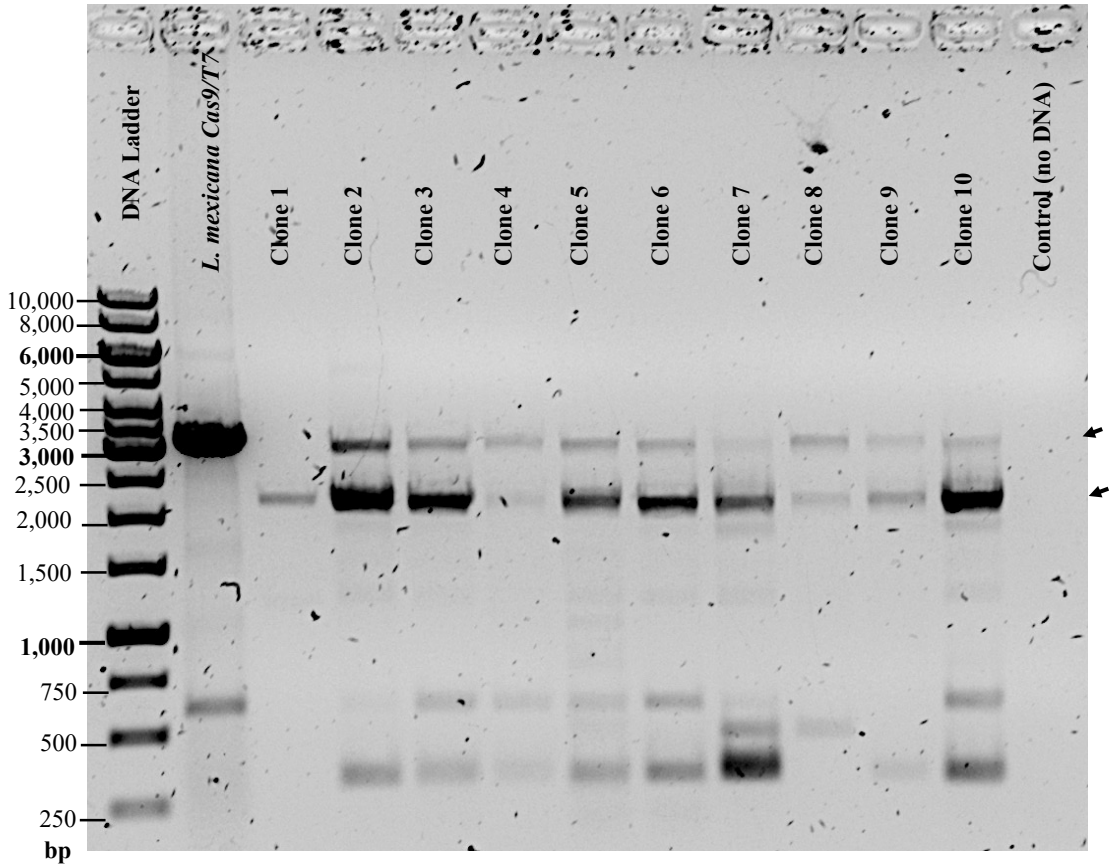

Figure 34: PCR diagnostic of the status of the potential sphingosine kinase knockout L. mexicana clones isolated as puromycin resistant. L. mexicana Cas9/T7 was used as control. Primer sets used flanking the sphingosine kinase locus (RP and FP).

Clones generated from the mixed puromycin-resistant population seen in Figure 33 were analysed by PCR using the diagnostic SK primer pair previously employed (RP and FP; Figure 34). The presence of a product matching the 3099bp fragment amplified from the *L. mexicana* Cas9/T7 parental line indicated the maintenance of the SK gene. In the 10 clones analysed, two high molecular weight DNA products were amplified (shown by arrows). The larger fragment of ~3000bp indicated the presence of the wild type locus (matching the 3099bp expected), whilst the ~2000bp fragment indicated the replacement of SK by the puromycin cassette (matching the 2137bp expected). Clones 2 to 10 presented both fragments, suggesting either that clonal selection was not complete or a single knockout

clonal population was achieved with only one SK allele missing (a single KO). The clone 1 PCR result showed only the 2137bp fragment suggesting a KO of the SK gene from both alleles (a double KO). 10 further clones were analysed but none demonstrated a double KO of SK.

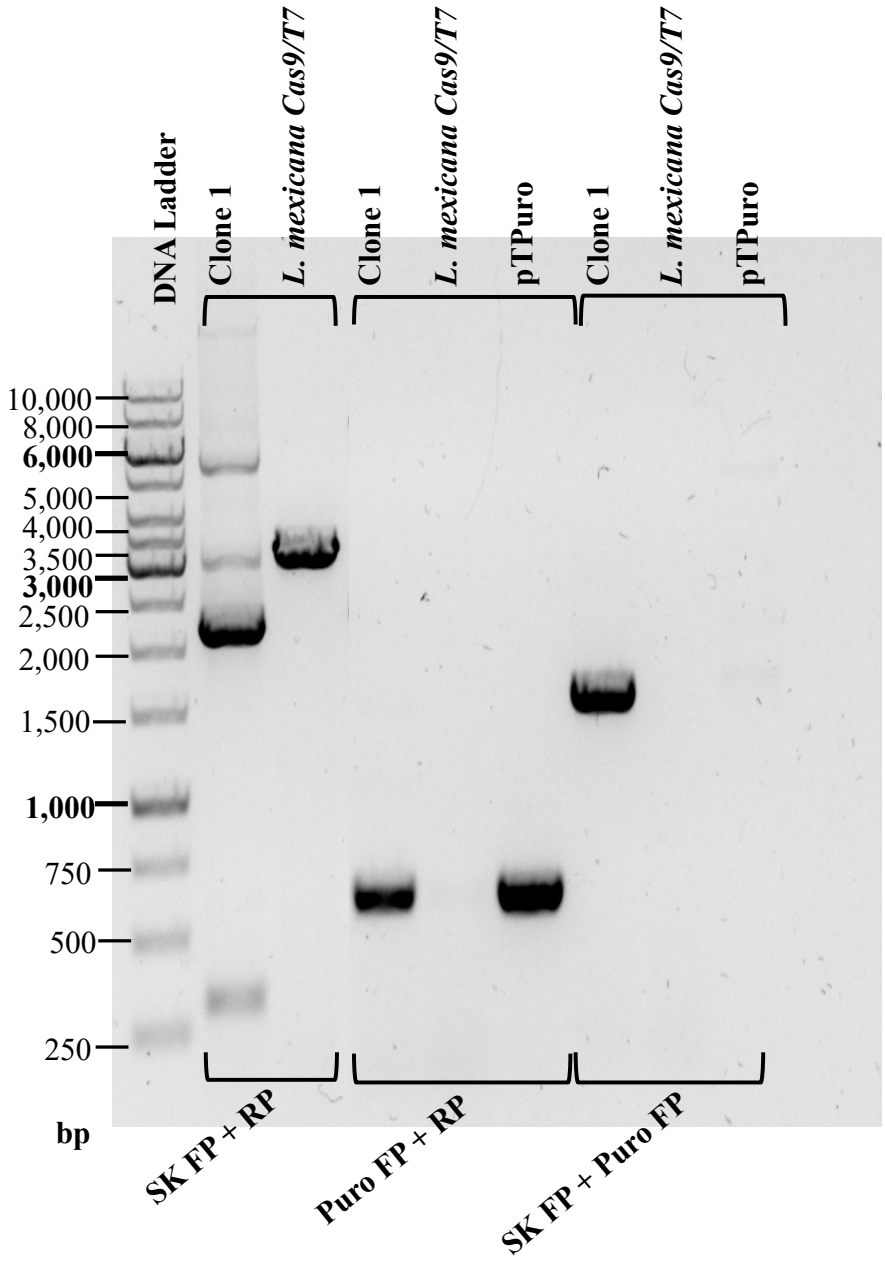

Figure 35: PCR diagnostic of the status of the sphingosine kinase knockout L. mexicana clone 1 isolated by puromycin resistance. L. mexicana Cas9/T7 and pTPuromycin plasmid were used as controls. Primer sets flanking the sphingosine kinase locus (SK RP and FP), flanking the puromycin resistance locus (Puro FP and RP) and primer set SK FP and Puro FP were used.

Clone 1 was further investigated through PCR analysis using the diagnostic SK primer pair (SK RP and FP), puromycin primer pair (Puro FP and RP), and the primer pair SK FP and Puro FP, to determine insertion of the puromycin repair cassette in the SK gene location. The parental *L. mexicana* Cas9/T7 line and pTPuromycin plasmid were used as a control (Figure 35). Using the SK diagnostic primer set a fragment of matching the 3099bp expected was generated from the parental line showing the presence of the SK gene. A prominent fragment of ~2000bp (matching the 2137bp in Figure 29) was seen in Clone 1 suggesting knockout of the SK gene, however two fainter unknown fragments of ~3000bp and ~6000bp could also be visualised on the gel. The ~3000bp fragment suggested that amongst the double knockout is a population containing a single knockout therefore retaining the SK gene in one allele (matching the expected 3099bp expected). However, the source of the ~6000bp band was unclear. The intensity of the 2137bp fragment suggested the knockout was highly abundant, and it was therefore likely that the population was non-clonal and formed of a majority SK double KO cells with a smaller population of single KO cells. The diagnostic primers within the resistance gene present in puromycin repair cassette resulted in the expected product of 587bp in Clone 1 and the pTPuromycin plasmid, which as expected was not present in the *L. mexicana* Cas9/T7 line (Figure 35). The third diagnostic primer pair (flanking the puromycin resistance and the SK UTR) resulted in a PCR product of the expected size 1505bp in Clone 1 only. Together, these data confirmed the puromycin cassette had replaced the SK gene as planned, however the apparent mixed population suggested the need to re-clone of Clone 1.

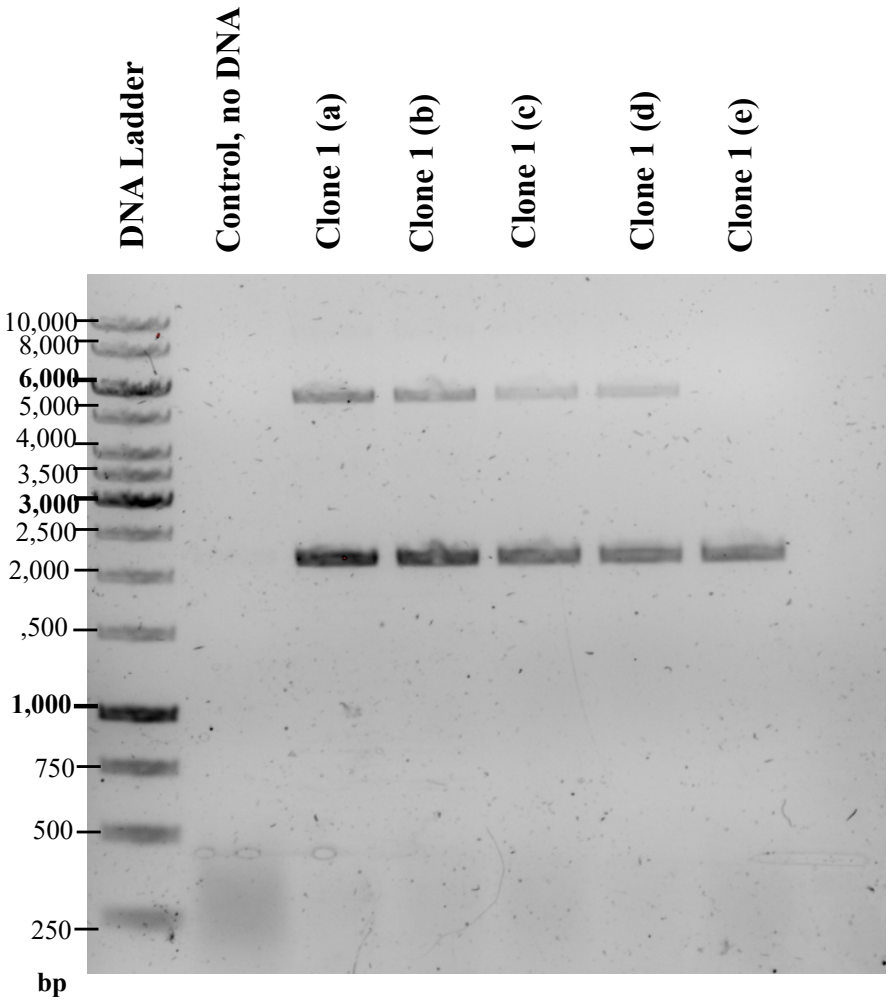

Figure 36: PCR diagnostic of the 5 clonally selected populations of sphingosine kinase knockout L. mexicana clone 1 isolated for puromycin resistance. Water (no DNA) was used as control. Primer sets used flanking the sphingosine kinase locus (SK RP and FP).

Clone 1 was re-cloned yielding five clones denoted a-e. These, along with a no DNA control, were analysed using PCR diagnostic primers SK FP and RP (Figure 36). Fragments of 2137bp and ~6000bp were generated. All clones (a-e) now lacked the WT SK 3099bp fragment, suggesting that original clone 1 (Figure 29 and 30) was not fully clonal and the population contained parasites which maintained the SK locus. However, all clones (1a-e) showed a fragment matching the 2137bp expected when the puromycin cassette inserted in place of the SK gene. However, Clone 1a-d also showed a ~6000bp fragment of unknown origin. This left clone 1e as an apparently clean SK KO, where both alleles had been replaced

with the puromycin resistance cassette. However, a repeat of the PCR protocol increasing the extension time showed that this ~6000bp fragment was present in Clone 1e (Figure 37).

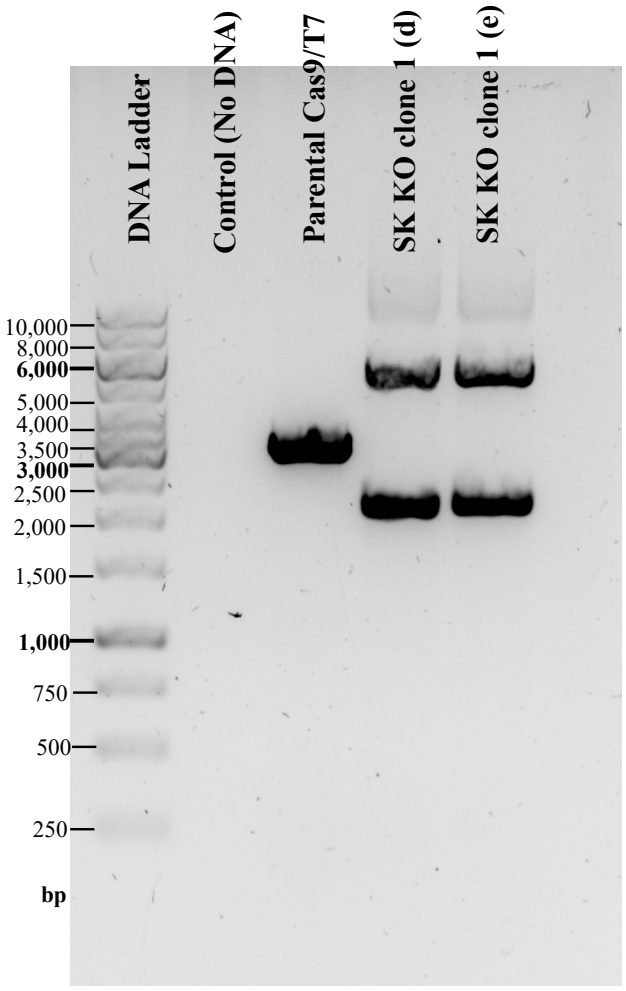

Figure 37: PCR diagnostic of the clonal selected population of sphingosine kinase knockout L. mexicana clone 1 isolated for puromycin resistance. Water (no DNA) was used as control. Primer sets flanking the sphingosine kinase locus (SK RP and FP) used.

Analyses of SK clone 1e. Clone 1e was further investigated through PCR analysis using the diagnostic SK primer pairs FP and RP, UR and DF, and SK FP and Puro FP to determine insertion of the puromycin repair cassette in the SK gene locus. The parental *L. mexicana* Cas9/T7 line was used as a control (Figure 38).

The diagnostic primer pair SK FP and RP resulted in a PCR product in Clone 1e which confirmed that the puromycin resistance marker has been inserted in the correct location, replacing the SK genes. However, the SK primers located within the SK gene (UR and DF) gave a product matching the 1245bp SK fragment (Figure 29) in both Clone 1e and the parental line, indicating the maintenance of all or part of the gene. In contrast, further mapping using primer pair FP and Puro FP (flanking the puromycin resistance and the SK UTR) demonstrated that the insert of the resistance marker was correct in Clone1e. This, left a conundrum – how was the SK maintained in Clone 1e? The ~6000bp fragment of unknown providence suggested that SK had perhaps been relocated to another location in the genome, where (based on fragment size) is may exist as some form derived tandem duplicate of the WT gene.

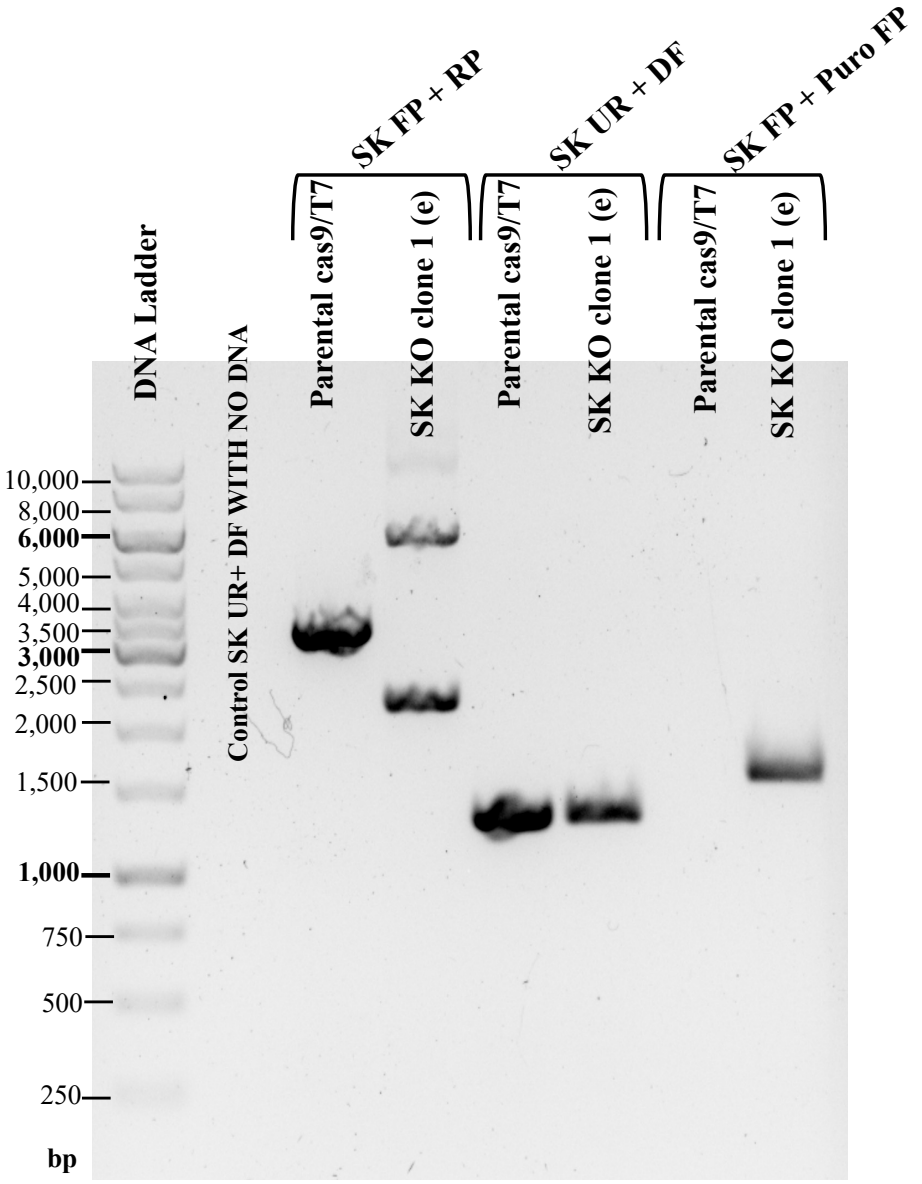

Figure 38: PCR diagnostic of the status of the sphingosine kinase knockout L. mexicana clone 1e isolated containing puromycin resistance. L. mexicana Cas9/T7 and water (no DNA) was used as control. Primer sets used flanking the sphingosine kinase locus (SK RP and FP), within the SK gene (SK UR and DF) and primer set SK FP and Puro FP.

Analyses of SK clone 1d. Like Clone 1e, Clone 1d was further investigated through PCR using the diagnostic SK primer pairs FP and RP, UR and DF, and the primer pair SK FP and Puro FP (Figure 39). The parental *L. mexicana* Cas9/T7 line was used as a control. As with Clone 1e, Clone 1d showed correct positioning of the resistance cassette and replacement of

the SK gene locus. However, like its sister clone, it also showed maintenance of SK and an undefined product of ~6000bp.

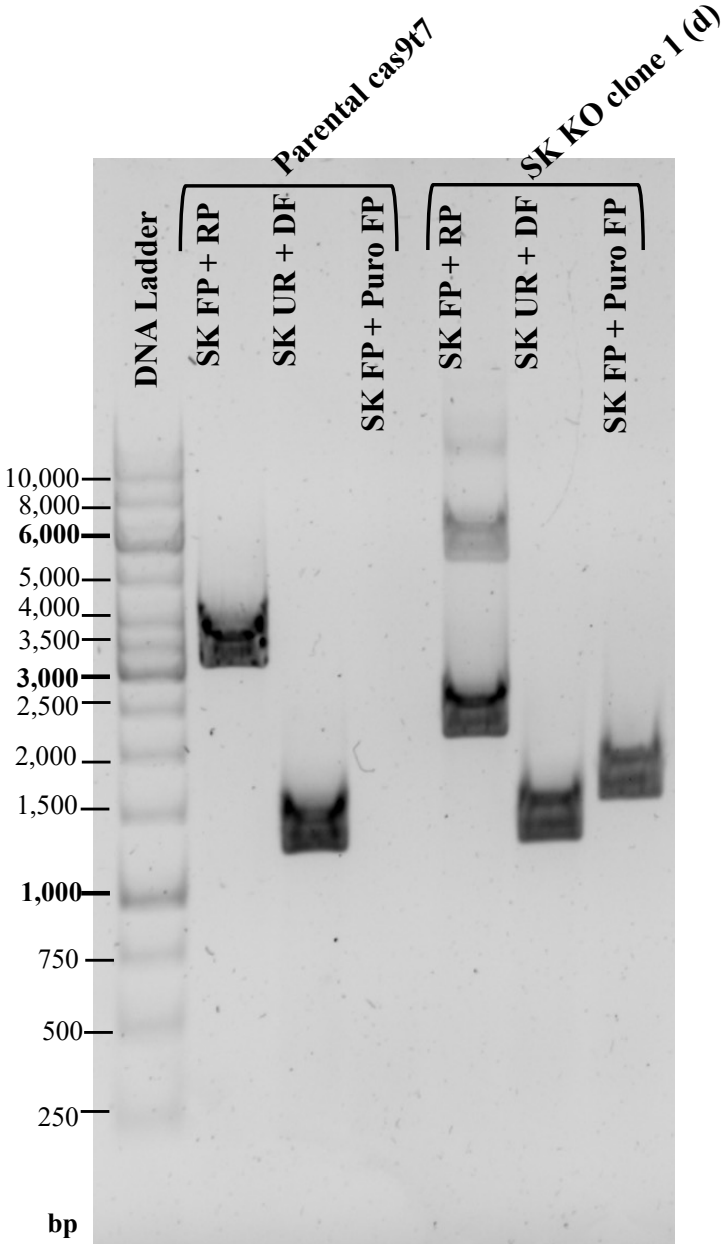

Figure 39: PCR diagnostic of the status of the sphingosine kinase knockout L. 108exicana clone 1d isolated containing puromycin resistance. L. mexicana Cas9/T7 was used as control. Primer sets used flanking the sphingosine kinase locus (SK RP and FP), within the SK gene (SK UR and DF) and primer set SK FP and Puro FP.

These results supported the theory that SK is translocated in these KO lines and maintained in a form which is amplified as a ~6000bp fragment when using primer pair SK FP and RP.

This strongly suggested that SK was essential and demonstrated the plasticity of the *Leishmania* genome.

In summary, although the generation of a double KO seemed possible using the puromycin repair cassette, PCR-based analyses indicated that SK was maintained via genomic rearrangements and is thus highly likely to be essential for *L. mexicana* fitness. In light of this prediction based on the CRISPR Cas9 analysis, the DiCRE system (Duncan et al., 2016) should in future be used to achieve an inducible knockout of the SK gene to enable full assessment of essentiality.

5.3 Analyses of *Leishmania mexicana* sphingosine kinase partial knockout and addback

To facilitate further analyses, Clone 1e (SK KO) above was transfected with an PCR cassette generated from plasmid pGL2277 (a version of pRM006 (Beneke et al., 2017a)) including the sphingosine (SK) gene for integration into the β-tubulin locus. This created a SK KO + addback with SK enzyme expression and functionality with the addition of a kanamycin resistance gene. Subsequently, the growth and morphology of the *L. mexicana* lines was assessed over 4 days (Figure 40) with raw data and ANOVA in appendix. With no variance initially as starting values were identical, the growth of all 3 lines starts of similar but diverge. This is showed by the decrease in the p-value from 0.121 on day 1 to 2.91E-06 on day 5 providing evidence that the three populations are not equal. Visually, the growth was near identical until cell density reached $1x10^7$/ml and the SK KO and SK KO + addback fell behind the parental line, Cas9/T7. The growth of SK KO addback appeared even slower than its direct parent, with cell death visible at higher densities. This contrasts sharply with the observations of Zhang et al, 2013 in that reconstitution of enzyme expression did not fully

restore the SK KO to a wildtype morphology. The rapid demise of the SK KO addback shown in Figure 40 is possibly due to SK being expressed at a higher level than the wildtype endogenous level. As a protein required for the balance of the sphingolipid biosynthetic pathway (Zhang et al,2013), high levels of SK expression in the SK KO + addback may have led to sub-optimal levels of sphingosine and reduced ceramide complex sphingolipid and increased bioactive S1P levels. Both are likely to be detrimental to the parasite leading to low proliferation and death.

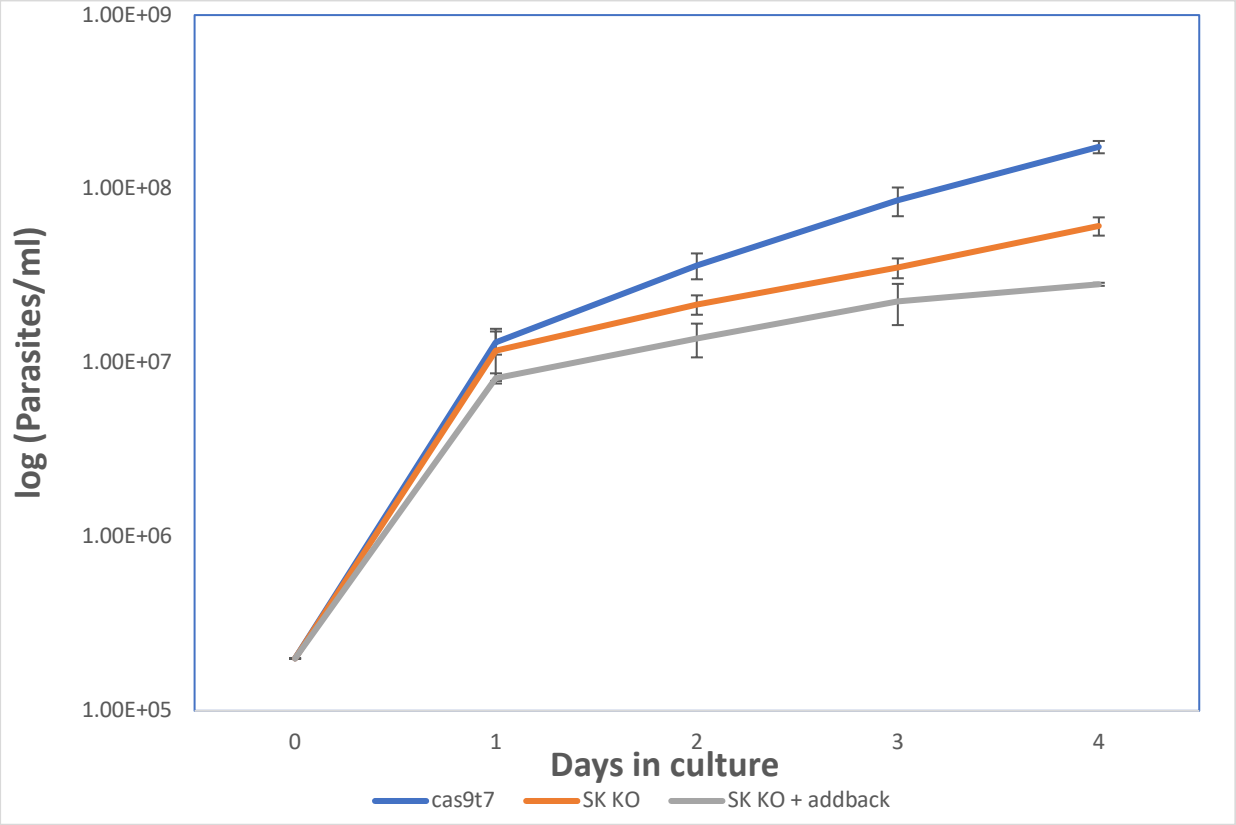

Figure 40: Growth curve of the parental Cas9/T7 , SK KO clone 1e and SK KO + addback over 4 days of growth, Standard deviation shown. n=3

Studies aiming to interfere *Leishmania* in SL metabolism include the KO of the LCB2 subunit of serine palmitoyltransferase (SPT), *L. major* Δ*Lmj*LCB2-/- (Denny et al., 2004). In this work Δ*Lmj*LCB2-/- parasites were shown to lack all sphingolipids and described as 'rounded compared with the classical bullet shape of the wild-type parasites'. *L. major* SK knockout parasites demonstrated a similar morphology (Zhang et al, 2013). SK KO (Clone

1e) and SK KO + addback morphology was analysed in comparison to the parental line. Figure 41 shows the morphology of the 3 cell lines at similar stage of growth (day 3 of culture in stationary phase). The parental cell line has the classic shape of *L. mexicana* parasites, whilst the SK KO and the SK KO + addback cells were slightly rounded towards the flagellum. These phenotypes were not similar to those reported for Δ*Lm*LCB2-/- (Denny et al., 2004) or SK knockout *L. major* (Zhang et al, 2013), or as dramatic.

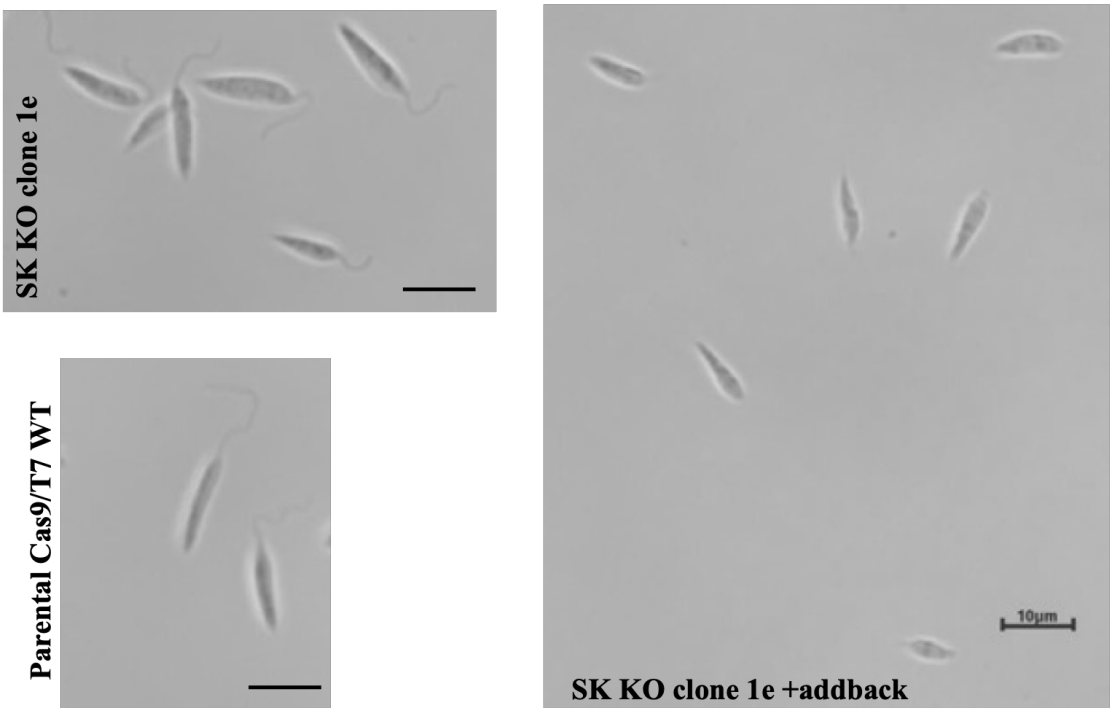

Figure 41: Differential interference contrast images of parasites from day 3 stationary phase cultures

5.4 The essential sphingosine kinase is retained through the plasticity of the *Leishmania* genome

The deletion of sphingosine kinase (SK) in *Leishmania major* was confirmed using Southern blot with five distinct probes (Zhang et al, 2013 supplementary Figure S3). Analysing the data confirmed targeted KO of SK in this species, both alleles replaced by the puromycin and blasticidin resistance markers. However, the data presented do not allow for complete consideration of the translocation of SK to a different genomic position. Without SK in its native location within the *L .major* genome and the designed the probe encompassing the

entire gene (4048bp – including UTRs), 1240bp (30%) of the probe's sequence is non-complementary to the SK gene in a new position. This may affect the hybridization process and lead to the probe being removed in the wash stage. The result shown here demonstrated that puromycin generated SK KO *L. mexicana* (Clone 1e or 1d) have translocated SK in some form to another genomic location, a Southern blot approach as described by Zhang et al,. 2013 may have failed to detect this.

5.5 Conclusion and proposed future experiments

The push for a sphingosine kinase (SK) knockout (KO), whilst successful in disrupting the loci, demonstrated that the plasticity of the genome facilitated maintenance of the presumably essential enzyme elsewhere in the *Leishmania* DNA. Through use of Southern blotting and probes containing a large quantity of the UTR, it is likely that Zhang et al, 2013 missed this event in their study in *L. major* and the residual SK activity in their 'KO' was the result of translocation of SK rather than another protein activity. Due to the crucial role of SK within the sphingolipid biosynthetic pathway, toxic sphingoid base (SB) accumulation or substrate diminution when SK expression is reduced (Zhang et al, 2013; SK KO Clone 1e) or overexpressed (SK KO + addback) is likely to be detrimental to *Leishmania* proliferation. Together these data strongly suggest that SK is an essential gene for these parasites and, given its divergence from the mammalian orthologue, may prove to be an ideal drug target. However, further confirmation of the essentiality of SK should be gained using the DiCre recombinase system (Duncan et al., 2016).

The aim set in Chapter 1 of generating and selecting for a SK KO clone in *L. mexicana* using CRISPR Cas9 was achieved as a SKO clone was generated and various clones troubleshooted. The result from this chapter gives insight into the essentiality of SK in *Leishmania* parasites and brought about research questions into the mechanisms that allow

for genetic changes that were not engineered for such as the availability of a SK in a different location to retain a gene copy. This pertains to the high plasticity of the *Leishmania* genome. Due to the results suggesting that the sphingolipid biosynthetic pathway is highly important, an assessment into the first enzyme within the pathway is required (Chapter 6).

Chapter 6: Compensatory deletions - serine palmitoyltransferase knockout in *Leishmania* resulted in non-targeted gene deletions

The inability to generate a knockout (KO) of sphingosine kinase (SK) using the CRISPR Cas9 system shown and discussed in Chapter 5, lead me to hypothesize that the enzyme is essential and required for homeostasis of the sphingolipid biosynthetic pathway. The only enzyme upstream of SK is serine palmitoyltransferase (SPT), the first enzyme in the *de novo* pathway and responsible for regulation of sphingolipid (SL) biosynthesis (Merrill and Jones, 1990). Chapter 5 suggests SK to be an essential gene, and previous chapters suggested the SK protein to be divergence. As SK is unable to be fully ablated, further knowledge of upstream genetic assessment on enzymes of the sphingolipid biosynthetic pathway is important. This will facilitate an understanding of the pathway. Objectives from Chapter 6 are:

1. Assessing published data where SPT has been ablated from *Leishmania* parasite genome.
2. Generating clones of *L. mexicana* parasites with SPT knockout.
3. Monitoring the multiple non-targeted gene ablations in *L. major* Δ*Lm*LCB2-/- using CRISPR Cas9.
4. Monitoring of the sphingolipidome to investigate the lipidomic changes that occur when the sphingolipid biosynthesis pathway is genetically probed.

In humans, SPT is encoded by two subunits, Long Chain Base (LCB)1 and LCB2, which form a heterodimer (Nagiec et al., 1994, Hanada et al., 1998). Both subunits have been reported to be required for enzymatic activity (Nagiec et al., 1994), however deletion studies have focussed on the catalytic LCB2, with LCB1 thought to stabilise the dimer (Hanada, 2003). Notably, in human keratinocytes SPT activity increases in parallel to LCB2 mRNA levels and not those of LCB1 (Farrell et al., 1998). However, Chinese hamster ovary (CHO)

cells lacking LCB1 showed a much lower level of LCB2 protein (Hanada et al., 1998) without a reduction in mRNA levels (Yasuda et al., 2003). Yasuda et al., 2003 demonstrated that LCB2 protein levels could not increase beyond those of LCB1 in CHO cells, however LCB1 protein can be increased to levels higher than that of LCB2 (Yasuda et al., 2003). Similarly, in yeast the level of expressed LCB2 protein is seen to be reduced in cells lacking LCB1 (Gable et al., 2000). Taken together, these data showed that the absence of SPT activity seen in LCB1 null cells is due to LCB2 instability and indicated functional stoichiometry – this makes both LCB1 and LCB2 targets for generating SPT nulls.

Genetic deletions of LCB1 and LCB2 have been shown to affect cell fitness, with LCB1 ablation in CHO cells leading to sphingolipid-free cells with low growth (Hanada et al., 2000), *Trypanosoma brucei* LCB2 deletion affecting cell growth and cytokinesis (Fridberg et al., 2008) and *Saccharomyces cerevisiae* lacking LCB1 losing cell viability (Pinto et al., 1992) when LCBs could not be scavenged from the media. Unlike in mammalian cells (Hanada et al., 1998), yeast (Pinto et al., 1992) and typanosomatid *T. brucei* (Fridberg et al., 2008), where SPT ablation or inhibition was shown to affect cell viability, genetic KO of LCB2 caused a complete loss of sphingolipids in *Leishmania major* but did not lead to a decline in cell viability (Zhang, 2003, Denny et al., 2004).

In these studies, LCB2 and so SPT functionality, was successfully targeted for deletion using two rounds of homologous recombination and gene replacement in *L. major* (Zhang, 2003, Denny et al., 2004, Zhang et al., 2003). *L. major* LCB2 null promastigotes grew slightly slower than wildtype parasites reaching stationary phase at much lower densities (Zhang et al., 2003, Denny et al., 2004), suggesting that LCB2 and SPT is not essential for *L. major* viability or growth during log phase. The morphology of LCB2 null parasites was described

as less elongated and “rounded” (Zhang et al., 2003) with failure to differentiate into the infectious metacyclic parasites. LCB2 null promastigotes also showed lower infectivity in macrophages and *in vivo* (Zhang et al., 2003, Denny et al., 2004). The lack of a strong phenotype in infective forms was proposed to be due to metacyclic and amastigote parasites synthesizing little or no LCB2 and intracellular amastigotes having the ability to sequester host SLs into their plasma membrane (Winter et al., 1994) Denny et al., 2004). This absence of LCB2 however did not completely ablate the synthesis of SLs (Zhang et al., 2003). Lipid profiling of LCB2 null promastigotes using thin layer chromatography (TLC) showed a complete loss of ceramide and inositol phosphorylceramide (IPC) synthesis (Zhang et al., 2003, Denny et al., 2004) evidencing a lack of *de novo* sphingolipid synthesis in the LCB2 mutants. Further investigation using electrospray ionization mass spectrometry (ESI MS, negative ion mode) confirmed showed this specific loss of IPC species IPC-d16:1 and IPC-d18:1 (Zhang et al., 2003, Denny et al., 2004), as well as loss of certain glycerophospholipids (Zhang et al., 2003).

Subsequent Whole Genome Sequencing (WGS) of the *L. major* LCB2 knockout (Δ*Lm*LCB2-/-) (Denny et al., 2004) and comparison to the wild type parental line (Friedlin Virulent 1) revealed non-targeted gene deletions. These included LmjF.08.0740, LmjF.11.1240, LmjF.13.1540 and LmjF.13.1530 (see appendix for Genome report).

LmjF.08.0740 encodes an amastin-like protein, one of a family of immunogenic surface protein expressed specifically on amastigote parasites (Wu et al., 2000) (Stober et al., 2006). Amastin-like protein is reported to play a role in parasite virulence (Rochette et al., 2005), however their exact function is unknown. LmjF.11.1240 encodes a putative adenosine triphosphate (ATP) binding cassette (ABC) 1 transporter 3A protein belonging to the ABCA

subfamily. There are 42 putative ABC proteins encoded by *Leishmania* parasites clustered into eight subfamilies (ABCA, ABCB, ABCC, ABCD, ABCE, ABCF, and ABCG each containing 10, 4, 8, 3, 1, 3 and 6 proteins respectively) (Leprohon et al., 2006). ABCA3 proteins transport phospholipids across cell membranes (Schmitz and Langmann, 2001) and their expression is upregulated in axenic amastigotes (Leprohon et al., 2006). Neighbouring genes, LmjF.13.1540 and LmjF.13.1530, encode a hypothetical protein with unknown function and a phospholipid-transporting ATPase 1-like protein known as the miltefosine transporter (MT). The hypothetical protein has 36 orthologues from kinetoplastids all of which are unknown function or hypothetical proteins. Conserved Domain Architecture Retrieval Tool (Geer et al., 2002) resulted in no valid domain hit for architecture search and InterProScan (Paysan-Lafosse et al., 2023) search resulted in no predicted domain or important sites. Due to this, a possible function cannot be gathered.

MT's function in *Leishmania* parasites includes the transportation of antileishmanial miltefosine and glycerophospholipids in an inward-directed translocation activity across the plasma membrane (Perez-Victoria et al., 2003b). Studies have shown that when the MT gene is mutated or lost, *Leishmania* species show a reduction in their ability to uptake miltefosine due to defective transport machinery (Coelho et al., 2014, Pérez-Victoria et al., 2003). The neighbouring hypothetical protein has also been shown to be ablated in many miltefosine resistant *L. donovani* clinical isolates (Shaw et al., 2016), and is therefore a known associated deletion when the MT gene is ablated from a population. When the hypothetical protein gene alone is ablated no change to the level of miltefosine resistance is recorded (Coelho et al., 2012). This suggests that the hypothetical protein gene deletion seen in MT null mutants is due to the genes' proximity to each other and not as a requirement or to infer miltefosine resistance. Mapping quality showed that genes encoding ABC3A transporter and LCB2 are

both completely deleted in the Δ*Lm*LCB2-/- population, whilst hypothetical protein, MT and amastin-like protein encoding genes were only absent in a subset of the whole population.

As an adaptive mechanism to respond to changes in environmental conditions, genomes of *Leishmania* parasites have been reported to have a high level of plasticity with events such as aneuploidy to alter gene expression (Rogers et al., 2011) (Dumetz et al., 2017) and genetic events thought to be tightly organised, such as mitosis, perturbed leading to asymmetric chromosome allotments (Sterkers et al., 2011). This plasticity plays an important role when probing the *Leishmania* genome to ablate target genes that may be essential (Jones et al., 2018). When double homologous recombination was employed to generate KO of potential essential genes, a high failure rate due to changes in ploidy allowing genetic adaptations and parasite survival was noted (Jones et al., 2018).

The first question this raises is whether LCB2 alone can be ablated from the genome of *Leishmania* spp or if these additional ablations were critical to compensate for the loss of SPT functionality. For this to be investigated, the CRISPR Cas9 system in *L. mexicana* was employed to generate KOs of LmxM.13.1540 hypothetical protein, LmxM.13.1530 phospholipid-transporting ATPase 1-like protein (miltefosine transporter), LmxM.11.1240 ABC1 transporter 3a, LmxM.08.0740 amastin like protein and LmxM.34.0320 serine palmitoyltransferase (LCB2 subunit). Ceramide synthase (LmxM.30.1780 ,CS) was added to the list of genes (Table 12). CS is one of the two second enzymes in the sphingolipid biosynthetic pathway from SPT, CS being the integral enzyme for ceramide production and SK for the generation of S-I-P. CS's function of N-acetylation of sphinganine to form ceramide which is further converted to complex sphingolipids and its proximity to SPT as a second key enzyme in the sphingolipid biosynthetic pathway shown in Figure 1 made CS an additional gene to investigate along with LCB2.

Table 12: Genes associated with LCB2 ablation according to FastQC analysis of ΔLmLCB2-/- population compared to WT L. major, and ceramide synthase. Copy number (CN) from TriTrypDB.

Gene 1D	Gene	Copy Number
LmxM.13.1540	hypothetical protein, unknown function	2
LmxM.13.1530	phospholipid-transporting ATPase 1-like protein, miltefosine transporter	2
LmxM.11.1240	ABC1 transporter, putative	14
LmxM.08.0740	amastin-like protein, putative	20
LmxM.34.0320	serine palmitoyltransferase, putative	2
LmxM.30.1780	Sphingosine N-acyltransferase, ceramide synthase, putative	4

Miltefosine resistance has been reported in *L. major* Δ*Lm*LCB2-/- parasites, with an EC_{50} of 21.21μM over three times higher than the 6.83μM reported for the wild-type (Armitage et al., 2018). Although exhibiting miltefosine resistance, *L. major* Δ*Lm*LCB2-/- parasites treated with miltefosine analysed by CE-MS had no significant difference in the relative concentration of miltefosine within the parasite and therefore influx of miltefosine was not inhibited (Armitage et al., 2018).

Many of the genes ablated in the *L. major* Δ*Lm*LCB2-/- population listed in Table 12 have previously been reported to be involved in drug resistance. Amastin-like proteins are differentially expressed in trivalent antimony, amphotericin B and paromomycin drug resistant *Leishmania* parasite lines (Rastrojo et al., 2018). When looking at antimony-resistant lines, expression is downregulated in *L. braziliensis* however upregulated in *L. panamensis* (Patino et al., 2019). Within these antimony-resistant lines, Patino et al also showed the expression of putative ABC transporter downregulated in *L. braziliensis* and putative ABC1 transporter (an orthologue to *L. mexicana* putative ABC1 transporter) upregulated in *L. panamensis* (Patino et al., 2019). This downregulation in expression of both amastin-like protein and ABC transporter in *L. braziliensis* is unusual, however other unknown events within genome may have occurred to compensate for this. Due to the function of ABC

transporters, changes in the expression of this protein can confer resistance to multiple drugs (Leprohon et al., 2006). It is therefore generally reported that ABC transporter expression is increased in drug resistant *Leishmania* (Purkait et al., 2012), (Verma et al., 2017), Leprohon et al., 2006). The increase in ABC transporters in the plasma membrane (Legare et al., 2001) aids parasite survival by reducing intracellular drug concentrations due to an increase in efflux (Henderson et al., 1992) and a decrease in drug sequestration (Ouellette et al., 1998). Investigating potential new antileishmanials, such as the antimalarial drug artemisinin, *L. donovani* resistant lines were found to differentially express genes within the ABC transporters gene family (Ghosh et al., 2020). This showed the important role that cell surface transporters play in conferring drug resistance. Similar to ABC transporters, phospholipid-transporting ATPase 1-like protein (miltefosine transporter) has been reported widely in miltefosine drug resistance (Cojean et al., 2012), (Carnielli et al., 2019), (Rijal et al., 2013), (Prajapati et al., 2013), (Bhandari et al., 2012). Analysis of *L. braziliensis* promastigotes and intracellular amastigotes reveal miltefosine transporter to be the main protein responsible for miltefosine drug resistance (Perez-Victoria et al., 2003b, Espada et al., 2019). Miltefosine resistant *L. donovani* parasites have modified sterol biosynthesis, increased cholesterol content and higher level of short alkyl chain fatty acid possibly due to inactivation of fatty acid elongation enzyme, suggesting a more rigid plasma membrane (Rakotomanga et al., 2005). Many of these genes are involved in the regulation of membrane lipid distribution (Andrade et al., 2020), consequently changes in gene expression affect drug internalisation and efflux to benefit parasite survival, conferring drug resistance.

Due to the multiple non-targeted gene ablations in *L. major* Δ*Lm*LCB2-/- being associated with miltefosine resistance, the question of which gene or genes confer this phenotype

remained unanswered. For this to be investigated, the KOs generated in this Chapter underwent drug sensitivity assays.

6.1 Attempted deletion of genes associated with Long Chain Base 2 ablation.

CRISPR-Cas9 Knockout (KO) of the genes associated with LCB2 ablation (Table 12)**.** KO of the genes LmxM.13.1540 hypothetical protein, LmxM.13.1530 phospholipid-transporting ATPase 1-like protein (miltefosine transporter), LmxM.11.1240 ABC1 transporter 3a (ABC3A), LmxM.08.0740 amastin like protein, ceramide synthase (LmxM.30.1780, CS) and LmxM.34.0320 serine palmitoyltransferase (LCB2 subunit) were attempted using the CRISPR-Cas9 system designed for use in *L. mexicana*. Genes may be referred to by their gene names from here onwards.

Using the online resource LeishGEdit, primers were designed for this purpose. 3'sgRNA, 5'sgRNA, blasticidin repair cassette and puromycin repair cassette were generated through PCR and confirmed by agarose gel electrophoresis. These sgRNA's and repair cassettes were then transfected into *L. mexicana* Cas9 T7 parasites (Beneke et al., 2017b), selected using puromycin, G418 and blasticidin drug resistance.

Serine palmitoyltransferase knockout. With a CN of two, the use of puromycin and blasticidin resistance cassette for transfection would allow both copies of the LmxM.34.0320 gene (SPT) to be concurrently deleted with one round of transfection. Although the generation of an LCB2 KO was attempted three times, the selection procedure led to parasite death 1-3 days after the addition of antibiotics and therefore no clones were generated following transfection with both the blasticidin and puromycin repair cassettes. The fact that a double knockout of both alleles of SPT was not possible infers possible essentiality of the

gene for *L. mexicana* parasites, differing from (Denny et al., 2004) where a KO of SPT is generated from HR.

Hypothetical Protein and Phospholipid-transporting ATPase 1-like protein knockouts. Apart from LCB2, the hypothetical protein gene and phospholipid-transporting ATPase 1-like protein gene (also known as miltefosine transporter protein) are the only targets associated with the ablation of SPT with a CN of 2 (Table 12).

A.

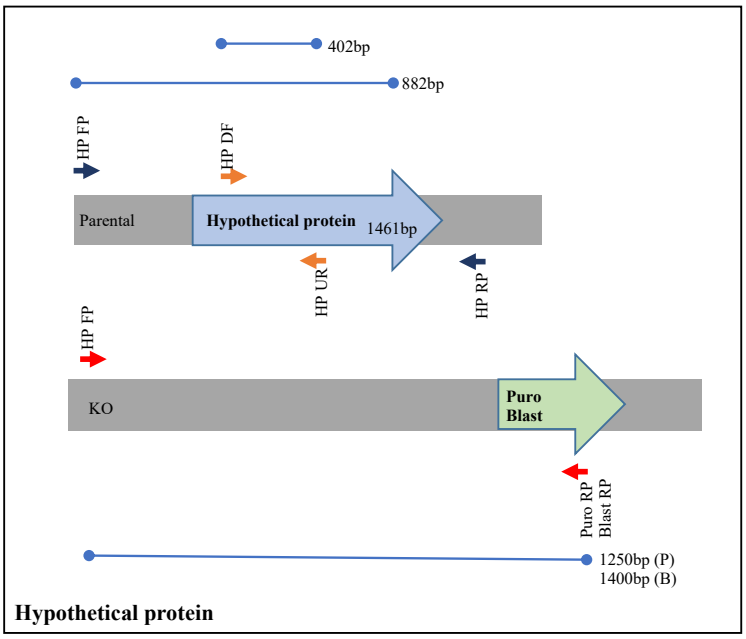

B.

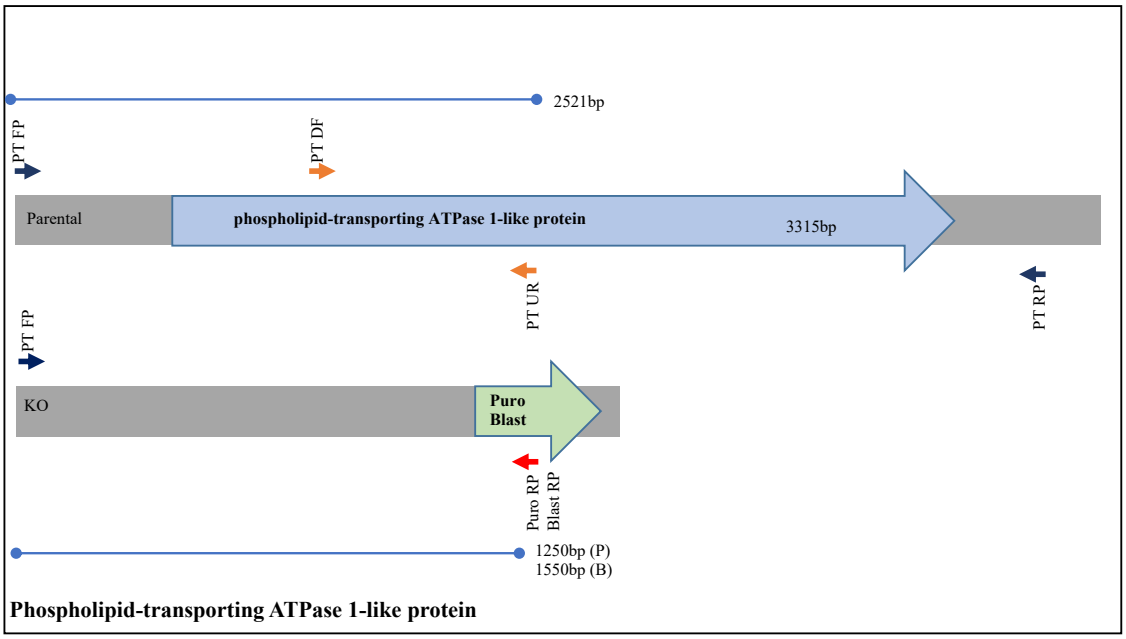

Figure 42: Primer sizes and location for hypothetical protein (A) and phospholipid-transporting ATPase 1-like protein gene (B) used for diagnostic PCR. Blue representing the parental and green representing the insertion of drug resistance in location.

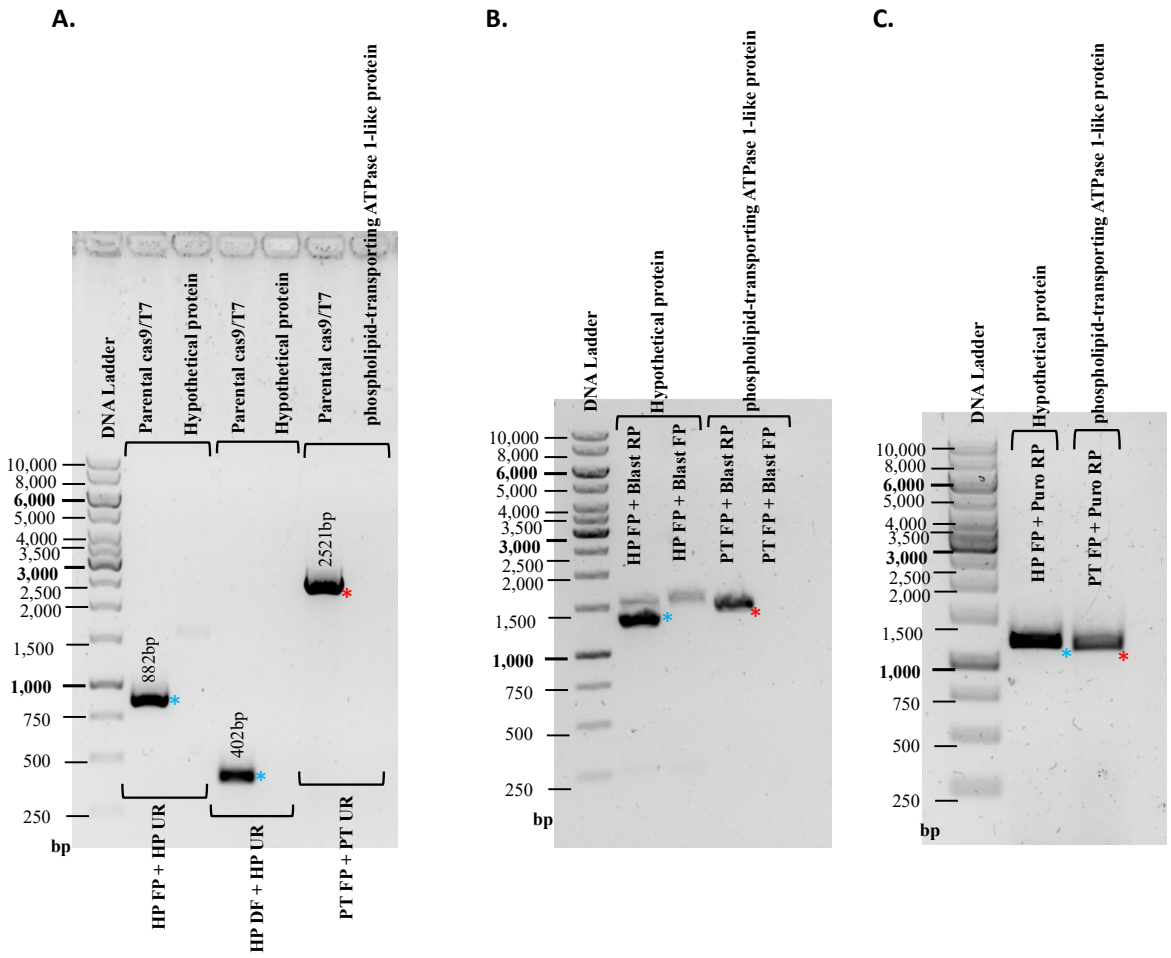

Figure 43: PCR diagnostics of the status of cloned knockouts of hypothetical protein(*) and phospholipid-transporting ATPase 1-like protein(*) using blasticidin and puromycin resistance. Size of expected fragment annotated. Starred fragments discussed.

Hypothetical protein KO parasites underwent PCR diagnostics using three primer sets primer sets schematically shown in Figure 42A. Primer set HP DF and HP UR within the target gene ORF amplifies a 402bp fragment confirming the presence or loss of the hypothetical protein gene. Positional primer sets HP FP and HP UR to confirm the presence of target gene locus *in-situ* by amplifying a fragment of 882bp, and primer set HP FP and Puro/Blast RP to amplify a 1250bp or 1400bp fragment respectively to confirm positional integration of drug resistance cassette. Figure 43A shows primer set HP FP and HP UR amplified an 882bp fragment, and primer set HP DF and HP UR amplified a 402bp fragment within the parental

Cas9/T7 population (starred in blue). Using the hypothetical protein KO parasites, both these primer sets had no amplification in the hypothetical protein KO population confirming the complete loss of the hypothetical protein from target locus and whole genome. Primer set HP FP and Blast RP resulted in a fragment in the region of 1400bp (starred in blue in Figure 43B) and primer set HP FP and Puro RP resulted in a fragment in the region of 1250bp (starred in blue in Figure 43C). This confirms the integration of blasticidin and puromycin resistance cassettes respectively *in situ* of the miltefosine transporter gene in both alleles.

As expected from the schematic shown in Figure 42B for the phospholipid-transporting ATPase 1-like protein gene, primer set PT FP and PT UR resulted in a 2521bp fragment in the Parental Cas9/T7 population (starred in red in Figure 43A) but not in the ATPase 1-like protein gene KO population confirming the deletion of miltefosine transporter (Figure 43A). Positional primer sets, PT FP and Blast RP amplified a 1550bp fragment (starred in red in Figure 43B) and PT FP and Puro RP amplified a 1250bp (starred in red in Figure 43C), confirming the integration of blasticidin and puromycin resistance cassettes respectively in situ of the miltefosine transporter gene in both alleles

ABC3A transporter knockout. Within the Δ*Lm*LCB2-/- population, LCB2 and ABC3A transporter were both ablated completely from the population. With LCB2 was not possible to KO, high priority was placed on the ABC3A transporter. Two clones were generated each possibly having the ABC3A transporter protein encoding gene ablated. These populations were labelled as ABC3A transporter (P/P), integration of only the puromycin resistance cassette, and ABC3A transporter (P/B), the integration of puromycin and blasticidin resistance cassettes.

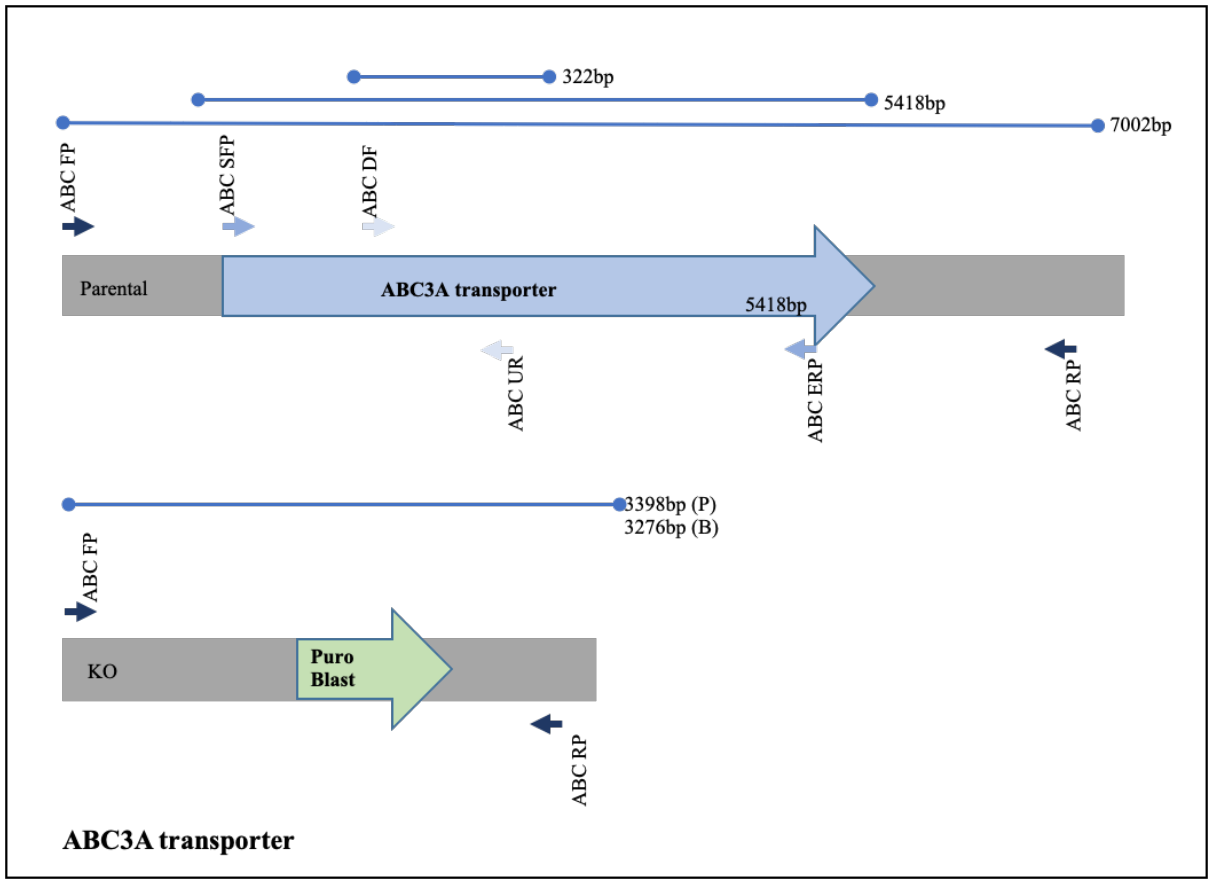

Figure 44: Primer sizes and location for ABC3a transporter protein gene used for diagnostic PCR. Blue representing the parental and green representing the insertion of drug resistance in location.

Putative ABC3A transporter protein KO parasites underwent PCR diagnostics using three primer sets primer sets schematically shown in Figure 44. Primer set ABC DF and ABC UR amplified a 322bp fragment within the ORF of ABC3A transporter gene, and primer set ABC SFP and ABC ERP amplified the full-length gene (5418bp). Positional primer set within the UTR of the target gene ABC FP and ABC RP amplified a 7002bp fragment when ABC3A transporter was *in-situ* and 3398bp or 3276bbp when puromycin or blasticidin were integrated respectively.

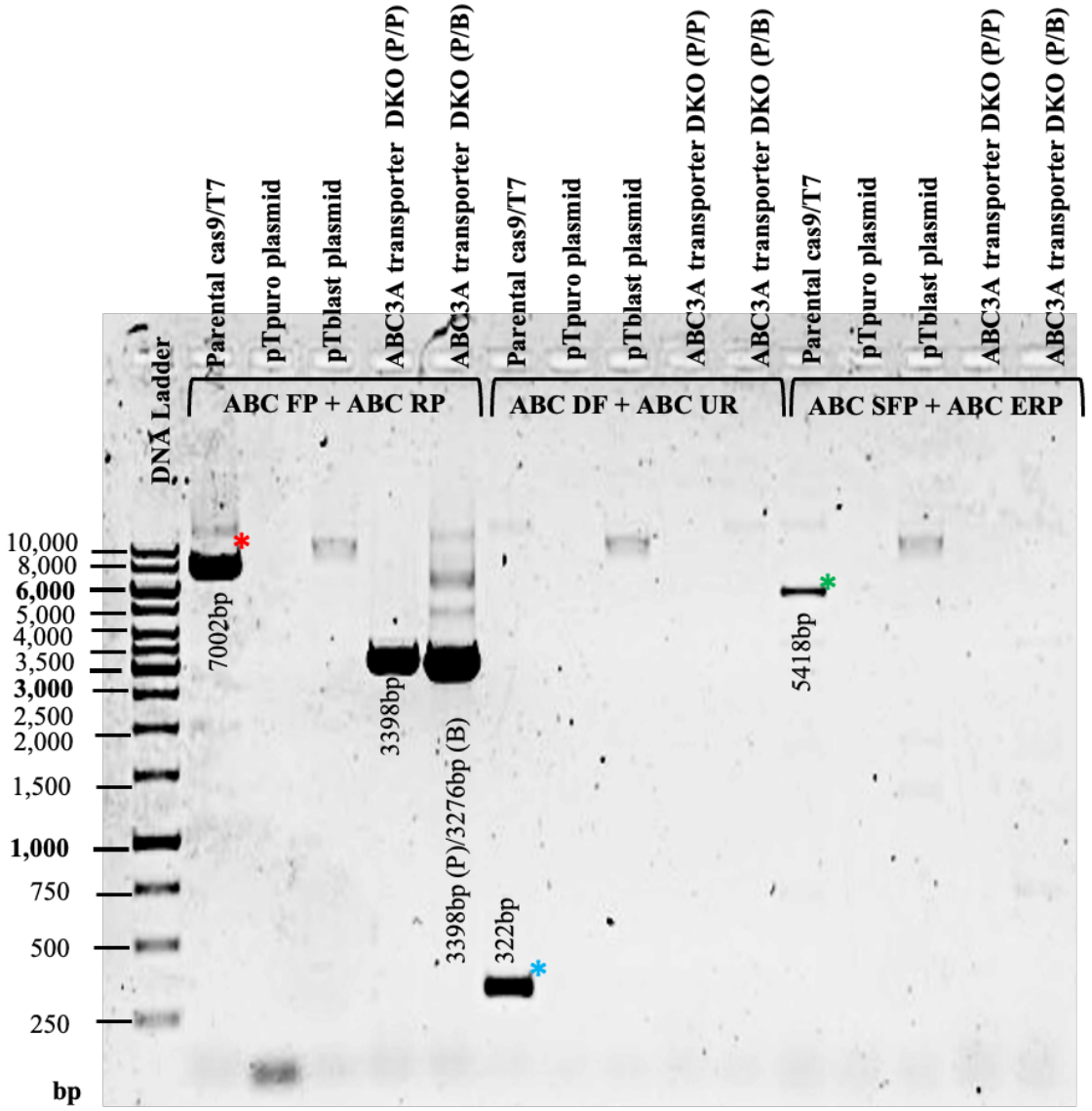

Figure 45: PCR diagnostics of the status of cloned ABC1 transporter3a knockout using blasticidin and puromycin resistance. Size of expected fragment annotated. Starred fragments discussed.

Positional primer set ABC FP and ABC RP results in the expected 7002bp amplified fragment in the Parental Cas9/T7 population (starred in red in Figure 45), however this band is lost in both ABC3A (P/P) and ABC3A (P/B) KO populations and replaced with a ~3300bp fragment (Figure 45). This suggested the successful excision of the ABC3A transporter gene and replacement with the puromycin resistance cassette (3398bp) alone, or with the blasticidin resistance cassette (3276bp), at the correct loci (Figure 45. The primer

sets within the target gene ORF, ABC DF and ABC UR resulted in a band of 322bp (starred in blue in Figure 45) only in the Parental Cas9/T7 population showing the lack of the ABC3A gene in the KO population genome. To further confirm this primer pair ABC SFP and ABC ERP, containing the start and stop codons of the gene, was used to amplify the full-length ORF. This only showed successful amplification in the Parental Cas9/T7 population (starred in green in Figure 45), providing further evidence that ABC3A gene is completely ablated from the genome of both ABC3A (P/P) and ABC3A(P/B) KO populations.

Ceramide synthase knockout. Although not ablated within the Δ*Lm*LCB2-/- population, ceramide synthase (CS) is important in the pathway for IPC synthesis. Putative KO parasites underwent PCR diagnostics using four primer sets primer sets schematically shown in Figure 46. Primer set CS DF and CS UR was designed to amplify a 609bp fragment within the CS ORF. Primer set CS FP and CS RP were designed within the UTR could be used positionally, amplifying a 1655bp fragment when the CS gene is *in-situ* or a 2086bp or 1955bp fragment confirming integration of puromycin or blasticidin in place of CS (Figure 46).

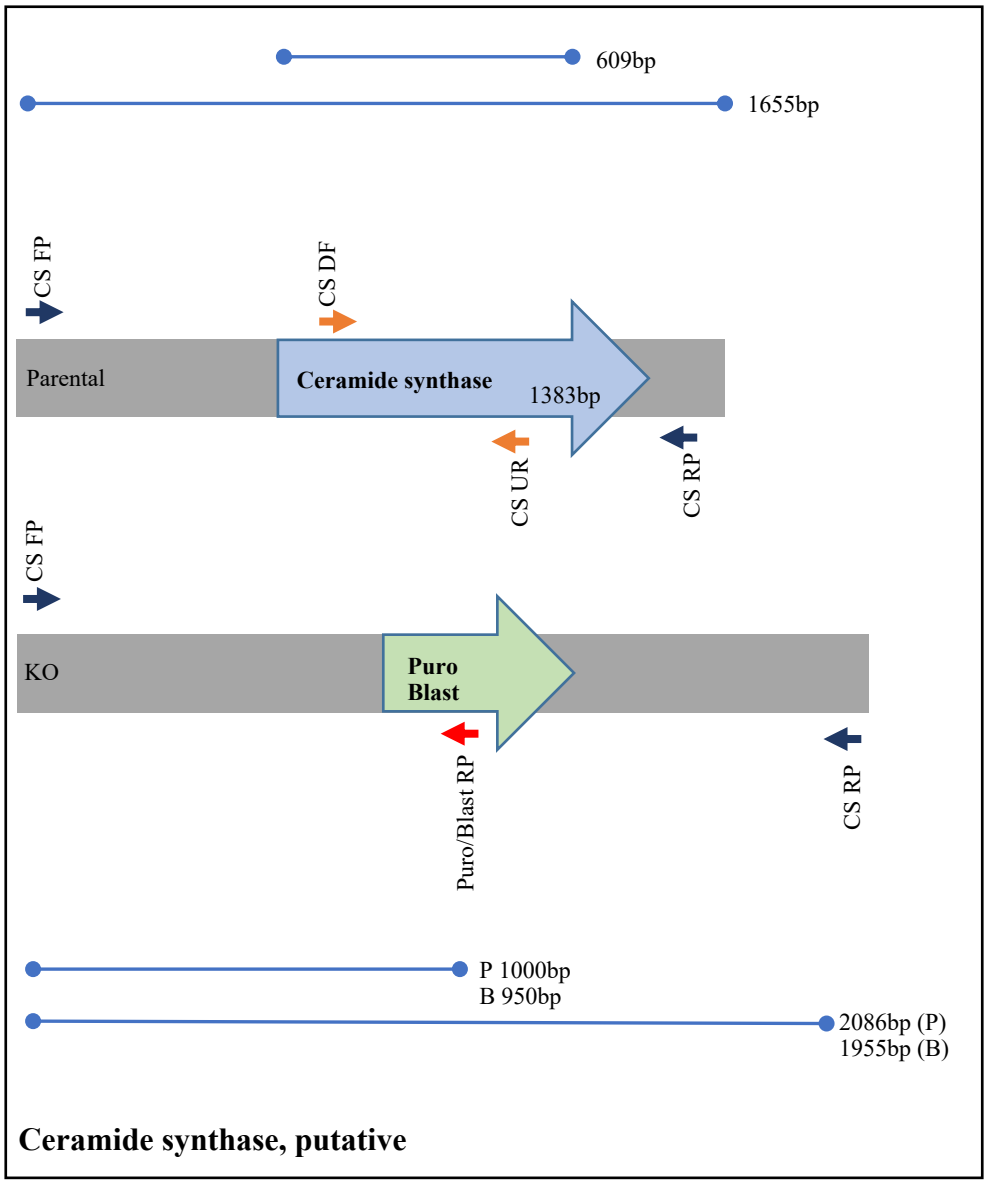

Figure 46: Primer sizes and location for Ceramide synthase protein gene used for diagnostic PCR. Blue representing the parental and green representing the insertion of drug resistance in location.

CS KO parasites were confirmed, the primer set CS FP and CS RP showing loss of the parental 1655bp fragment and replacement with a ~2000bp product, indicating the integration of either the puromycin or blasticidin cassettes (Figure 47). Further, the primer set within the CS ORF amplifying a 609bp fragment the Parental Cas9/T7 population, shown no product in the KO population (Figure 47). Primers Puro RP and Blast RP, coupled with the CS FP primer, amplified products of 1000bp and 950bp respectively in the CS KO population,

confirming the correct integration of the puromycin and blasticidin resistance cassettes within the CS locus.

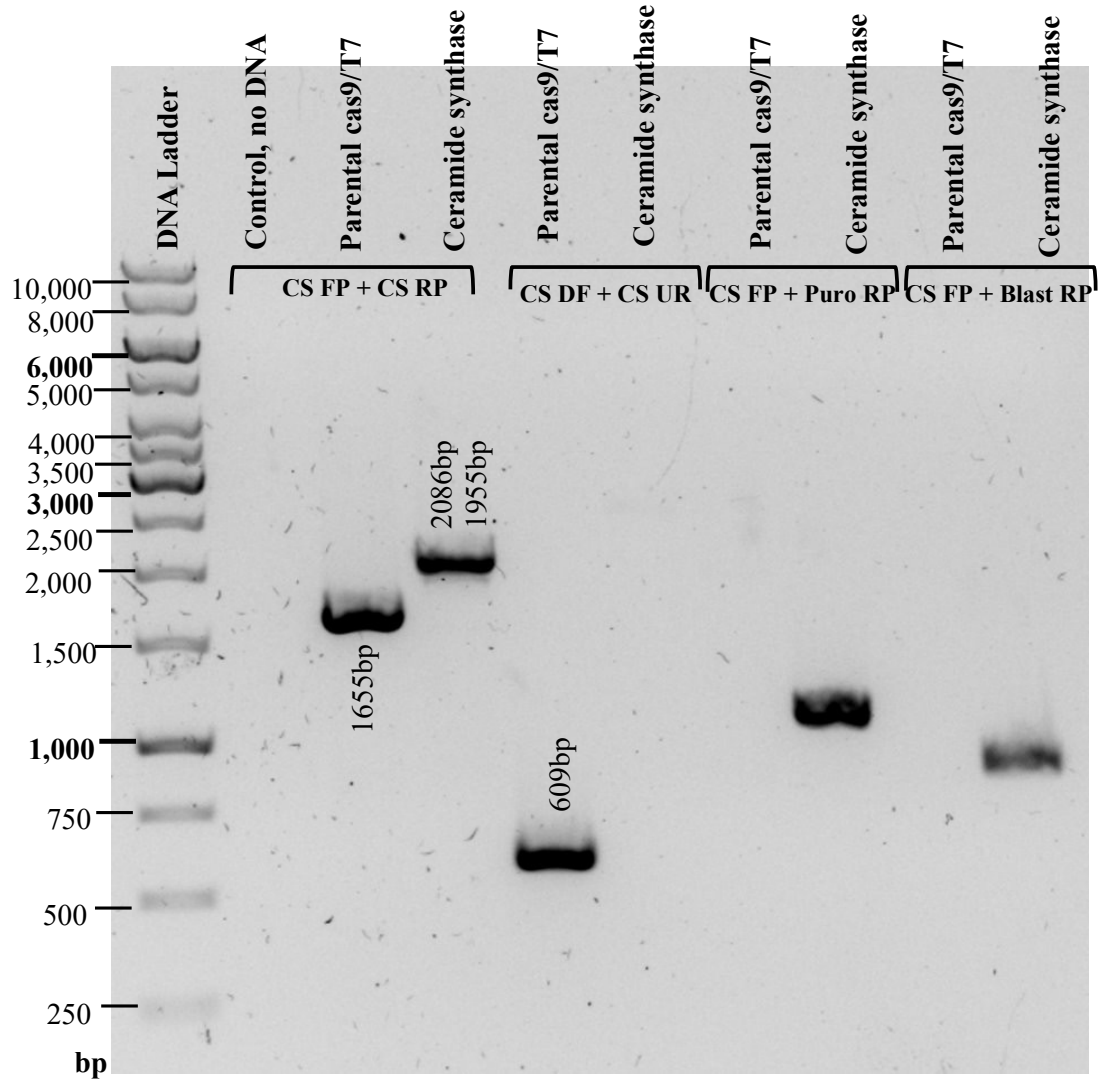

Figure 47:PCR diagnostics of the status of cloned Ceramide synthase knockout using blasticidin and puromycin resistance. Size of expected fragment annotated.

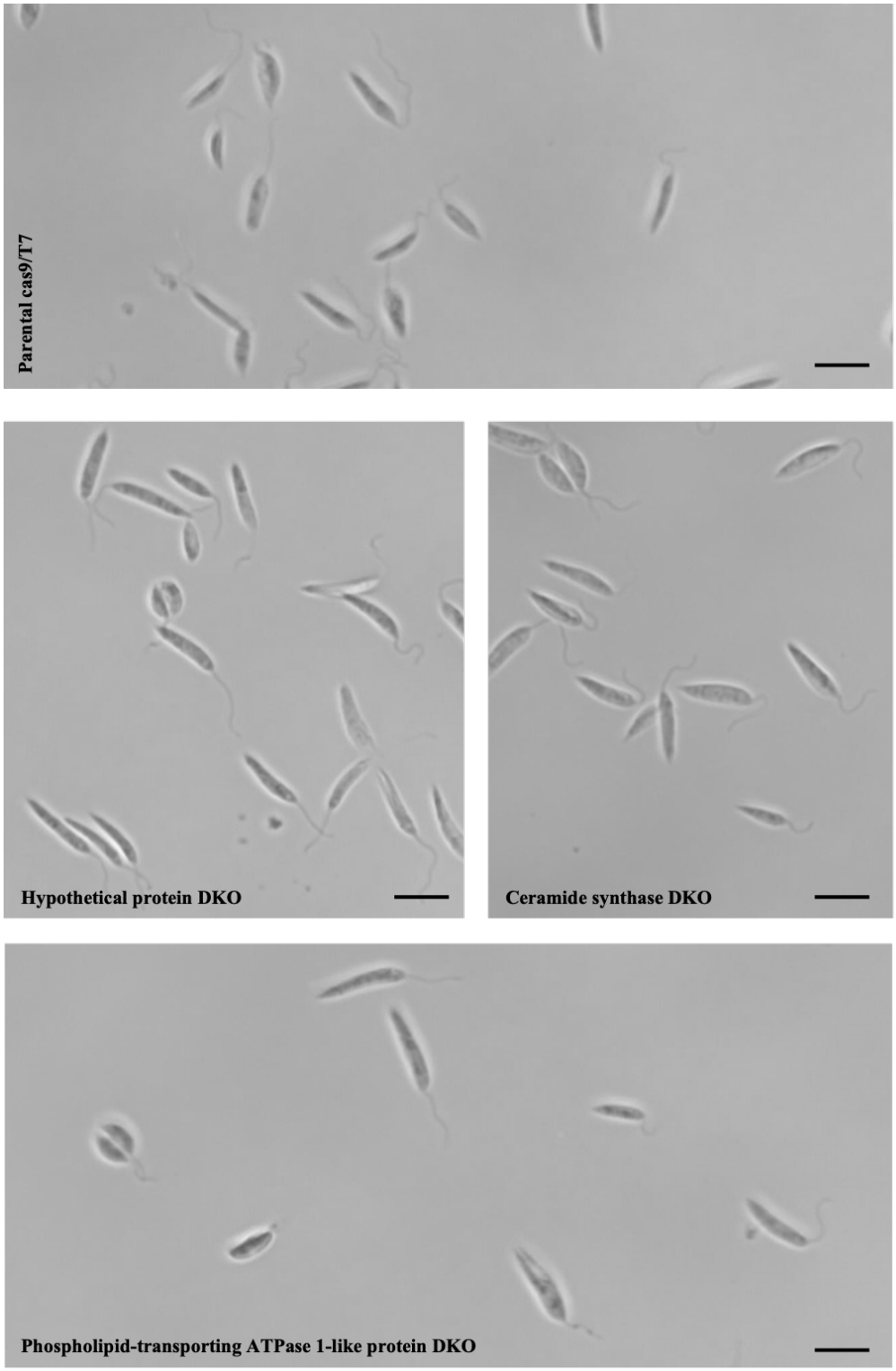

Figure 48: Differential interference contrast images of parasites from 3 days in culture

Morphological analyses of gene ablations associated with Δ*Lm*LCB2-/- showed no clear differences with the parental Cas9/T7 parasites. Morphology of parasites 3 days in culture shown in Figure 48 showed no differences between hypothetical protein, ceramide synthase, phospholipid-transporting ATPase 1-like protein and the parental Cas9/T7 parasites. This was further showed to be the case between in Figure 55 between ABC3A transporter and the parental Cas9/T7 parasites.

In summary, investigation the genes associated in SPT ablation within the Δ*Lm*LCB2-/- population listed in Table 12, showed that the hypothetical protein gene, phospholipid-transporting ATPase 1-like protein (miltefosine transporter) gene, ABC3A transporter gene, and the ceramide synthase gene can be fully ablated using CRISPR Cas9 suggesting they are non-essential. Genes encoding the amastin-like protein and LCB2 cannot be fully ablated however, the amastin-like protein gene due to it being encoded by multi-copy genes, and the LCB2 probably due to essentiality in *Leishmania* spp parasites.

6.2 Double gene ablations within the Sphingolipid biosynthetic pathway

Having shown that LCB2 (SPT) alone cannot be ablated from parental Cas9/T7 population, the question of if the additional ablations recovered from the Δ*Lm*LCB2-/- population listed in Table 12 were critical to compensate for the loss of SPT needed to be answered. Complete KO populations of the genes encoding the hypothetical protein gene, phospholipid-transporting ATPase 1-like protein (miltefosine transporter), ABC3A gene and the ceramide synthase were used to attempt the ablation of LCB2 (SPT). However, this approach was unsuccessful in all cases, with cell death after drug selection. It was therefore important to attempt concurrent KO of each of these genes (encoding hypothetical protein, phospholipid-transporting ATPase 1-like protein (miltefosine transporter), ABC3A transporter and ceramide) with LCB2 (SPT). This was done using a slight modification of the CRISPR Cas9 methodology to transfect gRNA and repair constructs for two gene ablations rather than just one. The inability to ablate LCB2 (SPT) from already KO populations but possible when two genes are targeted for ablation concurrently may be due to unknown genomic changes/adaptation being selected for along with these two KOs which allows for clones which are adapted for survival.

Ceramide synthase and serine palmitoyl transferase knockout. Following transfection and selection, two clones labelled clone 3 and 4 survived the selection process. These clones (3 and 4) were analysed using PCR diagnostics using primers shown in Figure 49. The detection of the full-length CS and the SPT gene was essential to confirming the loss of both genes within the 'CS (P/P) + LCB2 SPT (B/N) KO' and 'CS (P/B) +LCB2 (N)' clonal populations.

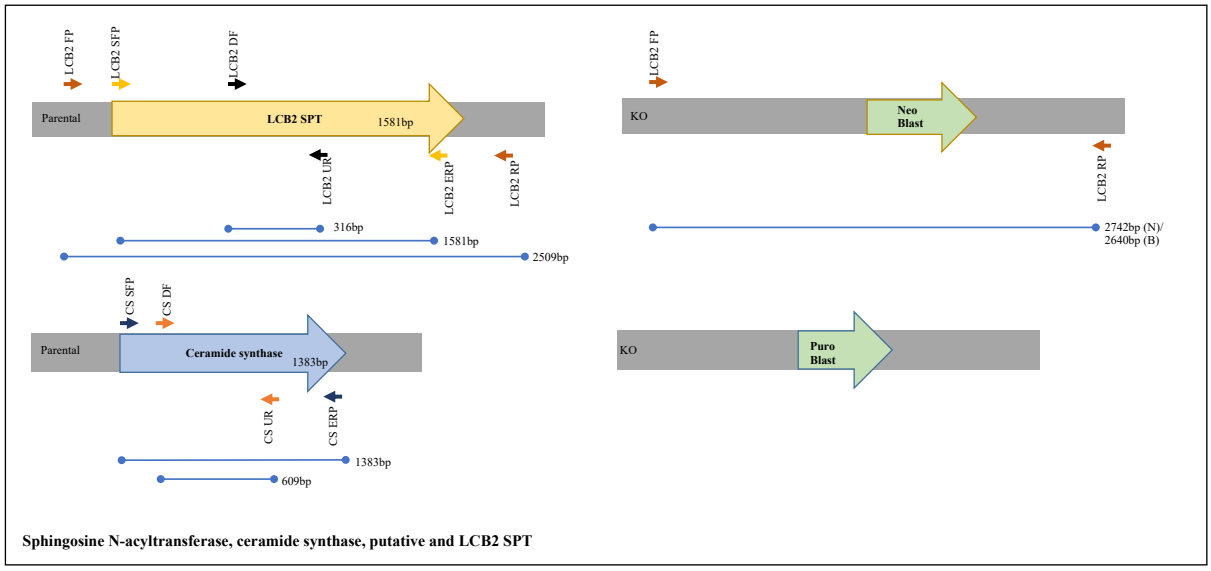

Figure 49: Primer sizes and location for ceramide synthase gene and LCB2 (SPT) gene used for diagnostic PCR. Blue and yellow representing the parental and green representing the insertion of drug resistance in location.

Primer sets designed are shown in Figure 49. For the analysis of CS, two primer sets were designed. Primer set CS DF and CR UR were designed to amplify a 609bp fragment from the CS gene. Primer set CS SFP and CS ERP containing the start and stop codon of the CS gene to amplify the full-length 1383bp fragment of the target gene. For the analysis of SPT, three primer sets were designed. Primer set LCB2 DF and LCB2 UR were designed to amplify a 316bp fragment from the SPT gene. Primer set LCB2 RP and LCB2 FP within the UTR was designed to amplify a 2509bp fragment containing the SPT gene or a 2742bp or 2640bp fragment when neomycin or blasticidin has replaced SPT respectively. Primer set LCB2 SFP

and LCB2 ERP containing the start and stop codon of the SPT gene was designed to amplify the full-length 1581bp fragment of the target gene.

These primers were used to analyse the different clones generated as shown in Figure 50. Figure 50A shows the analysis of the clones using the CS primer sets. All clonal populations analysed potentially had CS ablated. Primer set CS DF and CS UR amplified a 303bp fragment only from the parental Cas9/T7 population confirming loss of CS gene from all other populations. This was further supported by the primer set CS SFP and CS ERP only amplifying a 1383bp fragment from the parental Cas9/T7 population confirming the loss of full-length CS from the genome of all the KO populations. This group of CS KO populations were analysed using the LCB2 primer sets for the detection of SPT in the population's genome shown in Figure 50B. To detect if full length SPT was present, primer set LCB2 SFP and LCB2 ERP was used to amplify the 1581bp SPT gene from the parental Cas9/T7 population. Amplification also occurred in the CS DKO (P/B) +LCB2 (N) clonal population where only one drug cassette (neomycin) was used to attempt the KO of SPT from both alleles, however no amplification occurred in the combined CS (P/P) + LCB2 (P/N) KO populations (clone 3 and 4). To further confirm the loss of SPT gene, primer set LCB2 DF and LCB2 UR was used to amplify the 316bp CS fragment from the parental Cas9/T7 population. Again, amplification occurred in the CS DKO (P/B) +LCB2 (N) clonal population but not in both CS (P/P) + LCB2 (P/N) KO populations (clone 3 and 4). As previously stated, the LCB2 FP and LCB2 RP primer set cannot be used entirely for diagnostic here as the 2509bp fragment in the parental Cas9/T7 is very similar to the 2640bp and 2742bp fragment when blasticidin and neomycin has replaced the SPT gene respectively. CS KO (P/B) + LCB2 (N) where only one drug cassette was used to KO SPT from both

alleles was not successful. This suggests a requirement of two drug resistance cassettes to encourage a full LCB2 loss.

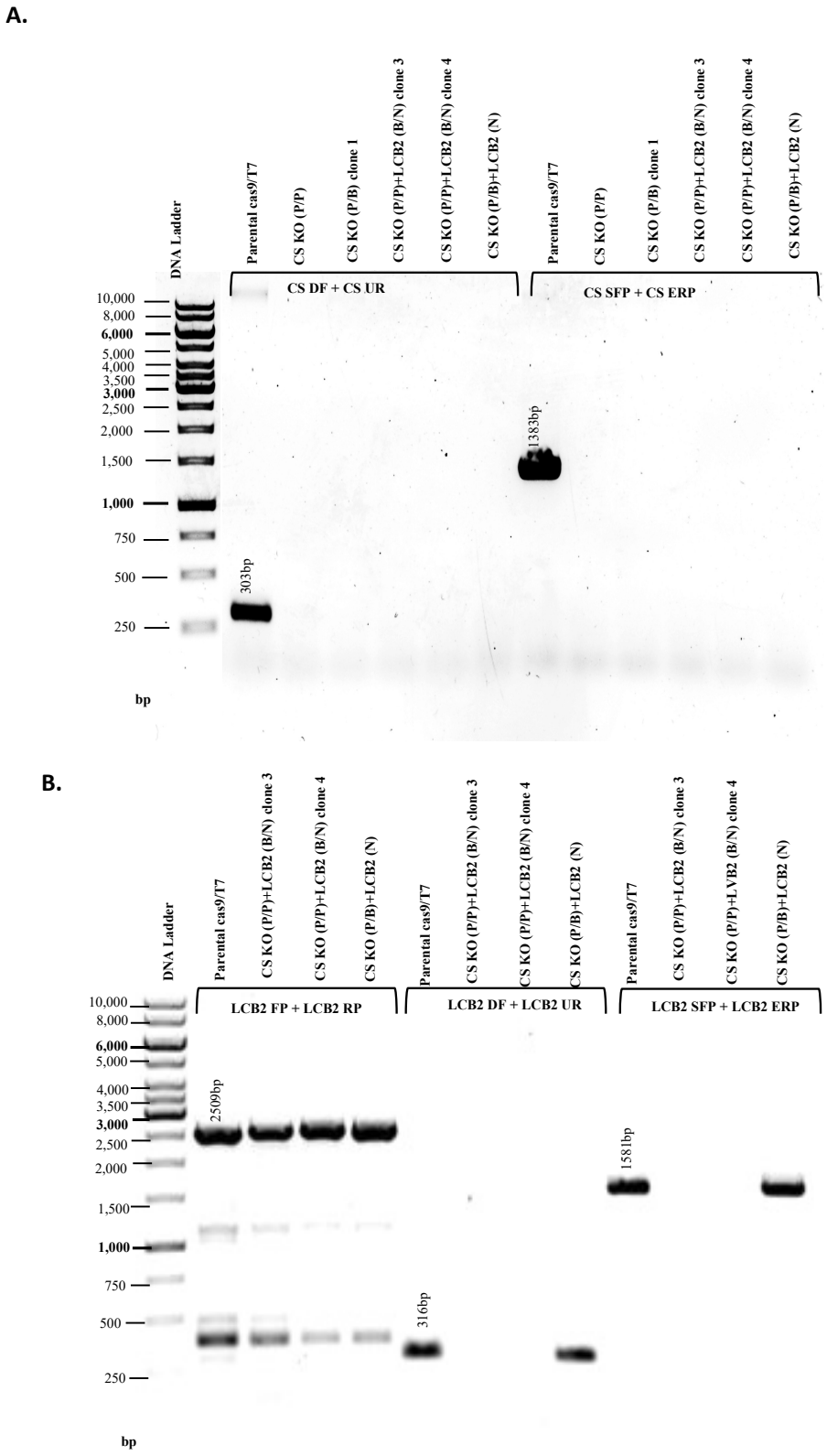

Figure 50: PCR diagnostics of the status of cloned ceramide synthase and LCB2 (SPT) knockout using blasticidin, puromycin and neomycin (G418) resistance. Size of expected fragment annotated.

Miltefosine transporter and LCB2 knockout. This combination of genes to be concurrently ablated was attempted three times however led to *L.mexicana* parasite death following selection with blasticidin, puromycin and neomycin. This possibly suggests that unlike ABC3A transporter and hypothetical protein, miltefosine transporter is not involved in any compensatory effects to allow the loss of LCB2 from the genome and parasite survival.

Hypothetical protein and serine palmitoyltransferase knockout. Dual transfected parasites were selected for blasticidin, puromycin and neomycin (G418) drug resistance and cloned. Clones (B2 and B8) were analysed using PCR diagnostics with the primers shown in Figure 51. The loss of the full-length hypothetical protein and the LCB2 (SPT) genes would evidentially confirms the loss of both genes within the 'Hypothetical protein (P/P) + LCB2 SPT (N/B) KO' clonal populations.

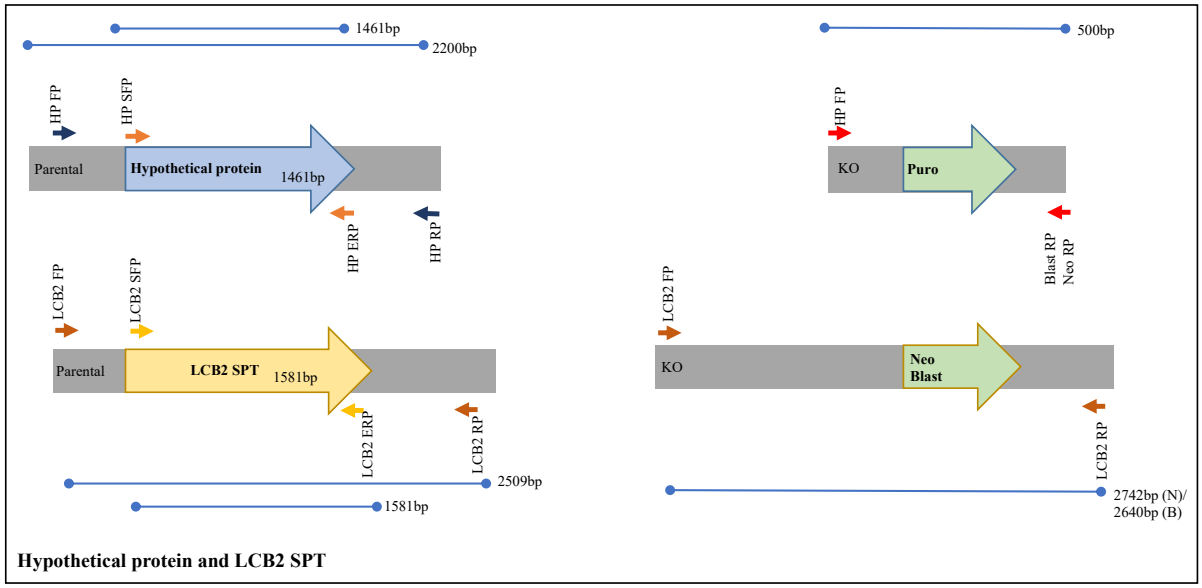

Figure 51: Primer sizes and location for hypothetical protein gene and LCB2 (SPT) gene used for diagnostic PCR. Blue and yellow representing the parental and green representing the insertion of drug resistance in location.

The primer set HP SFP and HP ERP contained the start and stop codon and was used to amplify a 1461bp fragment containing the hypothetical protein gene. The amplification of this fragment confirming the presence of the hypothetical protein. The primer set LCB2 SFP and LCB2 ERP contained the start and stop codon and was used to amplify a 1581bp fragment containing the LCB2 (SPT) gene confirming its presence. As well as to confirm the presence of the full-length gene, primers were designed within the 3' and 5' UTR of the target gene. These were used to confirm the loss of target gene and integration of drug resistance cassette. Primer set HP FP and HP RP within the UTR of the hypothetical protein gene amplifies a 2200bp fragment when target gene is present but 500bp fragment when the puromycin resistance cassette is inserted. Primer set LCB2 FP and LCB2 RP within the UTR of the SPT gene amplifies a 2509bp fragment when target gene is present but a 2640bp and 2742bp fragment when target gene is replaced with the blasticidin and neomycin resistance cassette respectively.

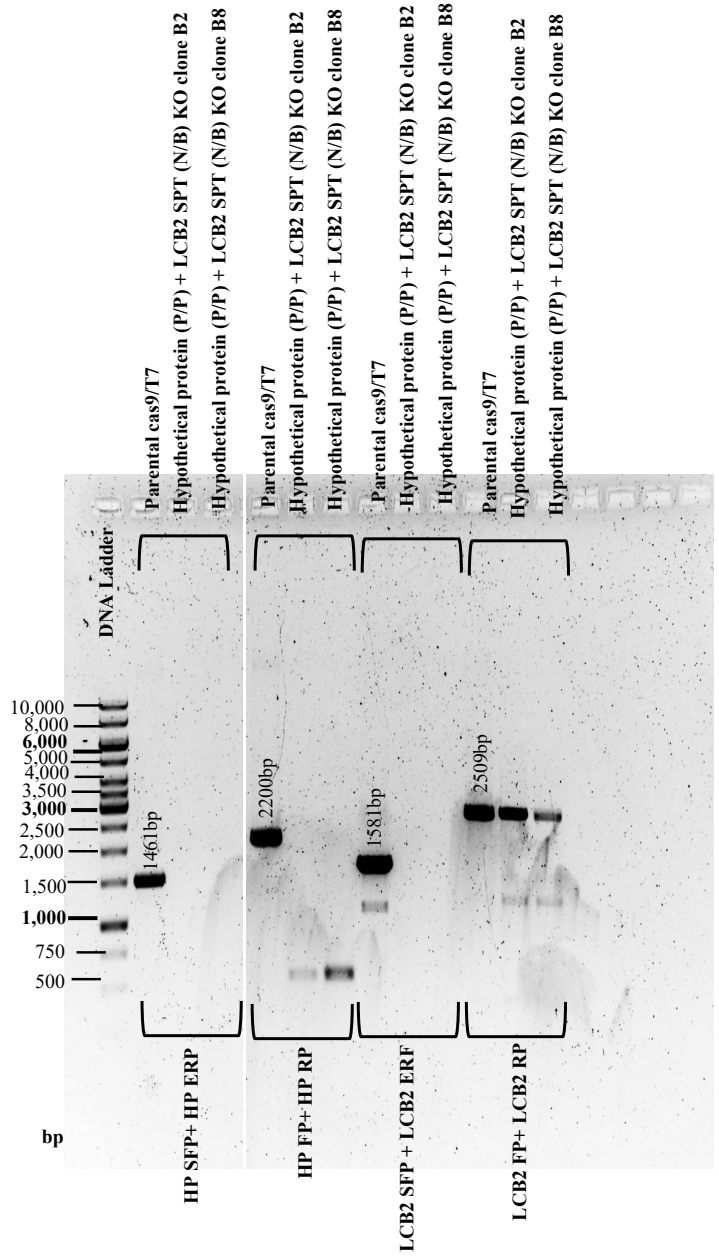

Figure 52: PCR diagnostics of the status of cloned hypothetical protein and LCB2 (SPT) knockout using blasticidin, puromycin and neomycin (G418) resistance. Size of expected fragment annotated.

Using these primer sets, the recovered Hypothetical protein (P/P) + LCB2 SPT (N/B) KO clonal populations B2 and B8 were analysed. This is shown in Figure 52. Using the primer set HP SFP and HP ERP, the full-length hypothetical protein was shown to be present in the parental Cas9/T7 population however lost in both B2 and B8 KO populations. The primer set LCB2 SFP and LCB2 ERP showed the loss of the 1581bp fragment (the full-length SPT gene) lost in both B2 and B8 KO populations. Using primers within the UTR regions of both

genes, primer set HP FP and HP RP amplified a 2200bp fragment and primer set LCB2 FP and LCB2 RP amplified a 2509bp fragment from the control parental Cas9/T7 population. These were the expected outcomes as shown in Figure 51. From both B2 and B8 KO populations, primer set HP FP and HP RP amplified a 500bp fragment and primer set LCB2 FP and LCB2 RP amplified a ~2500bp fragment. The LCB2 FP and LCB2 RP primer set cannot be used entirely for diagnostic purposes here as the 2509bp fragment from the parental Cas9/T7 is very similar to the 2640bp and 2742bp fragment when blasticidin and neomycin has replaced the SPT gene respectively. In its entirety, Figure 52 confirms the deletion of both full-length SPT and the hypothetical protein gene from both 'hypothetical protein (P/P) + LCB2 SPT (N/B) KO' clonal populations B2 and B8. These data suggested that deletion of the hypothetical protein gene facilitated loss of that encoding SPT.

ABC3A transporter and serine palmitoyl transferase knockout. Following transfection and selection for the concurrent ablation of ABC3A transporter and LCB2, the clones that survived the selection process (1 and 6) were analysed using PCR diagnostics using primers shown in Figure 53. The detection of the full-length ABC3A transporter and the SPT gene was essential to confirming the loss of both genes within the 'ABC3A1 transporter + LCB2 SPT KO' clonal populations.

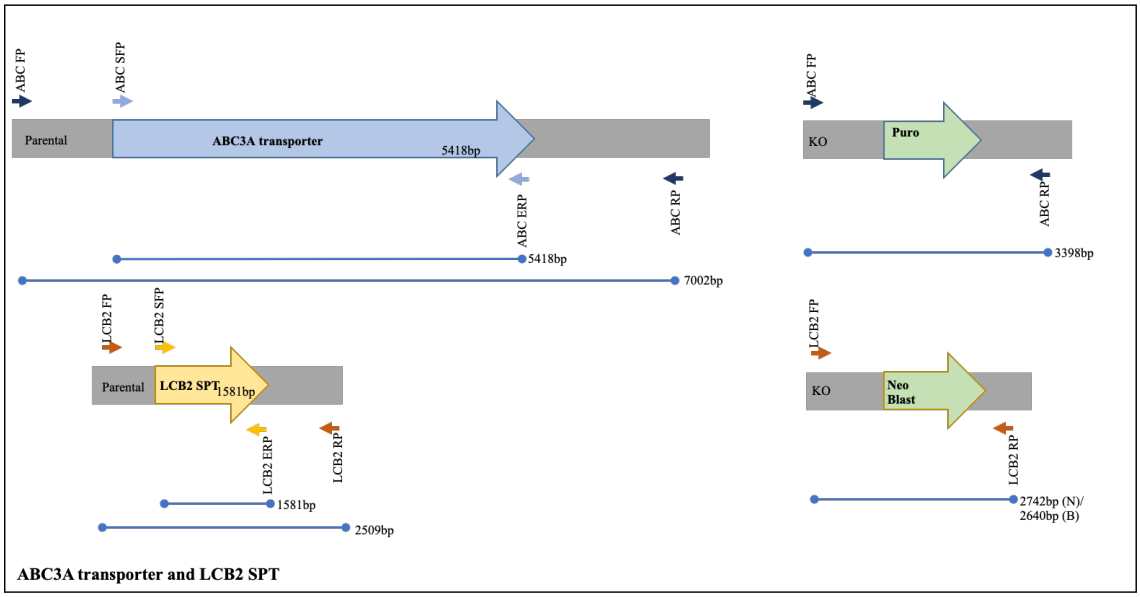

Figure 53: Primer sizes and location for ABC3A transporter gene and LCB2 (SPT) gene used for diagnostic PCR. Blue and yellow representing the parental and green representing the insertion of drug resistance in location.

Two primer sets for each target gene was designed and shown in Figure 53. Primers for containing the start and stop codon of ABC3A transporter (ABC SFP and ABC ERP) and of SPT (LCB2 SFP and LCB2 ERP) were designed to amplify a 5418bp and 1581bp fragment respectively containing the full-length gene. Primer sets for within the 3' and 5' UTR of each target gene was also designed. ABC FP and ABC RP amplified a 7002bp fragment containing ABC3A transporter from parental Cas9/T7 however would amplify a 3398bp fragment with the replacement of ABC3A transporter gene with the puromycin resistance cassette. LCB2 FP and LCB2 RP amplified a 2509bp fragment containing LCB2 from

parental Cas9/T7 however would amplify a 2742bp or 2640bp fragment with the replacement of LCB2 gene with neomycin or blasticidin resistance cassette respectively.

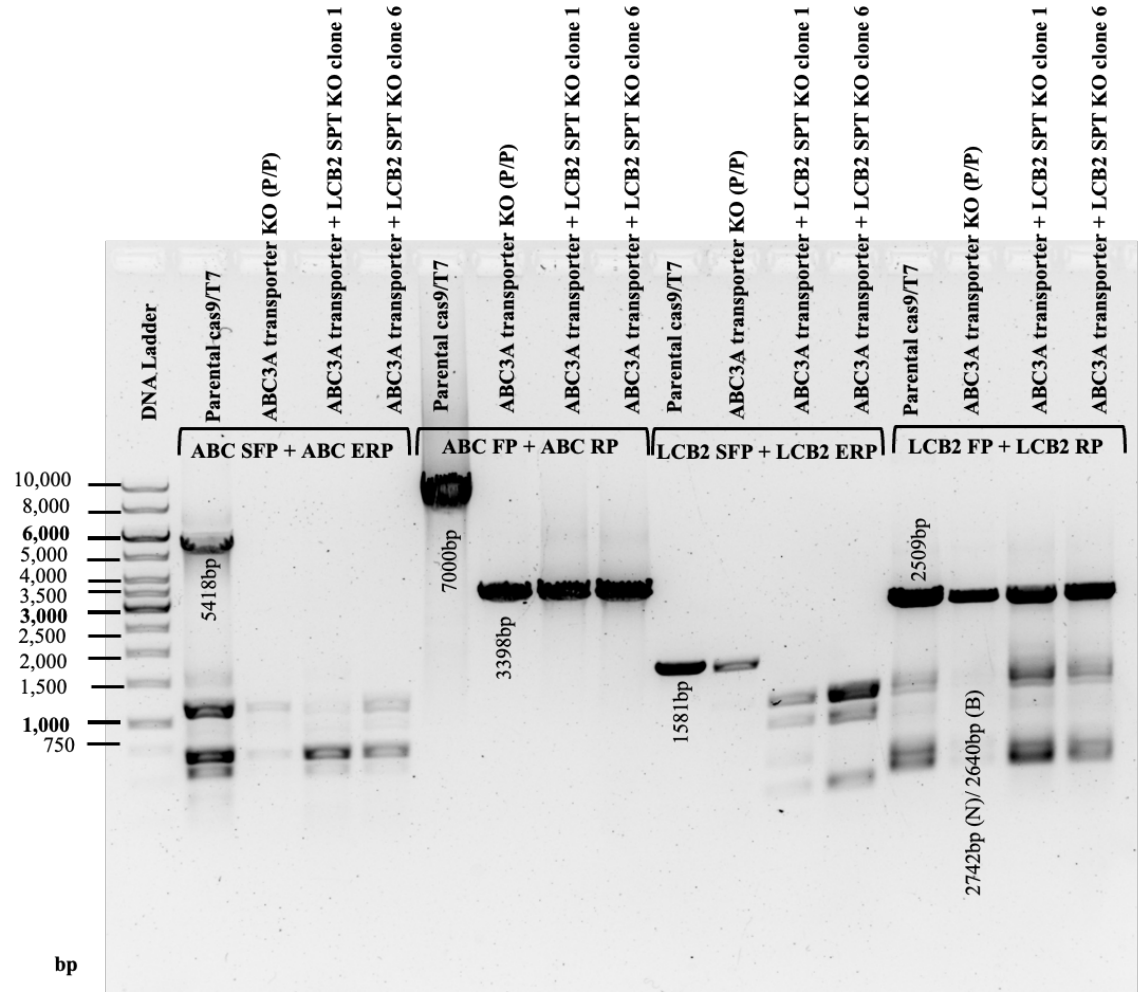

Figure 54: PCR diagnostics of the status of cloned ABC3A transporter and LCB2 (SPT) knockout using blasticidin, puromycin and neomycin (G418) resistance. Size of expected fragment annotated.

These primer sets were used to analyse the ABC3A transporter + LCB2 SPT KO clones 1 and 6 shown in Figure 54. Analysing the potential loss of the full length ABC3A transporter, primer set ABC SFP and ABC ERP was used to amplify the target gene in full. The expected 5418bp fragment was amplified from parental Cas9/T7 however not in any of the ABC3A transporter + LCB2 SPT KO clonal populations. This was similar when analysing for the loss of full length SPT using LCB2 SFP and LCB2 ERP. The expected 1581bp fragment was

amplified from parental Cas9/T7 and ABC3A transporter KO however not in any of the ABC3A transporter + LCB2 SPT KO clonal populations. This shows a complete loss of both SPT and ABC3A transporter gene from the ABC3A transporter + LCB2 SPT KO clonal populations (clone 1 and 6). To analyse the replacement of ABC3A transporter with puromycin repair cassette, ABC FP and ABC RP primer pair was used. This amplified a 7002bp fragment containing ABC3A transporter from parental Cas9/T7 and a smaller 3398bp fragment supporting the replacement with puromycin resistance cassette. As previously stated, the LCB2 FP and LCB2 RP primer set cannot be used entirely for diagnostic here as the 2509bp fragment in the parental Cas9/T7 is very similar to the 2640bp and 2742bp fragment when blasticidin and neomycin has replaced the SPT gene respectively.

Morphology analyses of all ABC3A transporter + LCB2 SPT KO, CS (P/P) + LCB2 SPT (B/N) KO and Hypothetical protein (P/P) + LCB2 SPT (N/B) KO clonal populations were noted with the only morphological changes seen in the ABC3A transporter + LCB2 (SPT) KO population. This is shown in Figure 55 where ABC3A transporter + LCB2 SPT KO clones 1 and 6 have a rounded cell body morphology, compared to the bullet shaped parental Cas9/T7 cells. This is similar to the morphology of ΔLmLCB2-/- population (Denny et al., 2004).

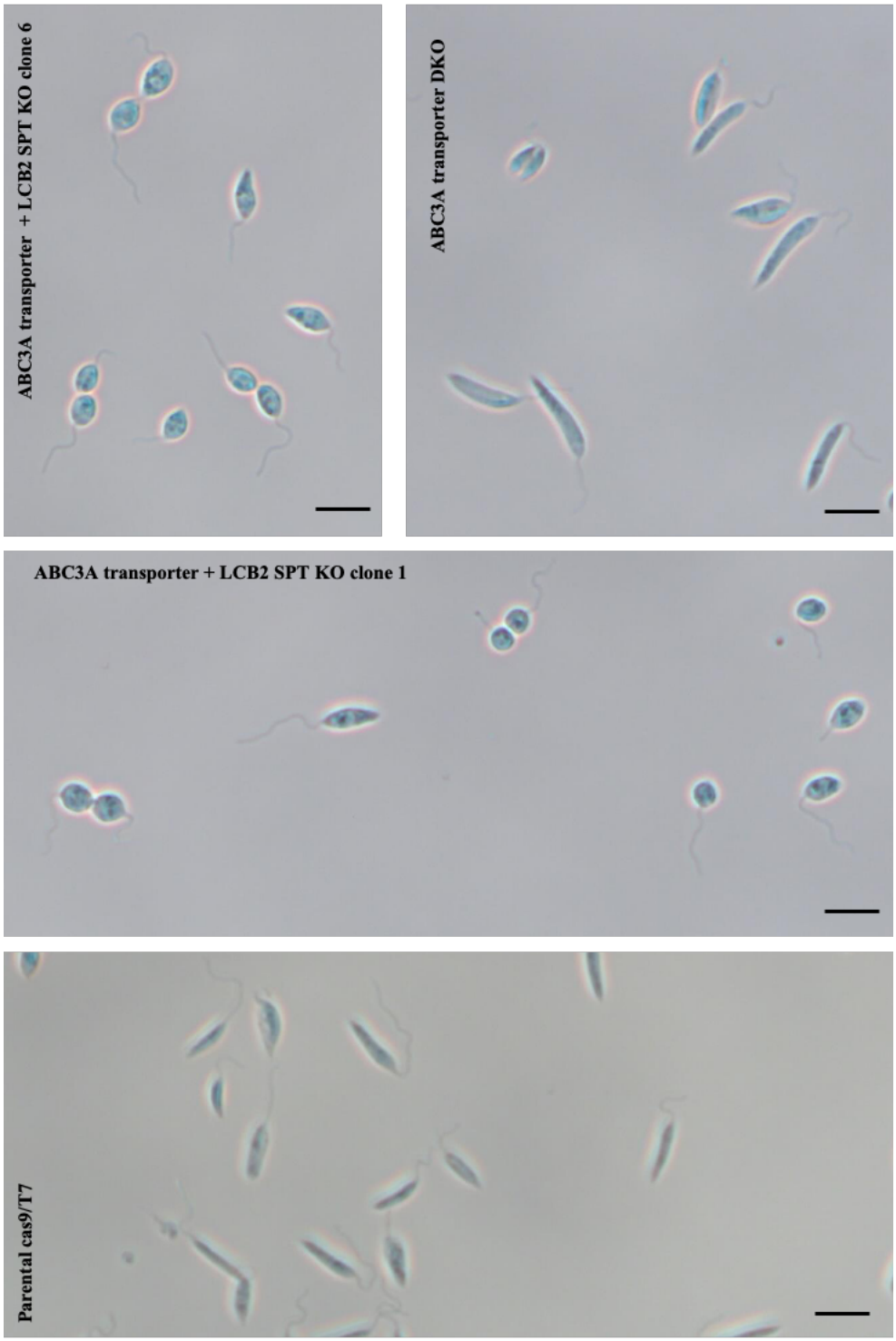

Figure 55: Differential interference contrast images of parasites from 3 days in culture

The observance of no morphological cAhanges in any of the other concurrent double targeted genes (CS + LCB2 and Hypothetical protein + LCB2), the lack of change of morphology in the ABC3A transporter KO (P/P) (labelled as ABC3A transporter DKO in Figure 55) and the

FastQC evidence of ABC3A transporter being the only gene completely ablated in all ΔLmLCB2-/- population collectively suggests that this ABC3A transporter + LCB2 SPT KO is very close genetically and phenotypically to the ΔLmLCB2-/- population which was stated to be a sphingolipid free leishmania cell line with no *de novo* sphingolipid (Denny et al., 2004). Further investigation to analyse the lipid profile of this ABC3A transporter + LCB2 SPT KO may provide information into some compensatory effects that ABC3A transporter gives *L. mexicana* parasites, allowing the loss of LCB2 from the genome.

6.3 Lipid profiles of ABC3A transporter and Serine Palmitoyltransferase knockout

Denny et al., 2004 reported the *ΔLmLCB2-/-* population to be sphingolipid free by metabolic labelling and mass spectrometry analysis. Parasites labelled with [^{3}H]-serine detected changes in the *de novo* synthesis of ceramide as well as ^{3}H-inositol to detect reduced IPC levels which is the predominant *de novo* synthesized sphingolipid in these *Leishmania* parasites (Denny et al., 2004). Mass spectrometry further confirmed the loss of the sphingolipid IPC in the *ΔLmLCB2-/-* population. This therefore confirmed that the ablation of LCB2 (SPT) in *Leishmania* affects the *de novo* synthesis of ceramides and sphingolipids, with glycolipid upregulation possibly compensating for sphingolipid downregulation to maintain the integrity of the cell membrane (Denny et al., 2004). With the morphological and genetic similarity between the ΔLmLCB2-/- population and ABC3A transporter, targeted lipid analysis of the sphingolipid biosynthetic pathway of ABC3A transporter was carried out as stated in the Materials and Methods to detect if it contained a similar lipid profile to *ΔLmLCB2-/-* as reported by Denny et al., 2004.

CER = Ceramides	GSL = Glycosphingolipids
TAG = Triacylglycerol	IPC = Inositol phosphorylceramide
SE = Sterol ester	LPC = Lysophosphatidylcholine
PS = Phosphatidylserine	LPE = Lysophosphatidylethanolamine
PG = Phosphatidylglyvcerol	LPI = Lysophosphatidylinositol
PI = Phosphatidylinositol	MAG = Monoacylglycerol
PE = Phosphatidylethanolamine	PC = Phosphatidylcholine
DAG = Diacylglycerol	CL = Cardiolipin

Table 13: List of lipids found in samples analysed by LC-MS with abbreviations used in Figures

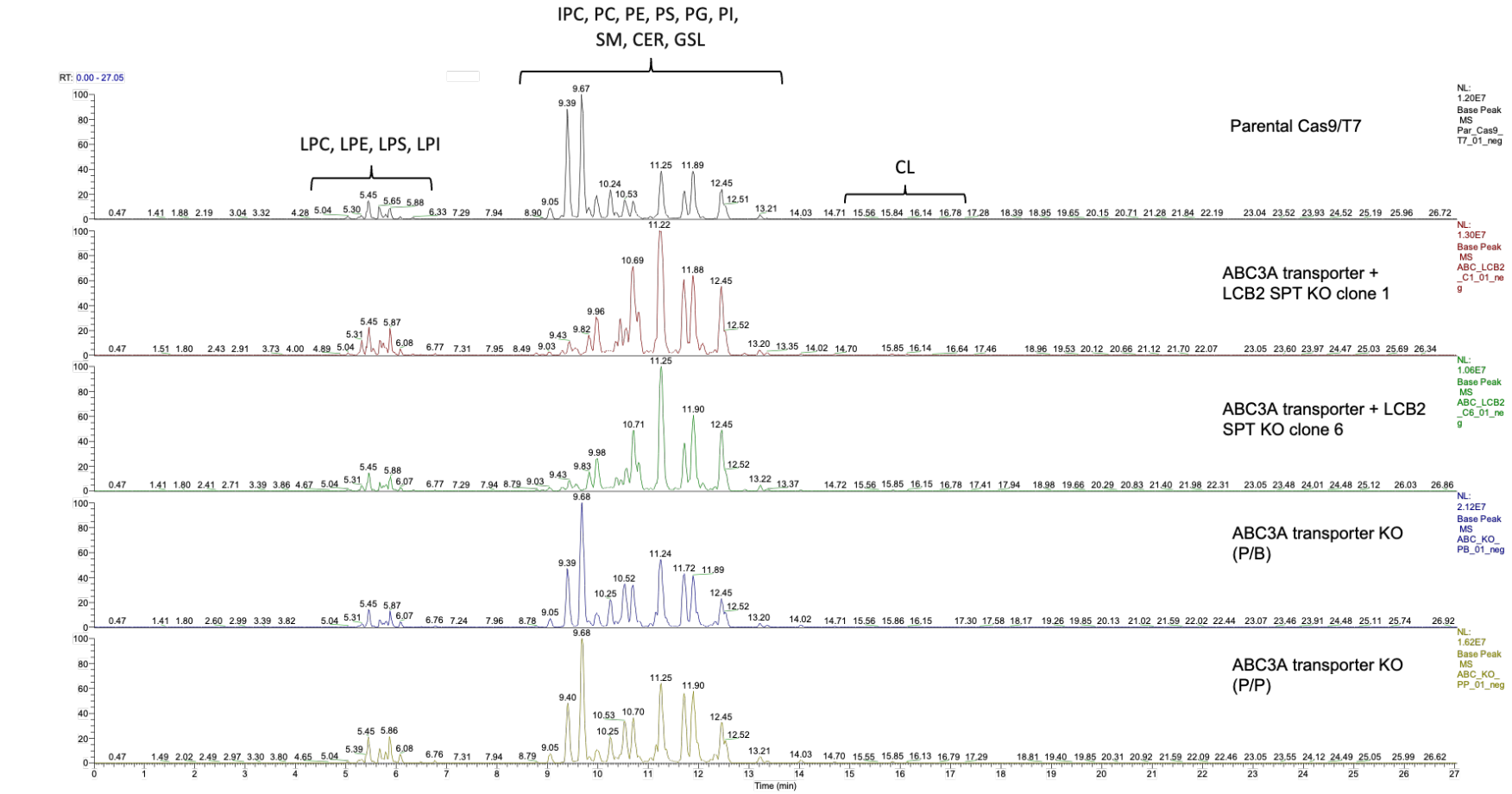

Figure 56:Global lipidomic analysis of KO populations (n=5 replicates) and the parental Cas9/T7 (n=3 replicates) populations analysed by LC-MS on a Thermo Orbitrap Exactive system in negative ion modes.

Global lipidomic analysis of lipids listed in Table 13 as shown in Figure 56 using LC-MS in the negative ion mode. The graph shows no large differences of lysophospholipids and phospholipid cardiolipin (CL) between populations, however changes of ion signal profile can be visualised on the chromatograph within the region containing ion signals attributable to inositol phosphorylceramide (IPC) and ceramides peaks. Levels of IPC, ceramides and sterols were analysed in more detail shown in Figure 58, Figure 59 and Figure 60 respectively.

Global lipidomic analysis of lipids listed in Table 13 and shown in Figure 57 using LC-MS in the positive ion mode. The chromatograph generally shows no large differences between populations. ABC3A transporter KO samples show a slight reduction of ion signals attributable to triacyglycerol (TAG) and sterol ester (SE) compared to both parental Cas9/T7 and ABC3A transporter + LCB2 SPT KO samples. However, this slight increase in lipid components (TAG and SE) which may potentially be lipid droplets suggests parasites undergoing autophagy for managing lipid metabolism (Guhe et al., 2023).

LC-MS Chromatograms - Positive Ion Mode

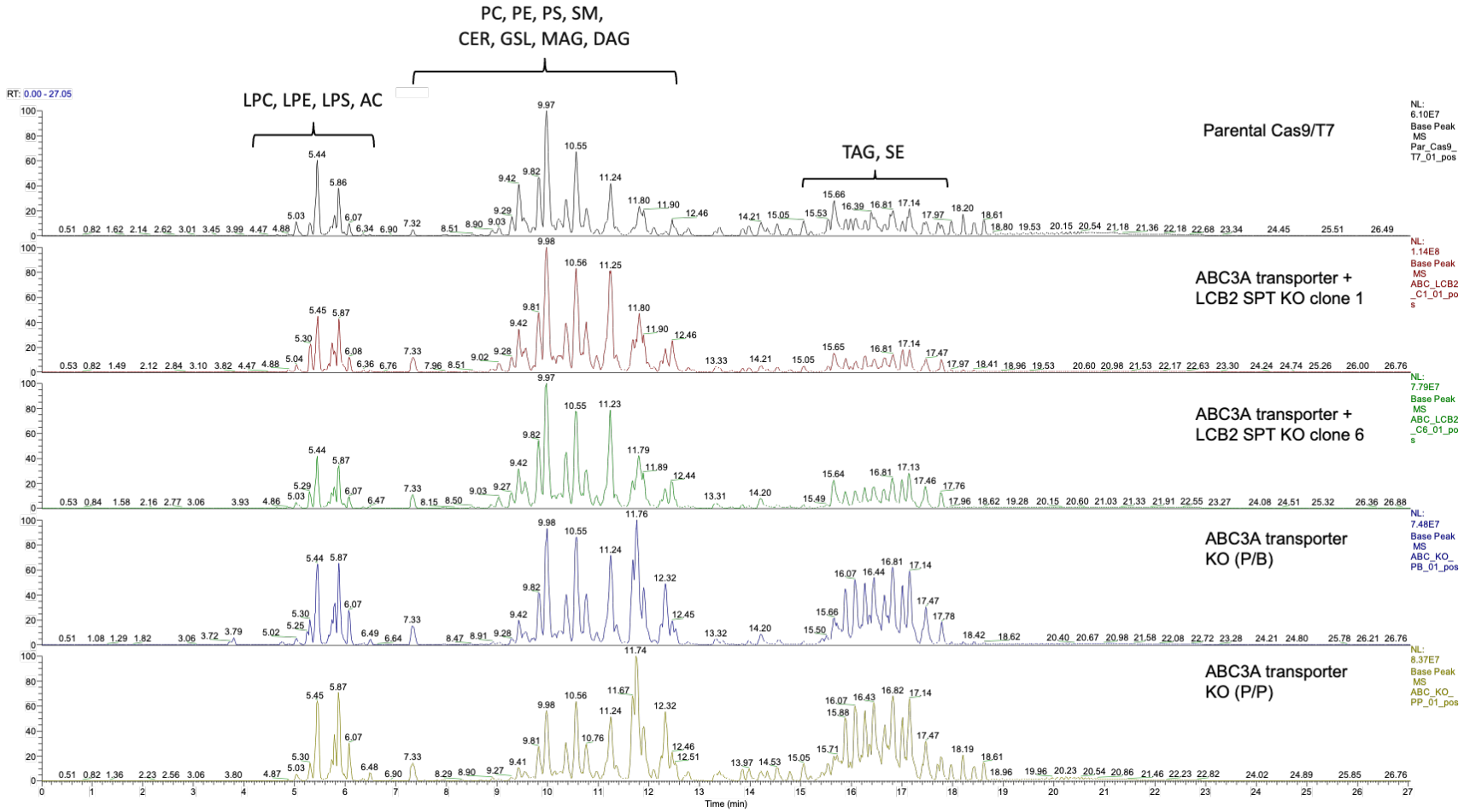

Figure 57: Global lipidomic analysis of KO populations (n=5 replicates) and the parental Cas9/T7 (n=3 replicates) populations analysed by LC-MS on a Thermo Orbitrap Exactive system in positive ion modes.

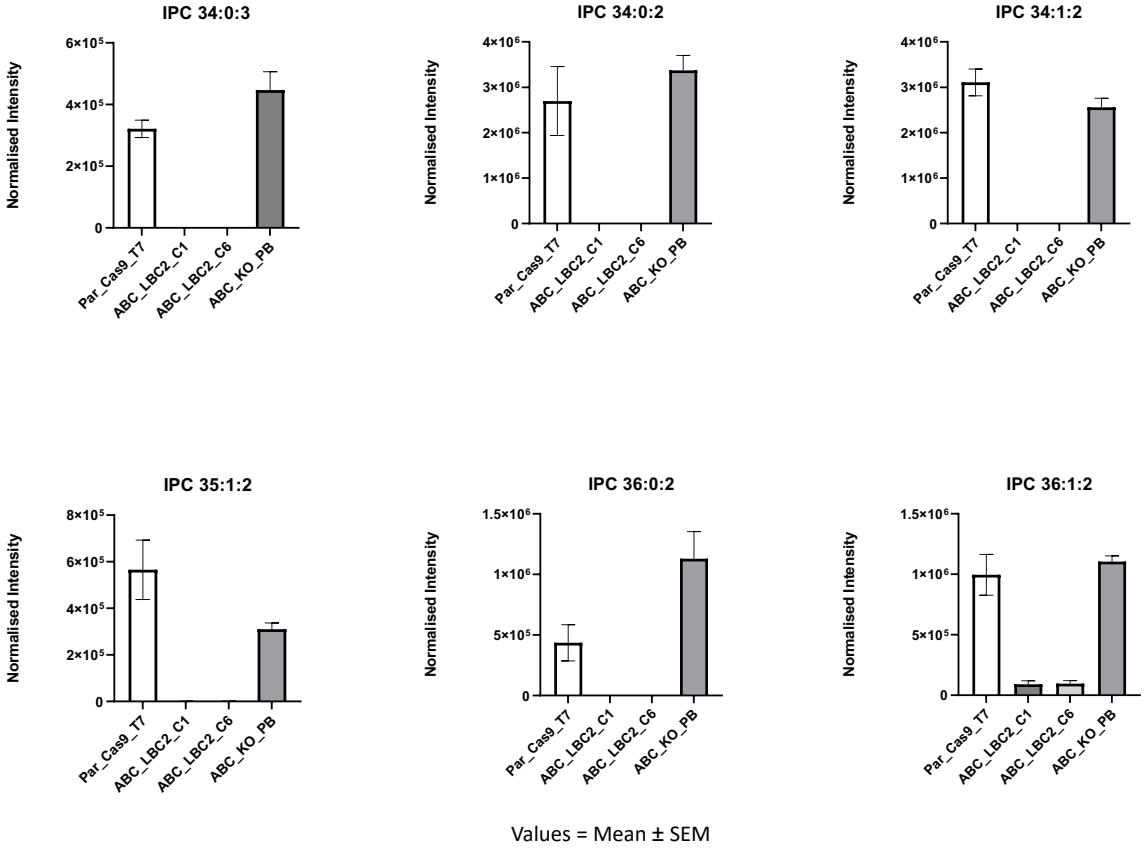

Figure 58: Relative Levels of Inositol Phosphorylceramide (IPC) in KO populations (n=5 replicates) and the parental Cas9/T7 (n=3 replicates) populations

Six different forms of IPC were analysed for their relative levels within parental Cas9/T7, ABC3A transporter KO populations (P/B) and (P/P), and ABC3A transporter + LCB2 SPT KO clones 1 and 6 (Figure 58). The data shows an ablation of ion signals attributable to these molecular species of inositol phosphorylceramide (IPC) in ABC3A transporter + LCB2 SPT KO clones 1 and 6. This ablation is not present in the ABC3A transporter KO populations (P/B) and (P/P) samples.

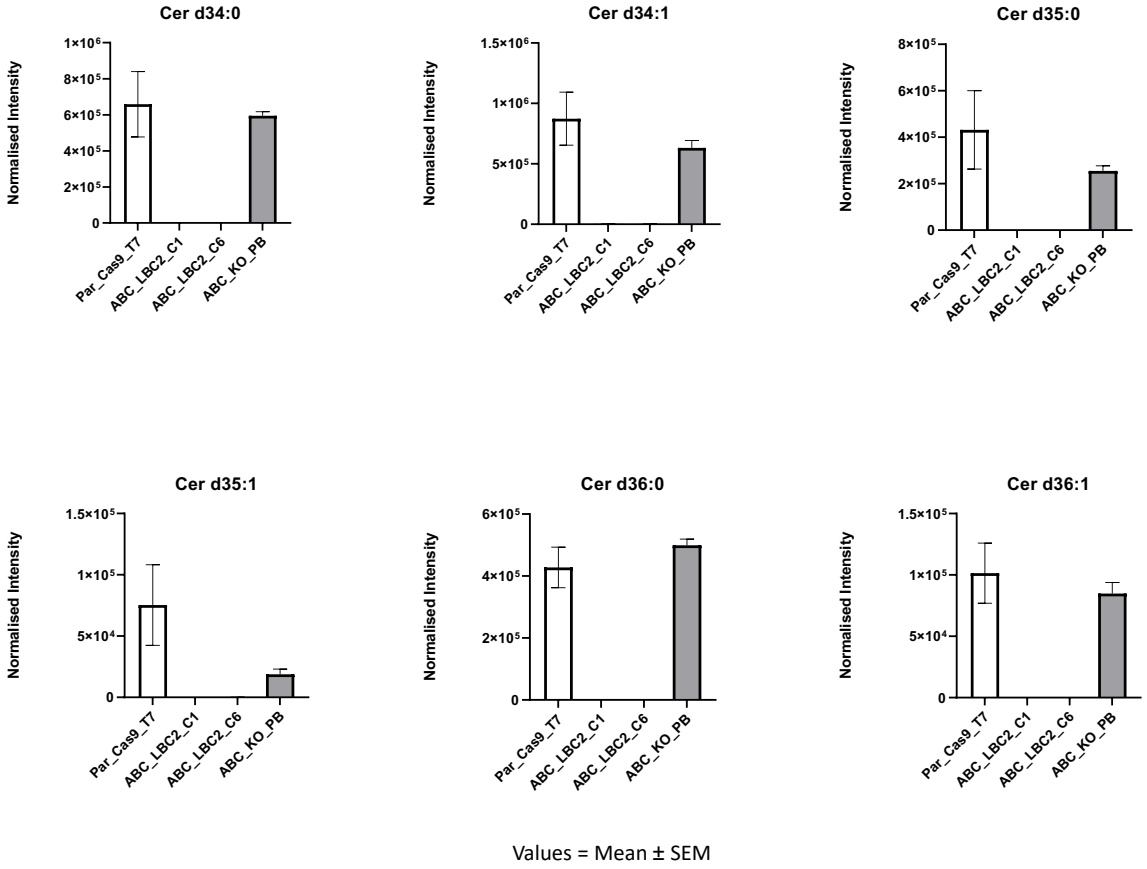

Figure 59: Relative Levels of ceramides (Cer) in KO populations (n=5 replicates) and the parental Cas9/T7 (n=3 replicates) populations analysed by LC-MS

Six different forms of ceramide were analysed for their relative levels within parental Cas9/T7, ABC3A transporter KO populations (P/B) and (P/P), and ABC3A transporter + LCB2 SPT KO clones 1 and 6 (Figure 59). The data shows an ablation of ion signals attributable to these molecular species of ceramide in ABC3A transporter + LCB2 SPT KO clones 1 and 6. Similar to in the IPC data in Figure 58, this ablation is not present in the ABC3A transporter KO populations (P/B) and (P/P) samples.

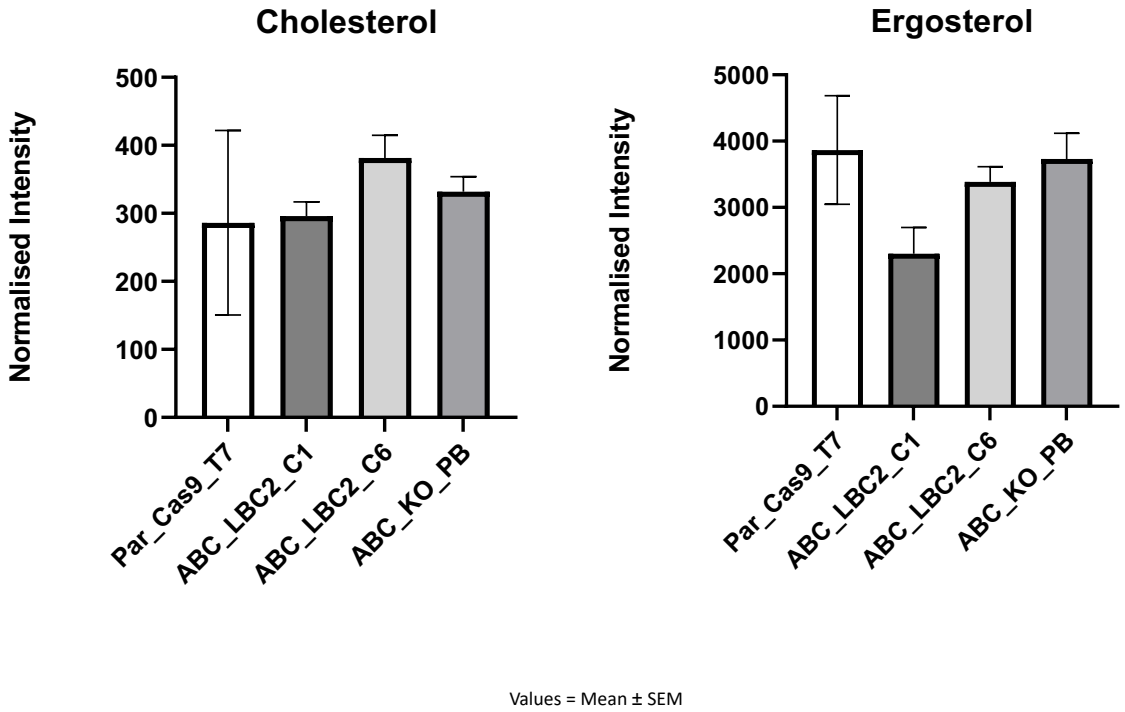

Figure 60:Relative Levels of sterols in KO populations (n=5 replicates) and the parental Cas9/T7 (n=3 replicates) populations analysed by LC-MS

The data comparing the ion signals attributable to cholesterol and ergosterol shown in Figure 60 is not as clear as data comparing ion signals for IPC and ceramide. With ABC3A transporter + LCB2 SPT KO clones 1 and 6, although genetically modified in the same manner to excise SPT and ABC3A transporter from the same locations they have differing levels of ion signals attributable to cholesterol and ergosterol. Generally, it suggests that the levels of cholesterol and ergosterol may differ slightly however no complete ablation occurs here. This may need follow-on analyses.

Summarizing the data showed in 6.3, the changes of lipid profile of ABC3A transporter and LCB2 KO is comparable to that of the ΔLmLCB2-/- population reported by Denny et.,al 2004 due to the loss of IPC (Figure 58) and ceramide (Figure 59) synthesis in these parasites suggesting similar lipid remodelling having occurred to survive the specific lipidomic changes associated with LCB2 and ABC3A transporter proteins being ablated.

6.4 Assessing drug resistance in gene ablations associated with Serine Palmitoyltransferase ablation.

Armitage et al., 2018 reported *L. major* Δ*Lm*LCB2-/- parasites to have a three-fold increase in miltefosine EC_{50} when compared to wild-type *L.major* parasites. With many gene ablations found within the Δ*Lm*LCB2-/- population, investigating each gene KO as well as the ABC3A transporter + LCB2 SPT KO clones 1 and 6 may inform which genes confers drug resistance. Growth curves prior to drug resistant assays showed no significant differences in the rate of cell division across the different KO populations.

Amphotericin B was tested against *L.mexicana* promastigotes CRISPR-Cas9 KO of the genes associated with LCB2 ablation (Table 12)**;** hypothetical protein KO, phospholipid-transporting ATPase 1-like protein (miltefosine transporter) KO, ABC3A transporter KO, Ceramide Synthase KO, ABC3A transporter and LCB2 KO (clone 1 and clone 6) and the parental Cas9/T7 line used as a control. This experiment (data shown in Figure 61) was done using three biological repeats with each containing three technical repeats. In the nonlinear curves (not shown), all KO curves show an increase in sensitivity to Amphotericin B compared to the parental cas9/T7 cell line curve. This is further indicated when collating the EC_{50} values to find the mean EC_{50} (Figure 61). The parental cell line with no gene ablation gave a mean EC_{50} of 83.47nm. Hypothetical protein KO, miltefosine transporter KO and ABC3A transporter KO populations have EC_{50} values of 51.09nm, 48.88nm and 54.94nm respectively; a 0.6-fold decrease. Ceramide synthase KO, ABC3A transporter + LCB2 clone 1 and clone 6 populations show further sensitivity to Amphotericin B with EC_{50} values of 25.54, 19.88 and 26.95 respectively. Surprisingly, ABC3A transporter + LCB2 clone 1 and clone 6 populations although genetically have the same targeted gene ablations differ in amphotericin B sensitivity, with clone 6 being slightly more resistant to the drug compared to

clone 1. Overall, this shows that all the gene ablations conferred heightened sensitivity to amphotericin B.

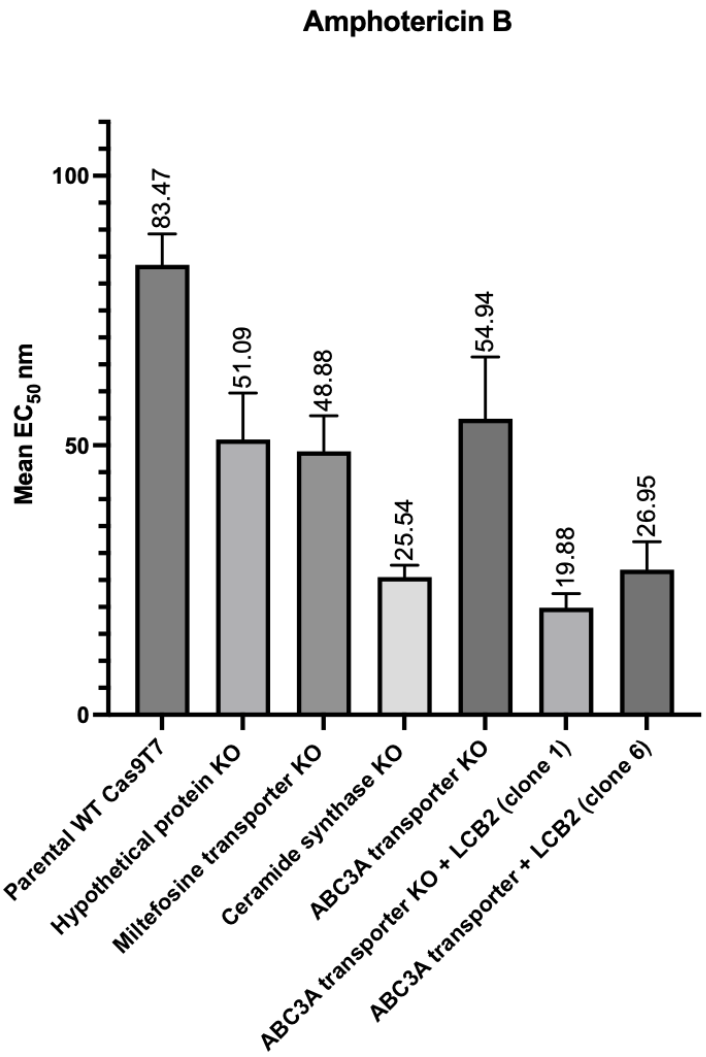

Figure 61: Amphotericin B sensitivity assay showing EC_{50} of KO populations (n=9 replicates). GraphPad Prism 7 software was used for analysis as described in Materials and Methods.

Miltefosine was tested against *L.mexicana* promastigote CRISPR-Cas9 KO of the genes associated with LCB2 ablation (Table 12). This drug sensitivity assay was repeated three times (biological repeats) each containing three technical repeats. In the nonlinear curves, the cell viability decreases with increase in drug concentration, similar to amphotericin B. However, the miltefosine transporter KO population result has very little sensitivity to

miltefosine even at high concentrations of 100μM drug. This was shown when collating the EC_{50} values to find the mean EC_{50} (Figure 62) which are all statistically significant. The parental cell line has an EC_{50} value of 6.79μM. Hypothetical protein KO, ABC3A transporter KO, ABC3A transporter + LCB2 KO clone 1 and clone 6 has EC_{50} values of 1.72μM, 2.32μM, 1.75μM and 0.28μM respectively; all more sensitive to miltefosine compared to the parental cell line. Miltefosine transporter KO population showed a mean EC_{50} value 179.69μM, a 26-fold increase in resistance compared to the parental cell line. Similar to in the amphotericin B sensitivity assay, ABC3A transporter + LCB2 KO clone 1 and clone 6 have different EC_{50} values with, ABC3A transporter + LCB2 KO clone 1 being more resistant to miltefosine than ABC3A transporter + LCB2 KO clone 6 (a 144.8276% difference).

Both amphothericin B and miltefosine drug sensitivity assays suggests that the three fold increase in miltefosine resistance showed by Δ*Lm*LCB2-/- parasites reported by Armitage et al., 2018 is confered to the population not through the ablation of miltefosine transporter gene and not the ablation of hypothetical protein, ABC3A transporter or LCB2 (SPT) however further experimentation will be needed to confirm whether or not amastin-like protein confers any resistance to Δ*Lm*LCB2-/- parasites.

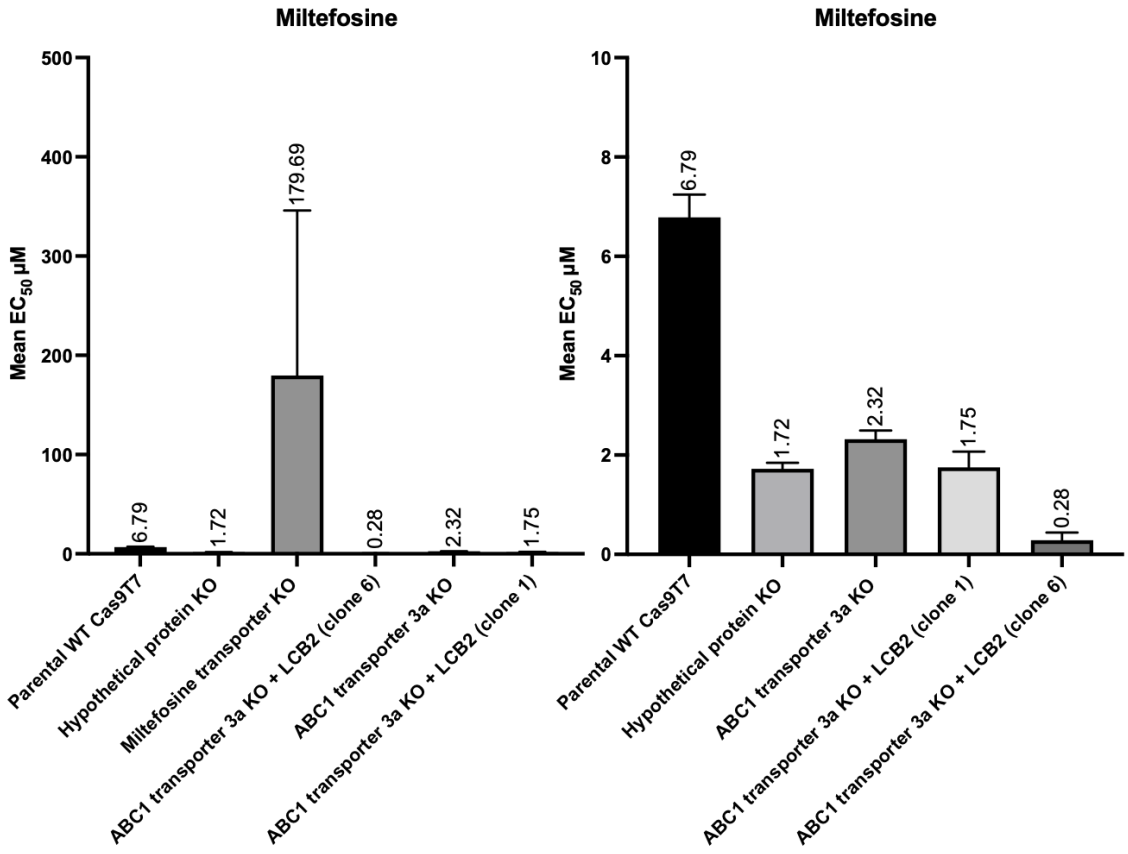

Figure 62: Miltefosine sensitivity assay showing EC_{50} of KO populations (n=9 replicates). GraphPad Prism 7 software was used for analysis as described in Materials and Methods. Statistical data in appendix.

6.5 Conclusion and future work

Δ*Lm*LCB2-/- parasites generated by two rounds of homologous recombination and drug selection (Zhang et al., 2003, Denny et al., 2004) were successfully generated, showing the LCB2 protein as being inessential to the survival of *Leishmania* parasites. With the role of SPT being important for the sphingolipid biosynthetic pathway (Hanada, 2003), the highly plastic genome of *Leishmania* causing KO failures (Jones et al., 2018) and the findings of additional non-targetted null genes within the Δ*Lm*LCB2-/- population; it was important to probe these genes individually and in addition to LCB2. With the inability to KO LCB2 (SPT) from *L.mexicana* using the CRIPSR Cas9 system, the findings of additional non-targetted null genes within the Δ*Lm*LCB2-/- population was hypothesised to confer genetic advantages for parasite survival and play a role in the three fold miltefosine drug resistance reported by Armitage et al.

The hypothetical protein (Figure 52), ceramide synthase (Figure 50) and ABC3A transporter (Figure 50) allowed for the ablation of LCB2 when concurrently generated. Ceramide synthase is within the sphingolipid biosynthetic pathway and therefore it was predicted to facilitate the KO of LCB2 as downstream of SPT is rendered ineffective, therefore a control. The inability to KO LCB2 using CRISPR Cas9 where the chances of additional ablations occurring is low suggests that LCB2 is essential in wildtype *Leishmania* parasites. However, in *Leishmania* parasites 'modified' by the loss of ABC3A transporter or hypothetical protein, the additional ablation of LCB2 (SPT) is possible due to the loss of LCB2 functionality compensated for. The ability to KO ABC3A and hypothetical protein in parallel to LCB2 KO suggests that at least one of these genes conferred some advantage. With ABC3A transporter

being the only gene with known function and shown to be 100% ablated from the Δ*Lm*LCB2-/- population, this dual KO was focussed on.

ABC3A transporter and SPT KO clone 1 and 6 had a similar rounded cell body morphology to Δ*Lm*LCB2-/- parasites (Figure 55) and had a complete loss in IPC (Figure 58) and ceramide synthesis (Figure 59) confirmed by mass spectrometry. Drug resistance of miltefosine (Figure 62) and amphotericin B (Figure 61) surprisingly showed all gene KOs exhibiting sensitivity to amphotericin B and only miltefosine transporter KO exhibiting complete resistance to miltefosine at a mean EC_{50} value of 179.69μM, a 26-fold increase to parental cell line (Figure 62). The parental cell line has an EC_{50} value of 6.79μM to miltefosine; ABC3A transporter + LCB2 KO clone 1 and clone 6 are hypersensitive to miltefosine with EC_{50} values of 1.75μM and 0.28μM respectively. As the Δ*Lm*LCB2-/- population is not clonal, the low level of parasites with the miltefosine transporter gene KO in the population allows for a small population to survive giving the 3-fold increases in resistance reported by Armitage et al.

The function of ABC3A transporter protein in transportation of lipids and in sterol trafficking across the PM may allow the ablation of LCB2 (SPT) and therefore *de novo* sphingolipid biosynthesis does not occur. This allows the membrane fluidity to be maintained without endogenously synthesised sphingolipids. LCB2 (SPT) KO may only be possible when concurrently KO with ABC3A due genome plasticity allowing further unknown adaptations/ genomic changes. We can conclude that as previously reported, genetic plasticity in *Leishmania* parasites is involved in the ability to create null genes. This data collectively indicates the importance in using WGS in genetically modified *Leishmania* parasites to investigate if other non-targeted events have occurred to allow and compensate for the

survival of parasites as observed in the Δ*Lm*LCB2-/- population, particularly in a long process of gene ablation such as homologous recombination.

The aims set in Chapter 1 of monitoring the multiple non-targeted gene ablations in *L. major* Δ*Lm*LCB2-/- using CRISPR Cas9 and monitoring of the sphingolipidome to investigate the lipidomic changes that occur when the sphingolipid biosynthesis pathway is genetically probed was achieved. The result from this chapter gives insight into the essentiality of the SPT the first enzyme of the pathway. LCB2 (SPT) not being able to be ablated along with the Genome Report (see appendix) of Δ*Lm*LCB2-/- locating additional ablations within the population brought about the research questions: Do these genes compensatory effects allow for LCB2 (SPT) to be ablated in the published Δ*Lm*LCB2-/- population? The results suggests that the ABC3A transporter protein does aid in the ability to ablate LCB2 (SPT). These compensatory deletions further support genome plasticity playing a role in published essential gene KO such as the Δ*Lm*LCB2-/- population.

Chapter 7: Conclusions on Sphingolipid Biosynthesis as an Antileishmanial Target and the Confounding Effects of Genome Plasticity

With the most activity *Hs*SK1 inhibitor PF-543 (Schnute et al., 2012), showing the second highest potency in the *Leishmania* cell-based assay. RB-005 was the most potent compound. However, in all cases Δ*Lm*LCB2-/- was more sensitive to the inhibitors indicating that SK and/or the sphingolipid biosynthetic pathway is not the target. This lack of specific *Leishmania* SK inhibition using inhibitors known to target *Hs*SK could be due to the overall divergence of sequence identity when looking outside of the conserved regions. The *Leishmania* SK protein has highly disordered areas predicted by HHPred, along with a divergence of sequence identity and a low resolution AlphaFold prediction suggesting a large divergence to the *Hs*SK protein. Looking at the predicted tertiary structure there are five conserved regions within the main hydrophobic pocket that makes up the active site, C1- C5 regions which contain the important residues for *Hs*SK inhibitor binding. Many of these residues are conserved across *Hs*SK to *Lmx*SK with conservative changes to those similar in properties and size. Δ*Lm*LCB2-/- (Denny et al., 2004), a reported sphingolipid-free *Leishmania* cell line predicted to lack SK activity, was used to test *Hs*SK inhibitors. Although there is conservation within the active site of the *Leishmania* enzyme, *Hs*SK inhibitors PF-543, ABC-29640, 55-21 and RB-005 were shown not to target the *Leishmania* sphingolipid biosynthetic pathway in these phenotypic assays. The result from Chapter 3 gives insight into the research questions and aims stated previously. It has confirmed the tested *Hs*SK inhibitors has suggested differences between the areas outside and potentially within the conserved regions. Bioinformatic analysis of the protein sequence of using COBALT MSA alignment and BLAST global alignment (using program Needleman-Wunsch alignment of two sequences), CLUSTAL sequence alignment and Alphafold predictions supported this divergence outside of the conserved regions. Overall, the tested Human SK inhibitors

suggests that the folded *LmjSK* protein is possibly divergent enough for cross-species interaction due to conserved regions to not occur. This however required a study into the structure of the *Leishmania* SK protein which is discussed in Chapter 4 and directed the need to produce the *Leishmania* sphingosine kinase enzyme.

In Chapter 4, small levels of full-length protein were confirmed by MS; however not sufficient expression was achieved for purification to be attempted. Attempt to solve this led to designing constructs that do not containing predicted disordered regions according to the HHpred report and only the active site and conserved regions. This however did not yield any soluble protein when using Shuffle, T7 Express and (B) BL21(DE3) Competent *E.coli* cell types. Lemo21 (DE3) did achieve a small amount of soluble protein. The change of expression cell type to ArcticExpress competent cell also showed some success in the expression of soluble protein. The conserved region (labelled LmxM.26.0710-whelix) can be expressed within the soluble fraction in certain cells such as ArcticExpress cells in the correct conditions. However, during purification, this protein was lost from the flowthrough and wash. This suggests a potential sequestration of the His tag within a fold of the protein thus making it unable to interact with the immobilized Nickel ion responsible for the affinity. This may be fixed by denaturation of proteins prior to purification, moving the His-tag to the opposite terminus of the protein to make it more accessible or using a different tag. The commercial production of the conserved region was not successful, suggesting that alternative expression systems may be required. Insect, yeast, or mammalian cell-based systems employ the benefits of protein folding and eukaryotic post-translational modifications. Without a purified protein, further understanding of *Leishmania* SK requires genetic evidence of its essentiality which was discussed in Chapter 5. Knowledge of its essentiality by generating a SK free *Leishmania* cell line will aid in the understanding of the

effect targeting the *Leishmania* SK directly using an inhibitor will result in unlike the non-specific targeting showed in Chapter 3.

The inability to validate the potential of SK as a drug target chemically through phenotypic screening and the recent availability of the CRISPR-Cas9 system in *L. mexicana,* prompted a genetic approach to SK validation in Chapter 5. The push for a sphingosine kinase (SK) knockout (KO), whilst successful in disrupting the loci, demonstrated that the plasticity of the genome facilitated maintenance of the presumably essential enzyme elsewhere in the *Leishmania* DNA. Generating a SK null was successfully published by Zhang et al, 2013, however these null population maintained enzyme activity. Coupled with the inability to easily KO SK using CRISPR-Cas9 in *L. mexicana* without selecting for unwanted genetic changes such as a translocation of SK in some form to another genomic location, it is proposed in Chapter 5 that SK in *Leishmania* spp is essential. Due to the crucial role of SK within the sphingolipid biosynthetic pathway, toxic sphingoid base (SB) accumulation or substrate diminution when SK expression is reduced (Zhang et al, 2013) or overexpressed is likely to be detrimental to *Leishmania* proliferation. Together these data strongly suggest that SK is an essential gene for these parasites and, given its divergence from the mammalian orthologue, may prove to be an ideal drug target. However, further confirmation of the essentiality of SK should be gained using the DiCre recombinase system (Duncan et al., 2016). The results suggested that the sphingolipid biosynthetic pathway is highly important, therefore an assessment into the first enzyme within the pathway (SPT) is required (Chapter 6).

SPT, the first enzyme in the *de novo* pathway and responsible for regulation of SL biosynthesis has been reported to have been successfully ablated (Zhang et al., 2003, Denny

et al., 2004), suggesting LCB2 protein to be inessential to the survival of *Leishmania* parasites. Due to the importance of the sphingolipid biosynthetic pathway and the plasticity shown in SK null generation, the clonal Δ*Lm*LCB2-/- population was probed using whole genome sequencing (WGS) revealing additional non-targetted null genes. With the inability to produce an LCB2 null from *L .mexicana* using the CRIPSR Cas9 system, it was proposed that the longer process of null generation by using HR allowed these additional null genes to be selected for. This was hypothesized to be due to their conferring a genetic advantage for parasite survival, leading to the ability for LCB2 to be ablated within the population. Along with LCB2, ABC3A transporter was deleted in 100% of the Δ*Lm*LCB2-/- clonal population. Ablation of these genes concurrently in *L. mexicana* was shown to be straightforward. The generated *Lmx*LCB2/*Lmx*ABC3A null had very similar morphology to the Δ*Lm*LCB2-/- population, with a rounded cell body. The putative function of the ABC3A transporter protein in transportation of sterols across the plasma membrane may allow the ablation of LCB2, facilitating membrane fluidity to be maintained without endogenously synthesised sphingolipids. The results from the SK and LCB2 ablation, illustrates two main points. Firstly, the importance in using WGS in genetically modified *Leishmania* to determine if other non-targeted events have occurred to compensate, hence allowing the survival of target gene null parasites as observed in the Δ*Lm*LCB2-/- population. Without knowledge of these additional genetic changes, the wrong phenotypes may be associated to target gene. Secondly, SK has the potential to be a drug target. This has been described throughout, with the *Leishmania* SK divergence from the *Hs*SK shown by the bioinformatics analysis in Chapter 4, the lack of cross species inhibitor binding analysed in Chapter 3, its essentiality in *Leishmania* species described in Chapter 5 where SK cannot be fully ablated with the process causing genetic changes and the sphingolipid biosynthetic pathway being essential described in Chapter 6.

References

AGRAWAL, N., DASARADHI, P. V., MOHMMED, A., MALHOTRA, P., BHATNAGAR, R. K. & MUKHERJEE, S. K. 2003. RNA interference: biology, mechanism, and applications. *Microbiol Mol Biol Rev,* 67**,** 657-85.

ALAWIEH, A., MUSHARRAFIEH, U., JABER, A., BERRY, A., GHOSN, N. & BIZRI, A. R. 2014. Revisiting leishmaniasis in the time of war: the Syrian conflict and the Lebanese outbreak. *Int J Infect Dis,* 29**,** 115-9.

ALI, H. Z., HARDING, C. R. & DENNY, P. W. 2012. Endocytosis and Sphingolipid Scavenging in Leishmania mexicana Amastigotes. *Biochemistry Research International,* 2012**,** 691363.

ALLENDE, M. L., SASAKI, T., KAWAI, H., OLIVERA, A., MI, Y., VAN ECHTEN-DECKERT, G., HAJDU, R., ROSENBACH, M., KEOHANE, C. A., MANDALA, S., SPIEGEL, S. & PROIA, R. L. 2004. Mice deficient in sphingosine kinase 1 are rendered lymphopenic by FTY720. *J Biol Chem,* 279**,** 52487-92.

ALPIZAR-SOSA, E. A., KUMORDZI, Y., WEI, W., WHITFIELD, P. D., BARRETT, M. P. & DENNY, P. W. 2022. Genome deletions to overcome the directed loss of gene function in Leishmania. *Front Cell Infect Microbiol,* 12**,** 988688.

ALTSCHUL, S. F., MADDEN, T. L., SCHAFFER, A. A., ZHANG, J., ZHANG, Z., MILLER, W. & LIPMAN, D. J. 1997. Gapped BLAST and PSI-BLAST: a new generation of protein database search programs. *Nucleic Acids Res,* 25**,** 3389-402.

ALVAR, J., VELEZ, I. D., BERN, C., HERRERO, M., DESJEUX, P., CANO, J., JANNIN, J., DEN BOER, M. & TEAM, W. H. O. L. C. 2012. Leishmaniasis worldwide and global estimates of its incidence. *PLoS One,* 7**,** e35671.

ANDRADE, J. M., GONÇALVES, L. O., LIARTE, D. B., LIMA, D. A., GUIMARÃES, F. G., DE MELO RESENDE, D., SANTI, A. M. M., DE OLIVEIRA, L. M., VELLOSO, J. P. L., DELFINO, R. G., PESCHER, P., SPÄTH, G. F., RUIZ, J. C. & MURTA, S. M. F. 2020. Comparative transcriptomic analysis of antimony resistant and susceptible Leishmania infantum lines. *Parasites & Vectors,* 13.

ARMITAGE, E. G., ALQAISI, A. Q. I., GODZIEN, J., PENA, I., MBEKEANI, A. J., ALONSO-HERRANZ, V., LOPEZ-GONZALVEZ, A., MARTIN, J., GABARRO, R., DENNY, P. W., BARRETT, M. P. & BARBAS, C. 2018. Complex Interplay between Sphingolipid and Sterol Metabolism Revealed by Perturbations to the Leishmania Metabolome Caused by Miltefosine. *Antimicrob Agents Chemother,* 62.

AULNER, N., DANCKAERT, A., ROUAULT-HARDOIN, E., DESRIVOT, J., HELYNCK, O., COMMERE, P. H., MUNIER-LEHMANN, H., SPATH, G. F., SHORTE, S. L., MILON, G. & PRINA, E. 2013. High content analysis of primary macrophages hosting proliferating Leishmania amastigotes: application to anti-leishmanial drug discovery. *PLoS Negl Trop Dis,* 7**,** e2154.

BAEK, D. J., MACRITCHIE, N., PYNE, N. J., PYNE, S. & BITTMAN, R. 2013. Synthesis of selective inhibitors of sphingosine kinase 1. *Chem Commun (Camb),* 49**,** 2136-8.

BATES, P. A. & TETLEY, L. 1993. Leishmania mexicana: induction of metacyclogenesis by cultivation of promastigotes at acidic pH. *Exp Parasitol,* 76**,** 412-23.

BEJAOUI, K., WU, C., SCHEFFLER, M. D., HAAN, G., ASHBY, P., WU, L., DE JONG, P. & BROWN, R. H., JR. 2001. SPTLC1 is mutated in hereditary sensory neuropathy, type 1. *Nat Genet,* 27**,** 261-2.

BENEKE, T., MADDEN, R., MAKIN, L., VALLI, J., SUNTER, J. & GLUENZ, E. 2017a. A CRISPR Cas9 high-throughput genome editing toolkit for kinetoplastids. *R Soc Open Sci,* 4**,** 170095.

BENEKE, T., MADDEN, R., MAKIN, L., VALLI, J., SUNTER, J. & GLUENZ, E. 2017b. A CRISPR Cas9 high-throughput genome editing toolkit for kinetoplastids. *Royal Society Open Science,* 4**,** 170095.

BERN, C., ADLER-MOORE, J., BERENGUER, J., BOELAERT, M., DEN BOER, M., DAVIDSON, R. N., FIGUERAS, C., GRADONI, L., KAFETZIS, D. A., RITMEIJER, K., ROSENTHAL, E., ROYCE, C., RUSSO, R., SUNDAR, S. & ALVAR, J. 2006. Liposomal amphotericin B for the treatment of visceral leishmaniasis. *Clin Infect Dis,* 43**,** 917-24.

BERN, C., MAGUIRE, J. H. & ALVAR, J. 2008. Complexities of assessing the disease burden attributable to leishmaniasis. *PLoS Negl Trop Dis,* 2**,** e313.

BHANDARI, V., KULSHRESTHA, A., DEEP, D. K., STARK, O., PRAJAPATI, V. K., RAMESH, V., SUNDAR, S., SCHONIAN, G., DUJARDIN, J. C. & SALOTRA, P. 2012. Drug susceptibility in Leishmania isolates following miltefosine treatment in cases of visceral leishmaniasis and post kala-azar dermal leishmaniasis. *PLoS Negl Trop Dis,* 6**,** e1657.

BODLEY, A. L., MCGARRY, M. W. & SHAPIRO, T. A. 1995. Drug cytotoxicity assay for African trypanosomes and Leishmania species. *J Infect Dis,* 172**,** 1157-9.

BOITZ, J. M., GILROY, C. A., OLENYIK, T. D., PARADIS, D., PERDEH, J., DEARMAN, K., DAVIS, M. J., YATES, P. A., LI, Y., RISCOE, M. K., ULLMAN, B. & ROBERTS, S. C. 2017. Arginase Is Essential for Survival of Leishmania donovani Promastigotes but Not Intracellular Amastigotes. *Infect Immun,* 85.

BUEDE, R., RINKER-SCHAFFER, C., PINTO, W. J., LESTER, R. L. & DICKSON, R. C. 1991. Cloning and characterization of LCB1, a Saccharomyces gene required for biosynthesis of the long-chain base component of sphingolipids. *J Bacteriol,* 173**,** 4325-32.

BUSSOTTI, G., GOUZELOU, E., CORTES BOITE, M., KHERACHI, I., HARRAT, Z., EDDAIKRA, N., MOTTRAM, J. C., ANTONIOU, M., CHRISTODOULOU, V., BALI, A., GUERFALI, F. Z., LAOUINI, D., MUKHTAR, M., DUMETZ, F., DUJARDIN, J. C., SMIRLIS, D., LECHAT, P., PESCHER, P., EL HAMOUCHI, A., LEMRANI, M., CHICHARRO, C., LLANES-ACEVEDO, I. P., BOTANA, L., CRUZ, I., MORENO, J., JEDDI, F., AOUN, K., BOURATBINE, A., CUPOLILLO, E. & SPATH, G. F. 2018. Leishmania Genome Dynamics during Environmental Adaptation Reveal Strain-Specific Differences in Gene Copy Number Variation, Karyotype Instability, and Telomeric Amplification. *mBio,* 9.

BYUN, H. S., PYNE, S., MACRITCHIE, N., PYNE, N. J. & BITTMAN, R. 2013. Novel sphingosine-containing analogues selectively inhibit sphingosine kinase (SK) isozymes, induce SK1 proteasomal degradation and reduce DNA synthesis in human pulmonary arterial smooth muscle cells. *Medchemcomm,* 4.

CARNIELLI, J. B. T., MONTI-ROCHA, R., COSTA, D. L., MOLINA SESANA, A., PANSINI, L. N. N., SEGATTO, M., MOTTRAM, J. C., COSTA, C. H. N., CARVALHO, S. F. G. & DIETZE, R. 2019. Natural Resistance of Leishmania infantum to Miltefosine Contributes to the Low Efficacy in the Treatment of Visceral Leishmaniasis in Brazil. *Am J Trop Med Hyg,* 101**,** 789-794.

CASTANYS-MUNOZ, E., ALDER-BAERENS, N., POMORSKI, T., GAMARRO, F. & CASTANYS, S. 2007. A novel ATP-binding cassette transporter from Leishmania is involved in transport of phosphatidylcholine analogues and resistance to alkyl-phospholipids. *Mol Microbiol,* 64**,** 1141-53.

CHAKRAVARTY, J. & SUNDAR, S. 2010. Drug resistance in leishmaniasis. *J Glob Infect Dis,* 2**,** 167-76.

CHAN, M. M., BULINSKI, J. C., CHANG, K. P. & FONG, D. 2003. A microplate assay for Leishmania amazonensis promastigotes expressing multimeric green fluorescent protein. *Parasitol Res,* 89**,** 266-71.

CHAURIO, R. A., JANKO, C., MUNOZ, L. E., FREY, B., HERRMANN, M. & GAIPL, U. S. 2009. Phospholipids: key players in apoptosis and immune regulation. *Molecules,* 14**,** 4892-914.

CHEN, J. K., LANE, W. S. & SCHREIBER, S. L. 1999. The identification of myriocin-binding proteins. *Chem Biol,* 6**,** 221-35.

CLAYTON, C. E. 2016. Gene expression in Kinetoplastids. *Curr Opin Microbiol,* 32**,** 46-51.

COELHO, A. C., LEPROHON, P. & OUELLETTE, M. 2012. Generation of Leishmania hybrids by whole genomic DNA transformation. *PLoS Negl Trop Dis,* 6**,** e1817.

COELHO, A. C., TRINCONI, C. T., COSTA, C. H. & ULIANA, S. R. 2014. In vitro and in vivo miltefosine susceptibility of a Leishmania amazonensis isolate from a patient with diffuse cutaneous leishmaniasis. *PLoS Negl Trop Dis,* 8**,** e2999.

COJEAN, S., HOUZE, S., HAOUCHINE, D., HUTEAU, F., LARIVEN, S., HUBERT, V., MICHARD, F., BORIES, C., PRATLONG, F., LE BRAS, J., LOISEAU, P. M. & MATHERON, S. 2012. Leishmania resistance to miltefosine associated with genetic marker. *Emerg Infect Dis,* 18**,** 704-6.

COPPOLINO, M. G., DIERCKMAN, R., LOIJENS, J., COLLINS, R. F., POULADI, M., JONGSTRA-BILEN, J., SCHREIBER, A. D., TRIMBLE, W. S., ANDERSON, R. & GRINSTEIN, S. 2002. Inhibition of phosphatidylinositol-4-phosphate 5-kinase Ialpha impairs localized actin remodeling and suppresses phagocytosis. *J Biol Chem,* 277**,** 43849-57.

CRUZ, A., COBURN, C. M. & BEVERLEY, S. M. 1991. Double targeted gene replacement for creating null mutants. *Proc Natl Acad Sci U S A,* 88**,** 7170-4.

DAWKINS, J. L., HULME, D. J., BRAHMBHATT, S. B., AUER-GRUMBACH, M. & NICHOLSON, G. A. 2001. Mutations in SPTLC1, encoding serine palmitoyltransferase, long chain base subunit-1, cause hereditary sensory neuropathy type I. *Nat Genet,* 27**,** 309-12.

DE FREITAS BALANCO, J. M., MOREIRA, M. E., BONOMO, A., BOZZA, P. T., AMARANTE-MENDES, G., PIRMEZ, C. & BARCINSKI, M. A. 2001. Apoptotic mimicry by an obligate intracellular parasite downregulates macrophage microbicidal activity. *Curr Biol,* 11**,** 1870-3.

DELGADO, G., PUENTES, F., MORENO, A. & PATARROYO, M. E. 2001. Flow cytometry, a useful tool for detecting the lethal effect of pentamidine on Leishmania viannia complex promastigote forms. *Pharmacol Res,* 44**,** 281-6.

DENNY, P. W., GOULDING, D., FERGUSON, M. A. J. & SMITH, D. F. 2004. Sphingolipid-free Leishmania are defective in membrane trafficking, differentiation and infectivity. *Molecular Microbiology,* 52**,** 313-327.

DUAN, J. & MERRILL, A. H., JR. 2015. 1-Deoxysphingolipids Encountered Exogenously and Made de Novo: Dangerous Mysteries inside an Enigma. *J Biol Chem,* 290**,** 15380-15389.

DUMETZ, F., IMAMURA, H., SANDERS, M., SEBLOVA, V., MYSKOVA, J., PESCHER, P., VANAERSCHOT, M., MEEHAN, C. J., CUYPERS, B., DE MUYLDER, G., SPATH, G. F., BUSSOTTI, G., VERMEESCH, J. R., BERRIMAN, M., COTTON, J. A., VOLF, P., DUJARDIN, J. C. & DOMAGALSKA, M. A. 2017. Modulation of Aneuploidy in Leishmania donovani during Adaptation to Different In Vitro and In Vivo Environments and Its Impact on Gene Expression. *mBio,* 8.

DUNCAN, S. M., JONES, N. G. & MOTTRAM, J. C. 2017. Recent advances in Leishmania reverse genetics: Manipulating a manipulative parasite. *Mol Biochem Parasitol,* 216**,** 30-38.

DUNCAN, S. M., MYBURGH, E., PHILIPON, C., BROWN, E., MEISSNER, M., BREWER, J. & MOTTRAM, J. C. 2016. Conditional gene deletion with DiCre demonstrates an essential role for CRK3 in Leishmania mexicana cell cycle regulation. *Mol Microbiol,* 100**,** 931-44.

ESPADA, C. R., MAGALHAES, R. M., CRUZ, M. C., MACHADO, P. R., SCHRIEFER, A., CARVALHO, E. M., HORNILLOS, V., ALVES, J. M., CRUZ, A. K., COELHO, A. C. & ULIANA, S. R. B. 2019. Investigation of the pathways related to intrinsic miltefosine tolerance in Leishmania (Viannia) braziliensis clinical isolates reveals differences in drug uptake. *Int J Parasitol Drugs Drug Resist,* 11**,** 139-147.

FADOK, V. A., VOELKER, D. R., CAMPBELL, P. A., COHEN, J. J., BRATTON, D. L. & HENSON, P. M. 1992. Exposure of phosphatidylserine on the surface of apoptotic lymphocytes triggers specific recognition and removal by macrophages. *J Immunol,* 148**,** 2207-16.

FARRELL, A. M., UCHIDA, Y., NAGIEC, M. M., HARRIS, I. R., DICKSON, R. C., ELIAS, P. M. & HOLLERAN, W. M. 1998. UVB irradiation up-regulates serine palmitoyltransferase in cultured human keratinocytes. *J Lipid Res,* 39**,** 2031-8.

FREARSON, J. A., WYATT, P. G., GILBERT, I. H. & FAIRLAMB, A. H. 2007. Target assessment for antiparasitic drug discovery. *Trends Parasitol,* 23**,** 589-95.

FRENCH, K. J., ZHUANG, Y., MAINES, L. W., GAO, P., WANG, W., BELJANSKI, V., UPSON, J. J., GREEN, C. L., KELLER, S. N. & SMITH, C. D. 2010. Pharmacology and antitumor activity of ABC294640, a selective inhibitor of sphingosine kinase-2. *J Pharmacol Exp Ther,* 333**,** 129-39.

FRIDBERG, A., OLSON, C. L., NAKAYASU, E. S., TYLER, K. M., ALMEIDA, I. C. & ENGMAN, D. M. 2008. Sphingolipid synthesis is necessary for kinetoplast segregation and cytokinesis in Trypanosoma brucei. *Journal of Cell Science,* 121**,** 522-535.

GABLE, K., SLIFE, H., BACIKOVA, D., MONAGHAN, E. & DUNN, T. M. 2000. Tsc3p is an 80-amino acid protein associated with serine palmitoyltransferase and required for optimal enzyme activity. *J Biol Chem,* 275**,** 7597-603.

GEER, L. Y., DOMRACHEV, M., LIPMAN, D. J. & BRYANT, S. H. 2002. CDART: protein homology by domain architecture. *Genome Res,* 12**,** 1619-23.

GHOSH, S., BHATTACHARYYA, S., DAS, S., RAHA, S., MAULIK, N., DAS, D. K., ROY, S. & MAJUMDAR, S. 2001. Generation of ceramide in murine macrophages infected with Leishmania donovani alters macrophage signaling events and aids intracellular parasitic survival. *Mol Cell Biochem,* 223**,** 47-60.

GHOSH, S., VERMA, A., KUMAR, V., PRADHAN, D., SELVAPANDIYAN, A., SALOTRA, P. & SINGH, R. 2020. Genomic and Transcriptomic Analysis for Identification of Genes and Interlinked Pathways Mediating Artemisinin Resistance in Leishmania donovani. *Genes (Basel),* 11.

GILLESPIE, P. M., BEAUMIER, C. M., STRYCH, U., HAYWARD, T., HOTEZ, P. J. & BOTTAZZI, M. E. 2016. Status of vaccine research and development of vaccines for leishmaniasis. *Vaccine,* 34**,** 2992-2995.

GRAETHER, S. P. 2019. Troubleshooting Guide to Expressing Intrinsically Disordered Proteins for Use in NMR Experiments. *Frontiers in Molecular Biosciences,* 5.

GRONDIN, K., PAPADOPOULOU, B. & OUELLETTE, M. 1993. Homologous recombination between direct repeat sequences yields P-glycoprotein containing amplicons in arsenite resistant Leishmania. *Nucleic Acids Res,* 21**,** 1895-901.

GUHE, V., INGALE, P., TAMBEKAR, A. & SINGH, S. 2023. Systems biology of autophagy in leishmanial infection and its diverse role in precision medicine. *Front Mol Biosci,* 10**,** 1113249.

HADDADI, N., LIN, Y., SIMPSON, A., NASSIF, N. & MCGOWAN, E. 2017. "Dicing and Splicing" Sphingosine Kinase and Relevance to Cancer. *International Journal of Molecular Sciences,* 18**,** 1891.

HANADA, K. 2003. Serine palmitoyltransferase, a key enzyme of sphingolipid metabolism. *Biochim Biophys Acta,* 1632**,** 16-30.

HANADA, K., HARA, T., FUKASAWA, M., YAMAJI, A., UMEDA, M. & NISHIJIMA, M. 1998. Mammalian cell mutants resistant to a sphingomyelin-directed cytolysin. Genetic and biochemical evidence for complex formation of the LCB1 protein with the LCB2 protein for serine palmitoyltransferase. *J Biol Chem,* 273**,** 33787-94.

HANADA, K., NISHIJIMA, M., FUJITA, T. & KOBAYASHI, S. 2000. Specificity of inhibitors of serine palmitoyltransferase (SPT), a key enzyme in sphingolipid biosynthesis, in intact cells. A novel evaluation system using an SPT-defective mammalian cell mutant. *Biochem Pharmacol,* 59**,** 1211-6.

HANNUN, Y. A. & OBEID, L. M. 2008. Principles of bioactive lipid signalling: lessons from sphingolipids. *Nat Rev Mol Cell Biol,* 9**,** 139-50.

HARRISON, P. J., DUNN, T. M. & CAMPOPIANO, D. J. 2018. Sphingolipid biosynthesis in man and microbes. *Nat Prod Rep,* 35**,** 921-954.

HATOUM, D., HADDADI, N., LIN, Y., NASSIF, N. T. & MCGOWAN, E. M. 2017. Mammalian sphingosine kinase (SphK) isoenzymes and isoform expression: challenges for SphK as an oncotarget. *Oncotarget,* 8**,** 36898-36929.

HENDERSON, D. M., SIFRI, C. D., RODGERS, M., WIRTH, D. F., HENDRICKSON, N. & ULLMAN, B. 1992. Multidrug resistance in Leishmania donovani is conferred by amplification of a gene homologous to the mammalian mdr1 gene. *Mol Cell Biol,* 12**,** 2855-65.

HORNEMANN, T., RICHARD, S., RUTTI, M. F., WEI, Y. & VON ECKARDSTEIN, A. 2006. Cloning and initial characterization of a new subunit for mammalian serine-palmitoyltransferase. *J Biol Chem,* 281**,** 37275-81.

HSU, F. F., TURK, J., ZHANG, K. & BEVERLEY, S. M. 2007. Characterization of inositol phosphorylceramides from Leishmania major by tandem mass spectrometry with electrospray ionization. *J Am Soc Mass Spectrom,* 18**,** 1591-604.

HUGHES, J. P., REES, S., KALINDJIAN, S. B. & PHILPOTT, K. L. 2011. Principles of early drug discovery. *Br J Pharmacol,* 162**,** 1239-49.

IMAMURA, H., MONSIEURS, P., JARA, M., SANDERS, M., MAES, I., VANAERSCHOT, M., BERRIMAN, M., COTTON, J. A., DUJARDIN, J. C. & DOMAGALSKA, M. A. 2020. Evaluation of whole genome amplification and bioinformatic methods for the characterization of Leishmania genomes at a single cell level. *Sci Rep,* 10**,** 15043.

JONES, N. G., CATTA-PRETA, C. M. C., LIMA, A. & MOTTRAM, J. C. 2018. Genetically Validated Drug Targets in Leishmania: Current Knowledge and Future Prospects. *ACS Infect Dis,* 4**,** 467-477.

KAPLER, G. M., COBURN, C. M. & BEVERLEY, S. M. 1990. Stable transfection of the human parasite Leishmania major delineates a 30-kilobase region sufficient for extrachromosomal replication and expression. *Mol Cell Biol,* 10**,** 1084-94.

KAWAMORI, T., KANESHIRO, T., OKUMURA, M., MAALOUF, S., UFLACKER, A., BIELAWSKI, J., HANNUN, Y. A. & OBEID, L. M. 2009. Role for sphingosine kinase 1 in colon carcinogenesis. *FASEB J,* 23**,** 405-14.

KELSO, A. A., WALDVOGEL, S. M., LUTHMAN, A. J. & SEHORN, M. G. 2017. Homologous Recombination in Protozoan Parasites and Recombinase Inhibitors. *Front Microbiol,* 8**,** 1716.

KOHAMA, T., OLIVERA, A., EDSALL, L., NAGIEC, M. M., DICKSON, R. & SPIEGEL, S. 1998. Molecular cloning and functional characterization of murine sphingosine kinase. *J Biol Chem,* 273**,** 23722-8.

LACHAUD, L., BOURGEOIS, N., KUK, N., MORELLE, C., CROBU, L., MERLIN, G., BASTIEN, P., PAGES, M. & STERKERS, Y. 2014. Constitutive mosaic aneuploidy is a unique genetic feature widespread in the Leishmania genus. *Microbes Infect,* 16**,** 61-6.

LEGARE, D., CAYER, S., SINGH, A. K., RICHARD, D., PAPADOPOULOU, B. & OUELLETTE, M. 2001. ABC proteins of Leishmania. *J Bioenerg Biomembr,* 33**,** 469-74.

LEPROHON, P., LEGARE, D., GIRARD, I., PAPADOPOULOU, B. & OUELLETTE, M. 2006. Modulation of Leishmania ABC protein gene expression through life stages and among drug-resistant parasites. *Eukaryot Cell,* 5**,** 1713-25.

LEPROHON, P., LEGARE, D., RAYMOND, F., MADORE, E., HARDIMAN, G., CORBEIL, J. & OUELLETTE, M. 2009. Gene expression modulation is associated with gene amplification, supernumerary chromosomes and chromosome loss in antimony-resistant Leishmania infantum. *Nucleic Acids Res,* 37**,** 1387-99.

LIU, H., SUGIURA, M., NAVA, V. E., EDSALL, L. C., KONO, K., POULTON, S., MILSTIEN, S., KOHAMA, T. & SPIEGEL, S. 2000. Molecular Cloning and Functional Characterization of a Novel Mammalian Sphingosine Kinase Type 2 Isoform. *Journal of Biological Chemistry,* 275**,** 19513-19520.

LOVERIDGE, C., TONELLI, F., LECLERCQ, T., LIM, K. G., LONG, J. S., BERDYSHEV, E., TATE, R. J., NATARAJAN, V., PITSON, S. M., PYNE, N. J. & PYNE, S. 2010. The sphingosine kinase 1 inhibitor 2-(p-hydroxyanilino)-4-(p-chlorophenyl)thiazole induces proteasomal degradation of sphingosine kinase 1 in mammalian cells. *J Biol Chem,* 285**,** 38841-52.

LUQUE-ORTEGA, J. R. & RIVAS, L. 2007. Miltefosine (hexadecylphosphocholine) inhibits cytochrome c oxidase in Leishmania donovani promastigotes. *Antimicrob Agents Chemother,* 51**,** 1327-32.

LYE, L. F., OWENS, K., SHI, H., MURTA, S. M., VIEIRA, A. C., TURCO, S. J., TSCHUDI, C., ULLU, E. & BEVERLEY, S. M. 2010. Retention and loss of RNA interference pathways in trypanosomatid protozoans. *PLoS Pathog,* 6**,** e1001161.

MAAROUF, M., DE KOUCHKOVSKY, Y., BROWN, S., PETIT, P. X. & ROBERT-GERO, M. 1997. In vivo interference of paromomycin with mitochondrial activity of Leishmania. *Exp Cell Res,* 232**,** 339-48.

MARSCHNER, N., KOTTING, J., EIBL, H. & UNGER, C. 1992. Distribution of hexadecylphosphocholine and octadecyl-methyl-glycero-3-phosphocholine in rat tissues during steady-state treatment. *Cancer Chemother Pharmacol,* 31**,** 18-22.

MERRILL, A. H. & JONES, D. D. 1990. An update of the enzymology and regulation of sphingomyelin metabolism. *Biochim Biophys Acta,* 1044**,** 1-12.

MERRILL, A. H., JR. 2011. Sphingolipid and glycosphingolipid metabolic pathways in the era of sphingolipidomics. *Chem Rev,* 111**,** 6387-422.

MERRILL, A. H., JR., WANG, M. D., PARK, M. & SULLARDS, M. C. 2007. (Glyco)sphingolipidology: an amazing challenge and opportunity for systems biology. *Trends Biochem Sci,* 32**,** 457-68.

MIZUGISHI, K., YAMASHITA, T., OLIVERA, A., MILLER, G. F., SPIEGEL, S. & PROIA, R. L. 2005. Essential role for sphingosine kinases in neural and vascular development. *Mol Cell Biol,* 25**,** 11113-21.

MURPHY, S. M., ERNST, D., WEI, Y., LAURA, M., LIU, Y. T., POLKE, J., BLAKE, J., WINER, J., HOULDEN, H., HORNEMANN, T. & REILLY, M. M. 2013. Hereditary sensory and autonomic neuropathy type 1 (HSANI) caused by a novel mutation in SPTLC2. *Neurology,* 80**,** 2106-11.

NAGIEC, M. M., BALTISBERGER, J. A., WELLS, G. B., LESTER, R. L. & DICKSON, R. C. 1994. The LCB2 gene of Saccharomyces and the related LCB1 gene encode subunits of serine palmitoyltransferase, the initial enzyme in sphingolipid synthesis. *Proceedings of the National Academy of Sciences,* 91**,** 7899-7902.

NAKAYAMA, G. R., CATON, M. C., NOVA, M. P. & PARANDOOSH, Z. 1997. Assessment of the Alamar Blue assay for cellular growth and viability in vitro. *J Immunol Methods,* 204**,** 205-8.

NAVA, V. E., HOBSON, J. P., MURTHY, S., MILSTIEN, S. & SPIEGEL, S. 2002. Sphingosine kinase type 1 promotes estrogen-dependent tumorigenesis of breast cancer MCF-7 cells. *Exp Cell Res,* 281**,** 115-27.

OLLIARO, P. L., GUERIN, P. J., GERSTL, S., HAASKJOLD, A. A., ROTTINGEN, J. A. & SUNDAR, S. 2005. Treatment options for visceral leishmaniasis: a systematic review of clinical studies done in India, 1980-2004. *Lancet Infect Dis,* 5**,** 763-74.

OMMEN, G., LORENZ, S. & CLOS, J. 2009. One-step generation of double-allele gene replacement mutants in Leishmania donovani. *Int J Parasitol,* 39**,** 541-6.

OUELLETTE, M. & BORST, P. 1991. Drug resistance and P-glycoprotein gene amplification in the protozoan parasite Leishmania. *Res Microbiol,* 142**,** 737-46.

OUELLETTE, M., LEGARE, D., HAIMEUR, A., GRONDIN, K., ROY, G., BROCHU, C. & PAPADOPOULOU, B. 1998. ABC transporters in Leishmania and their role in drug resistance. *Drug Resist Updat,* 1**,** 43-8.

PARIS, C., LOISEAU, P. M., BORIES, C. & BREARD, J. 2004. Miltefosine induces apoptosis-like death in Leishmania donovani promastigotes. *Antimicrob Agents Chemother,* 48**,** 852-9.

PATINO, L. H., IMAMURA, H., CRUZ-SAAVEDRA, L., PAVIA, P., MUSKUS, C., MÉNDEZ, C., DUJARDIN, J. C. & RAMÍREZ, J. D. 2019. Major changes in chromosomal somy, gene expression and gene dosage driven by SbIII in Leishmania braziliensis and Leishmania panamensis. *Scientific Reports,* 9.

PAYSAN-LAFOSSE, T., BLUM, M., CHUGURANSKY, S., GREGO, T., PINTO, B. L., SALAZAR, G. A., BILESCHI, M. L., BORK, P., BRIDGE, A., COLWELL, L., GOUGH, J., HAFT, D. H., LETUNIC, I., MARCHLER-BAUER, A., MI, H., NATALE, D. A., ORENGO, C. A., PANDURANGAN, A. P., RIVOIRE, C., SIGRIST, C. J. A., SILLITOE, I., THANKI, N., THOMAS, P. D., TOSATTO, S. C. E., WU, C. H. & BATEMAN, A. 2023. InterPro in 2022. *Nucleic Acids Res,* 51**,** D418-D427.

PEACOCK, C. S., SEEGER, K., HARRIS, D., MURPHY, L., RUIZ, J. C., QUAIL, M. A., PETERS, N., ADLEM, E., TIVEY, A., ASLETT, M., KERHORNOU, A., IVENS, A., FRASER, A., RAJANDREAM, M. A., CARVER, T., NORBERTCZAK, H., CHILLINGWORTH, T., HANCE, Z., JAGELS, K., MOULE, S., ORMOND, D., RUTTER, S., SQUARES, R., WHITEHEAD, S., RABBINOWITSCH, E., ARROWSMITH, C., WHITE, B., THURSTON, S., BRINGAUD, F., BALDAUF, S. L., FAULCONBRIDGE, A., JEFFARES, D., DEPLEDGE, D. P., OYOLA, S. O., HILLEY, J. D., BRITO, L. O., TOSI, L. R., BARRELL, B., CRUZ, A. K., MOTTRAM, J. C., SMITH, D. F. & BERRIMAN, M. 2007. Comparative genomic analysis of three Leishmania species that cause diverse human disease. *Nat Genet,* 39**,** 839-47.

PEREZ-VICTORIA, F. J., CASTANYS, S. & GAMARRO, F. 2003a. Leishmania donovani resistance to miltefosine involves a defective inward translocation of the drug. *Antimicrob Agents Chemother,* 47**,** 2397-403.

PEREZ-VICTORIA, F. J., GAMARRO, F., OUELLETTE, M. & CASTANYS, S. 2003b. Functional cloning of the miltefosine transporter. A novel P-type phospholipid translocase from Leishmania involved in drug resistance. *J Biol Chem,* 278**,** 49965-71.

PINTO, W. J., SRINIVASAN, B., SHEPHERD, S., SCHMIDT, A., DICKSON, R. C. & LESTER, R. L. 1992. Sphingolipid long-chain-base auxotrophs of Saccharomyces cerevisiae: genetics, physiology, and a method for their selection. *Journal of Bacteriology,* 174**,** 2565-2574.

PITSON, S. M., MORETTI, P. A., ZEBOL, J. R., ZAREIE, R., DERIAN, C. K., DARROW, A. L., QI, J., D'ANDREA, R. J., BAGLEY, C. J., VADAS, M. A. & WATTENBERG, B. W. 2002. The nucleotide-binding site of human sphingosine kinase 1. *J Biol Chem,* 277**,** 49545-53.

PONTE-SUCRE, A., GAMARRO, F., DUJARDIN, J. C., BARRETT, M. P., LOPEZ-VELEZ, R., GARCIA-HERNANDEZ, R., POUNTAIN, A. W., MWENECHANYA, R. & PAPADOPOULOU, B. 2017. Drug resistance and treatment failure in leishmaniasis: A 21st century challenge. *PLoS Negl Trop Dis,* 11**,** e0006052.

PRAJAPATI, V. K., SHARMA, S., RAI, M., OSTYN, B., SALOTRA, P., VANAERSCHOT, M., DUJARDIN, J. C. & SUNDAR, S. 2013. In vitro susceptibility of Leishmania donovani to miltefosine in Indian visceral leishmaniasis. *Am J Trop Med Hyg,* 89**,** 750-4.

PURKAIT, B., KUMAR, A., NANDI, N., SARDAR, A. H., DAS, S., KUMAR, S., PANDEY, K., RAVIDAS, V., KUMAR, M., DE, T., SINGH, D. & DAS, P. 2012. Mechanism of amphotericin B resistance in clinical isolates of Leishmania donovani. *Antimicrob Agents Chemother,* 56**,** 1031-41.

PÉREZ-VICTORIA, F. J., CASTANYS, S. & GAMARRO, F. 2003. Leishmania donovani resistance to miltefosine involves a defective inward translocation of the drug. *Antimicrob Agents Chemother,* 47**,** 2397-403.

RAKOTOMANGA, M., SAINT-PIERRE-CHAZALET, M. & LOISEAU, P. M. 2005. Alteration of fatty acid and sterol metabolism in miltefosine-resistant Leishmania donovani promastigotes and consequences for drug-membrane interactions. *Antimicrob Agents Chemother,* 49**,** 2677-86.

RASTROJO, A., GARCIA-HERNANDEZ, R., VARGAS, P., CAMACHO, E., CORVO, L., IMAMURA, H., DUJARDIN, J. C., CASTANYS, S., AGUADO, B., GAMARRO, F. & REQUENA, J. M. 2018. Genomic and transcriptomic alterations in Leishmania donovani lines experimentally resistant to antileishmanial drugs. *Int J Parasitol Drugs Drug Resist,* 8**,** 246-264.

RHEE, S. G. 2001. Regulation of phosphoinositide-specific phospholipase C. *Annu Rev Biochem,* 70**,** 281-312.

RIJAL, S., OSTYN, B., URANW, S., RAI, K., BHATTARAI, N. R., DORLO, T. P., BEIJNEN, J. H., VANAERSCHOT, M., DECUYPERE, S., DHAKAL, S. S., DAS, M. L., KARKI, P., SINGH, R., BOELAERT, M. & DUJARDIN, J. C. 2013. Increasing failure of miltefosine in the treatment of Kala-azar in Nepal and the potential role of parasite drug resistance, reinfection, or noncompliance. *Clin Infect Dis,* 56**,** 1530-8.

ROCHETTE, A., MCNICOLL, F., GIRARD, J., BRETON, M., LEBLANC, E., BERGERON, M. G. & PAPADOPOULOU, B. 2005. Characterization and developmental gene regulation of a large gene family encoding amastin surface proteins in Leishmania spp. *Mol Biochem Parasitol,* 140**,** 205-20.

ROGERS, M. B., HILLEY, J. D., DICKENS, N. J., WILKES, J., BATES, P. A., DEPLEDGE, D. P., HARRIS, D., HER, Y., HERZYK, P., IMAMURA, H., OTTO, T. D., SANDERS, M., SEEGER, K., DUJARDIN, J. C., BERRIMAN, M., SMITH, D. F., HERTZ-FOWLER, C. & MOTTRAM, J. C. 2011. Chromosome and gene copy number variation allow major structural change between species and strains of Leishmania. *Genome Res,* 21**,** 2129-42.

RUSSELL, D. G., XU, S. & CHAKRABORTY, P. 1992. Intracellular trafficking and the parasitophorous vacuole of Leishmania mexicana-infected macrophages. *J Cell Sci,* 103 (Pt 4)**,** 1193-210.

SAHA, A. K., MUKHERJEE, T. & BHADURI, A. 1986. Mechanism of action of amphotericin B on Leishmania donovani promastigotes. *Mol Biochem Parasitol,* 19**,** 195-200.

SCHMITZ, G. & LANGMANN, T. 2001. Structure, function and regulation of the ABC1 gene product. *Curr Opin Lipidol,* 12**,** 129-40.

SCHNUTE, MARK E., MCREYNOLDS, MATTHEW D., KASTEN, T., YATES, M., JEROME, G., RAINS, JOHN W., HALL, T., CHRENCIK, J., KRAUS, M., CRONIN, CIARAN N., SAABYE, M., HIGHKIN, MAUREEN K., BROADUS, R., OGAWA, S., CUKYNE, K., ZAWADZKE, LAURA E., PETERKIN, V., IYANAR, K., SCHOLTEN, JEFFREY A., WENDLING, J., FUJIWARA, H., NEMIROVSKIY, O., WITTWER, ARTHUR J. & NAGIEC, MAREK M. 2012. Modulation of cellular S1P levels with a novel, potent and specific inhibitor of sphingosine kinase-1. *Biochemical Journal,* 444**,** 79-88.

SHAW, C. D., LONCHAMP, J., DOWNING, T., IMAMURA, H., FREEMAN, T. M., COTTON, J. A., SANDERS, M., BLACKBURN, G., DUJARDIN, J. C., RIJAL, S., KHANAL, B., ILLINGWORTH, C. J., COOMBS, G. H. & CARTER, K. C. 2016. In vitro selection of miltefosine resistance in promastigotes of Leishmania donovani from Nepal: genomic and metabolomic characterization. *Mol Microbiol,* 99**,** 1134-48.

SINHA, R., C, M. M., RAGHWAN, DAS, S., DAS, S., SHADAB, M., CHOWDHURY, R., TRIPATHY, S. & ALI, N. 2018. Genome Plasticity in Cultured Leishmania donovani: Comparison of Early and Late Passages. *Front Microbiol,* 9**,** 1279.

SIQUEIRA-NETO, J. L., SONG, O. R., OH, H., SOHN, J. H., YANG, G., NAM, J., JANG, J., CECHETTO, J., LEE, C. B., MOON, S., GENOVESIO, A., CHATELAIN, E., CHRISTOPHE, T. & FREITAS-JUNIOR, L. H. 2010. Antileishmanial high-throughput drug screening reveals drug candidates with new scaffolds. *PLoS Negl Trop Dis,* 4**,** e675.

SRIVASTAVA, S., MISHRA, J., GUPTA, A. K., SINGH, A., SHANKAR, P. & SINGH, S. 2017. Laboratory confirmed miltefosine resistant cases of visceral leishmaniasis from India. *Parasit Vectors,* 10**,** 49.

STERKERS, Y., LACHAUD, L., CROBU, L., BASTIEN, P. & PAGES, M. 2011. FISH analysis reveals aneuploidy and continual generation of chromosomal mosaicism in Leishmania major. *Cell Microbiol,* 13**,** 274-83.

STOBER, C. B., LANGE, U. G., ROBERTS, M. T., GILMARTIN, B., FRANCIS, R., ALMEIDA, R., PEACOCK, C. S., MCCANN, S. & BLACKWELL, J. M. 2006. From genome to vaccines for leishmaniasis: screening 100 novel vaccine candidates against murine Leishmania major infection. *Vaccine,* 24**,** 2602-16.

STONE, N. R., BICANIC, T., SALIM, R. & HOPE, W. 2016. Liposomal Amphotericin B (AmBisome((R))): A Review of the Pharmacokinetics, Pharmacodynamics, Clinical Experience and Future Directions. *Drugs,* 76**,** 485-500.
SUNDAR, S., CHAKRAVARTY, J., RAI, V. K., AGRAWAL, N., SINGH, S. P., CHAUHAN, V. & MURRAY, H. W. 2007. Amphotericin B treatment for Indian visceral leishmaniasis: response to 15 daily versus alternate-day infusions. *Clin Infect Dis,* 45**,** 556-61.
SUNDAR, S., JHA, T. K., THAKUR, C. P., ENGEL, J., SINDERMANN, H., FISCHER, C., JUNGE, K., BRYCESON, A. & BERMAN, J. 2002. Oral miltefosine for Indian visceral leishmaniasis. *N Engl J Med,* 347**,** 1739-46.
SUNDAR, S., SINGH, A., RAI, M., PRAJAPATI, V. K., SINGH, A. K., OSTYN, B., BOELAERT, M., DUJARDIN, J. C. & CHAKRAVARTY, J. 2012. Efficacy of miltefosine in the treatment of visceral leishmaniasis in India after a decade of use. *Clin Infect Dis,* 55**,** 543-50.
TAHERI, T., SEYED, N., MIZBANI, A. & RAFATI, S. 2016. Leishmania-based expression systems. *Applied Microbiology and Biotechnology,* 100**,** 7377-7385.
TERNES, P., WOBBE, T., SCHWARZ, M., ALBRECHT, S., FEUSSNER, K., RIEZMAN, I., CREGG, J. M., HEINZ, E., RIEZMAN, H., FEUSSNER, I. & WARNECKE, D. 2011. Two pathways of sphingolipid biosynthesis are separated in the yeast Pichia pastoris. *J Biol Chem,* 286**,** 11401-14.
UZCANGA, G., LARA, E., GUTIERREZ, F., BEATY, D., BESKE, T., TERAN, R., NAVARRO, J. C., PASERO, P., BENITEZ, W. & POVEDA, A. 2017. Nuclear DNA replication and repair in parasites of the genus Leishmania: Exploiting differences to develop innovative therapeutic approaches. *Crit Rev Microbiol,* 43**,** 156-177.
VAN MEER, G., VOELKER, D. R. & FEIGENSON, G. W. 2008. Membrane lipids: where they are and how they behave. *Nat Rev Mol Cell Biol,* 9**,** 112-24.
VANCE, J. E. & STEENBERGEN, R. 2005. Metabolism and functions of phosphatidylserine. *Prog Lipid Res,* 44**,** 207-34.
VERHOVEN, B., SCHLEGEL, R. A. & WILLIAMSON, P. 1995. Mechanisms of phosphatidylserine exposure, a phagocyte recognition signal, on apoptotic T lymphocytes. *J Exp Med,* 182**,** 1597-601.
VERMA, A., BHANDARI, V., DEEP, D. K., SUNDAR, S., DUJARDIN, J. C., SINGH, R. & SALOTRA, P. 2017. Transcriptome profiling identifies genes/pathways associated with experimental resistance to paromomycin in Leishmania donovani. *Int J Parasitol Drugs Drug Resist,* 7**,** 370-377.
WANDERLEY, J. L., MOREIRA, M. E., BENJAMIN, A., BONOMO, A. C. & BARCINSKI, M. A. 2006. Mimicry of apoptotic cells by exposing phosphatidylserine participates in the establishment of amastigotes of Leishmania (L) amazonensis in mammalian hosts. *J Immunol,* 176**,** 1834-9.
WANG, J., KNAPP, S., PYNE, N. J., PYNE, S. & ELKINS, J. M. 2014. Crystal Structure of Sphingosine Kinase 1 with PF-543. *ACS Med Chem Lett,* 5**,** 1329-33.
WANG, X., SUN, Y., PENG, X., NAQVI, S., YANG, Y., ZHANG, J., CHEN, M., CHEN, Y., CHEN, H., YAN, H., WEI, G., HONG, P. & LU, Y. 2020. The Tumorigenic Effect of Sphingosine Kinase 1 and Its Potential Therapeutic Target. *Cancer Control,* 27**,** 1073274820976664.
WANG, Z., MIN, X., XIAO, S.-H., JOHNSTONE, S., ROMANOW, W., MEININGER, D., XU, H., LIU, J., DAI, J., AN, S., THIBAULT, S. & WALKER, N. 2013. Molecular Basis of Sphingosine Kinase 1 Substrate Recognition and Catalysis. *Structure,* 21**,** 798-809.
WEGERER, A., SUN, T. & ALTENBUCHNER, J. 2008. Optimization of an E. coli L-rhamnose-inducible expression vector: test of various genetic module combinations. *BMC Biotechnol,* 8**,** 2.
WILLIAMS, R. D., WANG, E. & MERRILL, A. H., JR. 1984. Enzymology of long-chain base synthesis by liver: characterization of serine palmitoyltransferase in rat liver microsomes. *Arch Biochem Biophys,* 228**,** 282-91.
WINBERG, M. E., HOLM, A., SARNDAHL, E., VINET, A. F., DESCOTEAUX, A., MAGNUSSON, K. E., RASMUSSON, B. & LERM, M. 2009. Leishmania donovani lipophosphoglycan inhibits phagosomal maturation via action on membrane rafts. *Microbes Infect,* 11**,** 215-22.
WINTER, G., FUCHS, M., MCCONVILLE, M. J., STIERHOF, Y. D. & OVERATH, P. 1994. Surface antigens of Leishmania mexicana amastigotes: characterization of glycoinositol phospholipids and a macrophage-derived glycosphingolipid. *Journal of Cell Science,* 107**,** 2471-2482.
WU, Y., EL FAKHRY, Y., SERENO, D., TAMAR, S. & PAPADOPOULOU, B. 2000. A new developmentally regulated gene family in Leishmania amastigotes encoding a homolog of amastin surface proteins. *Mol Biochem Parasitol,* 110**,** 345-57.

YASUDA, S., NISHIJIMA, M. & HANADA, K. 2003. Localization, topology, and function of the LCB1 subunit of serine palmitoyltransferase in mammalian cells. *J Biol Chem,* 278**,** 4176-83.
ZACKAY, A., COTTON, J. A., SANDERS, M., HAILU, A., NASEREDDIN, A., WARBURG, A. & JAFFE, C. L. 2018. Genome wide comparison of Ethiopian Leishmania donovani strains reveals differences potentially related to parasite survival. *PLoS Genet,* 14**,** e1007133.
ZHANG, K. 2003. Sphingolipids are essential for differentiation but not growth in Leishmania. *The EMBO Journal,* 22**,** 6016-6026.
ZHANG, K. & BEVERLEY, S. M. 2010. Phospholipid and sphingolipid metabolism in Leishmania. *Mol Biochem Parasitol,* 170**,** 55-64.
ZHANG, K., POMPEY, J. M., HSU, F. F., KEY, P., BANDHUVULA, P., SABA, J. D., TURK, J. & BEVERLEY, S. M. 2007. Redirection of sphingolipid metabolism toward de novo synthesis of ethanolamine in Leishmania. *EMBO J,* 26**,** 1094-104.
ZHANG, K., SHOWALTER, M., REVOLLO, J., HSU, F. F., TURK, J. & BEVERLEY, S. M. 2003. Sphingolipids are essential for differentiation but not growth in *Leishmania*. *EMBO J,* 22**,** 6016-26.
ZHANG, O., HSU, F.-F., XU, W., PAWLOWIC, M. & ZHANG, K. 2013a. Sphingosine kinase A is a pleiotropic and essential enzyme for *Leishmania* survival and virulence. *Molecular Microbiology,* 90**,** 489-501.
ZHANG, O., HSU, F.-F., XU, W., PAWLOWIC, M. & ZHANG, K. 2013b. Sphingosine kinase A is a pleiotropic and essential enzyme forLeishmaniasurvival and virulence. *Molecular Microbiology,* 90**,** 489-501.
ZIMMERMANN, L., STEPHENS, A., NAM, S.-Z., RAU, D., KÜBLER, J., LOZAJIC, M., GABLER, F., SÖDING, J., LUPAS, A. N. & ALVA, V. 2018. A Completely Reimplemented MPI Bioinformatics Toolkit with a New HHpred Server at its Core. *Journal of Molecular Biology,* 430**,** 2237-2243.
ZULFIQAR, B., SHELPER, T. B. & AVERY, V. M. 2017. Leishmaniasis drug discovery: recent progress and challenges in assay development. *Drug Discov Today,* 22**,** 1516-1531.

Appendix

Leishmania Sphingosine Kinase Protein Sequences

>LmjF.26.0710
MHSLSSNNTPSPHPATHRHTNHSSTHTSSLLPPTASPVLQASCMSAKEDHIGADAQGI
PSSALFTPKPRIFAVPASTESPPSPGATCHHAPTGGINVSAATGVSAAHHSDSGSNTAA
PTASSSSPALQKQQPEHCVPAAYRGKLDDAPHAVDDNMEAVILSKGRICTLAYFPSR
GSFRITHVSSNGKTRVVFNIPVRMIINIETAAERDARQRARQANDDTIKLVFAESGRN
TRSLLCSFPSGAGEDNEGVVLAHSVNTASLTLSLLGGPPPTPTASHFGAHTAACAAA
TAAPSIRYYVHYVQQRNKENPSIRTLEFQSSGPAETVQHVVSTVVQHIYQKGSKHIIA
FISAKSGKGKGEHIFEKHVRPLLHFSRHTYQAHVTRRAHDCEDYVANLENPMDSNT
VIAAVGGDGMIHETVNGVHRRKLALVRWLRSVTANVSTGNGSVVSPDLSVHLNEER
CAAVLLKSGSANKVVHHGEASVDSPSSPFIELGCEENKRDGYGGNGVTPSAEATARE
AYRLARCLVQGGWDALMPLVATVATGSACGLAKSLDVLSVTEAALSLVHLSTVHM
DLLLLNFTPNEDMVEFHRCRMSSRRLDAAQREFSRYKEDKAAELQERSRLGEAPQLP
PRTLTAADCMTPFLKDGSNVYRDAVSCAMRMPELHSRVAFMSLSFGSANDIDHGSE
SLRWMGNARFQVYGGYMILRGLKRYKGMLRYLPWGSKAGKTVEKLHTRCKMPST
DDFPLCTMRESCPHCRQYVFVHCGAPSLSSIQGDDTHPGPTPNTSRSTAQPISAAEVL
APYTDQQLLDEDVVDFKDERLPWVTVRGDFCIALLCNVRDVAQDMLMAPLAHMSD
GAIDIVYCRVDPITGRGGRMEMLKFVIGLESGSHVNLDFVNYVKARALEIKVDAGIS
MSDGELMPLSSVRVTKMRGSVQFVRSG
>LmjF.26.0710-_whelix
SGPAETVQHVVSTVVQHIYQKGSKHIIAFISAKSGKGKGEHIFEKHVRPLLHFSRHTY
QAHVTRRAHDCEDYVANLENPMDSNTVIAAVGGDGMIHETVNGVHRRKLALVRW
LRSVTANVSTGNGSVVSPDLSVHLNEERCAAVLLKSGSANKVVHHGEASVDSPSSPF
IELGCEENKRDGYGGNGVTPSAEATAREAYRLARCLVQGGWDALMPLVATVATGS
ACGLAKSLDVLSVTEAALSLVHLSTVHMDLLLLNFTPNEDMVEFHRCRMSSRRLDA
AQREFSRYKEDKAAELQERSRLGEAPQLPPRTLTAADCMTPFLKDGSNVYRDAVSC
AMRMPELHSRVAFMSLSFGSANDIDHGSESLRWMGNARFQVYGGYMILRGLKRYK
GMLRYLPWGSKAGKTV
>LmjF.26.0710-_wohelix
KGSKHIIAFISAKSGKGKGEHIFEKHVRPLLHFSRHTYQAHVTRRAHDCEDYVANLE
NPMDSNTVIAAVGGDGMIHETVNGVHRRKLALVRWLRSVTANVSTGNGSVVSPDL
SVHLNEERCAAVLLKSGSANKVVHHGEASVDSPSSPFIELGCEENKRDGYGGNGVTP
SAEATAREAYRLARCLVQGGWDALMPLVATVATGSACGLAKSLDVLSVTEAALSL
VHLSTVHMDLLLLNFTPNEDMVEFHRCRMSSRRLDAAQREFSRYKEDKAAELQERS
RLGEAPQLPPRTLTAADCMTPFLKDGSNVYRDAVSCAMRMPELHSRVAFMSLSFGS
ANDIDHGSESLRWMGNARFQVYGGYMILRGLKRYKGMLRYLPWGSKAGKTV
>LmxM.26.0710
MHSLTSDNTLNPQPATHRHTNHSSAHTSSLLPSTASPVLQASCMGAKEDHVDADAQ
GISSSALFTPKARISAAPASTKSPTSRGAACHHGPTSSINVSAAPSASSSLTAPQKQQPK
NGTPAADPENLDDATHPVEDSMEAAILNKDRVCTLAYFPSRGSFRITHVSSTGKTRV
VLNIPVRMIINIETAAECAARQLARSANDDTIKLGFAESGRSMGGLLCTFSGAGEDNE
RVVFADSHVNTTSSTLRLRGRSPPTPTASHLGTHTAARAVATAAPSIRYHVHYVQQR
NKESPSIRTLEFQSSGSVEGVQHVVTTVVQRIYQKGPKHIIAFISAKSGKGKGEDIFEK
QVRPVLHFSRHTYKIHVTRRAHDCEDYVANLENPMDSNTVIAAVGGDGMVHETVN
GVHRRKLALVRWLRSVTAEVSTGSTSVVSPNLSLHLNEETCAAVLKSGSANKAGLH
GEASVGFPSLFIQLGCEENKRNGHGGNGAMPSVEAKAREAYRLARCLVQDGWDAL

MPLVATVATGSGCGLAKSLDVLSVSEAALSLVHLSTVHMDLMLLNFTPNEDMLEFH
RRRMNARRLDAAKRKFSQYTKDKAAELQERSRLRETLQLPPGTLTAADCMTPFLKD
GSNVYRDAISCATRIPELHSRVAFMSLSFGAVNDIDHGSESLRWMGNARFNVYCGF
MLLRGLKRYNGILRYLPWESKTGKTVEKLHTRCKLPTTDHFPLCTMRETCPHCRQY
VFAHCGASSLSSMQGNDTHSGPTPNTSRSAAQPVSAAAALAPYTDQQLLDEDIVDFN
DERVPWVTIRGEFCVALMCNVRDVAQDVLMAPLAHMSDGSIDIVYCRVDPATDRR
GRMEMLKFLMGLESGSHVNLDFVNYVRARALEIKVDAGIAMSDGELMPLSSVRVT
KMRGSVQLVRSG

>LmxM.26.0710-whelix

SGSVEGVQHVVTTVVQRIYQKGPKHIIAFISAKSGKGKGEDIFEKQVRPVLHFSRHTY
KIHVTRRAHDCEDYVANLENPMDSNTVIAAVGGDGMVHETVNGVHRRKLALVRW
LRSVTAEVSTGSTSVVSPNLSLHLNEETCAAVLKSGSANKAGLHGEASVGFPSLFIQL
GCEENKRNGHGGNGAMPSVEAKAREAYRLARCLVQDGWDALMPLVATVATGSGC
GLAKSLDVLSVSEAALSLVHLSTVHMDLMLLNFTPNEDMLEFHRRRMNARRLDAA
KRKFSQYTKDKAAELQERSRLRETLQLPPGTLTAADCMTPFLKDGSNVYRDAISCAT
RIPELHSRVAFMSLSFGAVNDIDHGSESLRWMGNARFNVYCGFMLLRGLKRYNGIL
RYLPWESKTGKTV

>LmxM.26.0710-wohelix

KGPKHIIAFISAKSGKGKGEDIFEKQVRPVLHFSRHTYKIHVTRRAHDCEDYVANLEN
PMDSNTVIAAVGGDGMVHETVNGVHRRKLALVRWLRSVTAEVSTGSTSVVSPNLSL
HLNEETCAAVLKSGSANKAGLHGEASVGFPSLFIQLGCEENKRNGHGGNGAMPSVE
AKAREAYRLARCLVQDGWDALMPLVATVATGSGCGLAKSLDVLSVSEAALSLVHL
STVHMDLMLLNFTPNEDMLEFHRRRMNARRLDAAKRKFSQYTKDKAAELQERSRL
RETLQLPPGTLTAADCMTPFLKDGSNVYRDAISCATRIPELHSRVAFMSLSFGAVNDI
DHGSESLRWMGNARFNVYCGFMLLRGLKRYNGILRYLPWESKTGKTV

CRISPR Cas9 Primer Sequences used.

LmxSK UpstreamFPrimer	TTTCGCAGCTCCTTCTCCCGTCGTCGATCCGTATAATGCAGACCTGCTGC
LmxSK 5sgRNAprimer	GAAATTAATACGACTCACTATAGGTCGCGTGTTGCCTGCAGATCGTTTTAGAGCTAGAAATAGC
LmxSK DownstreamRPrimer	ATGAAAGTCTCTCTCCGCCCCCCCTCCCCGCCAATTTGAGAGACCTGTGC
LmxSK 3sgRNAprimer	GAAATTAATACGACTCACTATAGGGAGAGGGCAAGGATCCAGTAGTTTTAGAGCTAGAAATAGC
Lmx Diagnostic FP	AAAATAAAGGAGAAGCAGCGAAGCTATG
Lmx Diagnostic UR	AAACACATACTGACGGCAGTGC
Lmx Diagnostic DF	GCCGAAGCACATCATCGCTTT
Lmx Diagnostic RP	TCGTTTTGTTTAAGGCTGCGTGT
BlastREVdiagnose	TCCCACACATAACCAGAGGGCAGCAAT
BlastFRWdiagnose	TGCCTTTGTCTCAAGAAGAATCCA
PuroFWDdiagnose	ATGACTGAATACAAGCCAACGG
PuroREVdiagnose	TTACGTGTCATGCACCATGT
60S primer	ACTGTTCCTCGCACGCCCACGA
GLUT primer	GTATCCAATTCAAATACCCCAAACGA

Statistics for Figure 40

		Days in culture				
		0	**1**	**2**	**3**	**4**
Clone	**SK KO**	2.00E+05	1.49E+07	2.49E+07	3.84E+07	6.70E+07
	SK KO	2.00E+05	1.31E+07	2.01E+07	3.75E+07	5.30E+07
	SK KO	2.00E+05	7.40E+06	2.01E+07	3.00E+07	6.40E+07
	cas9t7	2.00E+05	1.09E+07	3.11E+07	6.84E+07	1.63E+08
	cas9t7	2.00E+05	1.47E+07	4.32E+07	8.91E+07	1.91E+08
	cas9t7	2.00E+05	1.39E+07	3.51E+07	1.00E+08	1.71E+08
	SK KO + addback	2.00E+05	7.60E+06	1.50E+07	1.95E+07	2.80E+07
	SK KO + addback	2.00E+05	8.20E+06	1.61E+07	1.86E+07	2.90E+07
	SK KO + addback	2.00E+05	8.70E+06	1.04E+07	2.94E+07	2.80E+07

Anova: Single Factor

DAY 0

SUMMARY

Groups	*Count*	*Sum*	*Average*	*Variance*
SK KO	3	600000	200000	0
cas9t7	3	600000	200000	0
SK KO + addback	3	600000	200000	0

ANOVA

Source of Variation	*SS*	*df*	*MS*	*F*	*P-value*	*F crit*
Between Groups	0	2	0	65535	#DIV/0!	5.14325285
Within Groups	0	6	0			
Total	0	8				

Anova: Single Factor

DAY 1

SUMMARY

Groups	*Count*	*Sum*	*Average*	*Variance*
SK KO	3	35400000	11800000	1.533E+13
cas9t7	3	39500000	13166666.7	4.0133E+12
SK KO + addback	3	24500000	8166666.67	3.0333E+11

ANOVA

Source of Variation	*SS*	*df*	*MS*	*F*	*P-value*	*F crit*
Between Groups	4.0069E+13	2	2.0034E+13	3.05921276	0.12137106	5.14325285
Within Groups	3.9293E+13	6	6.5489E+12			
Total	7.9362E+13	8				

Anova: Single Factor

DAY 2

SUMMARY

Groups	*Count*	*Sum*	*Average*	*Variance*
SK KO	3	65100000	21700000	7.68E+12
cas9t7	3	109350000	36450000	3.8273E+13
SK KO + addback	3	41400000	13800000	9.2025E+12

ANOVA

Source of Variation	*SS*	*df*	*MS*	*F*	*P-value*	*F crit*
Between Groups	7.93E+14	2	3.965E+14	21.5663584	0.00182113	5.14325285
Within Groups	1.1031E+14	6	1.8385E+13			
Total	9.0331E+14	8				

Anova: Single Factor

DAY 3

SUMMARY

Groups	*Count*	*Sum*	*Average*	*Variance*
SK KO	3	105900000	35300000	2.127E+13
cas9t7	3	257700000	85900000	2.6049E+14
SK KO + addback	3	67500000	22500000	3.591E+13

ANOVA

Source of Variation	*SS*	*df*	*MS*	*F*	*P-value*	*F crit*
Between Groups	6.7438E+15	2	3.3719E+15	31.8432335	0.00063828	5.14325285
Within Groups	6.3534E+14	6	1.0589E+14			
Total	7.3791E+15	8				

Anova: Single Factor

DAY 4

SUMMARY

Groups	*Count*	*Sum*	*Average*	*Variance*
SK KO	3	184000000	61333333.3	5.4333E+13
cas9t7	3	524125000	174708333	2.0157E+14
SK KO + addback	3	85000000	28333333.3	3.3333E+11

ANOVA

Source of Variation	*SS*	*df*	*MS*	*F*	*P-value*	*F crit*
Between Groups	3.5369E+16	2	1.7684E+16	207.04793	2.91E-06	5.14325285
Within Groups	5.1247E+14	6	8.5411E+13			
Total	3.5881E+16	8				

where P-value <0.05, we reject the null hypothesis. Our sample data provide strong enough evidence to conclude that the population means are not equal.

Statistics for Figure 62

Table Analyzed	Table 62				
Data sets analyzed	A-F				
ANOVA summary					
F	4.408				
P value	0.0189				
P value summary	*				
Significant diff. among means (P < 0.05)?	Yes				
R squared	0.6671				
Brown-Forsythe test					
F (DFn, DFd)	156206 (5, 11)				
P value	<0.0001				
P value summary	****				
Are SDs significantly different (P < 0.05)?	Yes				
Bartlett's test					
Bartlett's statistic (corrected)					
P value					
P value summary					
Are SDs significantly different (P < 0.05)?					
ANOVA table	SS	DF	MS	F (DFn, DFd)	P value
Treatment (between columns)	55434	5	11087	F (5, 11) = 4.408	P=0.0189
Residual (within columns)	27665	11	2515		
Total	83099	16			
Normality of Residuals					
Test name	Statistics	P value	Passed normality test (alpha=0.05)?	P value summary	
D'Agostino-Pearson omnibus (K2)	11.51	0.0032	No	**	
Anderson-Darling (A2*)	4.453	<0.0001	No	****	
Shapiro-Wilk (W)	0.4987	<0.0001	No	****	
Kolmogorov-Smirnov (distance)	0.4374	<0.0001	No	****	

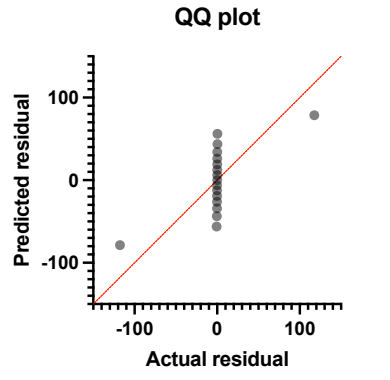

LCB2 genome report

Obtained the 75-bp pair ended Illumina reads for Lmj-LCB2 from Glasgow Polyomics:

Lmj_LCB2_S8_R1_001.fastq.gz
Lmj_LCB2_S8_R2_001.fastq.gz

Analyse using FastQC
Sequence content shows major anomalies in positions 73-5.
Otherwise the stats look good.
Clean up the reads with Trimmomatic-0.36

```
nohup java -jar ~/auxPackages/Trimmomatic-0.36/trimmomatic-
0.36.jar PE -threads 8 -phred33 -trimlog trimProcess.log
-validatePairs -basein Lmj_LCB2_S8_R1_001.fastq.gz -baseout Lmj-
LCB2.fq.gz CROP:72 ILLUMINACLIP:TruSeq2-PE.fa:2:30:10:2:true
LEADING:3 TRAILING:3 SLIDINGWINDOW:5:20 MINLEN:45 &
```

Obtain the *L. major* Freiedlin genome (version 36, release date 19/2/18) from TriTrypDB and generate Bowtie2 and faidx indices from same:

```
bowtie2-build LmjFriedlin.fa LmjFV1_genome
samtools faidx LmjFriedlin.fa
```

perform bowtie2 remapping using the *L. major* Friedlin genome index using all valid read files from post Trimmomatic processing convert directly to a .bam format file :

```
bowtie2 -p 10 -x indexes/LmjFV1_genome -1 Lmj-LCB2_1P.fq.gz -2
Lmj-LCB2_2P.fq.gz -U Lmj-LCB2_1U.fq.gz,Lmj-LCB2_2U.fq.gz  --sam-RG
ID:LCB2_deletion | samtools view -bS - > output.bam

[samopen] SAM header is present: 36 sequences.
15863390 reads; of these:
  13126689 (82.75%) were paired; of these:
    1166282 (8.88%) aligned concordantly 0 times
    10464539 (79.72%) aligned concordantly exactly 1 time
    1495868 (11.40%) aligned concordantly >1 times
    ----
    1166282 pairs aligned concordantly 0 times; of these:
      166390 (14.27%) aligned discordantly 1 time
    ----
    999892 pairs aligned 0 times concordantly or discordantly; of
these:
      1999784 mates make up the pairs; of these:
        1563311 (78.17%) aligned 0 times
        326060 (16.30%) aligned exactly 1 time
        110413 (5.52%) aligned >1 times
  2736701 (17.25%) were unpaired; of these:
    224156 (8.19%) aligned 0 times
```

```
    2155680 (78.77%) aligned exactly 1 time
    356865 (13.04%) aligned >1 times
93.83% overall alignment rate
```

sort the output bam file and get a pileup of the mapped reads, producing a stripped down file with the chromosome identifier, base position, totals bases mapped to position and the reference base value, omitting the mapped base values and quality scores:

```
samtools sort output.bam x

samtools mpileup -d 5000 -f indexes/LmjFriedlin.fa  x.bam | awk
'{print $1,"\t",$2,"\t",$4,"\t",$3}'>LmjLCB2.mpl
```

File LmjLCB2.mpl processed with script pileupParse.py:

```
python pileupScoreParse.py LmjLCB2.mpl LmjChrom.list

pileupParse.py
'''
Script to produce a read depth summary of each chromosome, in
100base blocks each chromosome is output as a separate text file
for later parsing and querying
'''
files pileupParse.py and LmjChrom.list are appended
```

Determine the distribution of read depths per chromosome and hence (from the median value for read depth) the relative ploidy for each chromosome.

```
python depthDistro.py LmjLCB2.mpl LmjChrom.list

depthDistro.py
'''
Script to produce a read depth summary of each chromosome,
histogram of depth of mappings in each chromosome
'''

LmjF.01.dst:Peak read depth   LmjF.01 = 28
LmjF.02.dst:Peak read depth   LmjF.02 = 54
LmjF.03.dst:Peak read depth   LmjF.03 = 54
LmjF.04.dst:Peak read depth   LmjF.04 = 53
LmjF.05.dst:Peak read depth   LmjF.05 = 74
LmjF.06.dst:Peak read depth   LmjF.06 = 54
LmjF.07.dst:Peak read depth   LmjF.07 = 53
LmjF.08.dst:Peak read depth   LmjF.08 = 52
LmjF.09.dst:Peak read depth   LmjF.09 = 53
LmjF.10.dst:Peak read depth   LmjF.10 = 52
LmjF.11.dst:Peak read depth   LmjF.11 = 55
LmjF.12.dst:Peak read depth   LmjF.12 = 54
```

```
LmjF.13.dst:Peak read depth   LmjF.13 = 50
LmjF.14.dst:Peak read depth   LmjF.14 = 52
LmjF.15.dst:Peak read depth   LmjF.15 = 53
LmjF.16.dst:Peak read depth   LmjF.16 = 53
LmjF.17.dst:Peak read depth   LmjF.17 = 52
LmjF.18.dst:Peak read depth   LmjF.18 = 52
LmjF.19.dst:Peak read depth   LmjF.19 = 53
LmjF.20.dst:Peak read depth   LmjF.20 = 53
LmjF.21.dst:Peak read depth   LmjF.21 = 53
LmjF.22.dst:Peak read depth   LmjF.22 = 55
LmjF.23.dst:Peak read depth   LmjF.23 = 55
LmjF.24.dst:Peak read depth   LmjF.24 = 51
LmjF.25.dst:Peak read depth   LmjF.25 = 52
LmjF.26.dst:Peak read depth   LmjF.26 = 51
LmjF.27.dst:Peak read depth   LmjF.27 = 51
LmjF.28.dst:Peak read depth   LmjF.28 = 52
LmjF.29.dst:Peak read depth   LmjF.29 = 51
LmjF.30.dst:Peak read depth   LmjF.30 = 53
LmjF.31.dst:Peak read depth   LmjF.31 = 128
LmjF.32.dst:Peak read depth   LmjF.32 = 52
LmjF.33.dst:Peak read depth   LmjF.33 = 51
LmjF.34.dst:Peak read depth   LmjF.34 = 51
LmjF.35.dst:Peak read depth   LmjF.35 = 52
LmjF.36.dst:Peak read depth   LmjF.36 = 52
```

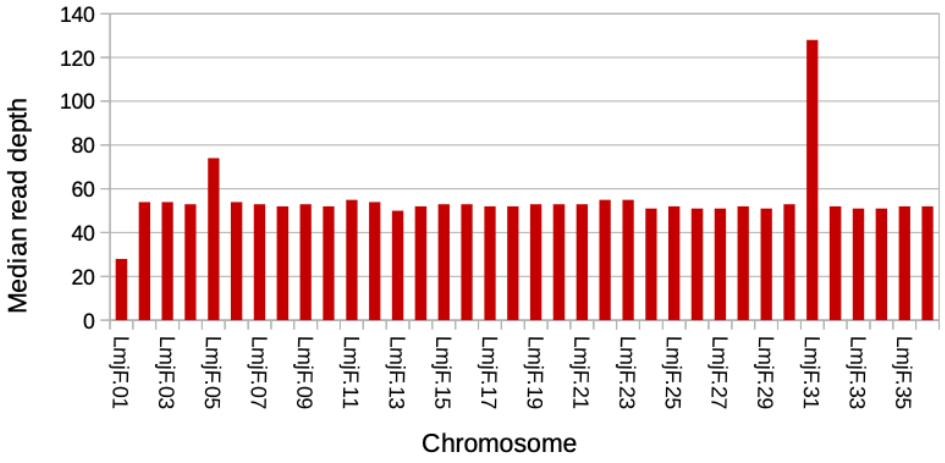

Three chromosomes appear to have aberrant ploidy. If the norm is diploid, then chromosome 1 seems to have a single copy, 5 is triploid and 31 (as found in other Leishmania species) is tetra- or penta- ploid.

Determine regions of the pileup summaries that seem to indicate potential deletions in the chromosomes:

```
echo Lmj01 >> ablated.list
awk -F "\t" '{if($2<5) {print}}'  LmjF.01.mpl >> ablated.list
echo Lmj02 >> ablated.list
awk -F "\t" '{if($2<5) {print}}'  LmjF.02.mpl >> ablated.list
echo Lmj03 >> ablated.list

…

echo Lmj36 >> ablated.list
awk -F "\t" '{if($2<5) {print}}'  LmjF.36.mpl >> ablated.list

ablated.list is appended.

14 regions are flagged as being potential deletions.
The representative regions including these potential deletions
were extracted from the base-by-base pileup file (LmjLCB2.mpl),
and the same regions visualised in the TriTrypDB genome browser.
The knockout region (LmjF.35:85,000..88,000) shows clear and
unambiguous ablation of sequence including the coding region for
Lmj.35.0320 – serine palmitoyl transferase. Three other cases
indicated a correspondence between very low/absent read depth and
annotated genes. The remaining 'deletions' in intergenic regions
were investigated – the reference sequences generated by TriTrypDB
(LCB2_KO_ablate.fas, file appended). All such regions showed
highly repetitive low complexity sequence often with a high GC
content e.g. :

>LmjF.11:551600..552100
gcggcctccatccctttcctctccactctcacgcacgatttcacagaagcgatgcgcttt
cttgccccctgtcctcctcctcccctcctcctcctcccctcctcctcctcccctcctcct
cctcccctgtcctcctcctcctcccctcccctgtcctcctcccctcctcctcccctgtcc
tcctcctcccctgtcctcctcctcctcccctcctcctcctcccctcccctcccctcccct
cctctcctcctcctcccctgtcctcctcctcctcccctcccctcccctgtcctctcctcc
cctcctcctcctcctcccctcctcctcccctcccctcccctgtcctctcctcctcctccc
ctcccctcctctgtccttcaaccagccgtgcaactaaagcgccgtttggaacccttttt
ggttgatgtgcatcgatttgtggctattcatgtgtttacgtgtgtgtatctttgtgtgtg
cacgcatggaattcatgtatg

>LmjF.12:107000..107800
aggtcggcgcacacgcgcatgcgtgggcgagccagagatcaagtgatgccgggatatacc
atgcgtgtctgtgtgggtgtgggtgtatgtgtgtgtgggggtgtgtgtgtgtctgtgagt
gtgtgtgggtgggtgggtgggtgtgggtgtgggtgtgggtgtgggtgtgggtgggtgggt
gtgggtgtgggtgtgtgtgtgtgtgggtgggtgtgggtgtgtgtgtgtgtgtgagtgtgtgt
gtgtgtgtgtgtgtgtgtgtgtgtccgtgtgtgtgtgtatgtgtgtgtgtgtgtgtgtgt
gtgtgtgtgtgtgtgtgtgcgtgtgtgtgtgggtgtgtgtgtgtgtgtgtgtgtctgt
gtgtgtgggtgtgggtgtgtgtgtgtgtgtgggtgtgggtgtgggtgtgggtgtgagtgt
gtgggtgtgtgtgtgtgggtgggtgggtgtgtgtgggtgtgggtgtgtgtgtgtgtgtgt
atgtgtgtgggtgtgggtgtgggtgtgtctgtgagtgtgtgtgtgtgtgggtaggtgggt
gtgtgtggtgtgggtgtgcggagcttatcccgttgtcgctatcgctgtccccgctgttgt
tgctgaatggcctggtgccggttagcctccccccccccctccccctcccccctcccctcc
```

atgttcttgtagcgcgcgcagtactaagacgttcactgacaccatagtgaataacaatgt
catgtaaagagcgcgcttgagggagggaggaagacagcgacgtgtccgtgtgtgtgtgtg
tgtgggtgggtggcagcggag

The low/absent level of reads covering these regions may reflect deficiencies in amplification of reads covering such regions, rather than any actual deletion of sequence.

The knock-out region on chromosome 35 shows complete ablation of the sequence. This represents the ideal of a complete deletion. The other three sites show a different pattern. The regions covering LmjF.11.1240 and LmjF.08.0740 demonstrate regions of zero mapping interspersed with peaks of mapping of read-depth lower than surrounding sequence. The low-mapping region including LmjF.13.1530 and 1540 shows a low level of mapping, but no strong evidence for complete ablation. The sorted .bam file was interrogated for the read mappings in the low/absent mapping regions as follows:

```
samtools view -h x.bam|awk -F "\t" '{if($3=="LmjF.11" &&
($4>508700 && $4 < 517100)) {print}}' > Lmj11spot.txt

samtools view -h x.bam|awk -F "\t" '{if($3=="LmjF.13" &&
($4>564753 && $4 < 573440)) {print}}' > Lmj13spot.txt

samtools view -h x.bam|awk -F "\t" '{if($3=="LmjF.08" &&
($4>327500 && $4 < 328300)) {print}}' > Lmj08spot.txt
```

These read mapping entries were investigated for the presence of the XS:i: optional field, the presence of which indicates that the read has at least one alternative mapping position.

```
grep -c AS:i Lmj*txt          grep -c XS:i Lmj*txt
Lmj08spot.txt:88              Lmj08spot.txt:85
Lmj11spot.txt:182             Lmj11spot.txt:179
Lmj13spot.txt:392             Lmj13spot.txt:7
```

The regions of chromosomes 8 and 11 show a large majority of reads that also map to alternative regions of the genome, The discrete peaks within in potential deletion site represent 'islands of identity' with other regions of the genome and it is therefore consistent with the region being completely deleted.

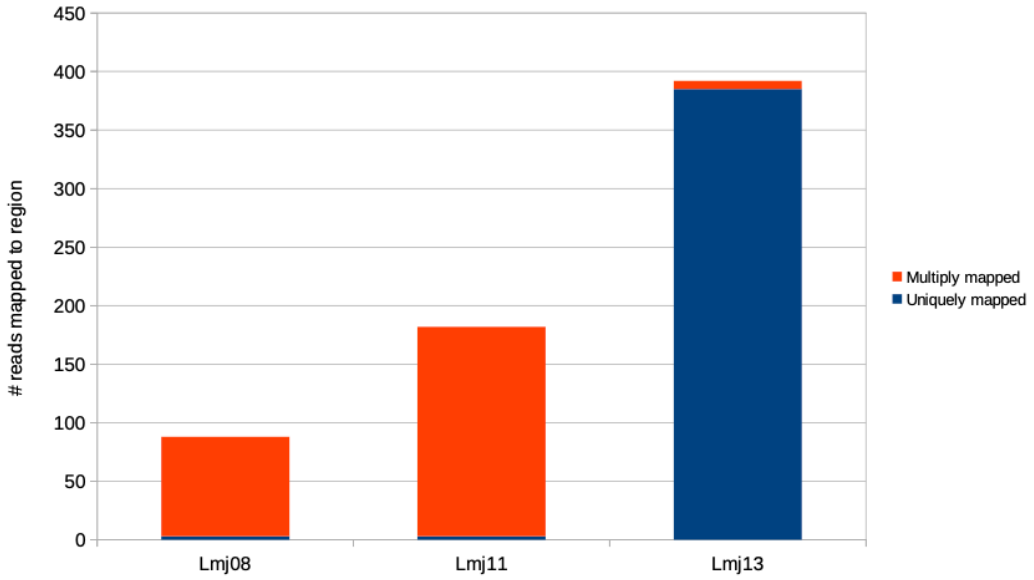

The region in chromosome 13 is different. A large majority of reads have a unique mapping locus, but are present in a much reduced abundance. One interpretation of this is that the sample consists of two populations, one in high abundance with a deletion covering the region, a second low abundance population retaining the region. This may be due to a differential growth effect, with the population losing the region having a higher growth rate and hence overgrowing the 'wild-type' (wrt chr13 564000..573500) population. The annotated genes covered by the potential deletions are :

LmjF.08.0740 amastin-like protein

LmjF.11.1240 ATP-binding cassette protein subfamily A, member 3, putative

LmjF.13.1530 phospholipid-transporting ATPase 1-like protein

(*Annotator's note Implicated in miltefosine and amphotericin B resistance in Leishmania. Resistance mutations change lipid composition (PMID:27911896; PMID:16785229; PMID:27123924); eupathdb_uc=100051073; date_20170104***)**

LmjF.13.1540 hypothetical protein, unknown function

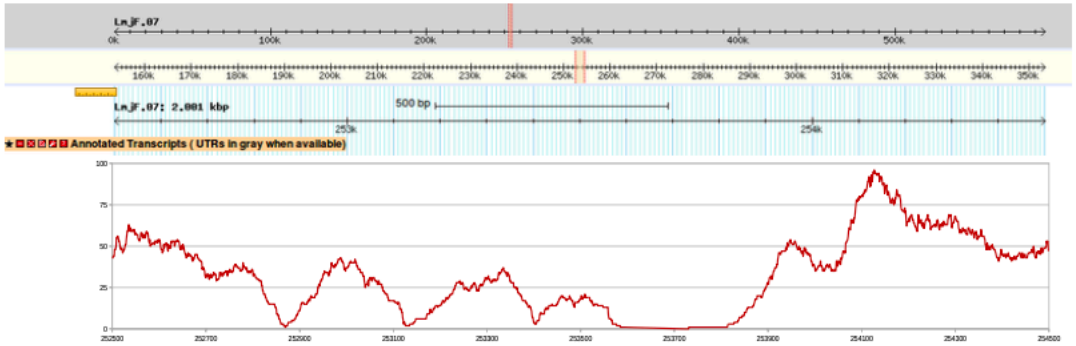

LmjF.07:252,500..254,500

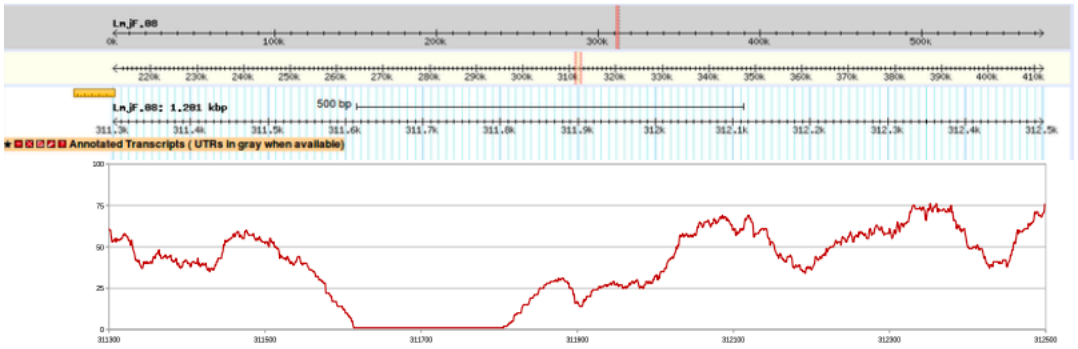

LmjF.08:311,300..312,500

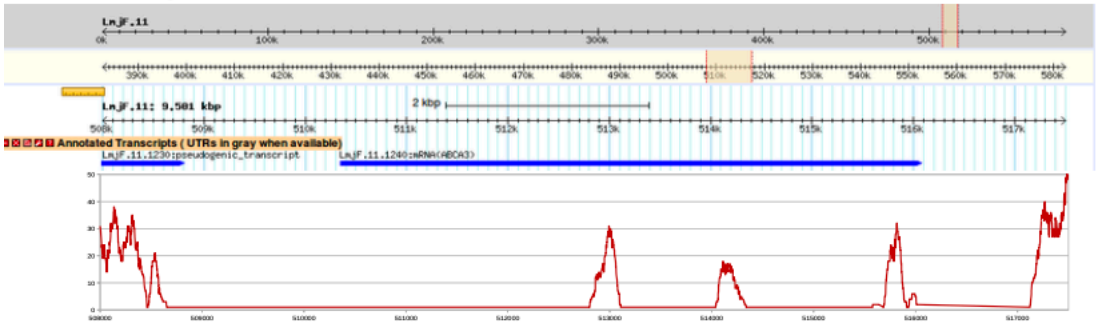

LmjF.11:508,000..517,500

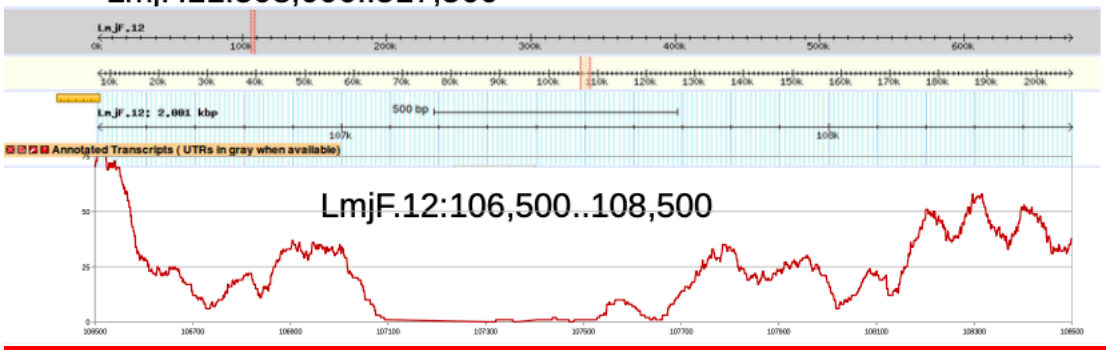

LmjF.12:106,500..108,500

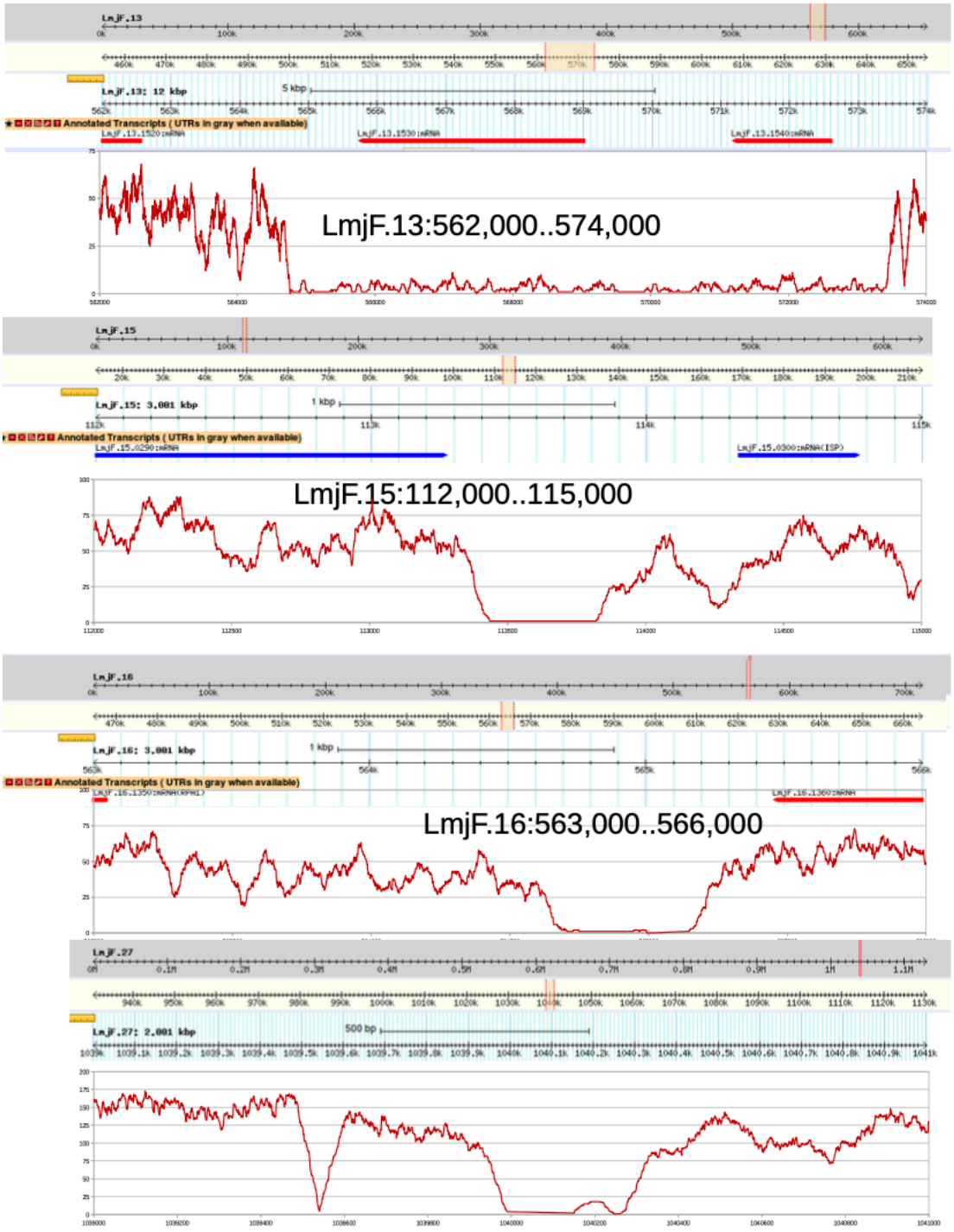

LmjF.27:1,039,000..1,041,000


LmjF.33
LmjF.33: 2.001 kbp
500 bp
Annotated Transcripts (UTRs in gray when available)
LmjF.33.2000:mRNA
LmjF.33:890,500..892,500

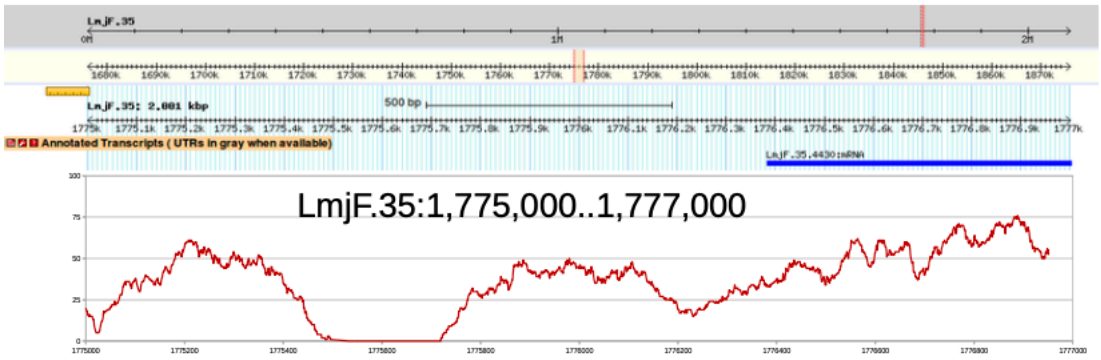
LmjF.35
LmjF.35: 2.001 kbp
500 bp
Annotated Transcripts (UTRs in gray when available)
LmjF.35.4430:mRNA
LmjF.35:1,775,000..1,777,000

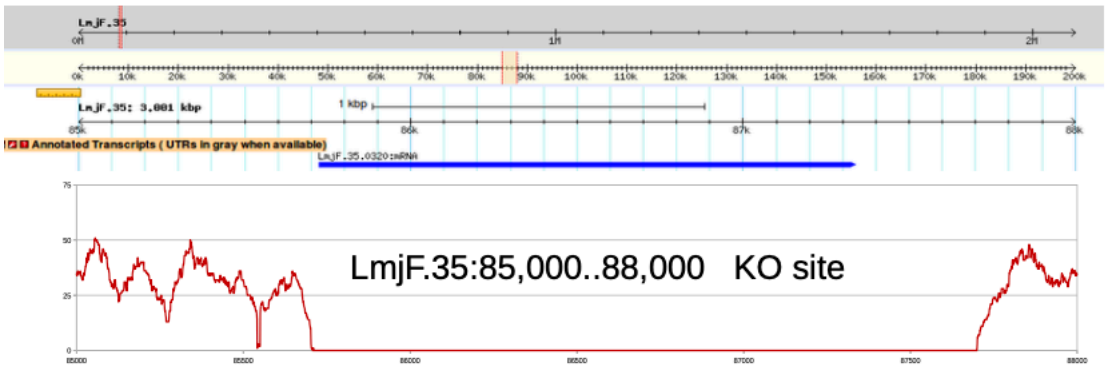
LmjF.35
LmjF.35: 3.001 kbp
1 kbp
Annotated Transcripts (UTRs in gray when available)
LmjF.35.0320:mRNA
LmjF.35:85,000..88,000 KO site

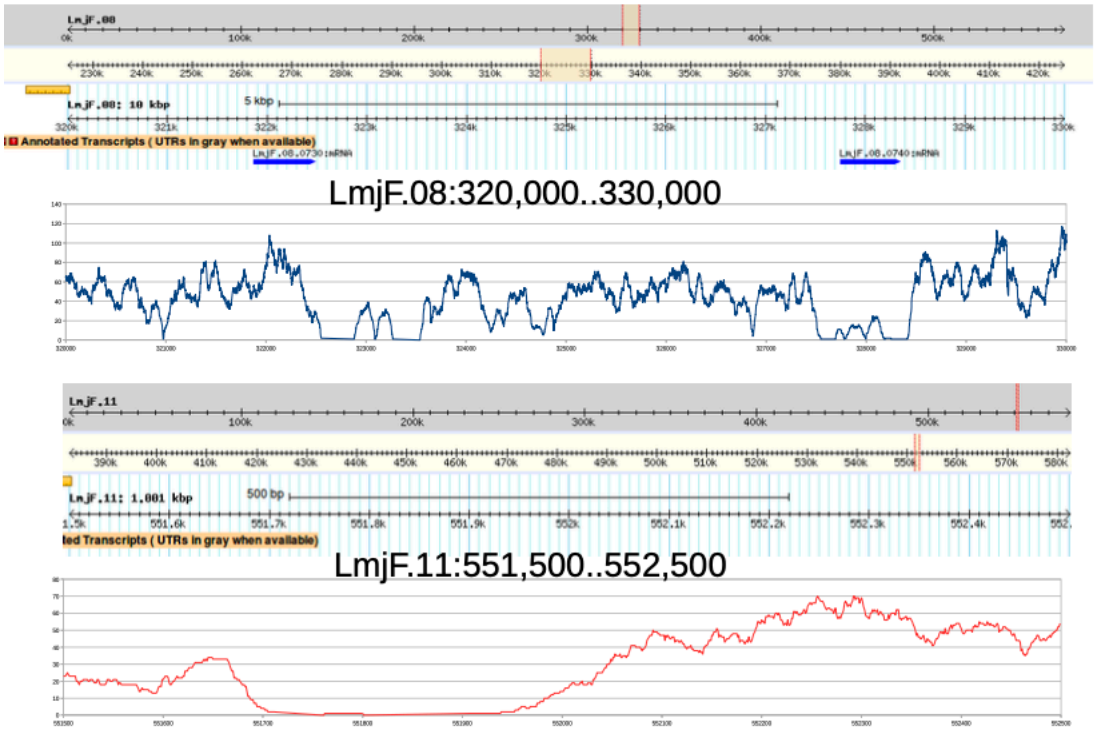
LmjF.08
LmjF.08: 10 kbp
5 kbp
Annotated Transcripts (UTRs in gray when available)
LmjF.08:320,000..330,000
LmjF.11
LmjF.11: 1.001 kbp
500 bp
led Transcripts (UTRs in gray when available)
LmjF.11:551,500..552,500